

SYNTHESIS, CHARACTERIZATION AND ANION BINDING PROPERTIES OF  
BORON-BASED LEWIS ACIDS

A Dissertation

by

HAIYAN ZHAO

Submitted to the Office of Graduate Studies of  
Texas A&M University  
in partial fulfillment of the requirements for the degree of

DOCTOR OF PHILOSOPHY

May 2012

Major Subject: Chemistry

Synthesis, Characterization and Anion Binding Properties of Boron-based Lewis Acids

Copyright 2012 Haiyan Zhao

SYNTHESIS, CHARACTERIZATION AND ANION BINDING PROPERTIES OF  
BORON-BASED LEWIS ACIDS

A Dissertation

by

HAIYAN ZHAO

Submitted to the Office of Graduate Studies of  
Texas A&M University  
in partial fulfillment of the requirements for the degree of

DOCTOR OF PHILOSOPHY

Approved by:

Chair of Committee,	François P. Gabbaï
Committee Members,	Marcetta Y. Darensbourg
	Hongcai Zhou
	Kathryn J. Ryan
Head of Department,	David H. Russell

May 2012

Major Subject: Chemistry

## ABSTRACT

Synthesis, Characterization and Anion Binding Properties of Boron-based  
Lewis Acids. (May 2012)

Haiyan Zhao, B.S., Nankai University

Chair of Advisory Committee: Dr. François P. Gabbaï

The recognition and capture of fluoride, cyanide and azide anions is attracting great deal of attention due to the negative effects of these anions on the environment and on human health. One of common methods used for the recognition and capture of these anions is based on triarylboranes, the Lewis acidity of which can be enhanced via variation the steric and electronic properties of the boron substituents.

This dissertation is dedicated to the synthesis of novel boron-based anion receptors that, for the most part, feature an onium group bound to one of the aryl substituents. The presence of this group is shown to increase the anion affinity of the boron center via Coulombic effects. Another interesting effect is observed when the onium group is juxtaposed with the boron atom. This is for example the case of naphthalene-based compounds bearing a dimesitylboryl moiety at one of the peri-position and a sulfonium or telluronium unit at the other peri position. Fluoride anion complexation studies with these sulfonium or telluronium boranes, show that the boron-bound fluoride anion is further stabilized by formation of a B-F $\rightarrow$ Te/S bridge involving a lp(F) $\rightarrow$  $\sigma^*$ (Te/S-C) donor acceptor interaction. Some of the sulfonium boranes



investigated have been shown to efficiently capture fluoride anions from wet methanolic solutions. The resulting fluoride/sulfonium borane adducts can be triggered to release a “naked” fluoride equivalent in organic solution and thus show promise as new reagents for nucleophilic fluorination chemistry. Interestingly, the telluronium systems show a greater fluoride anion affinity than their sulfonium analogs. This increase is assigned to the greater spatial and energetic accessibility of the  $\sigma^*$  orbital on the tellurium atom which favors the formation of a strong B–F→Te interaction.

This dissertation is concluded by an investigation of the Lewis acidic properties of B(C<sub>6</sub>Cl<sub>5</sub>)<sub>3</sub>. This borane, which has been reported to be non-Lewis acidic by other researchers, is found by us to bind fluoride, azide and cyanide anions in dichloromethane with large binding constants. This borane is also reactive toward neutral Lewis bases, such as *p*-dimethylaminopyridine, in organic solvents.

## ACKNOWLEDGEMENTS

I would like to thank my advisor and committee chair, Dr. François Gabbai for supervising me through my graduate study. He is always helpful with enduring patience and kindness. Dr. Gabbai gives me great encouragement when I encounter challenges in research. I would also like to thank my committee members, Dr. M. Darensbourg, Dr. Zhou, and Dr. Ryan, for their guidance and support throughout the course of my research.

Thanks also go to the members of the Gabbai group: Dr. Mieock Kim, Dr. Chammi Palehepitiya Gamage, Dr. Takeshi Matsumoto, Dr. Zureima Hernandez, Dr. Hyun-Sue Huh, Dr. Duxia Cao, Dr. Ching-Wen Chiu, Dr. Todd Hudnall, Dr. Christopher Dorsey, Dr. Casey Wade, Dr. Youngmin Kim, Tzu-Pin Lin, Iou-Sheng Ke, James Jones, Lauren Learner, Masato Hirai, Kantapat Chansaenpak, Adriana Hampton, Haifeng Yang. I would especially like to thank Dr. Ching-Wen Chiu, Dr. Youngmin Kim and Dr. Casey Wade for their great help in my early years in the Gabbai group. I would also like to thank my friends in and out of the department, with whom I have had a great time when out of lab. Without these wonderful colleagues and friends, I would not have such enjoyable time during my graduate study.

Finally, I would like to thank my mother and father for their encouragement and support. I am extremely grateful to my husband, Yi Shu. His support and love accompany me to finish my PhD study.

## TABLE OF CONTENTS

	Page
ABSTRACT .....	iii
ACKNOWLEDGEMENTS .....	v
TABLE OF CONTENTS .....	vi
LIST OF FIGURES .....	ix
LIST OF TABLES .....	xvi
CHAPTER	
I INTRODUCTION AND BACKGROUND .....	1
1.1 Introduction .....	1
1.2 Lewis acidity and anion complexation by triarylboranes .....	2
1.3 Anion complexation by diboranes .....	4
1.4 Lewis acidity and anion complexation by cationic boranes .....	8
1.4.1 Effects induced by remote cationic functionality .....	8
1.4.2 Effects induced by proximal cationic functionality .....	14
II SYNTHESIS, CHARACTERIZATION AND ANION AFFINITY OF SULFONIUM BORANE .....	18
2.1 Introduction .....	18
2.2 Synthesis and characterization of sulfonium borane .....	19
2.3 Reaction of the sulfonium borane with fluoride ions .....	23
2.4 Reaction of the sulfonium borane with cyanide ions .....	30
2.5 Comparison of Lewis acidity of [ <b>30</b> ] <sup>+</sup> with another sulfonium borane .....	35
2.6 Conclusion .....	39
2.7 Experimental section .....	39
III THE APPLICATION OF A SULFONIUM BORANE IN FLUORIDE TRANSFER PROCESS .....	52
3.1 Introduction .....	52
3.2 Review of nucleophilic fluorinating reagents .....	53

CHAPTER	Page
3.3 Demethylation of the fluoride adduct of the sulfonium borane	62
3.4 Nucleophilic reactions using <b>30</b> -F <sup>-</sup> .....	69
3.4.1 TBACN as a nucleophile for demethylation .....	69
3.4.2 TBASPh as a nucleophile for demethylation .....	70
3.5 Conclusion.....	71
3.6 Experimental section .....	72
 IV    A BIDENTATE LEWIS ACID WITH A TELLURONIUM ION AS AN ANION-BINDING SITE.....	75
4.1 Introduction .....	75
4.2 Synthesis and characterization of the telluronium borane and its sulfur analog .....	77
4.3 Anion affinity of the sulfonium borane and telluronium borane	93
4.3.1 Fluoride affinity.....	93
4.3.2 Cyanide affinity.....	102
4.4 Conclusion.....	108
4.5 Experimental section .....	109
 V     ON THE SYNERGY OF COULOMBIC AND CHELATE EFFECTS IN BIDENTATE DIBORANES: SYNTHESIS AND ANION BINDING PROPERTIES OF A CATIONIC 1,8- DIBORYLNAPHTHALENE.....	131
5.1 Introduction .....	131
5.2 Synthesis and characterization of the cationic diborane .....	132
5.3 Fluoride anion complexation.....	137
5.4 Reaction with other anions.....	147
5.5 Conclusion.....	152
5.6 Experimental section .....	152
 VI    LEWIS ACIDITY BEHAVIOR OF TRIS(PENTACHLORO- PHENYL)BORANE. ....	163
6.1 Introduction .....	163
6.2 Fluoride ion complexation of B(C <sub>6</sub> Cl <sub>5</sub> ) <sub>3</sub> .....	164
6.3 DMAP complexation of B(C <sub>6</sub> Cl <sub>5</sub> ) <sub>3</sub> .....	170
6.4 Complexation of other anions and molecules by B(C <sub>6</sub> Cl <sub>5</sub> ) <sub>3</sub> ....	174
6.5 Conclusion.....	174
6.6 Experimental section .....	175

CHAPTER	Page
VII THE HYDROPHOBIC EFFECTS IN THE FLUORIDE COMPLEXATION BY A SERIES OF SULFONIUM BORANES ...	178
7.1 Introduction .....	178
7.2 Synthesis and characterization of sulfonium boranes .....	179
7.3 Lewis acidity and pH stability range studies.....	183
7.4 Fluoride ion complexation in methanol .....	185
7.5 Fluoride ion complexation in water .....	190
7.6 Lewis acidity and fluoride affinity in the presence of CTABr	192
7.7 Conclusion.....	194
7.8 Experimental section .....	195
VIII SUMMARY .....	208
8.1 Lewis acidity of a sulfonium borane and its application in fluorination chemistry .....	208
8.2 Fluoride affinity of a telluronium borane .....	210
8.3 Anion affinity of a cationic diborane .....	211
8.4 Lewis acidity behavior of $B(C_6Cl_5)_3$ .....	213
8.5 Hydrophobic effects in the fluoride complexation by cationic boranes .....	214
REFERENCES.....	217
VITA .....	223

## LIST OF FIGURES

	Page
Figure 1. The fluoride capture by triarylboranes.....	2
Figure 2. Top: the fluoride binding by triarylborane; Bottom: schematic representation of the switching of $\pi$ -conjugation in the LUMO of the triarylboranes. ....	3
Figure 3. The anion chelation by diboranes to form B-X-B bridging bond.....	6
Figure 4. The anion chelation process by <b>12</b> .....	7
Figure 5. The reactions of <b>13</b> with $\text{Cu}(\text{OH})_2$ and $\text{C}_2\text{Cl}_6$ .....	8
Figure 6. The cationic boranes of $[\mathbf{14}]^+$ , $[\mathbf{15}]^+$ , $[\mathbf{16}]^+$ , $[\mathbf{17}]^+$ and $[\mathbf{18}]^+$ .....	10
Figure 7. The synthesis of $[\mathbf{19}]^+$ and its reaction with fluoride under biphasic conditions.....	12
Figure 8. The synthesis of $[\mathbf{22}]^+$ .....	13
Figure 9. The synthesis of $[\mathbf{26}]^+$ , $[\mathbf{27}]^+$ and their anion binding reactions. ....	15
Figure 10. The competition reaction of $[\mathbf{28}]^+$ and <b>22-F</b> in $\text{CDCl}_3$ .....	17
Figure 11. Crystal structure of <b>28-F</b> (left) and the AIM and NBO analyses of the B-F $\rightarrow$ P donor-acceptor interaction (right).....	17
Figure 12 Synthesis of the sulfonium borane $[\mathbf{30}]\text{OTf}$ .....	20
Figure 13. Crystal structure of $[\mathbf{30}]\text{OTf}$ . ....	21
Figure 14. Reaction of $[\mathbf{30}]^+$ with KF to form <b>30-F</b> in methanol.....	23
Figure 15. Crystal structure of <b>30-F</b> . ....	26
Figure 16. NBO contour plots that show the two $\text{lp}(\text{F})\rightarrow\sigma^*(\text{S-C})$ donor-acceptor interactions involved in <b>30-F</b> . ....	28

Figure 17. Left: Changes in the UV-vis absorption spectra of a solution of <b>[30]OTf</b> ( $4.36 \times 10^{-5}$ M in THF: H <sub>2</sub> O, 9/1, vol.) upon the addition of a TBAF solution ( $9.5 \times 10^{-3}$ M in THF); Right: resulting 1:1 binding isotherm using $\epsilon([\mathbf{30}]\text{OTf}) = 16350 \text{ M}^{-1}\text{cm}^{-1}$ and $\epsilon(\mathbf{30-F}) = 4900 \text{ M}^{-1}\text{cm}^{-1}$ with $\lambda_{\text{max}} = 337\text{nm}$ . .....	29
Figure 18. Reaction of <b>[30]<sup>+</sup></b> with KCN to form <b>30-CN</b> in methanol. ....	30
Figure 19. Crystal structure of <b>30-CN</b> . ....	32
Figure 20. NBO contour plots showing $\pi(\text{C}\equiv\text{N}) \rightarrow \sigma^*(\text{S}-\text{C})$ (top) and $\text{lp}(\text{S}) \rightarrow \pi^*(\text{C}\equiv\text{N})$ (bottom) interactions in <b>30-CN</b> . ....	34
Figure 21. Left: Changes in the UV-vis absorption spectra of a solution of <b>[30]OTf</b> ( $4.67 \times 10^{-5}$ M in THF) upon the addition of a KCN solution ( $7.5 \times 10^{-3}$ M) in THF); Right: resulting 1:1 binding isotherm using $\epsilon([\mathbf{30}]\text{OTf}) = 16350 \text{ M}^{-1}\text{cm}^{-1}$ and $\epsilon(\mathbf{30-CN}) = 5800 \text{ M}^{-1}\text{cm}^{-1}$ with $\lambda_{\text{max}} = 337 \text{ nm}$ . ....	35
Figure 22. Spectrophotometric titration curve of <b>[30]<sup>+</sup></b> .....	37
Figure 23. Partial view of the molecule of <b>[30]<sup>+</sup></b> showing the contour of the NBOs involved in the $\text{lp}(\text{S}) \rightarrow \text{p}(\text{B})$ donor - acceptor interaction. ....	38
Figure 24. <sup>1</sup> H NMR and <sup>13</sup> C NMR spectra of <b>30-F</b> .....	43
Figure 25. DFT optimized structure of <b>[30]<sup>+</sup></b> .....	47
Figure 26. DFT optimized structure of <b>30-F</b> .....	47
Figure 27. DFT optimized structure of <b>30-CN</b> . ....	50
Figure 28. Nucleophilic fluorination reaction with KF in various solvents. ....	54
Figure 29. Bis-terminal hydroxyl polyether as multifunctional promoters in fluorination reactions: the polyether acts as the K <sup>+</sup> chelator and two OH groups reduce the basicity of fluoride anion (F <sup>-</sup> ) while activating the electrophile (E). ....	56
Figure 30. The two structures of R <sub>4</sub> PF, ionic and molecular form. ....	57
Figure 31. The synthesis of <b>32</b> . ....	57

	Page
Figure 32. The reaction of <b>34</b> with 1-bromooctane at 25 °C and its decomposition at 77 °C.....	58
Figure 33. The synthesis of <b>35</b> from Me <sub>4</sub> NOH and HF in water. ....	59
Figure 34. The synthesis of <b>36</b> from C <sub>6</sub> F <sub>6</sub> and TBACN.....	60
Figure 35. Fluoride relay from KF to anhydrous TBAF .....	61
Figure 36. Reactions sequence showing the use of [ <b>30</b> ] <sup>+</sup> for the capture of fluoride ions and their triggered release. ....	63
Figure 37. Changes of <sup>1</sup> H NMR spectra upon mixing <b>30-F</b> with TBASPh in d <sub>3</sub> -MeCN.....	65
Figure 38. <sup>19</sup> F NMR spectra of <b>30-F</b> <sup>-</sup> in d <sub>3</sub> -MeCN before and after addition of water.....	65
Figure 39. The optimized structure of borane <b>30</b> (hydrogen atoms omitted for clarity); Right: NBO contour plot showing the two lp(S)→p(B) donor-acceptor interactions in <b>30</b> . ....	67
Figure 40. Reaction of <b>30-F</b> <sup>-</sup> with p-tolylsulfonyl chloride in CD <sub>3</sub> CN.....	69
Figure 41. <sup>1</sup> H NMR spectra of reactions of entry 3, 4 and 5.....	73
Figure 42. Anion complexation by chelating cationic boranes and Lewis acidic properties of group 16 and 17 compounds.....	76
Figure 43. Synthesis and reactivity of the chalcogenium borane salts [ <b>37</b> ]OTf and [ <b>38</b> ]OTf. ....	79
Figure 44. Crystal structure of the neutral borane <b>37</b> .....	81
Figure 45. Crystal structure of the neutral borane <b>38</b> .....	82
Figure 46. NBO contour plots showing the lp(Ch)→p(B) donor-acceptor interactions in <b>37</b> (top left), <b>38</b> (top right), [ <b>37</b> ]OTf (bottom left) and [ <b>38</b> ]OTf (bottom right).....	84
Figure 47. Crystal structure of the neutral borane [ <b>37</b> ]OTf. ....	86



	Page
Figure 48. Crystal structure of the neutral borane <b>[38]</b> OTf. ....	87
Figure 49. Photophysical properties of the chalcogenium borane <b>[37]</b> <sup>+</sup> .....	91
Figure 50. Photophysical properties of the chalcogenium borane <b>[38]</b> <sup>+</sup> .....	92
Figure 51. Spectroscopic evidence for the formation and structure of <b>37-F</b> .....	95
Figure 52. Crystal structure of the fluoride adduct <b>37-F</b> .....	97
Figure 53. Crystal structure of the fluoride adduct <b>38-F</b> .....	98
Figure 54. Top: NBO contour plots showing the two lp(F)→σ*(Ch-C) donor-acceptor interactions involved in <b>37-F</b> and <b>38-F</b> . Bottom: AIM electron density maps in the B-F-Ch plane of <b>37-F</b> and <b>38-F</b> . ....	101
Figure 55. Synthesis of <b>37-CN</b> and <b>38-CN</b> in MeOH.....	102
Figure 56. Crystal structure of the fluoride adduct <b>37-CN</b> .....	104
Figure 57. Crystal structure of the fluoride adduct <b>38-CN</b> •CH <sub>2</sub> Cl <sub>2</sub> . ....	105
Figure 58. NBO NBO contour plots showing the donor-acceptor interactions involved in <b>37-CN</b> (left) and <b>38-CN</b> (right).....	108
Figure 59. DFT optimized structure of <b>37</b> .....	119
Figure 60. DFT optimized structure of <b>[37]</b> <sup>+</sup> .....	119
Figure 61. Computed structure of <b>37-F</b> .....	122
Figure 62. Computed structure of <b>37-CN</b> .....	122
Figure 63. DFT optimized structure of <b>38</b> .....	125
Figure 64. DFT optimized structure of <b>[38]</b> <sup>+</sup> .....	125
Figure 65. DFT optimized structure of <b>38-F</b> .....	128
Figure 66. DFT optimized structure of <b>38-CN</b> .....	128
Figure 67 Synthesis of the sulfonium diborane of <b>[40]</b> <sup>+</sup> .....	133

Figure 68. ORTEP drawing of $[\mathbf{40}]^+$ with thermal ellipsoid plots (50% probability). .....	135
Figure 69. Top: Experimental (chloroform) and calculated UV-vis spectra for $[\mathbf{40}]^+$ . Bottom: Views of LUMO and LUMO+1 of $[\mathbf{40}]^+$ and LUMO of $\mathbf{10}$ . (isovalue = 0.035). .....	137
Figure 70. Reactions of $[\mathbf{40}]^+$ with fluoride in chloroform. ....	137
Figure 71. ORTEP drawings of $\mathbf{40}\text{-}\mu_2\text{-F}$ with thermal ellipsoid plots (50% probability). .....	139
Figure 72. (a) Optimized structure of $\mathbf{40}\text{-}\mu_2\text{-F}$ . (b) The energy changes based on different B(2)-F(1) lengths in the optimization calculations of $\mathbf{40}\text{-}\mu_2\text{-F}$ . (c) AIM electron density maps with relevant bond paths and bond critical points of B(1)-F(1)-B(2) bond in $\mathbf{40}\text{-}\mu_2\text{-F}$ (left) and B(1)-N(1)-B(2) bond in $\mathbf{40}\text{-}\mu_2\text{-N}_3$ (right). .....	142
Figure 73. Left: Absorbance changes upon addition of $n\text{Bu}_4\text{NPh}_3\text{SiF}_2$ to a $\text{CHCl}_3$ solution of $[\mathbf{40}]^+$ (0.067 mM). Right: Binding isotherm monitored at $\lambda = 349$ nm ( $K_{\text{rel}}([\mathbf{40}]^+) > 10^5$ , $\epsilon = 10040$ for $[\mathbf{40}]\text{OTf}$ , $\epsilon = 3270$ for $\mathbf{40}\text{-}\mu_2\text{-F}$ ). .....	145
Figure 74. Competition reaction of $[\mathbf{40}]^+$ with $\mathbf{28}\text{-F}$ in $\text{CDCl}_3$ . .....	146
Figure 75. Reactions of $[\mathbf{40}]^+$ with other anions in chloroform .....	147
Figure 76. Left: Absorbance changes upon addition of $n\text{Bu}_4\text{NN}_3$ to a $\text{CHCl}_3$ solution of $[\mathbf{40}]^+$ (0.095 mM). Right: Binding isotherm monitored at $\lambda = 349$ nm ( $K > 10^7$ $\text{M}^{-1}$ , $\epsilon = 10040$ for $[\mathbf{40}]\text{OTf}$ , $\epsilon = 3100$ for $\mathbf{40}\text{-}\mu_2\text{-N}_3$ ). .....	148
Figure 77. ORTEP drawings of $\mathbf{40}\text{-}\mu_2\text{-N}_3$ with thermal ellipsoid plots (50% probability). .....	149
Figure 78. DFT optimized structure of $[\mathbf{40}]^+$ .....	159
Figure 79. DFT optimized structure of $\mathbf{40}\text{-}\mu_2\text{-F}$ .....	161
Figure 80. The reaction of $\text{B}(\text{C}_6\text{Cl}_5)_3$ with fluoride anion. .....	164

Figure 81. ORTEP drawing of $[\text{FB}(\text{C}_6\text{Cl}_5)_3]^-[\text{S}(\text{NMe}_2)_3]^+$ with thermal ellipsoid plots (50% probability).....	166
Figure 82. Left: Absorbance changes upon addition of TBAF ( $4.7 \times 10^{-3}$ M in $\text{CH}_2\text{Cl}_2$ ) to a $\text{CH}_2\text{Cl}_2$ solution of $\text{B}(\text{C}_6\text{Cl}_5)_3$ ( $4.84 \times 10^{-5}$ M). Right: Binding isotherm monitored at $\lambda = 331$ nm ( $\epsilon = 15000$ for $\text{B}(\text{C}_6\text{Cl}_5)_3$ , $\epsilon = 150$ for $[\text{FB}(\text{C}_6\text{Cl}_5)_3]^-$ ).....	169
Figure 83. The reaction of $\text{B}(\text{C}_6\text{Cl}_5)_3$ with DMAP.....	170
Figure 84. Left: Absorbance changes upon addition of DMAP (0.026 M in $\text{CH}_2\text{Cl}_2$ ) to a $\text{CH}_2\text{Cl}_2$ solution of $\text{B}(\text{C}_6\text{Cl}_5)_3$ ( $6.8 \times 10^{-5}$ M). Right: Binding isotherm monitored at $\lambda = 331$ nm ( $\epsilon = 15000$ for $\text{B}(\text{C}_6\text{Cl}_5)_3$ , $\epsilon = 0$ for $\text{B}(\text{C}_6\text{Cl}_5)_3$ -DMAP). .....	171
Figure 85. ORTEP drawing of $\text{B}(\text{C}_6\text{Cl}_5)_3$ -DMAP with thermal ellipsoid plots (50% probability).....	172
Figure 86. Synthesis of the sulfonium boranes $[\mathbf{47}]^+$ , $[\mathbf{48}]^+$ , $[\mathbf{49}]^+$ and $[\mathbf{50}]^+$ .....	180
Figure 87. ORTEP drawing of $[\mathbf{48}]^+$ .....	181
Figure 88. Spectrophotometric acid-base titration curve of $[\mathbf{48}]^+$ , or $[\mathbf{49}]^+$ and $[\mathbf{50}]^+$ in $\text{H}_2\text{O}/\text{MeOH}$ (95:5 vol.). .....	184
Figure 89. ORTEP drawing of $\mathbf{48}$ -F.....	186
Figure 90. ORTEP drawing of $\mathbf{50}$ -F.....	187
Figure 91. Top: Experimental data and calculated 1:1 binding isotherm with $K = 8.5(\pm 0.5) \text{ M}^{-1}$ for $[\mathbf{49}]^+$ (left) and $K = 33(\pm 1) \text{ M}^{-1}$ for $[\mathbf{50}]^+$ (right) monitored by UV-vis spectroscopy. Bottom: Fluorescence quenching titration data and calculated 1:1 binding isotherm with $K = 60(\pm 5) \text{ M}^{-1}$ for $[\mathbf{47}]^+$ (left) and $K = 1670(\pm 50) \text{ M}^{-1}$ for $[\mathbf{48}]^+$ (right). .....	192
Figure 92. Left: Absorbance change of a solution of $[\mathbf{48}]^+$ after successive additions of fluoride anions in $\text{H}_2\text{O}/\text{MeOH}$ (95:5, vol.; 9.5 mM pyridine buffer, pH = 4.6). Right: Experimental data and calculated 1:1 binding isotherm with $K = 2.65(\pm 0.2) \times 10^4 \text{ M}^{-1}$ for $[\mathbf{48}]^+$ using $\epsilon([\mathbf{48}]^+) = 9200 \text{ M}^{-1} \text{ cm}^{-1}$ , $\epsilon(\mathbf{48}\text{-F}) = 0 \text{ M}^{-1} \text{ cm}^{-1}$ .....	194
Figure 93. $^1\text{H}$ NMR and $^{13}\text{C}$ NMR spectra of $[\mathbf{49}]\text{OTf}$ . .....	199

	Page
Figure 94. $^1\text{H}$ NMR and $^{13}\text{C}$ NMR spectra of <b>49-F</b> .....	202
Figure 95. $^1\text{H}$ NMR and $^{13}\text{C}$ NMR spectra of [ <b>50</b> ]OTf.....	203
Figure 96. $^1\text{H}$ NMR and $^{13}\text{C}$ NMR spectra of <b>50-F</b> .....	204
Figure 97. DFT optimized structure of <b>47-F</b> .....	205
Figure 98. DFT optimized structure of <b>48-F</b> .....	205

## LIST OF TABLES

	Page
Table 1. Crystal data, data collections, and structure refinement for <b>[30]OTf</b> .....	22
Table 2. Crystal data, data collections, and structure refinement for <b>30-F</b> . ....	27
Table 3. Crystal data, data collections, and structure refinement for <b>30-CN</b> .....	33
Table 4. Absorbance of a solution of <b>[30]<sup>+</sup></b> after successive additions of fluoride anions in THF/H <sub>2</sub> O, 9:1, vol. ....	45
Table 5. Absorbance of a solution of <b>[30]<sup>+</sup></b> after successive additions of cyanide anions in THF.....	46
Table 6. Atom coordinates for the optimized structure of <b>[30]<sup>+</sup></b> .....	48
Table 7. Atom coordinates for the optimized structure of <b>30-F</b> .....	49
Table 8. Atom coordinates for the optimized structure of <b>30-CN</b> .....	51
Table 9. Solubility of KF in crown ether solution at 25 °C.....	54
Table 10. Nucleophilic fluorination reaction with KF under different conditions.....	55
Table 11. Nucleophilic reactions of <b>36</b> with various organic substrates.....	61
Table 12. Atom coordinates for the optimized structure of <b>30</b> . ....	68
Table 13. Fluorination reaction results.....	71
Table 14. Crystal data, data collections, and structure refinements for <b>37</b> and <b>38</b> .....	83
Table 15. Crystal data, data collections, and structure refinements for <b>[37]OTf</b> and <b>[38]OTf</b> .....	88
Table 16. Crystal data, data collections, and structure refinements for <b>37-F</b> and <b>38-F</b> .....	99
Table 17. Crystal data, data collections, and structure refinements of <b>37-CN</b> and <b>38-CN</b> .....	106

	Page
Table 18. Partial TD-DFT calculation output showing the nature of the low energy excitations for $[37]^+$ and $[38]^+$ .....	118
Table 19. Atom coordinates for the optimized structure of <b>37</b> .....	120
Table 20. Atom coordinates for the optimized structure $[37]^+$ .....	121
Table 21. Atom coordinates for the optimized structure of <b>37-F</b> .....	123
Table 22. Atom coordinates for the optimized structure of <b>37-CN</b> .....	124
Table 23. Atom coordinates for the optimized structure of <b>38</b> .....	126
Table 24. Atom coordinates for the optimized structure of $[38]^+$ : .....	127
Table 25. Atom coordinates for the optimized structure of <b>38-F</b> .....	129
Table 26. Atom coordinates for the optimized structure of <b>38-CN</b> .....	130
Table 27. Crystal data, data collections, and structure refinement for $[40]OTf \cdot CH_2Cl_2$ . .....	136
Table 28. Crystal data, data collections, and structure refinement for <b>40-<math>\mu_2</math>-F</b> . .....	140
Table 29. Crystal data, data collections, and structure refinement for <b>40-<math>\mu_2</math>-<math>N_3 \cdot (CH_3)_2CO</math></b> .....	150
Table 30. Atom coordinates for the optimized structure of $[40]^+$ .....	159
Table 31. Atom coordinates for the optimized structure of <b>40-<math>\mu_2</math>-F</b> .....	161
Table 32. Crystal data, data collections, and structure refinement for $[FB(C_6Cl_5)_3]^- [S(NMe_2)_3]^+ \cdot 1.5THF$ . .....	167
Table 33. Crystal data, data collections, and structure refinement for $B(C_6Cl_5)_3$ -DMAP. .....	173
Table 34. The binding constants of $B(C_6Cl_5)_3$ with different Lewis bases in dichloromethane and/or THF. .....	174
Table 35. Crystal data, data collections, and structure refinement for $[48]OTf$ . .....	182

	Page
Table 36. Crystal data, data collections, and structure refinements of <b>48-F</b> and <b>50-F</b> ...	188
Table 37. Atom coordinates for the optimized structure of <b>47-F</b> .....	206
Table 38. Atom coordinates for the optimized structure of <b>48-F</b> .....	207

## CHAPTER I

### INTRODUCTION AND BACKGROUND

#### 1.1 Introduction

The field of anion recognition has become a very active research area fueled by the role that these species play in biological systems and in the environment. One of these anions is the cyanide anion. It is highly toxic because of its ability to inhibit cell respiration by deactivating the cytochrome-c oxidase enzyme.<sup>1</sup> Unfortunately, cyanide is widely available in both research and industrial settings such that its unintentional release or its use for harmful purposes have become unavoidable.<sup>2</sup> The azide anion ( $\text{N}_3^-$ ) possess an analogous biological profile and is also highly toxic. Again, as for cyanide, the azide anion is found in many salts used in a number of widespread applications including explosives for car airbags. Another important nucleophilic anion is fluoride anion. This anion is often added to drinking water and toothpaste because of its beneficial effects in dental health. It is also administered in the treatment of osteoporosis.<sup>3</sup> High doses of this anion are however dangerous because they can trigger conditions such as skeletal fluorosis.<sup>4</sup> Thus, as for cyanide and azide, the development of analytical methods for the detection of these, especially in water, is a worthwhile objective. Water compatible receptors that operate in low concentration ranges must be

---

This dissertation follows the style and format of the *Journal of the American Chemical Society*.



designed to overcome the high hydration enthalpy of the fluoride ion ( $\Delta H^\circ = -504$  KJ/mol) or the competitive protonation of the anion as in the case of cyanide ( $pK_a(\text{HCN}) = 9.3$ ).

In turn, molecular receptors that can selectively bind these specific anions, especially in protic media, has become a Holy Grail of anion recognition. The approach chosen in the design of such receptors depends largely on the nature of the anionic analyte. While organic receptors that feature hydrogen-bond donor group as recognition sites are well suited for large anions, Lewis acidic receptors based on main group elements or transition metals have proven competent for the recognition of small nucleophilic anions.

### 1.2 Lewis acidity and anion complexation by triarylboranes

Among the Lewis acidic receptors, triarylboranes are a typical class that binds small anions efficiently in organic solvents. For example, simple triarylboranes, such as trimesitylborane **1** and tri(9-anthryl)borane **2**, capture fluoride in organic solvents with binding constants in the  $10^5$ - $10^6$   $\text{M}^{-1}$  range (Figure 1).<sup>5</sup> This simple reaction provides the basis for the construction of anion receptors.

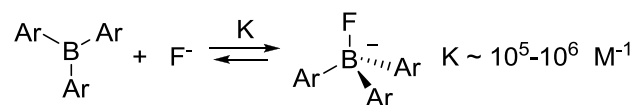


**Figure 1.** The fluoride capture by triarylboranes.

The anion binding process by triarylboranes can be monitored by UV-vis spectroscopy and/or fluorescence spectroscopy. Triarylboranes bear a low-energy absorbance band in the UV-vis spectrum caused by the presence of a low lying LUMO that bears a large contribution from the boron p-orbital. Anion binding to the boron center disrupts the LUMO, thus leading to the quenching of the low-energy absorbance band in the UV-vis spectrum (Figure 2). For instance, trimesitylborane **1** shows a low-energy absorption band at  $\lambda_{\max} = 331 \text{ nm}$  ( $\epsilon = 15500$ ) which can be quenched upon the addition of fluoride anions.

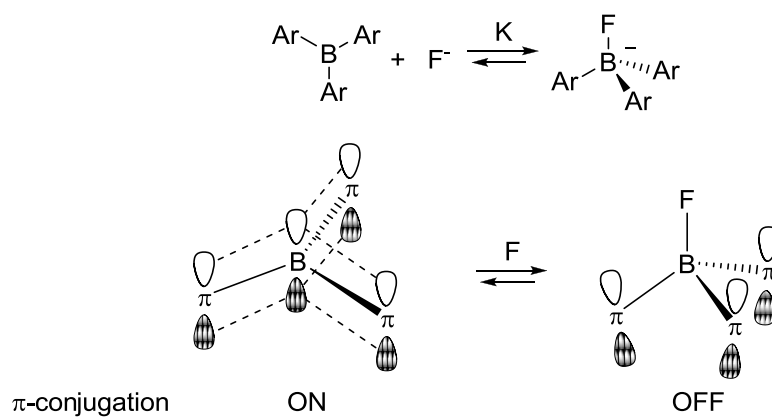


**Figure 2.** Top: the fluoride binding by triarylborane; Bottom: schematic representation of the switching of  $\pi$ -conjugation in the LUMO of the triarylboranes.

The Lewis acidity of triarylboranes can be easily adjusted by tuning the electronic properties and/or the steric bulk of the aryl substituents. Pentafluorophenylboranes which are strong Lewis acids due to the electron-withdrawing properties of the fluorine atoms, have been widely used in catalysis, small molecule

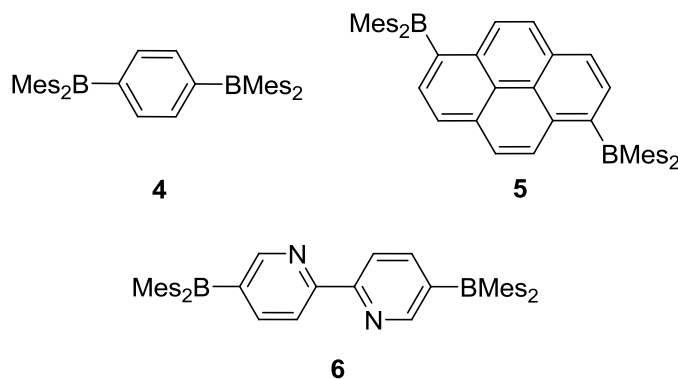
activation, and synthesis.<sup>6-15</sup> Decoration of peripheral cationic groups into triarylboranes is also a useful method to increase their Lewis acidity, a point that will be discussed later in this chapter.

The steric bulk of aryl substituents is another important tool which can be used to control the Lewis acidity of triarylboranes. Indeed, since anion binding is accompanied by pyramidalization of the boron center, a net increase in steric repulsion will be observed when a large aryl group is present. One simple example is that  $\text{BMes}_2\text{Ph}$  (**3**). This compound has a higher binding constant for fluoride ( $5.0 \times 10^6 \text{ M}^{-1}$ ) than  $\text{BMes}_3$  ( $3.3 \times 10^5 \text{ M}^{-1}$ ), which may be assigned to the lower steric demand of the phenyl group in **3**.<sup>16</sup> On the other hand, bulky groups such as the mesityl group play an important passivation role and impart water stability to triaryl boranes.

### 1.3 Anion complexation by diboranes

Diboranes discussed in this chapter consist of two species: one features well-separated boryl moieties while the other features juxtaposed boryl moieties sufficiently close to chelate small anions. Among the former species,  $\pi$ -conjugated diboranes are attracting a great deal of attention, because they are more electrophilic as well as more Lewis acidic than mononuclear triarylboranes. For instance, 1,4-bis(dimesitylboryl)benzene (**4**), as shown by Kaim, has a significantly more positive reduction potential than the corresponding mononuclear triarylboranes **1** under same conditions.<sup>17</sup> Also, diboranes **5** and **6** display a higher fluorophilicity than mononuclear triarylboranes when binding the first fluoride anion.<sup>18</sup> The increased electrophilicity and

Lewis acidity of these compounds can be attributed to a lowering of the LUMO which bears contributions from both inherently unsaturated boron centers.



Diboranes with juxtaposed boryl moieties sufficiently close to chelate small anions<sup>19-24</sup> have been used in the domains of anion complexation,<sup>25-26</sup> organometallic catalysis,<sup>27-30</sup> as well as small molecule activation.<sup>31-32</sup> In what might be the first example of a chelating diborane, it was demonstrated that the simple derivative **7** chelates methoxide anions effectively (Figure 3).<sup>33</sup> Later, several bidentate diboranes have been successfully synthesized and investigated. The *peri*-substituted naphthalene-based diborane **8** was the first example of a compound shown to complex chloride by forming a B-Cl-B bridge bond when treated with inorganic and organic chloride donors.<sup>34</sup> Diborane **9**, of similar structure to **8**, chelates hydride, fluoride as well as hydroxide anions to form the corresponding stable adducts.<sup>35-36</sup> A related behavior is observed for the naphthalene-based diborane **10** which shows a much higher fluoride anion affinity than mononuclear borane such as BMe<sub>3</sub>.<sup>37</sup> Diborane **11** can form the

hydride adduct by chelating hydride ion when treated with  $\text{H}_2$  (1.5 bar) at  $80\text{ }^\circ\text{C}$  in the presence of 2,2,6,6-tetramethylpiperidine (TMP).<sup>31</sup> The formation of a B-X-B bridging bond in these adducts is responsible for the high Lewis acidity of these diboranes.

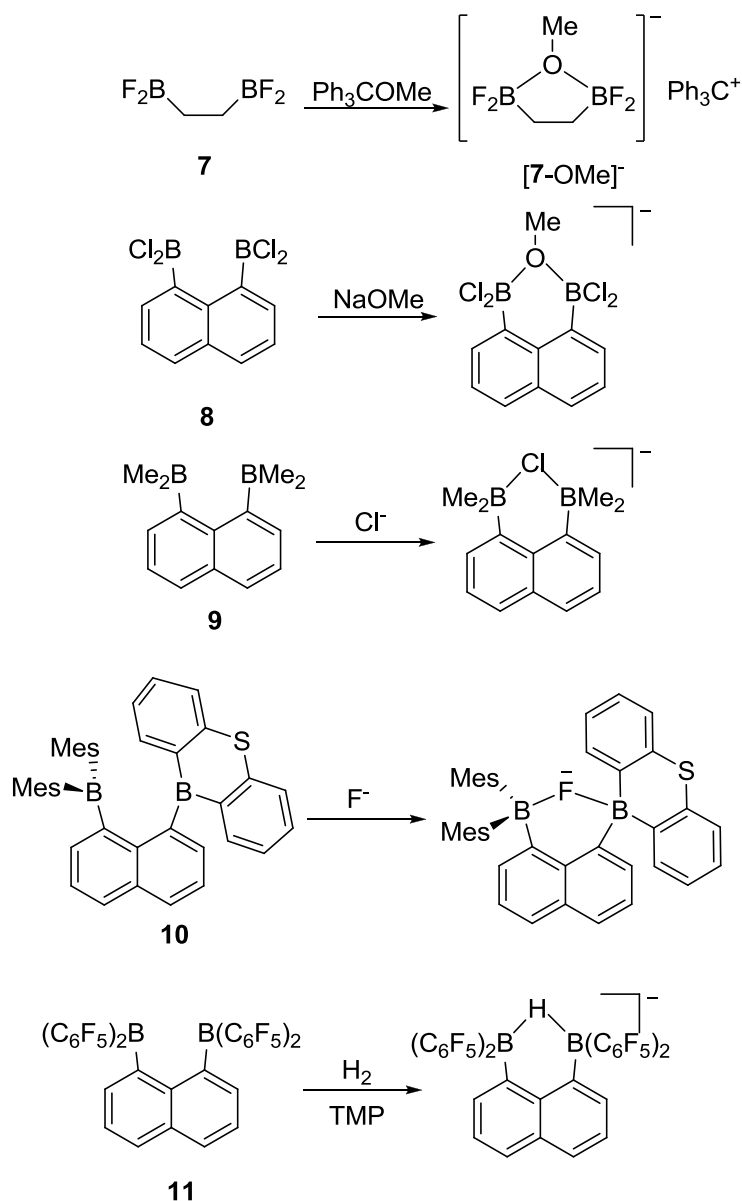


**Figure 3.** The anion chelation by diboranes to form B-X-B bridging bond.

Ortho-phenylene diboranes are also showing superior Lewis acidity for complexation of neutral electron-rich species and anions. A prototypical example of such diboranes is the 1,2-bis(bis(pentafluorophenyl)boryl)tetrafluorobenzene **12**, which chelates small anions efficiently including  $\text{OH}^-$ ,  $\text{F}^-$ ,  $\text{OMe}^-$ ,  $\text{OC}_6\text{F}_5^-$ ,  $\text{NMe}_2^-$  and  $\text{N}_3^-$  (Figure 4).<sup>27</sup>

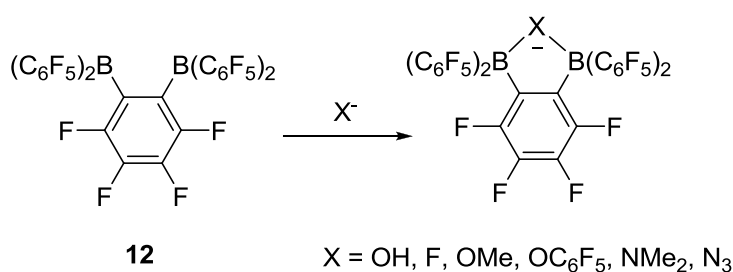


**Figure 4.** The anion chelation process by **12**.

Bidentate diboranes based on metallocene units have also been investigated as anion chelators. Reaction of compound **13** with  $\text{Cu}(\text{OH})_2$  affords a chelate complex with the formation of a B-O-B bridge along with oxidation of the cobalt center (Figure 5).<sup>38-39</sup> However, treatment of **13** with  $\text{C}_2\text{Cl}_6$  does not afford a chelate complex but instead leads to a zwitterion with only one tetrahedral chloride-bound boron center. In solution the chloride is highly fluxional as confirmed by detection of a single resonance in the  $^{11}\text{B}$  NMR spectrum as well as the equivalence of the  $\text{C}_5\text{H}_4\text{BPr}_2^i$   $^1\text{H}$  and  $^{13}\text{C}$  NMR resonances.

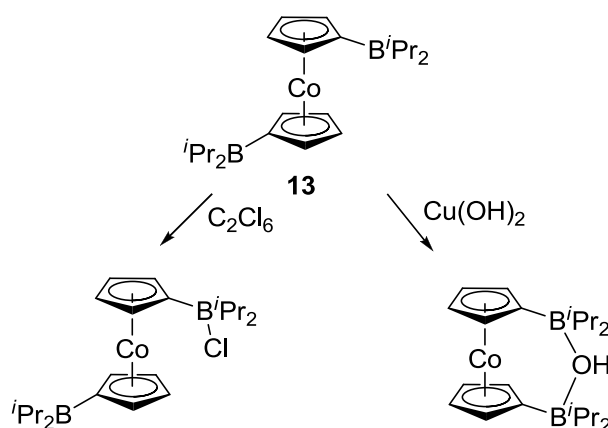


**Figure 5.** The reactions of **13** with  $\text{Cu}(\text{OH})_2$  and  $\text{C}_2\text{Cl}_6$ .

#### 1.4 Lewis acidity and anion complexation by cationic boranes

##### 1.4.1 Effects induced by remote cationic functionality

The incorporation of cationic functionality into triarylboranes is an approach that maybe better suited to applications of anion sensing in aqueous solutions because the cationic moiety can increase the Lewis acidity as well as the solubility of triarylboranes in aqueous environment. This approach was pioneered 16 years ago by Shinkai who showed that oxidation of  $\text{Fc-B}(\text{OH})_2$  ( $\text{Fc}$  = ferrocenyl) into the ferrocenium derivative  $[\text{Fc-B}(\text{OH})_2]^+$  leads to a significant increase of the Lewis acidity and fluoride ion affinity of the boron center.<sup>40</sup> As stated by Shinkai, his pioneering studies showed that the “oxidized species of ferroceneboronic acid has a stronger interaction with fluoride ions compared to the neutral boronic acid”. Inspired by this work, several groups have been implementing this strategy with triarylboranes.

The Gabbai group has observed that the presence of a somewhat distant and diffuse cationic group in organoboranes can have a marked effect on the anion affinity of

the boron center via favorable Coulombic effects. This phenomenon is appropriately illustrated by the behavior of the three cationic boranes **[14]**<sup>+</sup>, **[15]**<sup>+</sup>, and **[16]**<sup>+</sup> which have been synthesized by simple electrophilic methylation procedure using MeOTf in the case of **[14]**<sup>+</sup> or **[15]**<sup>+</sup> or by reaction of the pyridyl precursor with (bpy)<sub>2</sub>RuCl<sub>2</sub> and AgOTf in the case of **[16]**<sup>+</sup> (Figure 6).<sup>41-42</sup> A feature common to these three species is the distance and relative diffuseness of the cationic functionality. In the case of **[14]**<sup>+</sup> or **[15]**<sup>+</sup>, the positive charge is delocalized over the entire pyridinium ring, a factor that may further contribute to a lessening of Coulombic effects. A similar argument could be advanced in the case of **[16]**<sup>+</sup> where the charge is delocalized over the entire tris-chelate ruthenium complex. Despite the diffuseness of these cationic groups, these compounds feature a distinctly higher fluoride and cyanide affinity than the neutral boranes of similar bulks. Unlike neutral boranes of comparable bulk, these three compounds react quantitatively with fluoride and cyanide in organic solvents but show no affinity for other anions such as Cl<sup>-</sup>, Br<sup>-</sup>, and I<sup>-</sup>. Another distinguishing quality of these compounds pertains to their ability to capture fluoride ions under biphasic condition. These observations show that the presence of a distant and diffuse cationic group can still favorably impact the Lewis acidic properties.



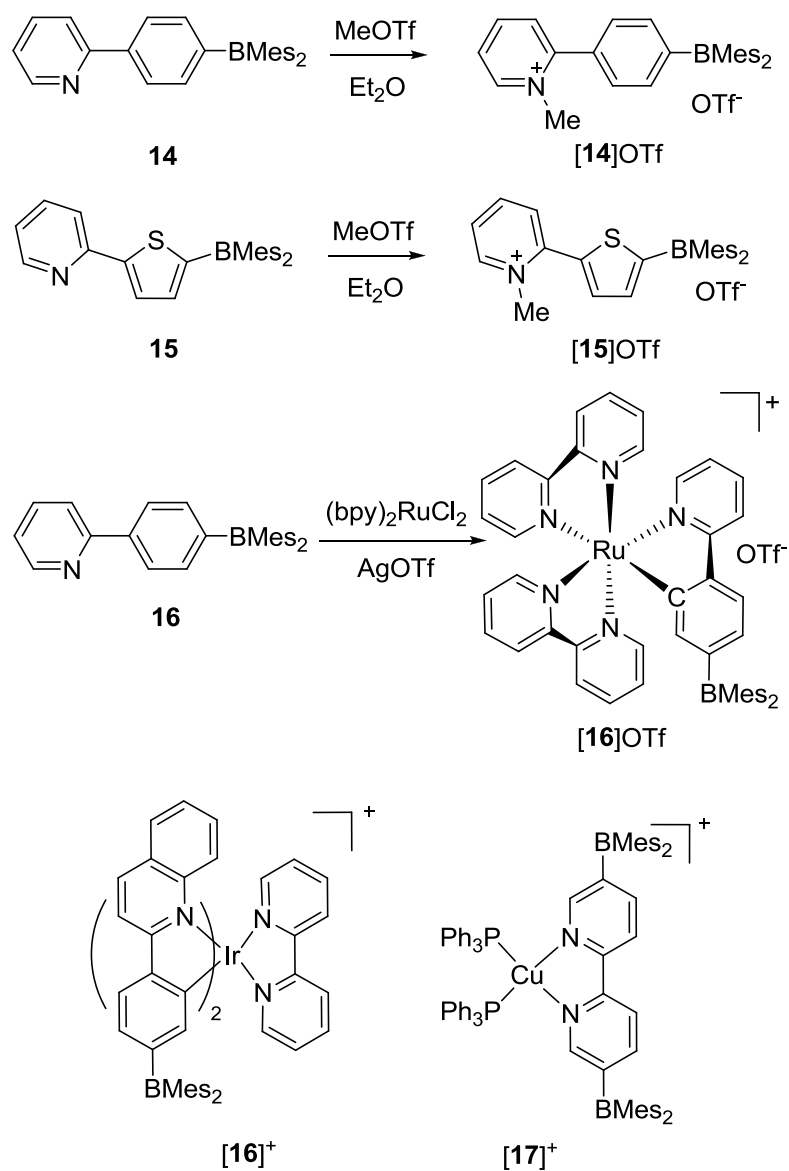


**Figure 6.** The cationic boranes of **[14]<sup>+</sup>**, **[15]<sup>+</sup>**, **[16]<sup>+</sup>**, **[17]<sup>+</sup>** and **[18]<sup>+</sup>**.

Similar results have also been obtained by other groups. For example, the Ir(III) derivative **[17]<sup>+</sup>**, isolated as PF<sub>6</sub><sup>-</sup> salt, captures two equivalents of fluoride ions in acetonitrile (CH<sub>3</sub>CN) (Figure 6).<sup>43</sup> The binding constant K<sub>1</sub> of **[17]<sup>+</sup>** significantly exceeds that of the free ligand 2-(4-dimesitylborylphenyl)quinoline. The Cu(I)

derivative **[18]**<sup>+</sup>, also shows elevated fluoride affinity compared to the corresponding free ligand 5,5'-bis(dimesitylboryl)-2,2'-bipyridine (Figure 6).<sup>44</sup>

Another compound that has been investigated is the cationic borane **[19]**<sup>+</sup>, which could be obtained by reaction of the tetrakis(THF)lithium salt of dimesityl-1,8-naphthalenediylborate with [Me<sub>2</sub>NCH<sub>2</sub>]I and subsequent methylation of the resulting borane **19** with MeOTf (Figure 7).<sup>45</sup> This cationic borane **[19]**<sup>+</sup>, containing a remote but localized cationic functionality, shows a much higher affinity towards fluoride and cyanide than the neutral borane **19** in organic solvents. More interestingly, **[19]**<sup>+</sup> could capture fluoride and cyanide ions under biphasic conditions (H<sub>2</sub>O/CHCl<sub>3</sub>). Surprisingly, the fluoride binding constant ( $K > 10^8 \text{ M}^{-1}$ ) of **[19]**<sup>+</sup> exceeds the cyanide binding constant ( $8.0 (\pm 0.5) \times 10^5 \text{ M}^{-1}$ ) in THF, even though cyanide ( $\text{p}K_{\text{a}} = 9.3$ ) is more basic than fluoride ( $\text{p}K_{\text{a}} = 3.18$ ).<sup>46</sup> This selectivity is attributed to the high steric encumbrance of the anion binding pocket boron of **[19]**<sup>+</sup> and the relatively larger size of the cyanide ion. The BF---HC hydrogen bond in **19-F**, confirmed by structural, NMR spectroscopic, and computational analysis, could also contribute to the higher stability constant of **19-F**. These results indicate that the incorporation of a distant cationic moiety can remarkably increase the anion affinity via Coulombic effects. These effects are however limited as none of these compounds show an affinity for any anions including fluoride and cyanide in aqueous solutions.

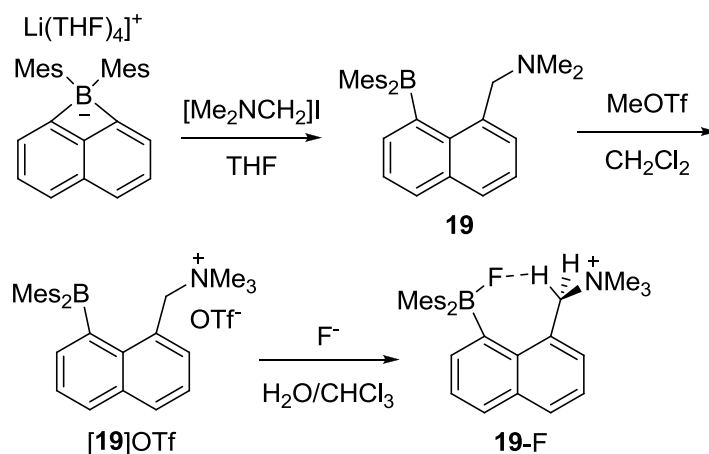
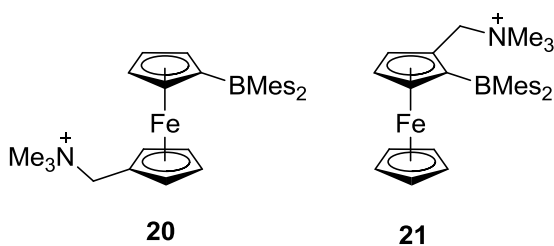


**Figure 7.** The synthesis of **[19]<sup>+</sup>** and its reaction with fluoride under biphasic conditions.

Similar examples in use of ammonium functionality contains the ammonium ferrocenyl boranes **[20]<sup>+</sup>** and **[21]<sup>+</sup>**. The cationic borane **[21]<sup>+</sup>** has a much higher fluoride affinity than **[20]<sup>+</sup>** due the presence of  $\text{BF} \cdots \text{HC}$  hydrogen bonding interaction in the fluoride adduct **21-F**.



In order to address the significance of the remote cationic functionality as well as to recognize fluoride in aqueous solutions, the phosphonium borane **[22]<sup>+</sup>** has been synthesized by simple methylation of the neutral borane **22** (Figure 8).<sup>47</sup> The fluoride titration of **[22]<sup>+</sup>** in  $\text{H}_2\text{O}/\text{MeOH}$  (9:1, v/v) monitored by UV-vis spectroscopy affords a

binding constant of  $10^3 \text{ M}^{-1}$ . This compound is also highly selective since its absorption spectrum shows negligible changes in the presence of  $\text{Cl}^-$ ,  $\text{Br}^-$ ,  $\text{NO}_3^-$  and  $\text{I}^-$ . The enhanced fluoride affinity of  $[\mathbf{22}]^+$  can be correlated to the favorable Coulombic effects introduced by the phosphonium moiety.

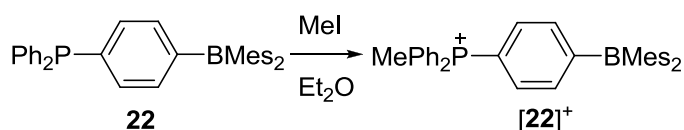
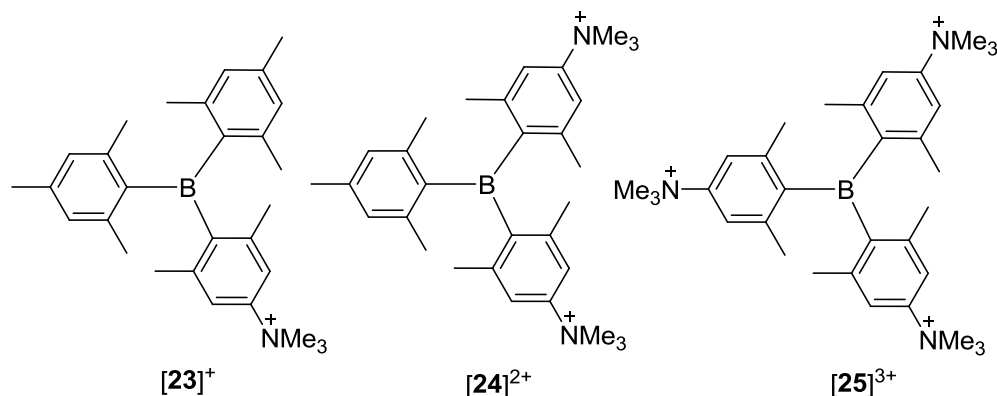


**Figure 8.** The synthesis of  $[\mathbf{22}]^+$ .

In an extension of these studies, the effects imparted by the introduction of multiple remote cationic groups have been investigated. Compounds  $[\mathbf{23}]^+$ ,  $[\mathbf{24}]^{2+}$  and  $[\mathbf{25}]^{3+}$  have been synthesized as their triflate salts. The reduction potential of  $\text{Mes}_3\text{B}$ ,  $[\mathbf{23}]^+$ ,  $[\mathbf{24}]^{2+}$  and  $[\mathbf{25}]^{3+}$  have been measured by cyclic voltammetry in  $\text{CH}_3\text{CN}$ . A comparison of the reduction peak potentials of these four boranes shows that substitution of a Mes group by a  $[4-(\text{Me}_3\text{N})-2,6-\text{Me}_2-\text{C}_6\text{H}_2]^+$  ( $\text{Ar}^{\text{N}^+}$ ) group leads to a linear increase of the reduction potential, indicating that  $[\mathbf{25}]^{3+}$  is the most electron-deficient compound in the series. Following these results, these boranes have been used for the complexation of the small anions in water. Among the three cationic boranes, only  $[\mathbf{25}]^{3+}$  could capture cyanide in pure water, in accordance with its higher reduction potential. In addition,  $[\mathbf{25}]^{3+}$  shows a high selectivity for cyanide since there is negligible change of the absorbance of the boron centered chromophore in the presence of  $\text{F}^-$ ,  $\text{Cl}^-$ ,  $\text{Br}^-$ ,  $\text{I}^-$ ,  $\text{OAc}^-$ ,  $\text{NO}_3^-$ ,  $\text{H}_2\text{PO}_4^-$ , and  $\text{HSO}_4^-$ . These results suggest that Coulombic effects are

additive, thus indicating that the Lewis acidity of triarylboranes can be enhanced by the introduction of multiple cationic groups.



#### 1.4.2 Effects induced by proximal cationic functionality

In order to address the way in which the proximity of the boron and cationic moiety affects the anion binding properties of the compounds, two ammonium boranes **[26]<sup>+</sup>** and **[27]<sup>+</sup>** were synthesized and their anion affinity has been evaluated (Figure 9).<sup>48</sup> Both compounds react with fluoride and cyanide ions in organic solvents, such as  $\text{CHCl}_3$ , leading to zwitterionic adducts which have been fully characterized. Following this studies in organic media, the complexation of small anions by **[26]<sup>+</sup>** and **[27]<sup>+</sup>** has been studied extensively in aqueous solutions. These two boranes show different anion affinity in  $\text{H}_2\text{O}/\text{DMSO}$  (6:4, v/v). Cation **[26]<sup>+</sup>** only complexes cyanide ions with an elevated binding constant ( $K(\text{CN}^-) = 3.9(\pm 0.1) \times 10^8 \text{ M}^{-1}$ ), while **[27]<sup>+</sup>** only binds fluoride ions ( $K(\text{F}^-) = 910 (\pm 50) \text{ M}^{-1}$ ). The anion binding selectivity of these cationic boranes most likely results from the interplay of both steric and electronic effects.

Because of the proximity of the ammonium functionality, the boron center of  $[27]^+$  is more Lewis acidic than  $[26]^+$ . However, in this case, the increased steric crowding of the boron center prevents coordination of the larger cyanide anion. Since cyanide is more basic than fluoride anion, it can be recognized by  $[26]^+$  with lower Lewis acidity and less steric crowding. The effects introduced by the proximal cationic functionality have been confirmed by Density Functional Theory (DFT) calculations.  $[27]^+$  features a lower LUMO (-2.02 eV) than  $[26]^+$  (-2.12 eV) thus corroborating the increased fluoride affinity of the ortho isomer  $[27]^+$ .

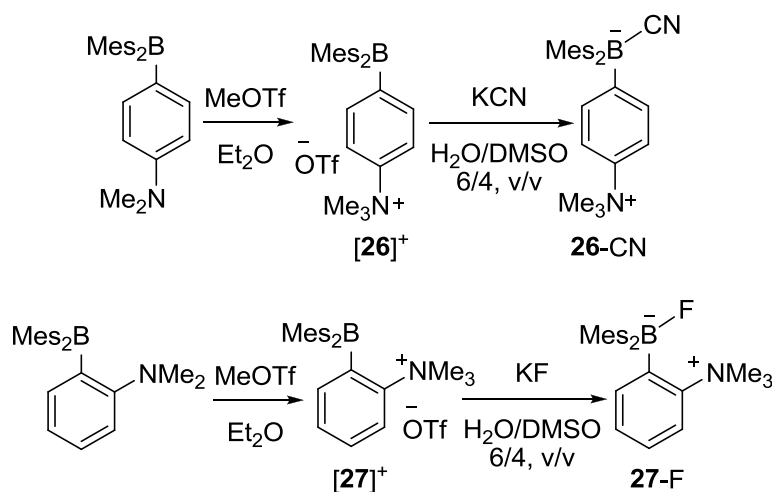


**Figure 9.** The synthesis of  $[26]^+$ ,  $[27]^+$  and their anion binding reactions.

In this vein, the phosphonium borane  $[28]^+$ , the ortho isomer of  $[22]^+$ , has been synthesized using the same method as for  $[22]^+$ .<sup>25</sup> The fluoride binding properties of  $[28]^+$  has been evaluated and compared to those of its para isomer  $[22]^+$ . Mixing the equimolar amounts of  $[28]^+$  and 22-F in CDCl<sub>3</sub> leads to a quantitative formation of 28-F

and  $[\mathbf{22}]^+$ , indicating that  $[\mathbf{28}]^+$  has a much higher fluoride affinity than  $[\mathbf{22}]^+$  (Figure 10). The fluoride titration in MeOH affords that the binding constant of  $[\mathbf{28}]^+$  exceeds the measurable range ( $K > 10^6 \text{ M}^{-1}$ ), which is at least four orders of magnitude higher than that of  $[\mathbf{22}]^+$  ( $K = 400 \pm 50 \text{ M}^{-1}$ ). The higher fluoride affinity of  $[\mathbf{28}]^+$  arises from the presence of a bonding B–F→P donor-acceptor interaction due to the Lewis acidity of the phosphonium moiety. The B–F→P donor-acceptor interaction has been confirmed by structural and computational analyses. The crystal structure of **28**-F shows that the distance between F and P atoms (2.66 Å) is shorter than the sum of the van der Waals radii (ca. 3.45 Å), and the angle of F-P-C<sub>Ph</sub> is 176.36° indicating the appropriate orientation of the orbitals involved in the B–F→P donor-acceptor interaction (Figure 11). A natural bond orbital (NBO) analysis identifies the lp(F)→σ\*(P-C) interaction. Energetically, this interaction contributes 5.0 kcal/mol to the stability of the complex **28**-F ( $E_{\text{del}} = 5.0 \text{ kcal/mol}$ ). An atom-in-molecule (AIM) analysis, probing the covalent component of the F-P interaction, shows a bond path connecting the P and F atoms with an electron density of 0.0205 e bohr<sup>-3</sup> at the bond critical point (BCP) (Figure 11). Cation  $[\mathbf{28}]^+$  can also capture azide from aqueous solutions into less polar solvents. For instance,  $[\mathbf{28}]^+$  transports azide ions from water into chloroform under D<sub>2</sub>O/CDCl<sub>3</sub> biphasic conditions by forming the azide adduct **28**-N<sub>3</sub>. Thus,  $[\mathbf{28}]^+$  can be regarded as a cationic bidentate Lewis acid with the boryl and phosphonium moieties as Lewis acidic centers.

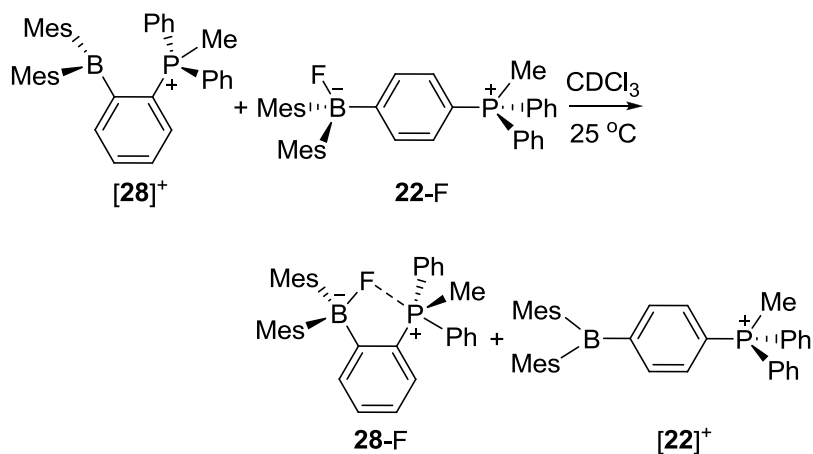


**Figure 10.** The competition reaction of  $[\mathbf{28}]^+$  and  $\mathbf{22-F}$  in  $\text{CDCl}_3$ .

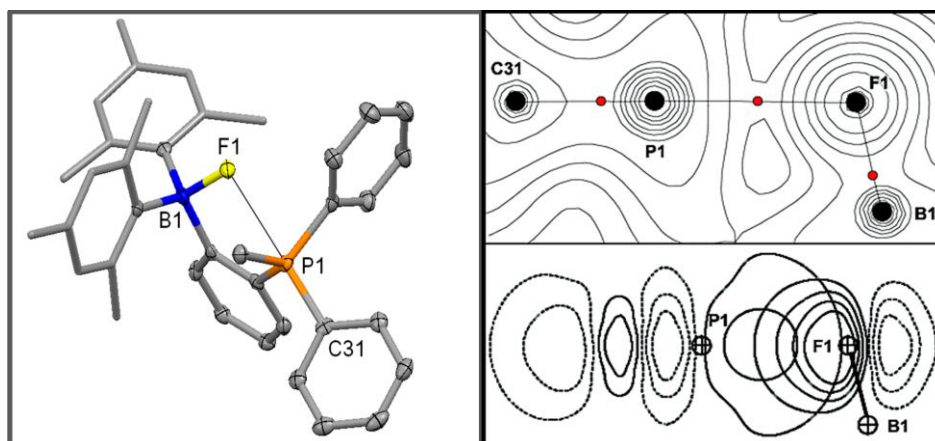


**Figure 11.** Crystal structure of  $\mathbf{28-F}$  (left) and the AIM and NBO analyses of the B-F $\rightarrow$ P donor-acceptor interaction (right).



CHAPTER II  
SYNTHESIS, CHARACTERIZATION AND ANION AFFINITY OF SULFONIUM  
BORANE\*

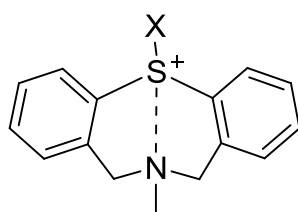
## 2.1 Introduction

As previously shown by Gabbai group and others, triarylboranes decorated with ammonium/phosponium groups can complex  $F^-$  ions under aqueous conditions. Among these anion receptors, the phosphonium borane [1-Mes<sub>2</sub>B-2-MePh<sub>2</sub>P-(C<sub>6</sub>H<sub>4</sub>)]<sup>+</sup> shows remarkably stronger fluoride affinity than its para analog, [1-Mes<sub>2</sub>B-4-MePh<sub>2</sub>P-(C<sub>6</sub>H<sub>4</sub>)]<sup>+</sup>.<sup>49</sup> The high fluorophilicity of the former compound arises from Coulombic effects which are complemented by the formation of a B-F→P interaction involving low lying  $\sigma^*$  orbitals of the P-C bond. Sulfonium ions, which also have low lying  $\sigma^*$  orbitals, are inherently Lewis acidic and can interact with electron-rich substrates to form donor-acceptor complexes. For example, the donor-acceptor interaction exists in the compounds **29a-e** from the lone pair of the amino group to the  $\sigma^*$  orbital of S-X, which is supported by the short distance between the N and S atoms in the crystal structure. Although this phenomenon has been documented,<sup>50-55</sup> efforts to use sulfonium ions as a binding site in Lewis acidic hosts have been only reported by the Gabbai group.

---

\*Reprinted in part permission from, "Sulfonium boranes for the selective capture of cyanide ions in water"; Kim, Y.; Zhao, H.; Gabbai, F. P. *Angew. Chem., Int. Ed.* **2009**, *48*, 4957. Copyright 2009 by John Wiley & Sons, Inc; and "Nucleophilic Fluorination Reactions Starting from Aqueous Fluoride Ion Solutions"; Zhao, H.; Gabbai, F. P. *Org. Lett.* **2011**, 1444. Copyright 2011 American Chemical Society.

As part of our fundamental interest in the chemistry of polydentate Lewis acidic boranes, probing the synthesis and properties of anion receptors containing accessible sulfonium ions appeared a worthwhile endeavor. As an added motivation for these studies, we anticipated that the anion binding properties of sulfonium boranes would also benefit from attractive Coulombic effects similar to those occurring in other cationic boron-based anion receptors.



X = Me, Et, MeO, EtO, Cl

**29a-e**

## 2.2 Synthesis and characterization of sulfonium borane

To test the validity of the aforementioned concepts, we synthesized the cationic borane **[30]<sup>+</sup>** which feature adjacent sulfonium and boryl moieties connected by a 1,8-naphthalenediyl. The salt **[30]OTf** was obtained by reaction of the tetrakis(THF)lithium salt of dimesityl-1,8-naphthalenediylborate with MeSSMe followed by methylation of the resulting sulfide MeOTf (Figure 12).<sup>56</sup> **[30]OTf** has been isolated in an analytically pure form and characterized by multinuclear NMR spectroscopy, UV-vis spectroscopy and single crystal X-ray diffraction. The <sup>1</sup>H NMR spectrum of this compound exhibits six distinct resonances that correspond to the aromatic CH groups of the

unsymmetrically substituted naphthalene backbone. In addition, six distinct methyl groups are observed for the mesityl substituents indicating that  $[30]^+$  has highly congested structure.<sup>45</sup> The detection of a  $^{11}\text{B}$  NMR resonance at 67 ppm and the presence of a low energy UV-vis absorption band at 340 nm for  $[30]^+$  indicates the presence of a coordinatively unsaturated boron center which mediates  $\pi$ -conjugation of the aromatic ligands. The resulting boron-centered chromophore is fluorescent and give rise to a broad emission band at 464 nm (quantum yield:  $\phi=0.02$ ) when excited at 350 nm in MeOH. As reported for other sulfonium salts,  $[30]^+$  is sensitive to UV light and should therefore not be irradiated for extended periods of time.

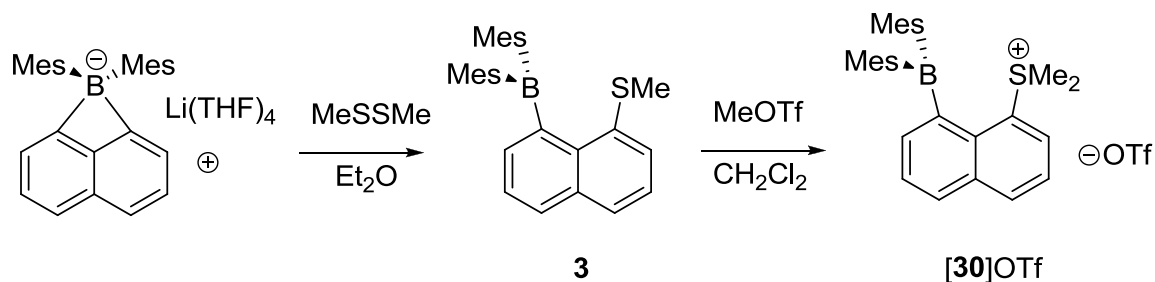


**Figure 12** Synthesis of the sulfonium borane  $[30]\text{OTf}$

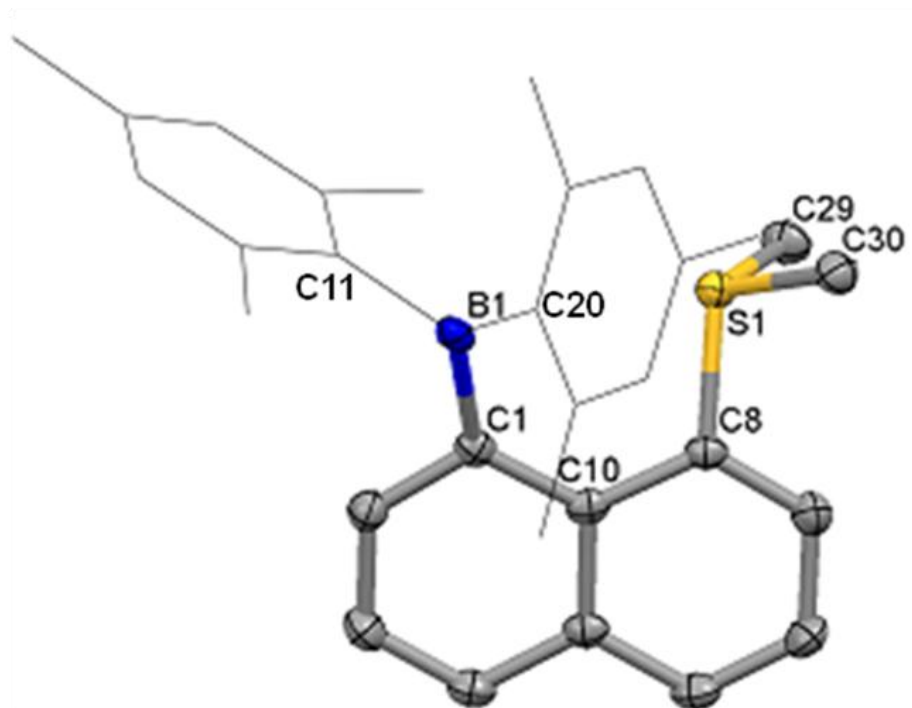


**Figure 13.** Crystal structure of [30]OTf (thermal ellipsoids are drawn at 50% probability levels; hydrogen atoms and triflate anion are omitted and the mesityl ligands are represented by thin lines for clarity). Selective bond distances [ $\text{\AA}$ ] and bond angles [ $^\circ$ ]: S(1)-C(8) 1.786(3), S(1)-C(30) 1.788(3), S(1)-C(29) 1.791(3), C(10)-C(8) 1.420(4), C(10)-C(1) 1.440(4), C(1)-B(1) 1.583(4), C(11)-B(1) 1.576(4), B(1)-C(20) 1.574(4); C(8)-S(1)-C(30) 103.59(13), C(8)-S(1)-C(29) 101.55(13), C(30)-S(1)-C(29) 102.94(13), C(8)-C(10)-C(1) 125.5(2), C(10)-C(1)-B(1) 129.0(2), C(10)-C(8)-S(1) 118.46(19), C(11)-B(1)-C(20) 120.6(2), C(11)-B(1)-C(1) 116.0(2), C(20)-B(1)-C(1) 123.0(2).

**Table 1.** Crystal data, data collections, and structure refinement for [30]OTf.

Crystal data	[30]OTf
formula	C <sub>32</sub> H <sub>36</sub> BCl <sub>2</sub> F <sub>3</sub> O <sub>3</sub> S <sub>2</sub>
$M_r$	671.44
crystal size (mm <sup>3</sup> )	0.20 x 0.10 x 0.10
crystal system	Triclinic
space group	P-1
$a$ (Å)	8.5182(17)
$b$ (Å)	10.144(2)
$c$ (Å)	18.638(4)
$\alpha$ (°)	104.31(3)
$\beta$ (°)	92.55(3)
$\gamma$ (°)	102.84(3)
$V$ (Å <sup>3</sup> )	1513.0(5)
$Z$	2
$\rho_{\text{calc}}$ (g cm <sup>-3</sup> )	1.474
$\mu$ (mm <sup>-1</sup> )	0.406
$F(000)$	700
Data Collection	
$T$ (K)	110(2)
scan mode	$\omega$
	-9 → +9
$hkl$ range	-11 → +11
	-21 → +21
measd reflns	13329
unique reflns [ $R_{\text{int}}$ ]	4735 [0.0228]
reflns used for refinement	4735
Refinement	
refined parameters	388
Goof	1.061
$R_1, {}^a wR_2^b$ all data	0.0448, 0.1216
$\rho_{\text{fin}}$ (max/min) (e Å <sup>-3</sup> )	0.676, -0.397

$${}^a R_1 = \frac{\sum ||F_o| - |F_c||}{\sum |F_o|}, {}^b wR_2 = \left[ \frac{\sum w(F_o^2 - F_c^2)^2}{\sum w(F_o^2)^2} \right]^{1/2}.$$

The crystal structure of  $[30]^+$  clearly shows that the boron center adopts a trigonal planar coordination geometry ( $\sum_{(C-B-C)} = 359.6^\circ$ ) and that it is only separated from sulfur atom by 3.07 Å (Figure 13, Table 1). This short separation indicates that: 1) the unsaturated boron center is sterically encumbered, in agreement with the large B(1)-C(1)-C(10) angle ( $129.0^\circ$ ) which substantially deviates from the ideal value of  $120^\circ$ ; 2) the boron center experiences electron donation from the neighboring sulfur atom through a  $lp(S) \rightarrow p(B)$  donor-acceptor interaction. More details on this bonding feature will be provided in 2.5.

### 2.3 Reaction of the sulfonium borane with fluoride ions

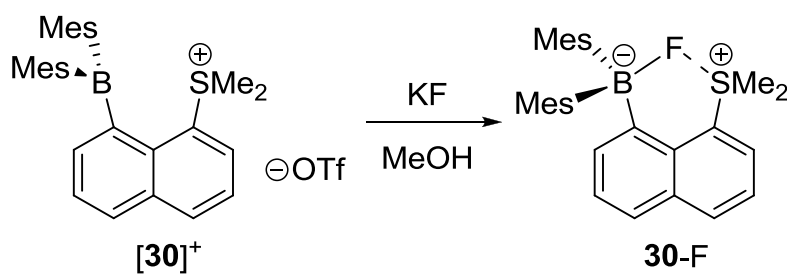


**Figure 14.** Reaction of  $[30]^+$  with  $KF$  to form  $30-F$  in methanol

Reactions of  $[\mathbf{30}]^+$  with fluoride anion in organic solvents or mixtures of organic solvent and water were examined. Reaction of  $[\mathbf{30}]^+$  with *n*-tetrabutylammonium fluoride (TBAF) in chloroform at ambient temperature results in a rapid formation of a new species, assigned to  $\mathbf{30-F}$ . Compound  $\mathbf{30-F}$  precipitates when  $[\mathbf{30}]^+$  reacts with excess KF in MeOH (Figure 14). Formation of  $\mathbf{30-F}$  does not require the use of dry methanol. Instead,  $\mathbf{30-F}$  also precipitates from concentrated MeOH/H<sub>2</sub>O solutions containing large fractions of water. For example, sonicating a mixture of  $\mathbf{30-OTf}$  (21 mg) and KF (45 mg) in 0.5 ml of a MeOH/H<sub>2</sub>O (3:2, v/v) solution results in the precipitation of  $\mathbf{30-F}$  (12 mg, 75% yield). The adduct  $\mathbf{30-F}$  has been fully characterized by multinuclear NMR spectroscopy and single crystal X-ray diffraction. The <sup>11</sup>B NMR resonance of  $\mathbf{30-F}$  at 9.0 ppm and the <sup>19</sup>F NMR signal at -161.1 ppm are consistent with the presence of a typical triarylfluoroborate anion.<sup>25-26</sup> The crystal structure of  $\mathbf{30-F}$  has been determined (Figure 15, Table 2). It crystallizes in the monoclinic *P*2<sub>(1)</sub>/*c* space group with two independent molecules in the asymmetric unit. Both independent molecules feature very similar structures. The boron atom adopts pyramidal geometry indicated by the sum of the C<sub>aryl</sub>-B-C<sub>aryl</sub> angles ( $\sum_{(C-B-C)} = 341.4^\circ$  and  $342.8^\circ$  for the two molecules) and is separated from fluoride by an average distance of 1.50 Å, a typical B-F bond in the triarylfluoroborate species.<sup>48, 57</sup>

The boron-bound fluorine atom is separated from the sulfur atom by an average distance of 2.53 Å, which is well within the sum of van der Waals radii of the two elements (ca. 3.3 Å).<sup>58</sup> The average F-S-C<sub>Me</sub> angle of 171.7° indicates that the fluorine atom occupies an axial coordination site directly opposite to one of the sulfur-bound methyl groups. These geometrical parameters, which are reminiscent of those observed in other fluoroborate sulfonium species,<sup>59-60</sup> suggest the presence of an interaction between the fluorine and sulfur atom. To confirm this view, the structure of **30-F** was computationally optimized (DFT, functional: B3LYP; mixed basis set: B, F: 6-31+g(d'); S: 6-31+g(d); C, H: 6-31g) and subjected to a Natural Bond Orbital (NBO) analysis. This analysis indicates that the short F-S separation present in **30-F** corresponds to a lp(F)→σ\*(S-C) donor-acceptor interaction which contributes 7.0 kcal/mol to the stability of the molecule (Figure 16). Altogether, these results suggest that the ability of [**30**]<sup>+</sup> to complex F<sup>-</sup> in wet methanol arises from favorable Coulombic effects which are complemented by the formation of a B-F→S chelate motif.<sup>25</sup>



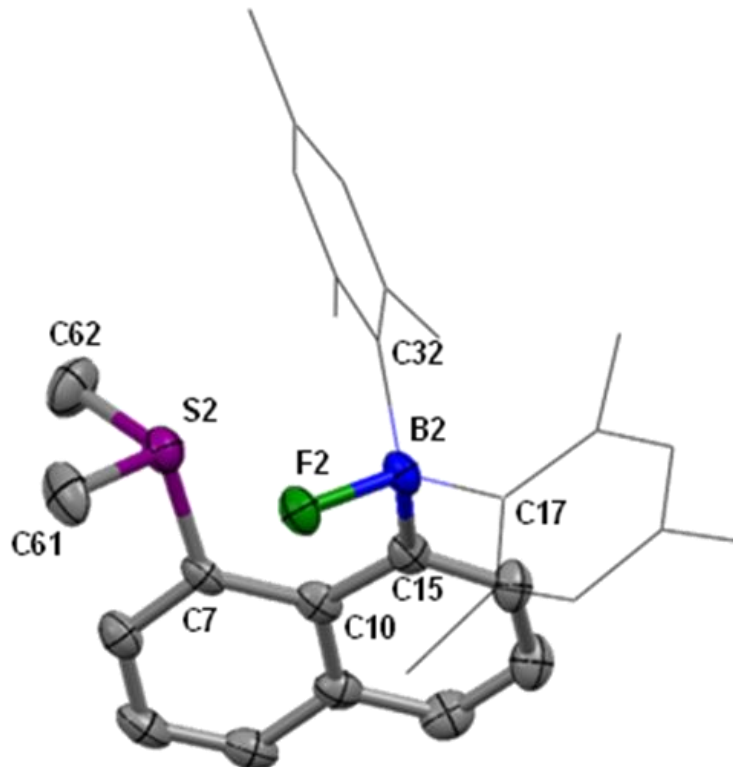


**Figure 15.** Crystal structure of **30-F** (only one independent molecule is shown; thermal ellipsoids are drawn at 50% probability levels; hydrogen atoms are omitted and the mesityl ligands are represented by thin lines for clarity). Selective bond distances [ $\text{\AA}$ ] and bond angles [ $^\circ$ ]: S(2)-C(7) 1.793(4), S(2)-C(62) 1.795(5), S(2)-C(61) 1.798(4), F(2)-B(2) 1.503(5), C(17)-B(2) 1.659(6), C(15)-B(2) 1.649(6), C(32)-B(2) 1.656(6), C(10)-C(15) 1.445(5), C(7)-C(10) 1.459(6); C(7)-S(2)-C(62) 103.0(2), C(7)-S(2)-C(61) 104.0(2), C(62)-S(2)-C(61) 100.2(2), C(10)-C(7)-S(2) 120.4(3), C(15)-C(10)-C(7) 126.9(3), C(10)-C(15)-B(2) 126.4(3), F(2)-B(2)-C(15) 103.2(3), F(2)-B(2)-C(32) 103.4(3), C(15)-B(2)-C(32) 116.8(3), F(2)-B(2)-C(17) 105.5(3), C(15)-B(2)-C(17) 110.8(3), C(32)-B(2)-C(17) 115.2(3).

**Table 2.** Crystal data, data collections, and structure refinement for **30-F**.

Crystal data	<b>30-F</b>
formula	C <sub>30</sub> H <sub>34</sub> BFS
$M_r$	456.44
crystal size (mm <sup>3</sup> )	0.15 x 0.06 x 0.03
crystal system	Monoclinic
space group	P2(1)/c
$a$ (Å)	9.486(9)
$b$ (Å)	26.43(2)
$c$ (Å)	20.531(19)
$\alpha$ (°)	90
$\beta$ (°)	102.677(12)
$\gamma$ (°)	90
$V$ (Å <sup>3</sup> )	5022(8)
$Z$	8
$\rho_{\text{calc}}$ (g cm <sup>-3</sup> )	1.207
$\mu$ (mm <sup>-1</sup> )	0.152
$F(000)$	1952
Data Collection	
$T$ (K)	110(2)
scan mode	$\omega$
	-10 $\rightarrow$ +11
$hkl$ range	-31 $\rightarrow$ +31
	-24 $\rightarrow$ +24
measd reflns	35548
unique reflns [ $R_{\text{int}}$ ]	0.1191
reflns used for refinement	8830
Refinement	
refined parameters	8830/0/595
GooF	1.058
$R_1$ , <sup>a</sup> $wR_2$ <sup>b</sup> all data	0.1286, 0.2132
$\rho_{\text{fin}}$ (max/min) (e Å <sup>-3</sup> )	0.412, -0.422

$$^a R_1 = \frac{\sum ||F_o| - |F_c||}{\sum |F_o|}, \quad ^b wR_2 = \left[ \frac{\sum w(F_o^2 - F_c^2)^2}{\sum w(F_o^2)^2} \right]^{1/2}.$$

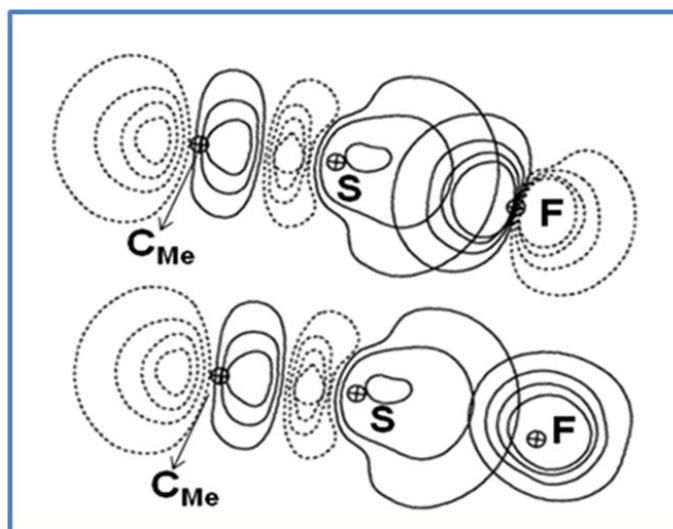


**Figure 16.** NBO contour plots that show the two  $lp(F) \rightarrow \sigma^*(S-C)$  donor-acceptor interactions involved in **30-F**. The difference in hybridization of the two fluorine lone pairs involved in this interaction is evident from this view.

Next we investigated the fluoride ion affinity of  $[30]^+$  under dilute conditions. Bearing in mind that anion binding to the boron center should result in a quenching of the low-energy band observed in the UV-vis spectrum of the borane, these studies were monitored by UV/Vis spectroscopy. The addition of 100 equiv. fluoride ions to  $[30]^+$  (0.045 mM) in MeOH did not result in any changes in the UV-vis spectrum, indicating that  $[30]^+$  has no or very little affinity for fluoride ions in this solvent under dilute conditions. When the titration experiment was carried out in THF, the absorbance of UV-vis spectrum was progressively quenched upon fluoride addition. The binding constant exceeds  $10^7 \text{ M}^{-1}$  by fitting the resulting data to a 1:1 binding isotherm. A

titration experiment was also carried out in aqueous solutions (THF: H<sub>2</sub>O, 9/1, v/v), affording a binding constant of  $2.05(\pm 0.5) \times 10^5 \text{ M}^{-1}$  (Figure 17).

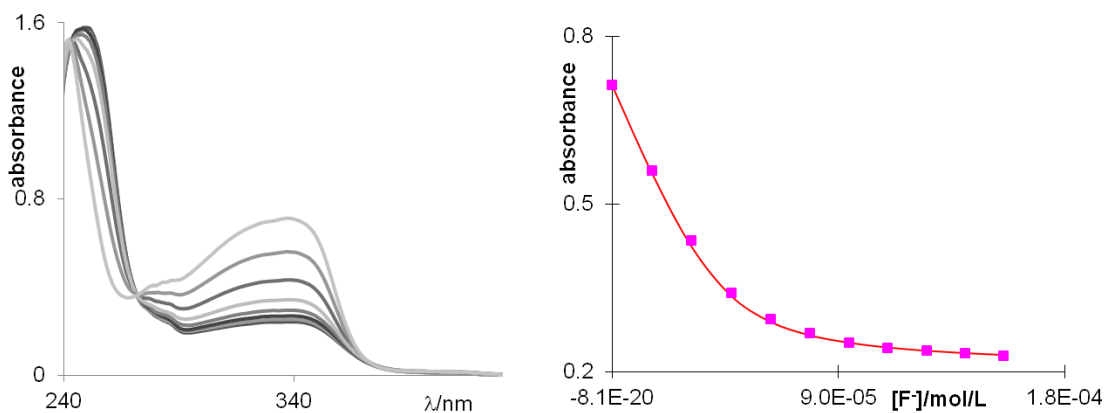


**Figure 17.** Left: Changes in the UV-vis absorption spectra of a solution of [30]OTf ( $4.36 \times 10^{-5} \text{ M}$  in THF: H<sub>2</sub>O, 9/1, vol.) upon the addition of a TBAF solution ( $9.5 \times 10^{-3} \text{ M}$  in THF); Right: resulting 1:1 binding isotherm using  $\epsilon([\mathbf{30}]\text{OTf}) = 16350 \text{ M}^{-1}\text{cm}^{-1}$  and  $\epsilon(\mathbf{30}\text{-F}) = 4900 \text{ M}^{-1}\text{cm}^{-1}$  with  $\lambda_{\text{max}} = 337\text{nm}$ .

## 2.4 Reaction of the sulfonium borane with cyanide ions

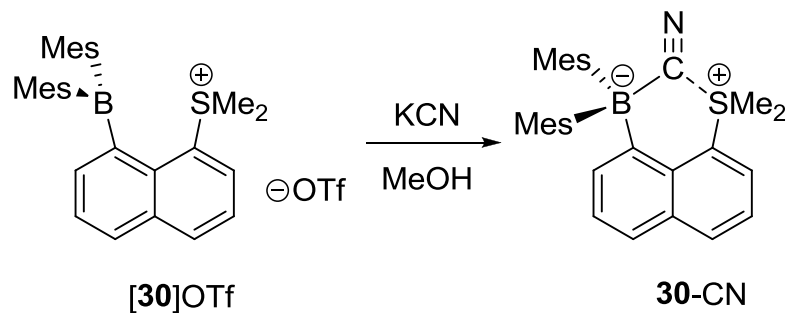


**Figure 18.** Reaction of  $[\mathbf{30}]^+$  with KCN to form  $\mathbf{30-CN}$  in methanol.

Similarly,  $[\mathbf{30}]^+$  reacts with TBACN in chloroform to affording the zwitterionic cyanoborate,  $\mathbf{30-CN}$ .  $\mathbf{30-CN}$  precipitates when  $[\mathbf{30}]^+$  reacts with excess KCN in MeOH (Figure 18). The adduct  $\mathbf{30-CN}$  has been characterized by multinuclear NMR spectroscopy and single crystal X-ray diffraction. The  $^{11}\text{B}$  NMR resonance of  $\mathbf{30-CN}$  at -13.0 ppm is consistent with the presence of a typical triarylborate anion and an intense IR band at  $2162\text{ cm}^{-1}$  confirms the presence of the boron-bound cyano group.<sup>46,</sup>

This compound crystallizes in the orthorhombic space group  $P2(1)2(1)2(1)$  with two independent molecules in the asymmetric unit (Figure 19, Table 3). Both molecules, arbitrarily denoted as molecule A and B, feature very similar structures. The boron atoms adopt pyramidal geometries (the sum of the  $C_{\text{aryl}}\text{-B-C}_{\text{aryl}}$  angles:  $\sum_{(\text{C-B-C})} = 340.5^\circ$ , A;  $\sum_{(\text{C-B-C})} = 339.9^\circ$ , B), and are separated from the cyanide carbon atom by 1.630(5) Å (A) and 1.624(6) Å (B). These B- $C_{\text{CN}}$ - distances are comparable to those typically found in triarylborate anions. The distances between the boron and the sulfur atoms are 3.247 Å (A) and 3.197 Å (B), much larger than that in [30]OTf (3.075 Å), which suggest an increase in steric crowding upon cyanide binding. This conclusion is in agreement with the large angle of B(1)-C(1)-C(9) ( $128.5(3)^\circ$  (A),  $129.9(3)^\circ$  (B)). Finally, the centroid of the  $C_{\text{CN}}\text{-N(1)}$  ( $C_{\text{tCN}}$ ) bond is separated from the sulfur atom by only 2.95 Å and forms a  $C_{\text{tCN}}\text{-S(1)-C}_{\text{Me}}$  angle of  $157.9^\circ$ . To investigate the presence of a possible interaction between the sulfur atom and the cyanide group, we carried out an NBO analysis of the DFT optimized structure (Figure 20). This analysis reveals the presence of a  $\pi(\text{C}\equiv\text{N})\rightarrow\sigma^*(\text{S-C})$  donor-acceptor interaction unexpectedly complemented by a back-bonding  $\text{lp}(\text{S})\rightarrow\pi^*(\text{C}\equiv\text{N})$  component. The concomitant deletion of these two interactions leads to an increase of the total energy of the molecule by  $4.1 \text{ kcal mol}^{-1}$ , an energy comparable to that of a strong hydrogen bond.

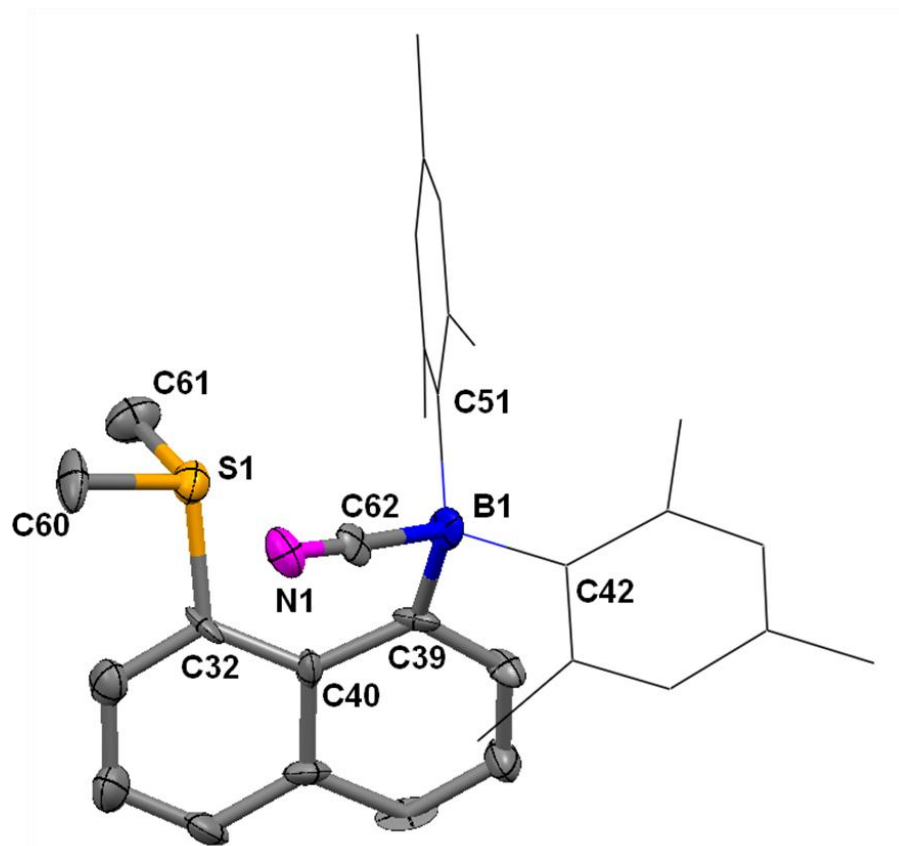


**Figure 19.** Crystal structure of **30-CN** (only one independent molecule is shown; ellipsoids are drawn at 50% probability levels; hydrogen atoms omitted and the mesityl groups are represented by thin lines for clarity). Selective bond distances [ $\text{\AA}$ ] and bond angles [ $^\circ$ ]: S(1)-C(32) 1.798(7), S(1)-C(61) 1.809(7), S(1)-C(60) 1.816(7), C(40)-C(39) 1.474(10), C(40)-C(32) 1.402(9), C(39)-B(1) 1.639(11), C(42)-B(1) 1.686(11), C(62)-B(1) 1.631(14), C(51)-B(1) 1.668(11), N(1)-C(62) 1.162(9); N(1)-C(62)-B(1) 176.7(7), C(32)-S(1)-C(61) 102.5(3), C(32)-S(1)-C(60) 104.2(4), C(61)-S(1)-C(60) 100.6(4), C(32)-C(40)-C(39) 127.5(6), C(40)-C(39)-B(1) 128.7(6), C(62)-B(1)-C(39) 106.4(6), C(62)-B(1)-C(51) 102.9(5), C(39)-B(1)-C(51)-119.1(6), C(62)-B(1)-C(42) 105.2(5), C(39)-B(1)-C(42) 108.5(6), C(51)-B(1)-C(42) 113.5(6).

**Table 3.** Crystal data, data collections, and structure refinement for **30-CN**.

Crystal data	<b>30-CN</b>
Formula	C <sub>63</sub> H <sub>70</sub> B <sub>2</sub> Cl <sub>2</sub> N <sub>2</sub> S <sub>2</sub>
$M_r$	1011.85
crystal size (mm <sup>3</sup> )	0.20 x 0.10 x 0.08
crystal system	Orthorhombic
space group	P2(1)2(1)2(1)
$a$ (Å)	8.9440(18)
$b$ (Å)	21.579(4)
$c$ (Å)	28.106(6)
$\alpha$ (°)	90
$\beta$ (°)	90
$\gamma$ (°)	90
$V$ (Å <sup>3</sup> )	5424.4(19)
$Z$	4
$\rho_{\text{calc}}$ (g cm <sup>-3</sup> )	1.239
$\mu$ (mm <sup>-1</sup> )	0.239
$F(000)$	2152
Data Collection	
$T$ (K)	110(2)
scan mode	$\omega$
$hkl$ range	-11 $\rightarrow$ +11 -28 $\rightarrow$ +28 -36 $\rightarrow$ +37
measd reflns	59911
unique reflns [ $R_{\text{int}}$ ]	12952 [0.0872]
reflns used for refinement	12952
Refinement	
refined parameters	640
GooF	1.000
$R_1, {}^a wR_2$ all data	0.0892, 0.1880
$\rho_{\text{fin}}$ (max/min) (e Å <sup>-3</sup> )	0.492 and -0.536

$${}^a R_1 = \frac{\sum ||F_o| - |F_c||}{\sum |F_o|}, {}^b wR_2 = \left[ \frac{\sum w(F_o^2 - F_c^2)^2}{\sum w(F_o^2)^2} \right]^{1/2}.$$



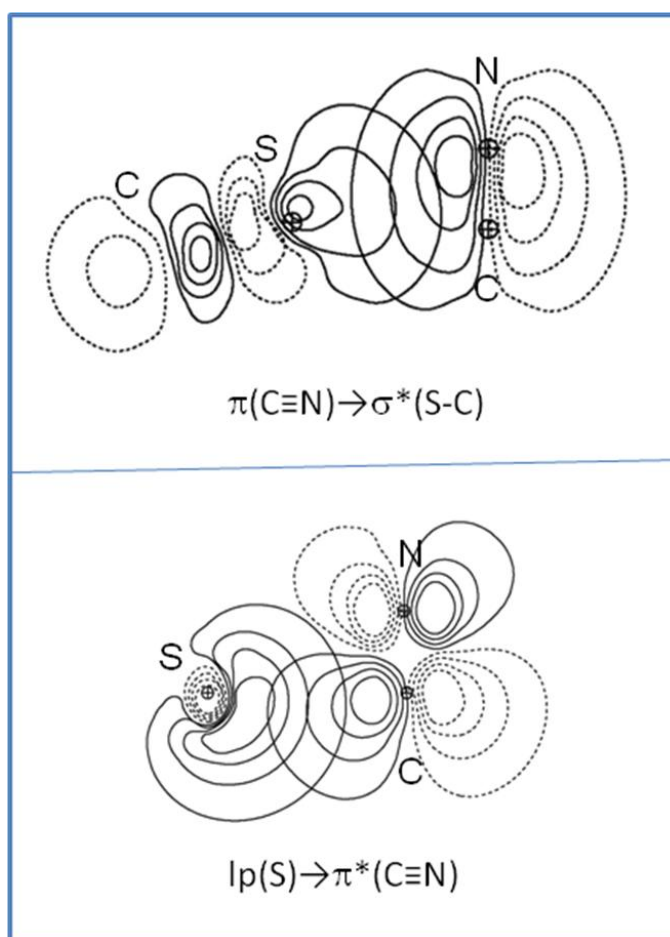


**Figure 20.** NBO contour plots showing  $\pi(\text{C}\equiv\text{N}) \rightarrow \sigma^*(\text{S}-\text{C})$  (top) and  $\text{lp}(\text{S}) \rightarrow \pi^*(\text{C}\equiv\text{N})$  (bottom) interactions in **30-CN**.

Next, titration experiments monitored by UV/Vis spectroscopy were carried out to investigate the cyanide ion affinity of  $[\mathbf{30}]^+$  under dilute conditions. The addition of 10 equivalents of  $\text{CN}^-$  into a methanol solution of  $[\mathbf{30}]\text{OTf}$  (0.063mM) resulted in a total quenching of the absorption spectrum within 30 minutes. On the other hand, the addition of  $\text{F}^-$  resulted in negligible absorption quenching, and  $\text{Cl}^-$ ,  $\text{Br}^-$ ,  $\text{I}^-$ ,  $\text{HSO}_4^-$ ,  $\text{H}_2\text{PO}_4^-$  did induce any change of the absorption spectrum. The difference between cyanide and

fluoride affinity probably arises from the basicity of the cyanide anion and the high hydration energy of fluoride ion in methanol. However, the binding process was very slow which precludes the determination of the accurate cyanide binding constant of [30]OTf in methanol. The titration carried out in THF shows that the binding constant exceeds  $10^7 \text{ M}^{-1}$  (Figure 21).

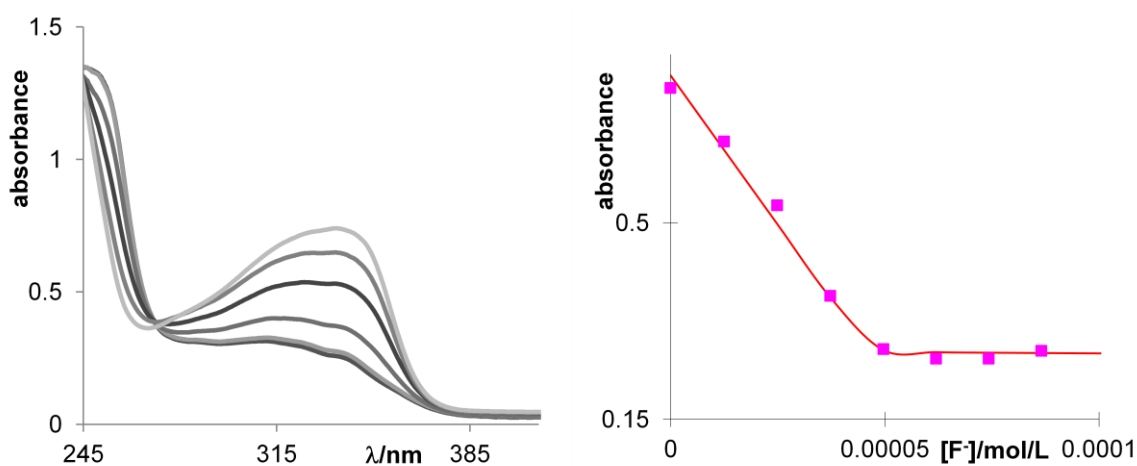


**Figure 21.** Left: Changes in the UV-vis absorption spectra of a solution of [30]OTf ( $4.67 \times 10^{-5} \text{ M}$  in THF) upon the addition of a KCN solution ( $7.5 \times 10^{-3} \text{ M}$ ) in THF); Right: resulting 1:1 binding isotherm using  $\epsilon([\mathbf{30}]\text{OTf}) = 16350 \text{ M}^{-1}\text{cm}^{-1}$  and  $\epsilon(\mathbf{30}\text{-CN}) = 5800 \text{ M}^{-1}\text{cm}^{-1}$  with  $\lambda_{\text{max}} = 337 \text{ nm}$ .

## 2.5 Comparison of Lewis acidity of [30]<sup>+</sup> with another sulfonium borane

In order to better understand the properties of the borane and its compatibility with aqueous environments, we have investigated its reaction with hydroxide anions. Interestingly, addition of NaOH to a solution of the cationic borane in  $\text{D}_2\text{O}/\text{MeOH-}d_4$

(9:1 vol.) for  $[30]^+$  results in the formation of the corresponding hydroxide adducts as confirmed by  $^{11}\text{B}$  NMR spectroscopy. The  $^{11}\text{B}$  NMR signal is detected at 2.1 ppm, thus confirming the presence of a coordinatively saturated boron center. This hydroxide binding has been discussed in previous papers from the Gabbai group.<sup>62</sup> Next, we decided to investigate the Lewis acidity of  $[30]^+$  by studying its behavior in aqueous solution as a function of pH. Since hydroxide binding to the boron center is expected to interrupt the  $\pi$  conjugation mediated by the vacant  $p$ -orbital on the boron atom, we monitored the absorbance of the boron-centered chromophore as a function of pH in MeOH/H<sub>2</sub>O (5:95, vol.). The absorption of the boron-centered chromophore is quenched as the pH becomes more basic, in agreement with the formation of the hydroxide adduct, which shows that  $[30]^+$  is stable up to pH 9.5 (Figure 22). These results suggest that  $[30]^+$  has a significantly lower Lewis acidity than other cationic boranes, such as the phosphonium borane  $[1\text{-Mes}_2\text{B-2-MePh}_2\text{P-(C}_6\text{H}_4)]^+$  ( $\text{p}K_{\text{R}^+}$  is between 2 and 3). In turn, the addition of 15 equivalents of  $\text{F}^-$  or  $\text{CN}^-$  to a 32  $\mu\text{M}$  solution of  $[30]^+$  in H<sub>2</sub>O/MeOH (95:5, vol.) at pH 7 did not result in any changes of the absorption spectrum, indicating the absence of any significant interactions.

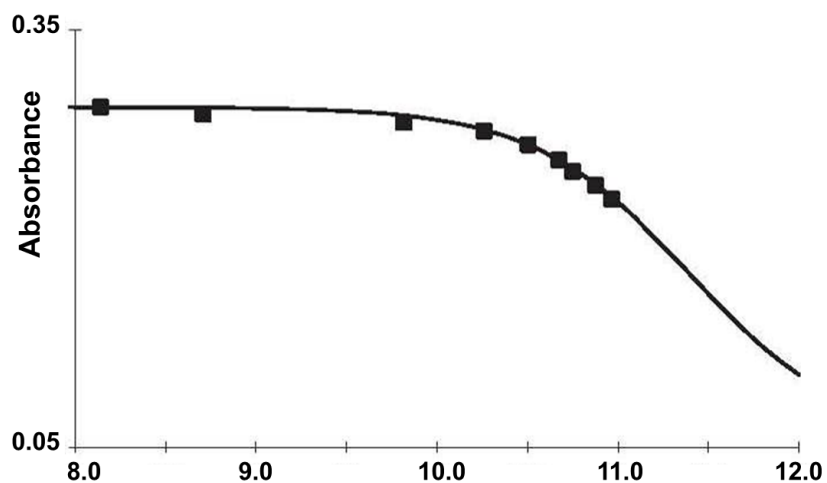
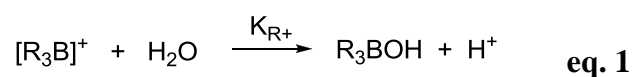


**Figure 22.** Spectrophotometric titration curve of  $[\mathbf{30}]^+$ . The absorbance was measured at 337 nm. The experimental data was fitted to eq. 1 using  $\epsilon([\mathbf{30}]^+) = 16350 \text{ M}^{-1} \text{ cm}^{-1}$ ,  $\epsilon(\mathbf{30-OH}) = 3000 \text{ M}^{-1} \text{ cm}^{-1}$ , and  $\text{p}K_{\text{R}^+} = 11.4$ . Data point above pH 11 could not be obtained because of precipitation. Because of the lack of reversibility observed in this experiment, the  $\text{p}K_{\text{R}^+}$  value use to fit the data does not provide a measure of the equilibrium described in eq. 1

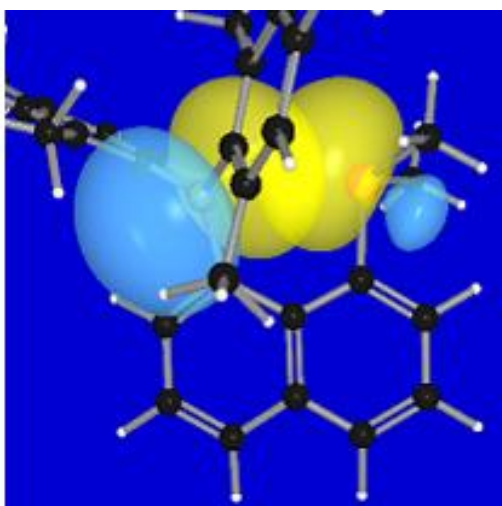


**Figure 23.** Partial view of the molecule of  $[30]^+$  showing the contour of the NBOs involved in the  $lp(S) \rightarrow p(B)$  donor–acceptor interaction.

The crystal structure of  $[30]^+$  clearly shows that the boron center is only separated from the sulfur atom by 3.07 Å, which indicates that the boron center experiences electron donation from the neighboring sulfur atom via a  $lp(S) \rightarrow p(B)$  donor–acceptor interaction. An NBO analysis carried out at the DFT optimized geometry of  $[30]^+$  indicates the presence of a  $lp(S) \rightarrow p(B)$  donor–acceptor interaction (Figure 23) whose deletion leads to an increase of the total energy of the molecule by  $E_{\text{del}}=6.8 \text{ kcal mol}^{-1}$ . Therefore, in addition to being sterically crowded, the boron center of  $[30]^+$  experiences electron donation from the neighboring sulfur atom, a phenomenon which would be expected to reduce its electron deficiency. In turn, the relatively weak Lewis acidity of  $[30]^+$  probably arises from the sterically encumbered boron center and the  $lp(S) \rightarrow p(B)$  donor–acceptor interaction caused by the short boron–sulfur separation.

## 2.6 Conclusion

In conclusion, a new cationic borane  $[30]^+$  incorporating a sulfonium moiety as a secondary Lewis acidic site has been synthesized successfully. The stability and Lewis acidity of  $[30]^+$  has been studied in aqueous environments. These studies indicate that there is limited use for  $[30]^+$  as an anion receptor in aqueous media due to its relatively weak Lewis acidity. However, this compound reacts with fluoride and cyanide anions in MeOH to afford the corresponding zwitterionic fluoroborate and cyanoborate species, **30-F** and **30-CN**, respectively. Titration experiments carried out in THF indicate the binding constants of  $[30]^+$  with fluoride and cyanide anions exceed  $10^7 \text{ M}^{-1}$ . The resulting fluoro- and cyano-borate species have been isolated and fully characterized. The structural and computational analysis of **30-F** and **30-CN** demonstrates that the sulfonium moiety interacts with the fluoride and cyanide guests through a donor-acceptor interaction. For **30-CN**, such interaction is complemented by the  $\text{lp}(\text{S}) \rightarrow \pi^*(\text{CN})$  back-bonding interaction.

## 2.7 Experimental section

**General Considerations.** Tetrakis(THF)lithium dimesityl-1,8-naphthalenediylborate was synthesized by following the published procedure (Hoefelmeyer, J. D.; Gabbaï, F. P. *Organometallics* **2002**, *21*, 982-985). Dimesitylboron fluoride, methyl triflate, potassium fluoride and potassium cyanide were purchased from Aldrich, dimethyl disulfide from Alfa Aesar. Solvents were dried by passing through an alumina column (hexanes, dichloromethane) or refluxing under  $\text{N}_2$  over Na/K ( $\text{Et}_2\text{O}$ ).

UV-vis spectra were recorded on an Ocean Optics USB4000 spectrometer with an Ocean Optics ISS light source. Elemental analyses were performed by Atlantic Microlab (Norcross, GA). pH Measurements were carried out with a Radiometer PHM290 pH meter equipped with a VWR SympHony electrode. NMR spectra were recorded on Varian Unity Inova 400 FT NMR (399.59 MHz for  $^1\text{H}$ , 128.19 MHz for  $^{11}\text{B}$ , 100.45 MHz for  $^{13}\text{C}$ ) spectrometers at ambient temperature. Chemical shifts  $\delta$  are given in ppm, and are referenced against external  $\text{BF}_3 \cdot \text{Et}_2\text{O}$  ( $^{11}\text{B}$  and  $^{19}\text{F}$ ).

**Crystallography.** The crystallographic measurements were performed using a Bruker APEX-II CCD area detector diffractometer (Mo- $\text{K}_\alpha$  radiation,  $\lambda = 0.71069 \text{ \AA}$ ) for [30]OTf, 30-F, and 30-CN. In each case, a specimen of suitable size and quality was selected and mounted onto a nylon loop. The structures were solved by direct methods, which successfully located most of the non-hydrogen atoms. Subsequent refinement on  $F^2$  using the SHELXTL/PC package (version 5.1) allowed location of the remaining non-hydrogen atoms.

**Synthesis of borane 30.** Dimethyl disulfide (0.247g, 2.62mmol) was added to a suspension of tetrakis(THF)lithium dimesityl-1,8-naphthalenediylborate in diethyl ether(40 mL) at  $-20 \text{ }^\circ\text{C}$ . After stirring overnight at room temperature, the reaction was quenched with water and extracted with diethyl ether (3 x 50 mL). The organic phases were combined and dried over  $\text{MgSO}_4$  and filtered. The solvent was removed under reduced pressure yielding light yellow solid. The solid was washed with hexanes to afford compound 30 (0.73 g, yield 73%).  $^1\text{H}$  NMR (400 MHz,  $\text{CDCl}_3$ )  $\delta$  1.81 (s, 3H), 1.98 (s, 12H), 2.23 (s, 6H), 6.74 (br s, 4H, Mes-CH), 7.39-7.47 (m, 3H, nap-CH), 7.66

(dd, 1H,  $^3J_{\text{H-H}} = 9.4$  Hz,  $^4J_{\text{H-H}} = 1.4$  Hz, nap-CH), 7.74 (t, 1H,  $^3J_{\text{H-H}} = 6.2$ Hz), 7.83 (dd, 1H,  $^3J_{\text{H-H}} = 10.8$  Hz,  $^4J_{\text{H-H}} = 1.2$  Hz, nap-CH).  $^{13}\text{C}$  NMR (100 MHz,  $\text{CDCl}_3$ )  $\delta$  20.98, 23.22, 24.59, 125.46, 126.95, 128.72, 129.12, 129.25, 131.45, 133.41, 136.66, 139.42, 141.11.  $^{11}\text{B}$  NMR (128 MHz,  $\text{CDCl}_3$ )  $\delta$  + 77 (bs).

**Synthesis of [30]OTf.** Methyl triflate (0.23 mL, 2.05 mmol) was added to a solution of compound **30** (0.72 g, 1.71 mmol) in dichloromethane (25 mL) at room temperature. The mixture was refluxed overnight and cooled to room temperature. The solvent was removed in *vacuo* to yield a yellow solid as crude. The solid was washed by hexanes to afford the pale product (0.8g, yield 88%). Single crystals of [30]OTf were obtained by evaporation of mixture solution of dichloromethane and diethyl ether.  $^1\text{H}$  NMR (400 MHz,  $\text{CDCl}_3$ )  $\delta$  0.73 (s, 3H), 1.84 (s, 3H), 2.16 (s, 3H), 2.19 (s, 3H), 2.34 (s, 6H), 2.46 (s, 3H), 3.21 (s, 3H), 6.54 (s, 1H, Mes-CH), 6.84 (s, 1H, Mes-CH), 6.94 (s, 2H, Mes-CH), 7.58 (t, 1H,  $^3J_{\text{H-H}} = 10.0$  Hz, nap-CH), 7.69 (d, 1H,  $^3J_{\text{H-H}} = 9.2$  Hz, nap-CH), 7.92 (t, 1H,  $^3J_{\text{H-H}} = 9.2$  Hz, nap-CH), 8.09 (d, 1H,  $^3J_{\text{H-H}} = 10.8$  Hz, nap-CH), 8.27 (d, 1H,  $^3J_{\text{H-H}} = 10.0$  Hz, nap-CH), 8.73 (d, 1H,  $^3J_{\text{H-H}} = 9.6$  Hz, nap-CH).  $^{13}\text{C}$  NMR (100 MHz,  $\text{CDCl}_3$ )  $\delta$  21.33, 21.52, 22.54, 23.02, 23.93, 24.45, 27.02, 33.67, 123.35, 128.14, 128.42, 128.63, 129.38, 130.98, 132.41, 133.46, 136.49, 137.60, 140.10, 141.15, 141.90, 144.32.  $^{11}\text{B}$  NMR (128 MHz,  $\text{CDCl}_3$ )  $\delta$  + 67 (bs). Anal. Calcd for  $\text{C}_{31}\text{H}_{36}\text{BF}_3\text{O}_4\text{S}_2$  ([30]OTf •  $\text{H}_2\text{O}$ ): C, 61.5; H, 6.00. Found: C, 61.03; H, 5.74.



**Synthesis of 30-F.** **30-OTf** (1.00 g, 1.7 mmol) was added to 20 ml methanol solution of KF (0.70 g) which resulted in the formation of a colorless precipitate. This precipitate was isolated by filtration, washed with methanol, and dried under vacuum to afford **30-F** (0.45 g, yield 58%). Single crystals of **30-F** were obtained by evaporation of a solution of acetonitrile. The purity of this compound was established by NMR spectroscopy (Figure 24).  $^1\text{H}$  NMR (400 MHz,  $\text{CD}_3\text{CN}$ )  $\delta$  1.54 (bs, 3H, Mes- $\text{CH}_3$ ), 1.83 (bs, 6H, Mes- $\text{CH}_3$ ), 2.02 (bs, 3H, Mes- $\text{CH}_3$ ), 2.16 (bs, 6H, S- $\text{CH}_3$ ), 2.41 (bs, 3H, Mes- $\text{CH}_3$ ), 3.09 (bs, 3H, Mes- $\text{CH}_3$ ), 6.49 (bs, 3H, Mes- $\text{CH}$ ), 6.66 (s, 1H, Mes- $\text{CH}$ ), 7.24 (t,  $J = 7.6$  Hz, 1H, nap- $\text{CH}$ ), 7.56-7.66 (m, 3H, nap- $\text{CH}$ ), 8.09 (d,  $J = 7.6$  Hz, 1H, nap- $\text{CH}$ ), 8.16 (d,  $J = 8.0$  Hz, 1H, Nap- $\text{CH}$ );  $^{13}\text{C}$  NMR (100 MHz,  $\text{CD}_3\text{CN}$ )  $\delta$  20.21(s, 2C, Mes- $\text{CH}_3$ ), 23.79(s, 2C, S- $\text{CH}_3$ ), 24.42(s, 1C, Mes- $\text{CH}_3$ ), 26.84(s, 1C, Mes- $\text{CH}_3$ ), 30.18(s, 1C, Mes- $\text{CH}_3$ ), 31.35(s, 1C, Mes- $\text{CH}_3$ ), 123.95, 125.40, 126.54, 128.05, 128.24, 128.75, 129.18, 132.47, 135.11, 136.08, 136.23, 137.62, 137.70, 140.36, 142.26 (Ar- $\text{H}$ );  $^{11}\text{B}$  NMR (128 MHz,  $\text{CD}_3\text{CN}$ )  $\delta$  9.0 (bs).  $^{19}\text{F}$  NMR (375.9 MHz,  $\text{CD}_3\text{CN}$ )  $\delta$  -161 (bs).

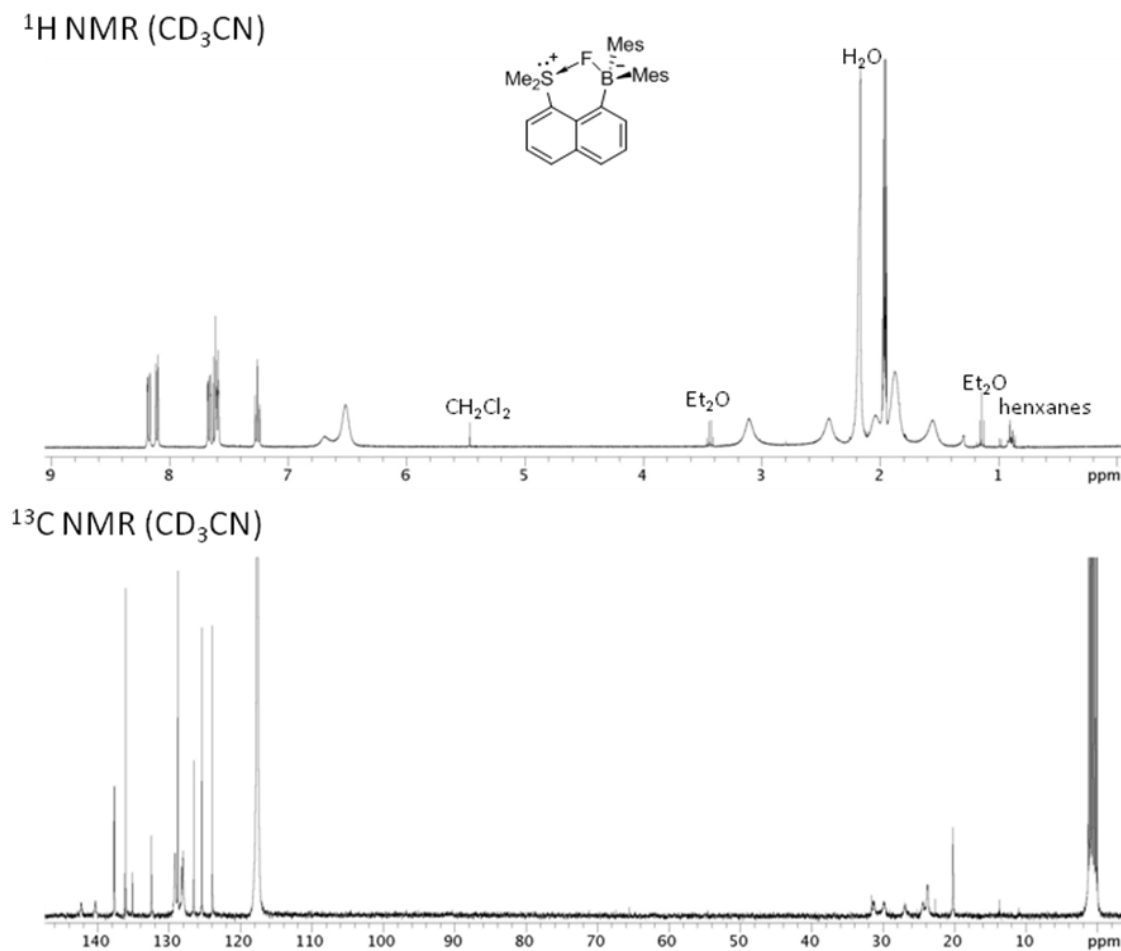


**Figure 24.**  $^1\text{H}$  NMR and  $^{13}\text{C}$  NMR spectra of **30-F**

**Synthesis of 30-CN.** **[30]OTf** (0.025g, 0.043mmol) was added to saturated KCN methanol solution. After stirring 30 min, the pale solid was formed. The solid was filtered, washed with methanol, and dried by vacuum to afford the product (0.015 mg, yield 75%). Single crystals of **30-CN** were obtained by evaporation of dichloromethane solution.  $^1\text{H}$  NMR (400 MHz,  $\text{CDCl}_3$ )  $\delta$  1.69 (s, 3H), 1.79 (s, 3H), 1.88 (s, 3H), 2.21 (s, 3H), 2.25 (s, 3H), 2.31 (s, 3H), 2.36 (s, 3H), 3.27 (s, 3H), 6.50 (s, 1H, Mes-CH), 6.70 (s,

1H, Mes-CH), 6.78 (s, 1H, Mes-CH), 6.83 (s, 1H, Mes-CH), 7.35 (t, 1H,  $^3J_{\text{H-H}} = 7.6$  Hz, nap-CH), 7.55 (d, 1H,  $^3J_{\text{H-H}} = 7.6$  Hz, nap-CH), 7.69 (d, 1H,  $^3J_{\text{H-H}} = 8.0$  Hz, nap-CH), 7.81 (d, 1H,  $^3J_{\text{H-H}} = 7.6$  Hz, nap-CH), 7.92 (d, 1H,  $^3J_{\text{H-H}} = 6.4$  Hz, nap-CH), 8.17 (d, 1H,  $^3J_{\text{H-H}} = 7.6$  Hz, nap-CH).  $^{13}\text{C}$  NMR (100 MHz,  $\text{CDCl}_3$ )  $\delta$  20.74, 20.78, 24.93, 25.27, 25.33, 27.55, 30.28, 31.44, 33.04, 123.46, 125.12, 126.71, 127.60, 127.66, 128.83, 129.22, 129.60, 129.92, 133.22, 133.42, 135.90, 136.66, 137.60, 141.04, 141.60, 142.80, 143.39.  $^{11}\text{B}$  NMR (128 MHz,  $\text{CDCl}_3$ )  $\delta$  -13.0 (s). Anal. Calcd for  $\text{C}_{31.5}\text{H}_{35}\text{BNCIS}$  (**30-CN** • 0.5 $\text{CH}_2\text{Cl}_2$ , the single crystal contains one  $\text{CH}_2\text{Cl}_2$  molecule in the unit cell and partial solvent was probably lost in the sample for analysis): C, 74.78; H, 6.97. Found: C, 73.57; H, 6.83.

**Fluoride titration in THF:  $\text{H}_2\text{O}$ , 9/1, v/v.** A solution of [**30**]OTf (3ml,  $4.36 \times 10^{-5}$  M in THF/ $\text{H}_2\text{O}$ , 9:1, vol.) was placed in the cuvette and titrated with incremental amounts of fluoride anions by addition of a solution of TBAF in THF ( $9.5 \times 10^{-3}$  M). The absorbance was monitored at  $\lambda = 337$  nm ( $\epsilon = 16350$  for [**30**]OTf,  $\epsilon = 4900$  for **30-F**). The experimental data obtained was fitted to a 1:1 binding isotherm which indicated that the fluoride binding constant of [**30**]OTf is about  $2.05(\pm 0.5) \times 10^5 \text{ M}^{-1}$  (Table 4).

**Table 4.** Absorbance of a solution of  $[30]^+$  after successive additions of fluoride anions in THF/H<sub>2</sub>O, 9:1, vol.

$C_{\text{Fluoride}}$	$Abs_{\text{exp}}$	$Abs_{\text{calc}}$
0	0.713	0.713
1.5807E-05	0.560	0.556
3.15615E-05	0.435	0.425
4.72637E-05	0.341	0.336
6.29139E-05	0.294	0.290
7.85124E-05	0.269	0.266
9.40594E-05	0.252	0.252
0.000109555	0.243	0.244
0.000125	0.237	0.238
0.000140394	0.233	0.233
0.000155738	0.229	0.230

**Cyanide titration in THF.** A solution of  $[30]OTf$  (3ml,  $4.67 \times 10^{-5}$  M in THF) was placed in the cuvette and titrated with incremental amounts of cyanide anions by addition of a solution of KCN in MeOH ( $7.5 \times 10^{-3}$  M). The absorbance was monitored at  $\lambda = 337$  nm ( $\epsilon = 16350$  for  $[30]OTf$ ,  $\epsilon = 5800$  for **30-F**). The experimental data obtained was fitted to a 1:1 binding isotherm which indicated that the fluoride binding constant of  $[30]OTf$  exceeds  $10^7$  M<sup>-1</sup> (Table 5).

**Table 5.** Absorbance of a solution of [30]<sup>+</sup> after successive additions of cyanide anions in THF.

C <sub>cyanide</sub>	Abs <sub>exp</sub>	Abs <sub>calc</sub>
0	0.74	0.763
1.24792E-05	0.645	0.630208
2.49169E-05	0.531	0.49801
3.73134E-05	0.37	0.367008
4.96689E-05	0.275	0.273348
6.19835E-05	0.258	0.269493
7.42574E-05	0.258	0.268584
8.64909E-05	0.272	0.26796

**Computational details:** DFT calculations (full geometry optimization) were carried out with the Gaussian 03 program using the gradient-corrected Becke exchange functional (B3LYP) and the Lee-Yang-Parr correlation functional (Figure 25, Figure 26, Figure 27, Table 6, Table 7, Table 8). Geometry optimization was carried out with the following mixed basis set: 6-31+g(d') for the boron, nitrogen and fluorine atom, 6-31+g(d) for the sulfur atom, 6-31g basis set was used for other remained carbon and hydrogen atoms. Frequency calculations, which were carried out on the optimized structure of the compound, confirmed the absence of any imaginary frequencies. The Natural Bond Orbital (NBO) analysis was carried out using the stand along PC version of GENNBO 5.0 program.

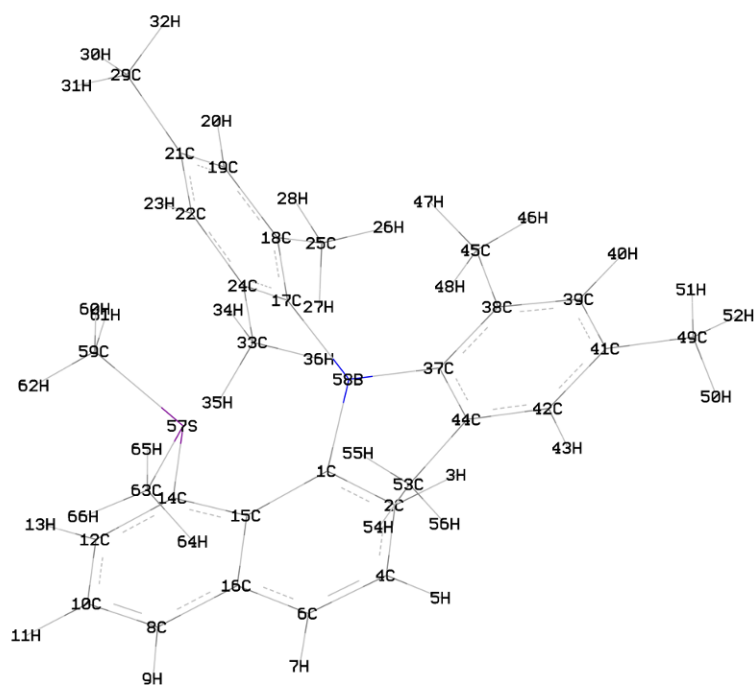


**Figure 25.** DFT optimized structure of [30]<sup>+</sup>

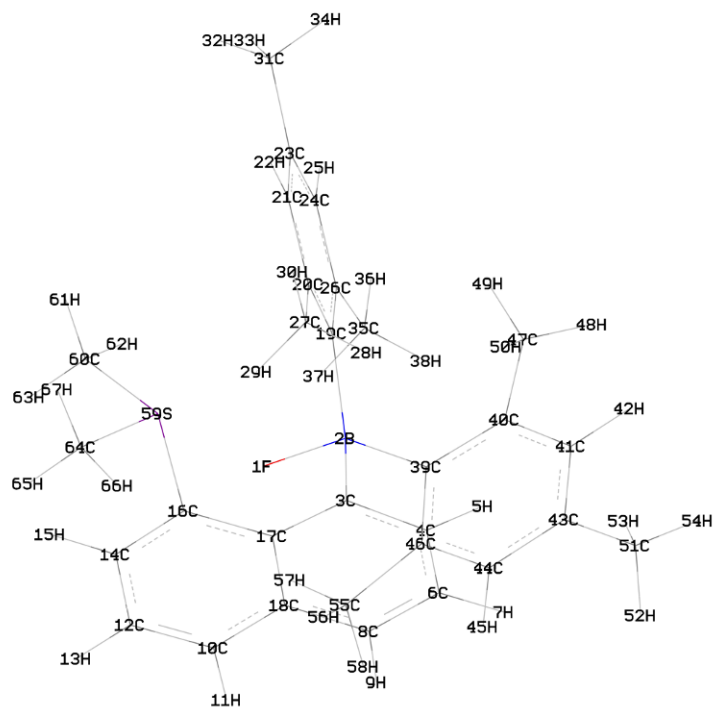


**Figure 26.** DFT optimized structure of 30-F

**Table 6.** Atom coordinates for the optimized structure of [30]<sup>+</sup>

Center Number	Coordinates(Angstroms)		
	X	Y	Z
C1	1.161769	-0.894605	0.835450
C2	1.138901	-1.934945	1.773123
H3	0.275232	-2.023975	2.422423
C4	2.206488	-2.846634	1.953639
H5	2.132468	-3.615742	2.714409
C6	3.336137	-2.731875	1.179778
H7	4.181740	-3.396889	1.322529
C8	4.577237	-1.663885	-0.652513
H9	5.393571	-2.349061	-0.447681
C10	4.684407	-0.746722	-1.679130
H11	5.583156	-0.684433	-2.280980
C12	3.588877	0.088781	-1.967087
H13	3.661737	0.764237	-2.813068
C14	2.434454	0.028369	-1.194358
C15	2.299581	-0.842564	-0.059599
C16	3.411413	-1.745774	0.153694
C17	0.351181	1.737449	1.196181
C18	-0.581613	2.707799	0.692731
C19	-0.301993	4.078236	0.791725
H20	-1.022070	4.789961	0.396029
C21	0.861782	4.561496	1.407090
C22	1.764209	3.619491	1.917818
H23	2.660692	3.970514	2.421793
C24	1.536752	2.235785	1.831265
C25	-1.897928	2.331492	0.032988
H26	-2.632867	1.996131	0.772032
H27	-1.801525	1.517711	-0.693655
H28	-2.323920	3.196763	-0.484924
C29	1.110620	6.044120	1.554399
H30	0.698420	6.609148	0.711935
H31	2.179235	6.268458	1.629286
H32	0.633182	6.429575	2.465114
C33	2.564854	1.341814	2.505159
H34	3.214017	1.939664	3.151240
H35	3.210402	0.825750	1.786289
H36	2.101393	0.572452	3.129427
C37	-1.409042	-0.367702	1.459890
C38	-2.017558	-0.045427	2.712116
C39	-3.272414	-0.577656	3.039615
H40	-3.705473	-0.339523	4.007480
C41	-3.982657	-1.408962	2.162955
C42	-3.385662	-1.723975	0.935031
H43	-3.915421	-2.371948	0.241425
C44	-2.122933	-1.233754	0.576966
C45	-1.338712	0.837290	3.745820
H46	-1.883364	0.800791	4.693737
H47	-1.299579	1.884787	3.427109
H48	-0.307977	0.525537	3.951761
C49	-5.352377	-1.935323	2.522715
H50	-5.544981	-2.906299	2.055051
H51	-6.140041	-1.248913	2.183475
H52	-5.466681	-2.049904	3.605234
C53	-1.594169	-1.606229	-0.796935
H54	-0.560302	-1.964540	-0.759268
H55	-1.629068	-0.749371	-1.486608
H56	-2.203713	-2.397213	-1.243784
S57	1.004309	0.975475	-1.737057
B58	0.023211	0.187161	1.105243
C59	1.614882	2.685035	-1.930322
H60	0.793283	3.285398	-2.325903
H61	1.884499	3.045757	-0.936892
H62	2.472378	2.712895	-2.603758
C63	0.806921	0.465990	-3.485796
H64	0.534424	-0.591050	-3.487762
H65	-0.010692	1.054985	-3.909310
H66	1.723819	0.620134	-4.056285

**Table 7.** Atom coordinates for the optimized structure of **30-F**

Center Number	Coordinates(Angstroms)		
	X	Y	Z
F1	0.210342	-0.111076	-0.117457
B2	0.264314	0.050418	1.402763
C3	1.530718	-0.952195	1.820898
C4	1.397534	-1.660591	3.017511
H5	0.541653	-1.439010	3.644332
C6	2.268552	-2.690297	3.438616
H7	2.094383	-3.185875	4.388858
C8	3.292323	-3.095893	2.615590
H9	3.939527	-3.925564	2.884078
C10	4.549562	-2.899760	0.527087
H11	5.127587	-3.760182	0.851741
C12	4.828779	-2.290856	-0.676836
H13	5.610505	-2.664428	-1.328695
C14	4.103313	-1.138031	-1.036743
H15	4.369696	-0.630139	-1.957742
C16	3.088373	-0.651581	-0.223715
C17	2.672577	-1.305777	0.995539
H18	3.511122	-2.434511	1.377400
C19	0.447194	1.689149	1.608227
C20	-0.474161	2.553598	0.931062
C21	-0.305165	3.948676	0.947398
H22	-1.027798	4.568229	0.419090
C23	0.746437	4.567173	1.634245
C24	1.629587	3.734529	2.326694
H25	2.442776	4.184487	2.893823
C26	1.496570	2.331908	2.331368
C27	-1.689370	2.032092	0.179999
H28	-2.308772	1.394750	0.818532
H29	-1.409410	1.419567	-0.681705
H30	-2.306511	2.866372	-0.171792
C31	0.886742	6.074023	1.668860
H32	0.595079	6.527679	0.714155
H33	1.917482	6.376135	1.886545
H34	0.247679	6.519287	2.444215
C35	2.526704	1.583335	3.165844
H36	3.139789	2.294384	3.730811
H37	3.206310	0.969748	2.562726
H38	2.062135	0.902718	3.885072
C39	-1.136828	-0.589424	2.012728
C40	-1.780466	-0.095365	3.188970
C41	-2.978678	-0.667898	3.654229
H42	-3.436476	-0.261051	4.553992
C43	-3.594030	-1.741550	3.007460
C44	-2.945508	-2.264682	1.884584
H45	-3.375731	-3.128432	1.380633
C46	-1.746581	-1.725006	1.389478
C47	-1.232788	1.048262	4.029840
H48	-1.744398	1.077804	4.998680
H49	-1.374585	2.021515	3.548536
H50	-0.161399	0.949748	4.226504
C51	-4.904641	-2.315170	3.500425
H52	-4.956872	-3.397814	3.335592
H53	-5.761968	-1.867339	2.977924
H54	-5.044837	-2.129235	4.571300
C55	-1.148087	-2.440815	0.188124
H56	-0.071078	-2.596046	0.297714
H57	-1.289674	-1.873883	-0.738072
H58	-1.622070	-3.421084	0.061621
S59	2.378630	0.948285	-0.686030
C60	3.872201	1.955007	-1.021031
H61	3.522040	2.944494	-1.327272
H62	4.416071	2.047455	-0.079139
H63	4.518625	1.526402	-1.787999
C64	1.766865	0.704766	-2.386869
H65	2.540528	0.287190	-3.033343
H66	0.914339	0.032753	-2.300748
H67	1.435970	1.678583	-2.756662



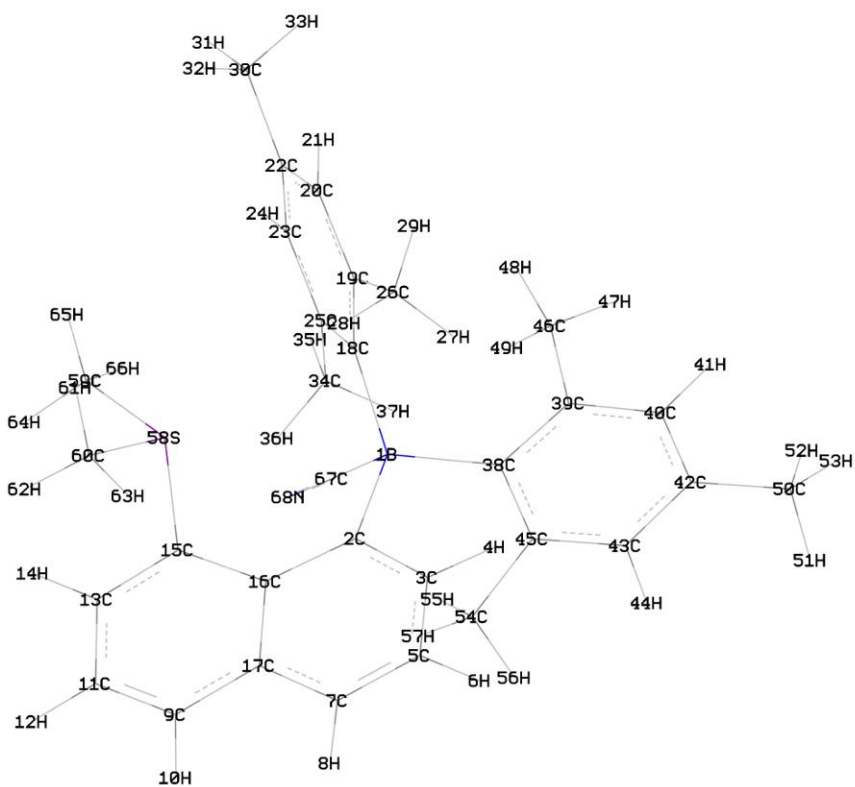


**Figure 27.** DFT optimized structure of **30-CN**.

**Table 8.** Atom coordinates for the optimized structure of **30-CN**

Center Number	Coordinates(Angstroms)		
	X	Y	Z
B1	-0.209269	-0.104473	1.508291
C2	1.109748	-1.069787	1.936514
C3	0.930637	-1.810077	3.109024
H4	0.024913	-1.638994	3.677194
C5	1.816974	-2.801175	3.583925
H6	1.590945	-3.325018	4.507527
C7	2.927729	-3.124816	2.845686
H8	3.601234	-3.919703	3.151520
C9	4.379743	-2.780530	0.924418
H10	4.967205	-3.615079	1.295708
C11	4.770383	-2.107285	-0.210688
H12	5.654502	-2.399474	-0.765769
C13	4.014613	-0.994935	-0.622203
H14	4.365427	-0.431753	-1.479706
C15	2.862526	-0.612329	0.055055
C16	2.346791	-1.325984	1.206878
C17	3.218443	-2.410009	1.652676
C18	0.016669	1.549602	1.653848
C19	-0.868625	2.437053	0.957923
C20	-0.643491	3.824667	0.942185
H21	-1.342302	4.458181	0.398770
C22	0.425438	4.419091	1.621365
C23	1.255932	3.569948	2.357649
H24	2.061778	4.004989	2.946691
C25	1.070093	2.173238	2.396477
C26	-2.115948	1.964724	0.227121
H27	-2.589988	1.119201	0.730196
H28	-1.901500	1.645013	-0.798898
H29	-2.846453	2.779834	0.173901
C30	0.625326	5.919572	1.620103
H31	0.387534	6.356685	0.643123
H32	1.658311	6.187298	1.869322
H33	-0.024142	6.410922	2.357790
C34	2.021006	1.427600	3.325224
H35	2.586873	2.145722	3.929195
H36	2.746184	0.795540	2.800903
H37	1.488226	0.766378	4.013746
C38	-1.596663	-0.693555	2.251121
C39	-2.258364	-0.036005	3.338635
C40	-3.459879	-0.541920	3.868680
H41	-3.928505	-0.006911	4.692314
C42	-4.062483	-1.706232	3.388918
C43	-3.387489	-2.396230	2.380259
H44	-3.797623	-3.337309	2.018539
C45	-2.185960	-1.929113	1.820078
C46	-1.730565	1.208366	4.036132
H47	-2.262893	1.353617	4.982890
H48	-1.863915	2.115629	3.439014
H49	-0.665157	1.136195	4.267195
C50	-5.379382	-2.202984	3.943309
H51	-5.450893	-3.295306	3.888053
H52	-6.230721	-1.793930	3.381013
H53	-5.511398	-1.907270	4.990406
C54	-1.571533	-2.848020	0.774201
H55	-1.854692	-2.564199	-0.245154
H56	-1.917884	-3.874843	0.938864
H57	-0.480380	-2.858261	0.810299
S58	2.118577	0.942605	-0.510084
C59	3.480135	2.138794	-0.260087
C60	2.109874	0.834293	-2.332947
H61	1.743313	1.798567	-2.694834
H62	3.097581	0.622578	-2.743202
H63	1.385617	0.057643	-2.582735
H64	4.407549	1.796938	-0.722169
H65	3.157460	3.091449	-0.687172
H66	3.604791	2.259471	0.816041
C67	-0.374299	-0.371059	-0.084044
N68	-0.423592	-0.558614	-1.236253

CHAPTER III  
THE APPLICATION OF A SULFONIUM BORANE IN FLUORIDE TRANSFER  
PROCESS\*

### 3.1 Introduction

The incorporation of fluorine in organic molecules and materials is gaining momentum because of the beneficial properties imparted by this small and highly electronegative halogen. Such properties may include: increased stability in the case of organic materials as well as increased metabolic stability, lipophilicity; and bioavailability in the case of drugs.<sup>63-67</sup> Fluorination chemistry is also becoming important in the domain of [<sup>18</sup>F]-positron emission tomography (PET), a technique that necessitates the radiolabeling of organic molecules with [<sup>18</sup>F]-fluorine atoms.<sup>68-71</sup>

For the reasons enumerated in the preceding paragraph, the field of fluorination chemistry is experiencing a surge of interest. While electrophilic fluorination strategies remain preponderant,<sup>72-80</sup> there is a growing need for the development of nucleophilic pathways. These research needs have fueled a series of recent efforts that have already afforded an array of nucleophilic fluorinating agents reviewed in the following sections.<sup>81-95</sup>

---

\*Reprinted in part with permission from, "Nucleophilic Fluorination Reactions Starting from Aqueous Fluoride Ion Solutions"; Zhao, H.; Gabbaï, F. *P. Org. Lett.* **2011**, 1444. Copyright 2011 American Chemical Society.

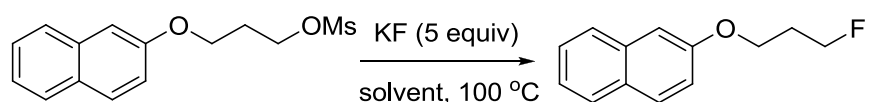
### 3.2 Review of nucleophilic fluorinating reagents

The simplest fluoride sources are alkali metal fluorides, such as KF. However, the applications of these inorganic salts in fluorination chemistry are limited because of their poor solubility in aprotic solvents. 'Calcine-dried' or 'spray-dried' KF can act as a fluorinating reagent in nucleophilic substitution reactions carried out in organic solvents.<sup>96</sup> However, these reactions occur slowly and necessitate harsh conditions due to the poor solubility of KF. In 1973, Liotta reported that 18-crown-6 can effectively increase the solubility of KF in dry CH<sub>3</sub>CN and benzene (Table 9), thus improving its reactivity as a fluorinating agent.<sup>97</sup> With this formulation, KF acts as a nucleophile which reacts with benzyl bromide (83 °C, 11.5 h), 2,4-dinitrochlorobenzene (25 °C, 5 h) and acetyl chloride (25 °C, 5.5 h) in CH<sub>3</sub>CN leading to the formation of the corresponding fluoride compounds, namely: benzyl fluoride, 2,4-dinitrofluorobenzene and acetyl fluoride. However, in the case of 1-bromooctane, the elimination product 1-octene is also formed with 8% in CH<sub>3</sub>CN at 83 °C. When bromocyclohexane is used in CH<sub>3</sub>CN at 83 °C, only elimination occurs leading to the formation of cyclohexene. It is important to note that 18-crown-6 serves as a phase transfer catalyst that promotes the dissolution of solid KF. These early results demonstrated that the solubilized fluoride ions are nucleophilic as well as basic.

**Table 9.** Solubility of KF in crown ether solution at 25 °C

Solvent	[18-crown-6], M	[KF], M
Benzene	1.01	$5.2 \times 10^{-2}$
	0.34	$1.4 \times 10^{-2}$
Acetonitrile	0.16	$3.5 \times 10^{-3}$

When bis-terminal hydroxyl polyethers, such as triethylene glycol and tetraethylene glycol, are used as solvents in fluorination reactions with KF as a fluoride source, the polyethers also act as multifunctional promoters which help solubilize KF.<sup>98</sup> The reaction of 2-(3-methanesulfonyloxypropoxy)naphthalene with KF was performed under different conditions in order to investigate the role played by bis-terminal hydroxyl polyethers (Figure 28, Table 10). Comparison of entries 1-6 clearly shows that the use of triethylene glycol and tetraethylene glycol as solvents efficiently increases the reaction rate as well as the yield. The results of entries 7-10 confirm the importance of the bis-terminal hydroxyl functionality present in the solvent molecule.

**Figure 28.** Nucleophilic fluorination reaction with KF in various solvents.

**Table 10.** Nucleophilic fluorination reaction with KF under different conditions.

Entry	Solvent	Time/h	Yield[%]
1	CH <sub>3</sub> CN	24	0
2	18-crown-6 in CH <sub>3</sub> CN	24	40
3	tBuOH	1.5	0
4	Tert-amyl alcohol	1.5	0
5	Triethylene glycol	1.5	93
6	Tetraethylene glycol	1.5	92
7	Triethylene glycol dimethyl ether	1.5	0
8	Triethylene glycol monoethyl ether	1.5	42
9	Triethylene glycol	1.5	>99
10	Triethylene glycol dimethyl ether/tBuOH (1:1, v/v)	1.5	0

In turn, there are several distinct characteristics of such polyethers as solvents: 1) the polyether can enhance the solubility and nucleophilicity of fluoride ion by capturing the potassium ion, a role similar to that played by 18-crown-6; 2) the basicity of the 'naked' fluoride is reduced by hydrogen bonding with one of the two OH groups; 3) the other OH group is able to activate the electrophilic substrates and thus stabilize the transition state, again via hydrogen bonding; 4) the negative result of entry 10 also shows that the presence of two hydroxyl groups in one molecule is required. This last

peculiarity supports the multi-functional role played by the polyethers as solvents (Figure 29).

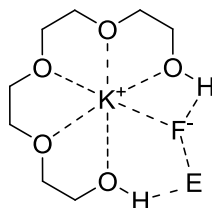


**Figure 29.** Bis-terminal hydroxyl polyether as multifunctional promoters in fluorination reactions: the polyether acts as the  $K^+$  chelator and two OH groups reduce the basicity of fluoride anion ( $F^-$ ) while activating the electrophile (E).

Tetraorganofluorophosphoranes  $R_4PF$ , such as  $Me_4PF$  **31** and  $MenBu_3PF$  **32**, are also potential fluorinating agents for organic substrates.<sup>89, 99-103</sup> These species may exist in an ionic phosphonium fluoride form ( $[R_4P]^+F^-$ ) or as trigonal bipyramidal fluorophosphorane (Figure 30). The structure of **31** has been investigated carefully in the gas phase, as well as in solution and in the solid state. In the gas phase, electron diffraction and vibrational spectra show that **31** is a fluorophosphorane with the fluorine atom in an axial position. The situation in solutions is more complicated. In protic and high-polar solvents, such as methanol, ethanol, water and acetonitrile, **31** possesses an ionic structure as confirmed by  $^{13}C$ ,  $^{19}F$  and  $^{31}P$  NMR spectra, while it exists in a molecular form when in aprotic solvents of low polarity, such as dimethyl ether, diethyl ether, THF and benzene. The single crystal structure of **31** shows an ionic structure in

the solid state. The fact the **31** is ionic in organic solvents indicates the possibility of **31** as a ‘naked’ fluoride source.

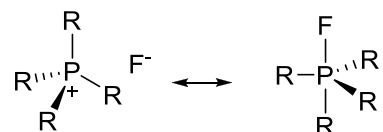


**Figure 30.** The two structures of  $\text{R}_4\text{PF}$ , ionic and molecular form.

The preparation of **32** can be achieved by the reaction of **33** with HF (Figure 31). Compound **32** is soluble in organic solvents where it behaves as a potent fluorinating reagent. Indeed, reactivity studies show that **32** can fluorinate benzyl chloride leading to the formation of benzyl fluoride in a 80% yield when the reaction is carried out in pentane. However, the fluoride ion of **32** is also highly basic as confirmed by the high production of  $\text{nC}_{10}\text{H}_{21}\text{-CH=CH}_2$  (50%) when  $\text{nC}_{12}\text{H}_{25}\text{Br}$  is used as a substrate.

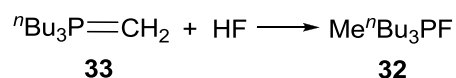


**Figure 31.** The synthesis of **32**.

The first example of naked fluoride salts with tetraorganoammonium as counteraction is ‘anhydrous’ tetrabutylammonium fluoride (TBAF) **34** containing 0.1 - 0.3 molar equiv of water, synthesized from  $\text{TBAF}\cdot 3\text{H}_2\text{O}$  under high vacuum at 40 °C.<sup>104</sup> Compound **34** can react with organohalides and tosylates to yield the corresponding



fluoro-organic products at lower temperature and shorter time when compared to the use of KF with 18-crown-6 ether. These results indicate the higher nucleophilicity of **34**. At the same time, the fluoride ion in **34** is also basic as indicated by the presence of the elimination product 1-octene (12%) when **34** reacts with 1-bromooctane (Figure 32). The hydrolysis reaction also occurs to produce the corresponding alcohol as one of the side products during the reaction with organohalides due to the presence of 0.1 - 0.3 molar equiv. of water left in **34**. Moreover, **34** would decompose at 77 °C by Hofmann degradation.

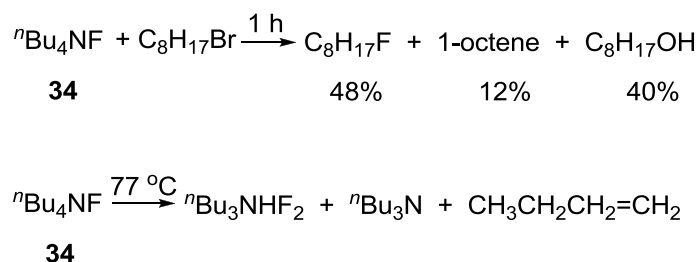


**Figure 32.** The reaction of **34** with 1-bromooctane at 25 °C and its decomposition at 77 °C.

The first stable naked fluoride salt with tetraorganoammonium as counteraction is Me<sub>4</sub>NF, **35**, reported by K. O. Christie in 1990 (Figure 33).<sup>105</sup> Since the methyl group cannot undergo Hofmann decomposition, **35** is stable up to about 150 °C under vacuum during the drying process. However, **35** is highly basic as indicated by its capacity to react with CH<sub>3</sub>CN to form the dimer. The solubility of **35** is low because of the high lattice energy. The most common application of **35** is for the synthesis inorganic fluoro-

anions, such as  $\text{XeF}_5^-$ ,  $\text{TeF}_7^-$ ,  $\text{ClF}_6\text{O}^-$ ,  $\text{SOF}_3^-$ , and  $\text{IF}_6^-$ , by the fluorination of the neutral compounds,  $\text{XeF}_4$ ,  $\text{TeF}_6$ ,  $\text{ClF}_5\text{O}$ ,  $\text{SOF}_2$ , and  $\text{IF}_5\text{O}$ .<sup>106-113</sup>

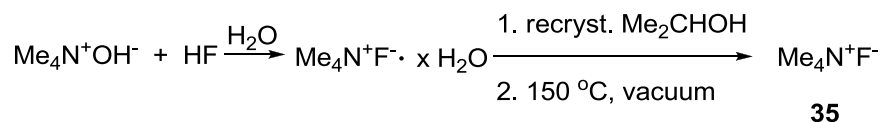


**Figure 33.** The synthesis of **35** from  $\text{Me}_4\text{NOH}$  and HF in water.

The synthesis of ‘truly’ anhydrous TBAF, **36**, was achieved through a nucleophilic aromatic substitution ( $\text{S}_{\text{N}}\text{Ar}$ ) process at low temperature by DiMugno’s group in 2005 (Figure 34 and Figure 35)<sup>87, 114-115</sup>. This approach is based on the nucleophilic displacement of a fluoride ion from hexafluorobenzene by a cyanide anion. This reaction can be carried out in THF,  $\text{CH}_3\text{CN}$  or DMSO at or below room temperature. The freshly made anhydrous TBAF is stable for hours in  $\text{CH}_3\text{CN}$ , and for more than 24 hours in THF and DMSO. The reactions of **36** with organic substrates, such as benzyl halides, afford higher yields of the corresponding fluorides. These reactions are characterized by short reaction time and require moderate or even on occasion low temperature. Altogether, the observed reactivity of **36** indicates that it is a more nucleophilic fluorination reagent than **35** (Table 11). Due to the complete absence of water in **36**, the hydrolysis side product alcohol is not formed during the reaction as when **35** is the fluoride source. **36** can also be used as a fluorinating reagent for aromatic fluorination reaction. Entry 4, 5 and 6 have shown that electron-withdrawing substituents are necessary in such reactions, and the reactions with aromatic compounds

bearing more electron-withdrawing substituents proceed faster. The fluorination process can tolerate various functional groups, such as ketones, ethers, esters and aldehydes.

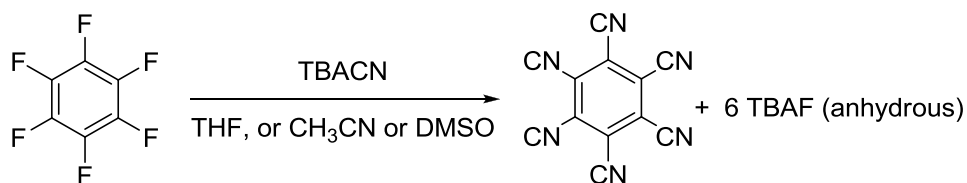
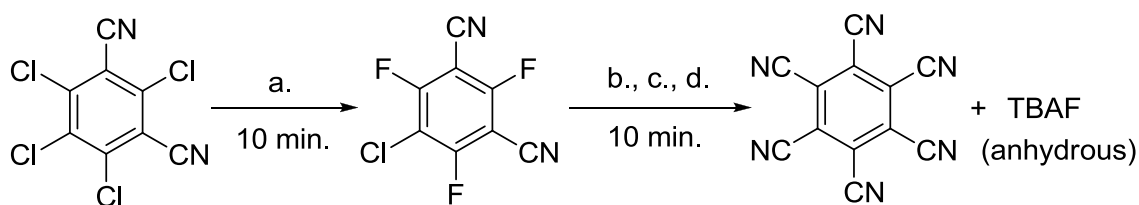


**Figure 34.** The synthesis of **36** from C<sub>6</sub>F<sub>6</sub> and TBAF.

The same group has also designed an elegant “fluoride relay” concept in which fluoride ions from KF are first incorporated onto an electron deficient benzene derivative before being nucleophilically displaced in dry organic solvent to generate **36** (Figure 35).<sup>87</sup> This general approach affords fluoride ions that, as confirmed by <sup>19</sup>F NMR spectroscopy, have a “naked” character. In line with this observation, the *in situ* generated TBAF\* is a very potent nucleophilic fluorinating agent that reacts with a variety of substrates including aromatic ones (Table 11). Despite the elegance of this approach, its compatibility with wet fluoride sources (rather than KF in DMF) has not yet been demonstrated. For these reasons, the discovery of reagents that could complex hydrated fluoride ions and deliver these ions to organic molecules should open new routes in fluorination and radiofluorination chemistry. Stimulated by this possibility, we propose to establish whether some of the cationic Lewis acids developed in this research could also be used for the capture and delivery of fluoride ions.



a. KF, DMF, reflux; b. EtOAc/H<sub>2</sub>O extraction; c. flash chromatography, evaporation; d. TBAF, DMSO, room temperature.

**Figure 35.** Fluoride relay from KF to anhydrous TBAF

**Table 11.** Nucleophilic reactions of **36** with various organic substrates.

Entry	Substrate	Conditions	Product	Yield(%)
1	PhCH <sub>2</sub> Br	CD <sub>3</sub> CN, -35 °C, < 5 min, 1.3-1.5 eq. TBAF	PhCH <sub>2</sub> F	100
2	PhCH <sub>2</sub> Cl	THF, RT, < 2 min, 1.5 eq. TBAF	PhCH <sub>2</sub> F	100
3	CH <sub>3</sub> (CH <sub>2</sub> ) <sub>7</sub> Br	THF, RT, < 5 min, TBAF	CH <sub>3</sub> (CH <sub>2</sub> ) <sub>7</sub> F	40-50
4		CD <sub>3</sub> CN, RT, < 2 min, 1 eq. TBAF		>95
5		DMSO, RT, 14 days, 4 eq. TBAF		80
6		DMSO, RT, 1 h, 2.5 eq. TBAF		>95

### 3.3 Demethylation of the fluoride adduct of the sulfonium borane

As shown in Chapter II, the sulfonium borane  $[30]^+$  can capture fluoride ions in methanol (Figure 36). Formation of **30-F** does not require the use of dry methanol. Instead, **30-F** also precipitates from concentrated MeOH/H<sub>2</sub>O solutions containing large fractions of water. For example, sonicating a mixture of  $[30]OTf$  (21 mg) and KF (45 mg) in 0.5 ml of a MeOH/H<sub>2</sub>O (3:2, v/v) solution results in the precipitation of **30-F** (12 mg, 75% yield). The ability of  $[30]^+$  to complex F<sup>-</sup> in wet methanol arises from favorable Coulombic effects which are complemented by the formation of a B-F→S chelate motif. Realizing that the absence of such interactions would greatly increase the liability of the boron-bound fluoride anion, we sought to determine if demethylation of the sulfonium moiety could be used to trigger the release of the fluoride anion.

With this in mind, we tested the reactivity of **30-F** toward soft nucleophiles such as tetrabutylammonium iodide (TBAI). When TBAI was mixed with **30-F** in dry CD<sub>3</sub>CN or THF, the demethylation of the sulfonium ion at ambient temperature occurred slowly with the formation of a new anionic fluoride adduct, namely **30-F<sup>-</sup>**. This demethylation produces MeI which quickly reacts with **30-F<sup>-</sup>** to form MeF, as indicated by the appearance of a quartet at -272 ppm in the <sup>19</sup>F NMR spectrum of the reaction

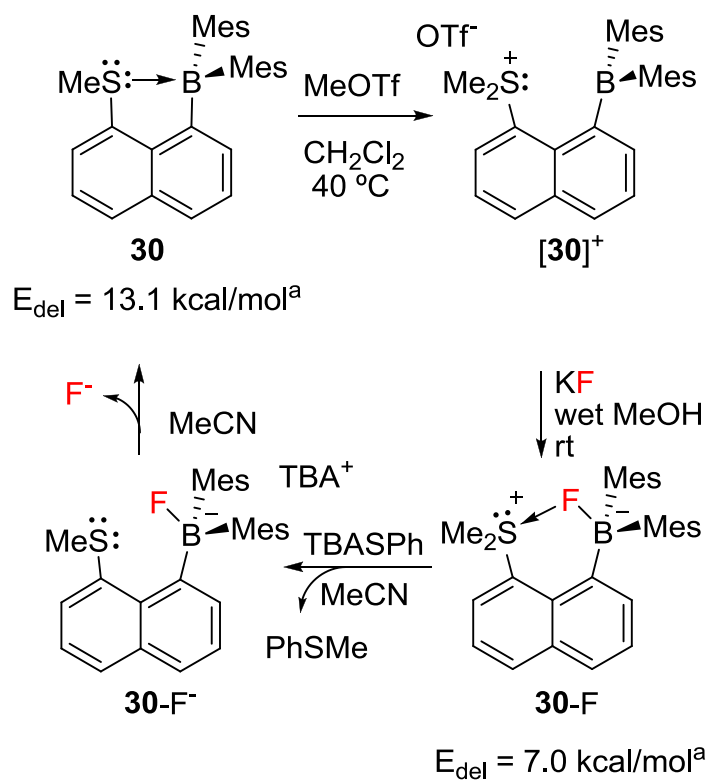


**Figure 36.** Reactions sequence showing the use of **[30]<sup>+</sup>** for the capture of fluoride ions and their triggered release. (<sup>a</sup>  $E_{\text{del}}$  corresponds to the energy provided by the  $\text{lp}(\text{S}) \rightarrow \text{p}(\text{B})$  and  $\text{lp}(\text{F}) \rightarrow \sigma^*(\text{S}-\text{C})$  interactions to the stability of **30** or **30-F**, respectively.)

mixture. Formation of MeF, which supports the notion that **30-F<sup>-</sup>** is an active fluorinating agent, indicates that iodide salts cannot be used in this approach. When TBAN<sub>3</sub> was used as a nucleophile instead of TBAI, the demethylation of the sulfonium ion also occurred with the formation of the anionic fluoride adduct **30-F<sup>-</sup>**. However, at elevated temperature (ca. 70 °C) MeF was also formed indicated by a quartet at -272 ppm in the <sup>19</sup>F NMR spectrum.

Next, we have used TBACN as a nucleophile towards the demethylation reaction. Mixing TBACN and **30-F** at ambient temperature for 6 h did not result in the demethylation indicated by the absence of any change in the <sup>1</sup>H NMR and <sup>19</sup>F NMR spectra. At 70 °C, the demethylation of the sulfonium ion proceeded slowly and completed after 2.5 h with the formation of the major product **30-F<sup>-</sup>**. The product **30-F<sup>-</sup>** can be stable at ambient temperature for at least 2 days. Even though the use of TBACN can help to limit the formation of MeF, the demethylation reaction requires elevated temperature and longer reaction time.

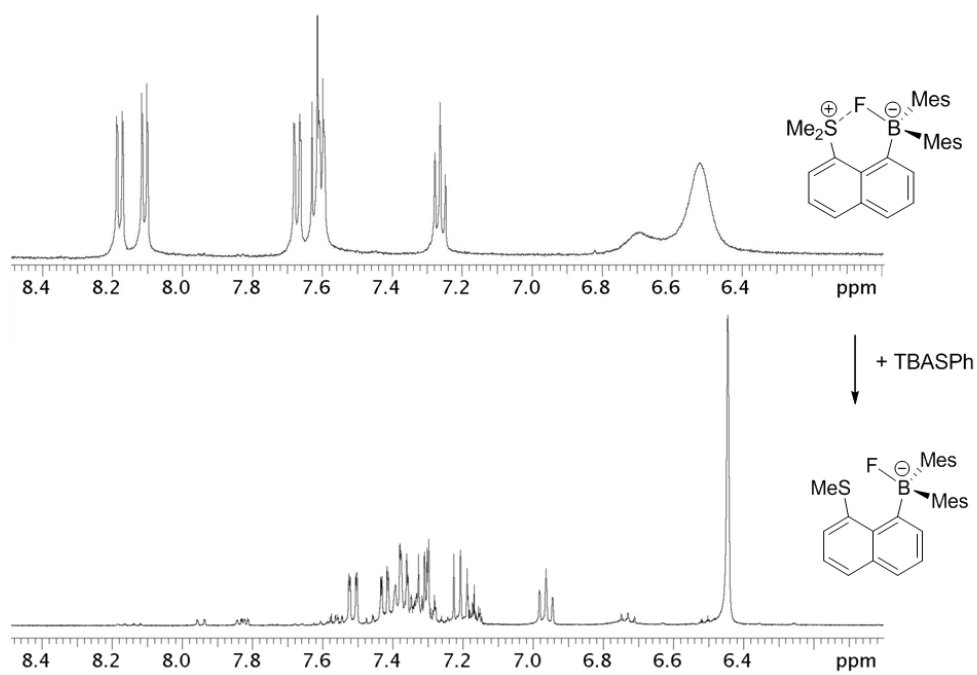


**Figure 37.** Changes of  $^1\text{H}$  NMR spectra upon mixing **30-F** with TBASPh in  $\text{d}_3\text{-MeCN}$ .

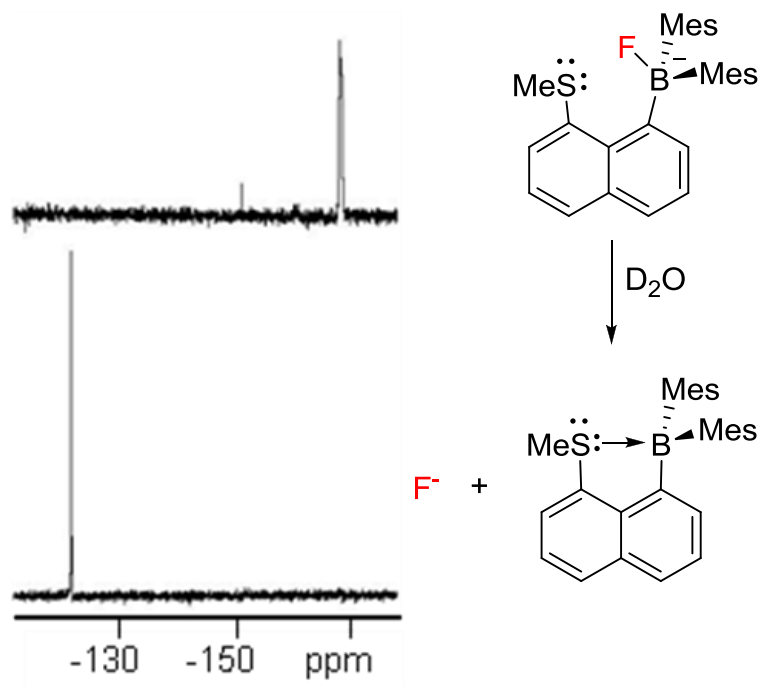


**Figure 38.**  $^{19}\text{F}$  NMR spectra of **30-F** in  $\text{d}_3\text{-MeCN}$  before and after addition of water.



For this reason, we turned our attention to the phenylthiolate anion ( $pK_a = 10.3$ ). Mixing an equimolar amount of tetrabutylammonium phenylthiolate (TBASPh) and **30-F** in dry  $CD_3CN$  at ambient temperature resulted, after 30 minutes, in elimination of PhSMe and formation of **30-F<sup>-</sup>** (Figure 37). Formation of the latter was accompanied by the appearance of ca. 5% of neutral borane **30**, suggesting that partial  $F^-$  release was possibly caused by traces of water (Figure 38). The anionic fluoride adduct **30-F<sup>-</sup>** has been characterized by multinuclear NMR spectroscopy. The  $^{11}B$  NMR resonance at 8.0 ppm is very close to that of **30-F**, consistent with the presence of a typical triarylfluoroborate anion. The  $^{19}F$  NMR signal at -168.9 ppm is shifted upfield compared to the compound **30-F** but remains within the range of triarylfluoroborate anions.<sup>25-26</sup> Solutions of this anion are stable for up to 3 days in  $CH_3CN$  or THF at ambient temperature. Addition of ca. 2 equivalents of water to solutions of **30-F<sup>-</sup>** in  $CH_3CN$  results in the formation of the neutral borane **30** and hydrated fluoride ions as indicated by the appearance of a  $^{19}F$  NMR signal at -121.9 ppm (Figure 38). By contrast, solutions of **30-F** in  $CH_3CN$  are perfectly stable when the same amount of water is added. This contrasting behavior can be assigned to: i) the absence of stabilizing Coulombic effects in **30-F<sup>-</sup>**; ii) the increased basicity of the sulfur atom in **30-F<sup>-</sup>** which competes with  $F^-$  for the Lewis acidic boron center. Thermodynamically, fluoride release from **30-F<sup>-</sup>** is further promoted by formation of a relatively strong  $lp(S) \rightarrow p(B)$  donor-acceptor interaction in **30** ( $E_{del} = 13.1$  kcal/mol) (Figure 39, Table 12).<sup>59</sup> The precipitation of the neutral borane from  $CH_3CN$  due to its poor solubility also

drives the release of  $F^-$  ions. These results suggest that  $30-F^-$  may be sufficiently labile to act as a potent nucleophilic  $F^-$  source.

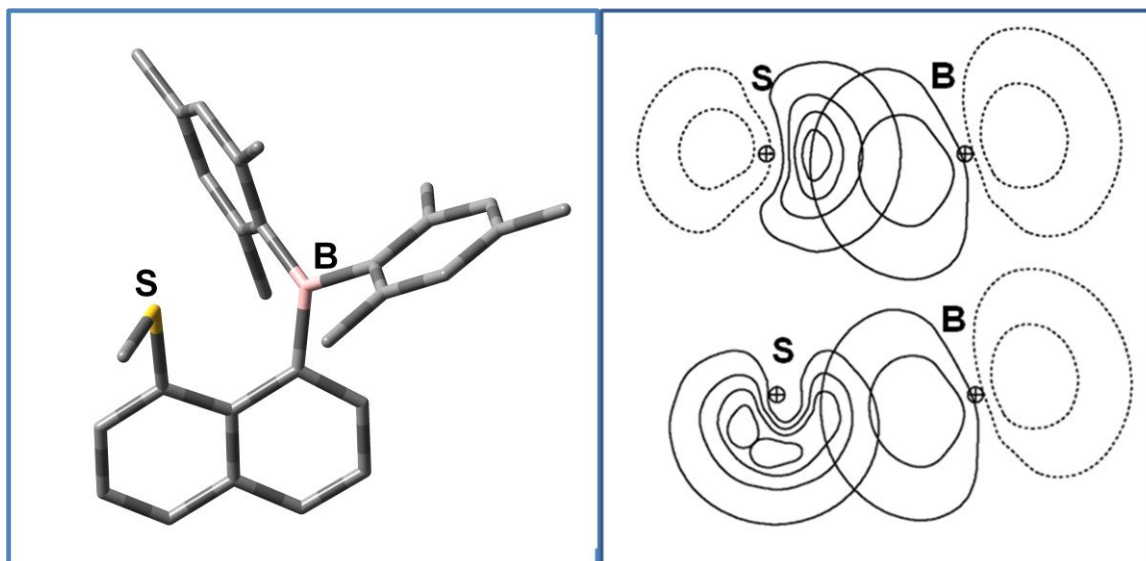


**Figure 39.** The optimized structure of borane **30** (hydrogen atoms omitted for clarity); Right: NBO contour plot showing the two lp(S)→p(B) donor-acceptor interactions in **30**.

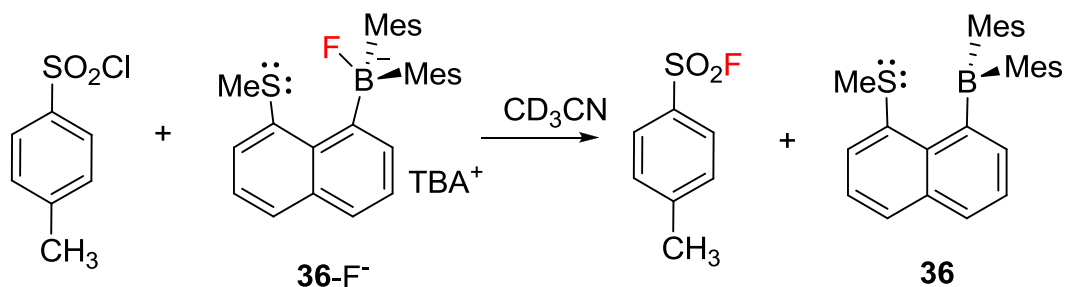
**Table 12.** Atom coordinates for the optimized structure of **30**.

Center Number	Coordinates(Angstroms)		
	X	Y	Z
S1	-1.535066	0.114487	2.088939
C2	-1.779487	-0.988091	3.544614
C3	-2.549280	-0.753046	0.880043
C4	-0.588595	-1.200698	-0.680511
C5	0.035846	1.477947	-0.259738
C6	-1.970266	-1.366018	-0.283552
C7	4.282373	-0.379272	-0.831505
H8	5.021934	0.048097	-1.504816
C9	1.948128	-0.507851	-0.079918
C10	-0.116600	-1.996841	-1.729095
H11	0.929451	-1.924232	-2.008895
C12	3.704916	-1.894252	0.931271
H13	3.989400	-2.653608	1.656263
C14	4.687344	-1.339476	0.103172
C15	-0.953663	-2.859915	-2.477050
H16	-0.535645	-3.438585	-3.294810
C17	-1.119897	3.413443	-1.243314
H18	-1.764503	3.814186	-2.022139
C19	-0.825085	2.040393	-1.254329
B20	0.427091	-0.063512	-0.235955
C21	2.949963	0.049908	-0.931627
C22	0.586840	2.378616	0.710207
C23	-4.213746	-2.329910	-0.755685
H24	-4.837288	-2.966329	-1.377004
C25	0.244023	3.737206	0.695550
H26	0.663130	4.390613	1.457208
C27	-0.612397	4.279336	-0.270415
C28	-2.833755	-2.210856	-1.076093
C29	2.358443	-1.509304	0.849378
C30	-3.909150	-0.874147	1.142318
H31	-4.330077	-0.369339	2.005612
C32	-2.293211	-2.939912	-2.174945
H33	-2.959140	-3.573124	-2.754436
C34	2.638536	1.096037	-1.989581
H35	3.494394	1.221575	-2.661007
H36	2.416563	2.072005	-1.544682
H37	1.773887	0.826122	-2.605797
C38	1.386357	-2.164746	1.810364
H39	0.489339	-2.528104	1.300221
H40	1.050231	-1.460730	2.581500
H41	1.858609	-3.012552	2.317470
C42	1.546660	1.930384	1.797309
H43	1.664437	2.719848	2.547077
H44	2.538986	1.702316	1.393423
H45	1.197247	1.029903	2.311025
C46	-1.424690	1.238470	-2.397562
H47	-1.819833	1.915415	-3.162019
H48	-2.251615	0.601682	-2.065825
H49	-0.694440	0.583001	-2.880963
C50	-4.750511	-1.654877	0.319862
H51	-5.807658	-1.732373	0.551850
C52	6.137348	-1.752882	0.222952
H53	6.231657	-2.795733	0.545224
H54	6.667858	-1.135652	0.961375
H55	6.665323	-1.643140	-0.730522
C56	-0.985686	5.744401	-0.251160
H57	-0.163621	6.362759	0.126172
H58	-1.852233	5.924158	0.400214
H59	-1.250457	6.103652	-1.251401
H60	-2.830913	-1.029222	3.838389
H61	-1.414567	-1.997122	3.337455
H62	-1.199392	-0.553984	4.364834

### 3.4 Nucleophilic reactions using **30-F<sup>-</sup>**

#### 3.4.1 TBACN as a nucleophile for demethylation

With freshly prepared solutions of **30-F<sup>-</sup>** from the reaction of **30-F** and TBACN in hand, we have decided to investigate the fluorination ability of **30-F<sup>-</sup>** with different substrates in CD<sub>3</sub>CN. We first studied the reaction of **30-F<sup>-</sup>** with *p*-tolylsulfonyl chloride (Figure 40), which as indicated by <sup>1</sup>H NMR and <sup>19</sup>F NMR spectroscopy, proceeded smoothly. The <sup>1</sup>H NMR spectrum shows the formation of the neutral borane **30** and a <sup>19</sup>F NMR resonance at 62 ppm, corresponding to *p*-tolylsulfonyl fluoride. Similarly, the addition of benzoyl chloride also results in formation of **30** and benzoyl fluoride which displays a resonance at 13.4 ppm in the <sup>19</sup>F NMR spectrum. For substrates such as benzylchloride and 1-bromooctane, the fluorination reactions only occur upon elevation of the temperature to about 70 °C. When benzylchloride is added, the major product is benzylfluoride with the major peak at -209 ppm in <sup>19</sup>F NMR spectrum. In the case of 1-bromooctane, formation of 1-octene is observed indicating that elimination occurs. This side reaction is non-negligible as the 1-fluorooctane/1-octene ratio is close to 1.

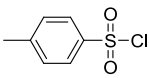
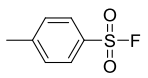
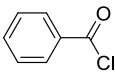
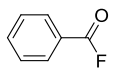
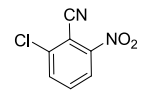
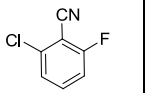
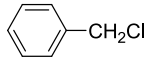
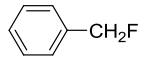


**Figure 40.** Reaction of **30-F<sup>-</sup>** with *p*-tolylsulfonyl chloride in CD<sub>3</sub>CN.

### 3.4.2 TBASPh as a nucleophile for demethylation

Addition of substrates such as *p*-tolylsulfonyl chloride or benzoyl chloride to solutions of **30-F**<sup>-</sup> obtained from **30-F** and TBASPh (Table 13, entries 1 and 2) results in the rapid and high yield fluorination of *p*-tolylsulfonyl fluoride and benzoyl chloride at room temperature. Using the same protocol, fluorination of activated aromatic substrates such as 1-chloro-2-cyano-3-nitrobenzene can also be implemented, albeit with longer reaction times (entry 3). For substrates such as benzylchloride and 1-bromooctane (entries 4 and 5), fluorination occurs upon elevation of the temperature to 70 °C. Formation of 1-fluorooctane is accompanied by elimination which produces 1-octene in 53% yield. The 1-fluorooctane/1-octene ratio observed with **30-F**<sup>-</sup> in MeCN at 70 °C is comparable to that observed with TBAF\* (~40%/60%) in THF at room temperature<sup>89</sup> and distinctly lower than that observed for TBAT (~85%/15%) in MeCN upon reflux for 24 h.<sup>92</sup> These comparisons suggest that the TBA salt of **30-F**<sup>-</sup> dissociates upon elevation of the temperature to produce **30** and TBAF\*. While the synthesis of the latter reagent necessitates the use of dry conditions, our approach can be implemented in two simple steps starting from aqueous fluoride solutions.

**Table 13.** Fluorination reaction results. (a. All yields are calculated from integration of the  $^1\text{H}$  NMR spectra.)

entry	substrate	conditions	product	yield (%) <sup>a</sup>
1		<b>30-F<sup>-</sup></b> (1.4 equiv) 25 °C CD <sub>3</sub> CN, 5 min		>95
2		<b>30-F<sup>-</sup></b> (1.4 equiv) 25 °C CD <sub>3</sub> CN, 5 min		>95
3		<b>30-F<sup>-</sup></b> (1.2 equiv) 25 °C CD <sub>3</sub> CN, 2 h		>95
4		<b>30-F<sup>-</sup></b> (2 equiv) 70 °C CD <sub>3</sub> CN, 1 h		80
5	1-C <sub>8</sub> H <sub>17</sub> Br	<b>30-F<sup>-</sup></b> (2 equiv) 70 °C CD <sub>3</sub> CN, 1 h	1-C <sub>8</sub> H <sub>17</sub> F	45

### 3.5 Conclusion

The results presented in this paragraph show that the cationic borane [**30**]OTf can capture the fluoride ions in wet protic solvents to form the anhydrous zwitterionic fluoroborate **30-F**. The latter is stabilized by strong Coulombic effects as well as by the formation of a B-F→S bridge. The stabilizing effects can be removed by demethylation of the sulfonium moiety. This demethylation reaction affords the fluoroborate **30-F<sup>-</sup>** which acts as a potent reagent for nucleophilic fluorination reactions in organic solvents. The reactivity of **30-F<sup>-</sup>** is reminiscent of that of anhydrous TBAF (**36**). While preparation of the latter necessitates the use of dry conditions, the new approach

described in this chapter can be implemented in two simple steps starting from aqueous fluoride solutions. We are currently testing the use of **[30]<sup>+</sup>** in [<sup>18</sup>F]-radiofluorination reactions.

### 3.6 Experimental section

**General Considerations.** **30-OTf** was prepared as described in the preceding chapter. Acetonitrile was dried by refluxing over phosphorus pentoxide, followed by distillation under N<sub>2</sub>. Methanol (ACS reagent grade) was used without purification or drying. NMR spectra were recorded on a Varian Unity Inova 400 FT NMR (399.59 MHz for <sup>1</sup>H, 375.96 MHz for <sup>19</sup>F, 128.19 MHz for <sup>11</sup>B, 100.45 MHz for <sup>13</sup>C) spectrometers at ambient temperature.

**Formation of 30-F in aqueous methanolic solutions.** KF (45 mg) was added to a 0.5 ml MeOH/H<sub>2</sub>O (3:2, v/v) solution of **30-OTf** (21 mg). Sonication of the mixture for 5 minutes resulted in the precipitation of **30-F** which was recovered by filtration in a 75% yield (12 mg).

**Fluorination reactions from mixing 30-F and TBACN.** In an NMR tube, TBACN (2.7 mg, 7.7 μmol) was added to a CD<sub>3</sub>CN solution of **30-F** (3.5 mg, 7.7 μmol). After 20 minutes, the substrate was added to the solution. The reaction was monitored by <sup>1</sup>H NMR and <sup>19</sup>F NMR spectroscopy.

**Fluorination reactions from mixing 30-F and TBASPh.** In an NMR tube, TBASPh (2.7 mg, 7.7 μmol) was added to a CD<sub>3</sub>CN solution of **30-F** (3.5 mg, 7.7 μmol). After 20 minutes, the substrate was added to the solution. The reaction, which was

allowed proceed under the conditions listed in Table 13 of the main text, was monitored by  $^1\text{H}$  NMR and  $^{19}\text{F}$  NMR spectroscopy. The yields were calculated by integration of the relevant  $^1\text{H}$  NMR spectra (Figure 41).

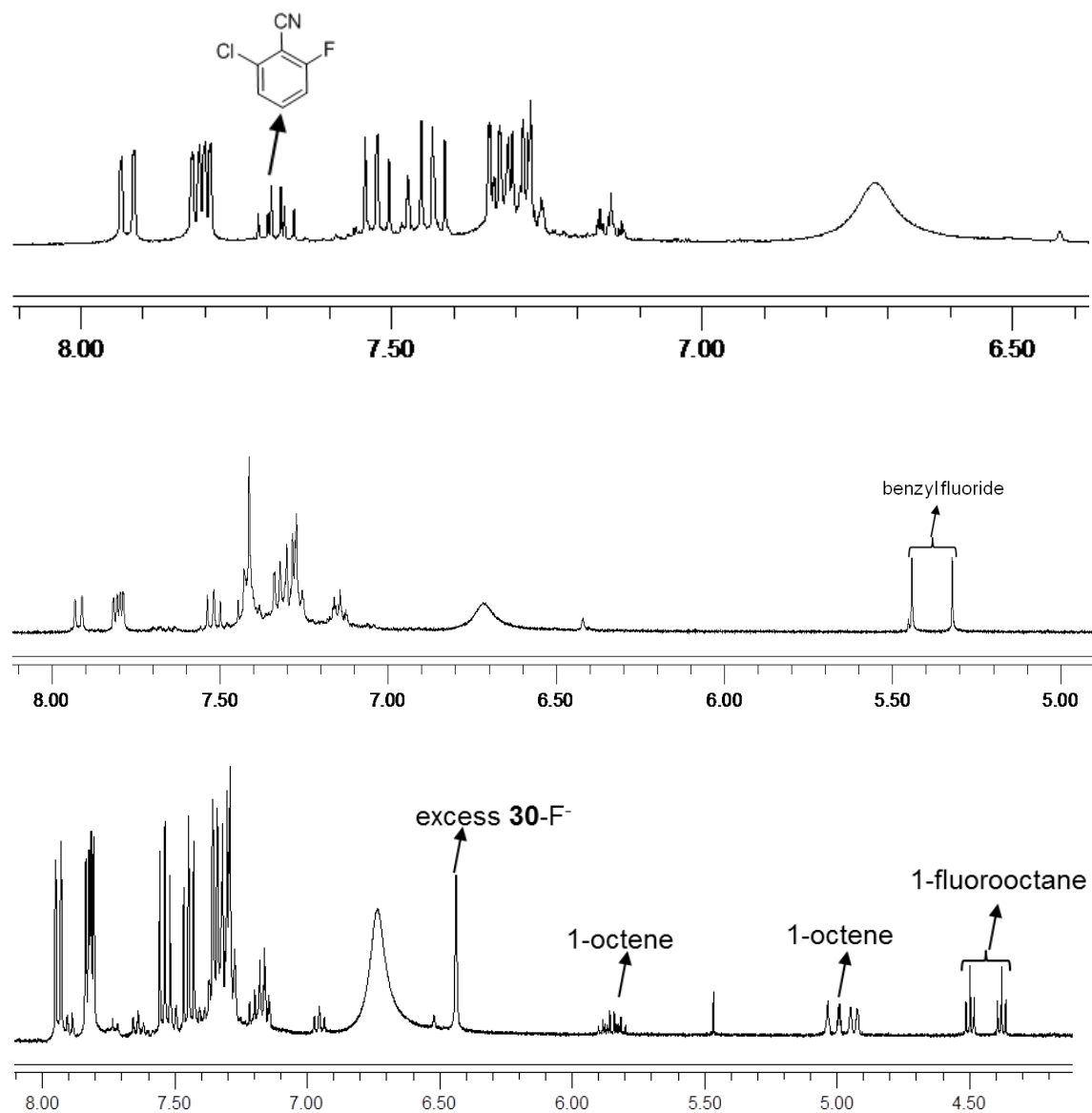


**Figure 41.**  $^1\text{H}$  NMR spectra of reactions of entry 3, 4 and 5.



**Computational details:** DFT calculations (full geometry optimization) were carried out with the Gaussian 03<sup>116</sup> program using the B3LYP functional. Geometry optimization was carried out with the following mixed basis set: B, F: 6-31+g(d'); S: 6-31+g(d); C, H: 6-31g. Frequency calculations, which were carried out on the optimized structure of the compound, confirmed the absence of any imaginary frequencies. The Natural Bond Orbital (NBO) analyses<sup>117</sup> were carried out using the stand along PC version of GENNBO 5.0 program.

CHAPTER IV  
A BIDENTATE LEWIS ACID WITH A TELLURONIUM ION AS AN ANION-  
BINDING SITE\*

#### 4.1 Introduction

The chemistry of polyfunctional Lewis acids constitutes a rapidly expanding field with important applications in anion sensing. Most of the polyfunctional Lewis acids investigated to date contain group 12,<sup>118-121</sup> 13<sup>10, 20, 23, 25, 122-124</sup> and 14<sup>125-128</sup> elements as Lewis acidic binding sites incorporated in both homonuclear<sup>10, 20, 23, 25, 118-128</sup> and heteronuclear<sup>57, 129-131</sup> motifs.<sup>26</sup> Advances in the chemistry of boron-based heteronuclear bidentate Lewis acids have shown that anion binding at the boron center can be assisted by the participation of a secondary Lewis acidic site.<sup>57, 129-131</sup> Unlike most bidentate diboranes, some of these heteronuclear Lewis acids display an increased stability to protic media as well as uncompromised anion affinities.<sup>57, 131</sup> In a fundamental effort aimed at broadening the type of Lewis acidic moiety that could be employed in such systems, we have recently become interested in the use of onium ions as secondary Lewis acidic sites. Initial results obtained in pursuit of this idea have revealed that the latent Lewis acidity of phosphonium or sulfonium ions can be exploited

---

\*Reprinted in part permission from, “A bidentate Lewis acid with a telluronium ion as an anion-binding site”; Zhao, H.; Gabbaï, F. P., *Nat. Chem.* **2010**, 2, 984. Copyright 2010 by the Nature Publishing Group.

for the recognition of potentially toxic anions such as fluoride and cyanide in protic environments.<sup>49, 61</sup> These favourable effects can be illustrated by the anion affinity of the boron-based Lewis acids  $[28]^+$  which is enhanced by electron donation from a filled orbital of the anion ( $A^-$ ) into a low lying E-C  $\sigma^*$ -orbital of the onium center in the corresponding complexes (Figure 42).

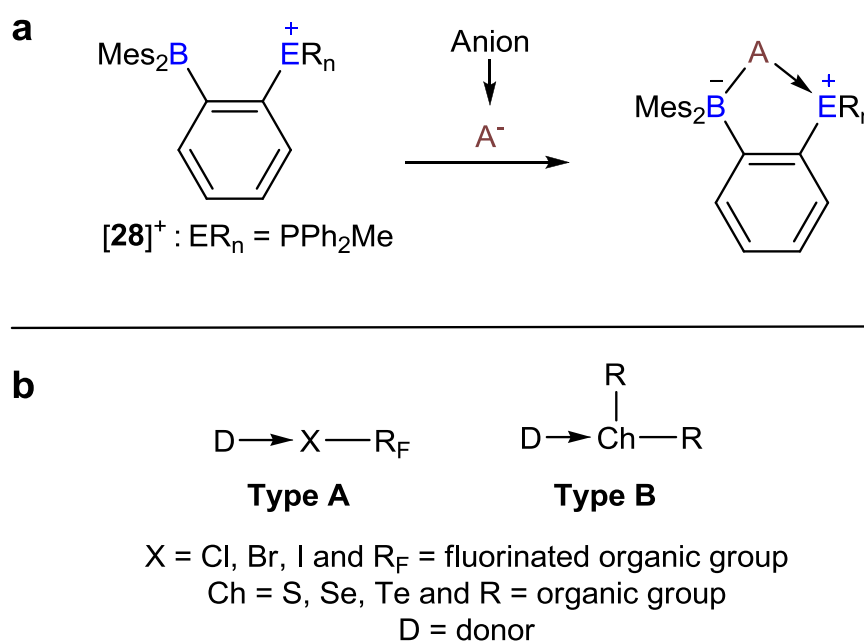


**Figure 42.** Anion complexation by chelating cationic boranes and Lewis acidic properties of group 16 and 17 compounds. a, Anion chelation by *ortho*-phenylene-phosphonium and -sulfonium boranes. b, Donor-acceptor interactions in halogen-bonded and chalcogen-bonded complexes.

These  $A^- \rightarrow E^+$  donor-acceptor interactions are reminiscent of those involved in halogen-bonded (Type A)<sup>132</sup> or chalcogen-bonded (Type B)<sup>133-138</sup> complexes. Although

electron donation from the filled-orbital of the donor into the  $\sigma^*$ -orbital of the X-C or Ch-C bond (X = halogen, Ch = chalcogen) plays a role in the formation of such complexes, electrostatic effects arising from the polarisability and relative electropositivity of the X or Ch atom may be the most important factor.<sup>75, 132, 136</sup> In agreement with this view, the strength of the donor-acceptor interactions observed in these complexes has been shown to increase in the order Cl < Br < I for complexes of Type A<sup>132</sup> and S < Se < Te for complexes of Type B.<sup>136</sup> Realizing that similar effects may control the strength of  $A^- \rightarrow E^+$  donor-acceptor interactions, we are now considering the use of heavier onium ions as Lewis acidic sites. In an initial exploration of this idea, we have decided to synthesize and investigate a bidentate Lewis acid containing a telluronium ion and compare its properties to its sulfur analogue. Although evidence for the Lewis acidity of telluronium ions can be gleaned from short anion-cation contacts in the crystal structures of their salts,<sup>139-142</sup> efforts to use such onium ions for catalysis or anion recognition have never been reported.

#### 4.2 Synthesis and characterization of the telluronium borane and its sulfur analog

Implementing some of the synthetic approaches that we have recently employed for the synthesis of sulfonium boranes,<sup>61</sup> the tetrakis(THF)lithium salt of dimesityl-1,8-naphthalenediylborate<sup>56</sup> (THF = tetrahydrofuran) was allowed to react with diphenylditelluride to afford the corresponding telluro-borane (**37**, Figure 43). The latter reacted smoothly with methyltriflate (MeOTf) to afford the borane/telluronium [**37**]<sup>+</sup> which has been isolated as triflate salt. For comparative purposes, we also synthesized

the sulfonium analog of [37]OTf, namely [38]OTf, by an analogous series of steps. Compounds **37**, **38**, [37]OTf and [38]OTf have been characterized by multinuclear Nuclear Magnetic Resonance (NMR) spectroscopy and elemental analysis. In all four cases, the boron centre remains trigonal planar in agreement with the detection of a broad  $^{11}\text{B}$ -NMR resonance in the 60 – 70 ppm range.<sup>49, 61</sup> For **37** and **38**, the  $^1\text{H}$  NMR spectrum exhibits six distinct resonances that correspond to the aromatic CH groups of the asymmetrically substituted naphthalene backbone. Four aryl ( $\text{CH}^{\text{Mes}}$ ) and six methyl proton ( $\text{CH}_3^{\text{Mes}}$ ) resonances are observed for the two mesityl groups, thus, indicating the existence of a congested structure. The  $^1\text{H}$  NMR spectra of [37]OTf and [38]OTf are consistent with the existence of two diastereomers arising from chirality at the group 16 onium centre and helical chirality at the boron centre. Each of these diastereomers gives rise to four  $\text{CH}^{\text{Mes}}$  resonances and six  $\text{CH}_3^{\text{Mes}}$  resonances leading to a total of eight  $\text{CH}^{\text{Mes}}$  and twelve  $\text{CH}_3^{\text{Mes}}$  signals. Accordingly, two resonances are observed for the group 16-bound methyl group. In the case of [37]<sup>+</sup>, the presence of these diastereomers can be further ascertained by the detection of two  $^{125}\text{Te}$  NMR resonances at 660 and 677 ppm,<sup>143-144</sup> whose integration ratio corresponds to that observed for the  $^1\text{H}$  NMR signals of each diastereomer.

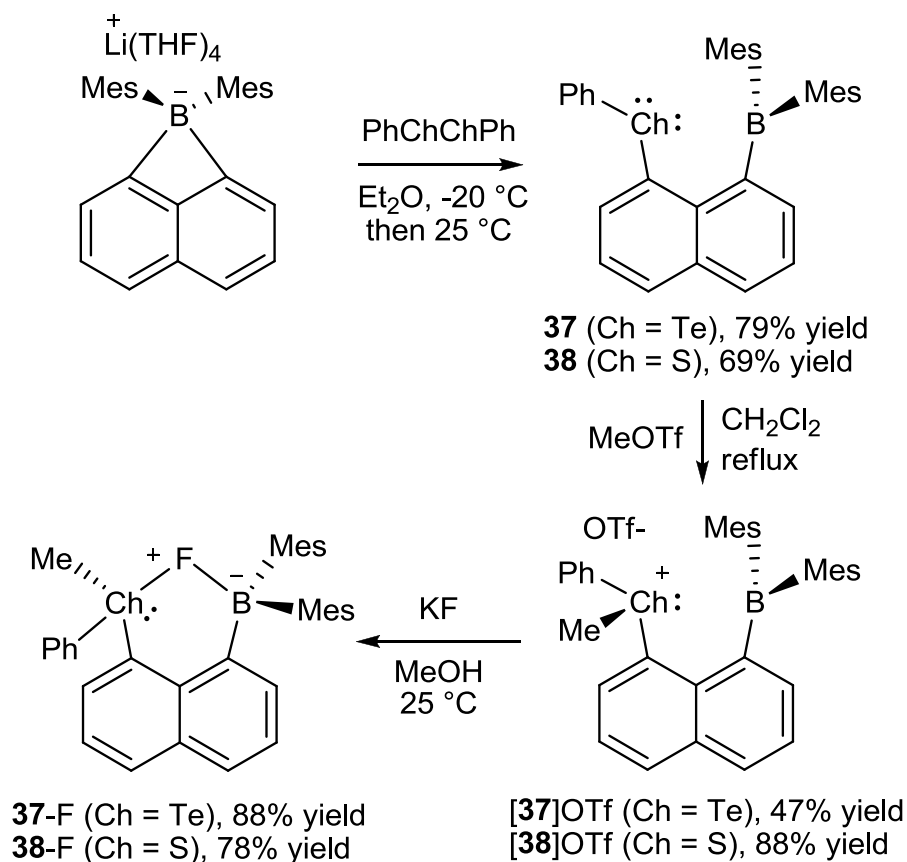


**Figure 43.** Synthesis and reactivity of the chalcogenium borane salts **[37]OTf** and **[38]OTf**. The chalcogenium borane triflate salts **[37]OTf** and **[38]OTf** are converted into the corresponding fluoride complexes **37-F** and **38-F** by reaction with KF in methanol.

The crystal structures of **37** and **38** have been determined experimentally (Figure 44 and Figure 45, Table 14).<sup>145</sup> The B-Ch (Ch = chalcogen) distances in **37** (B-Te = 3.007(2) Å) and **38** (B-S = 2.952(3) Å) are well within the sum of the van der Waals radii of the two elements (1.50 Å for F, 1.80 Å for S, 2.10 Å for Te), thus suggesting the presence of a donor–acceptor interaction in these two compounds.<sup>58</sup> In agreement with

this view, the boron atom in each compound adopts a slightly pyramidalized structure as indicated by sum of the C-B-C angles ( $\Sigma(\text{B-C-B}) = 357.21(2)^\circ$  for **37** and  $358.3(2)^\circ$  for **38**). This small angular distortion may also partly result from steric effects inherent to *peri*-substituted naphthalene derivatives. The existence of such effects is corroborated by the observation that C(9)-C(1)-B angles in **37** ( $126.1(2)^\circ$ ) and **38** ( $126.9(2)^\circ$ ) deviate markedly from the ideal value of  $120^\circ$ . To shed further light on the bonding characteristics of **37** and **38**, the geometry of these two compounds has been optimized using Density Functional Theory (DFT) methods (functional: BP86; mixed basis set: Te: aug-cc-pvTz-pp; B: 6-31+g(d<sup>7</sup>); S: 6-31+g(d); C, H: 6-31g). The optimized geometries, which are close to those experimentally determined ( $\text{B-Te}_{\text{calc}} = 3.014 \text{ \AA}$  and  $\text{B-S}_{\text{calc}} = 2.971 \text{ \AA}$ ), were subjected to a Natural Bond Orbital (NBO) analysis which identified a  $\text{lp}(\text{Ch}) \rightarrow \text{p}(\text{B})$  donor-acceptor interaction (lp = lone-pair orbital; p = p orbital) (Figure 46). As shown by deletion calculations,<sup>49</sup> this interaction contributes to the stability of the molecules by  $E_{\text{del}} = 32.4 \text{ kcal/mol}$  in the case of **37** and  $E_{\text{del}} = 16.5 \text{ kcal/mol}$  in the case of **38**. In turn, the boron center of these derivatives experiences significant electron donation from the chalcogen.

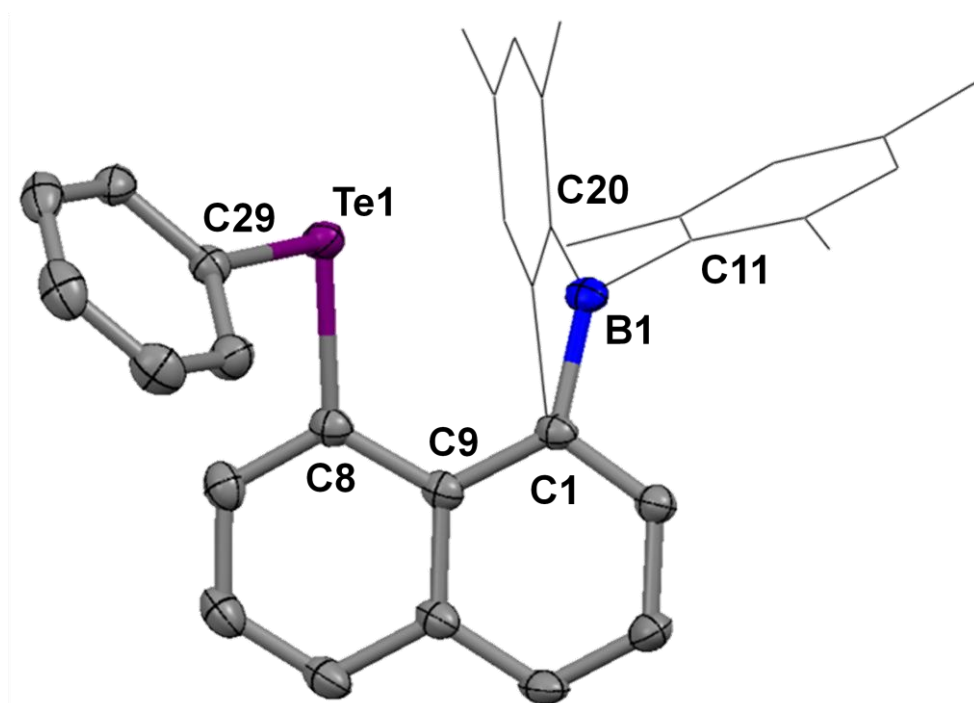


**Figure 44.** Crystal structure of the neutral borane **37** (thermal ellipsoids are drawn at 50% probability levels; hydrogen atoms are omitted and the mesityl ligands are represented by thin lines for clarity). Selective bond distances [ $\text{\AA}$ ] and bond angles [ $^\circ$ ]: Te(1)-C(8) 2.108(2), Te(1)-C(29) 2.119(2), C(8)-C(9) 1.422(3), C(1)-C(9) 1.434(3), C(1)-B(1) 1.576(3), C(11)-B(1) 1.590(3), C(20)-B(1) 1.597(3); C(8)-Te(1)-C(29) 93.11(8), C(9)-C(1)-B(1) 126.88(19), C(9)-C(8)-Te(1) 120.34(15), C(8)-C(9)-C(1) 123.34(19), C(1)-B(1)-C(11) 115.30(18), C(1)-B(1)-C(20) 123.46(19), C(11)-B(1)-C(20) 118.45(18).



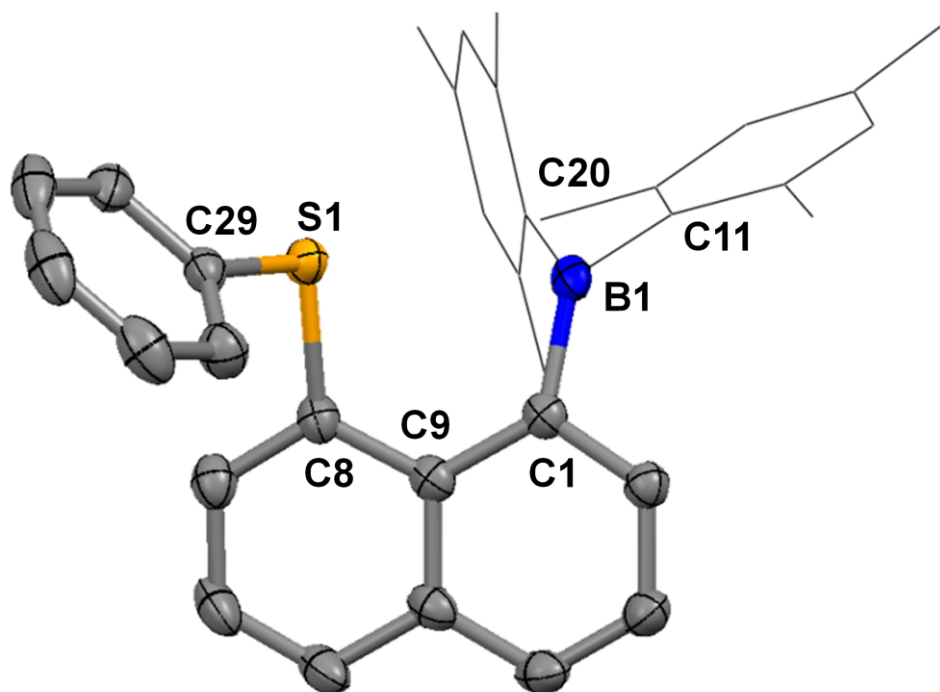


**Figure 45.** Crystal structure of the neutral borane **38** (thermal ellipsoids are drawn at 50% probability levels; hydrogen atoms are omitted and the mesityl ligands are represented by thin lines for clarity). Selective bond distances [ $\text{\AA}$ ] and bond angles [ $^\circ$ ]: S(1)-C(29) 1.779(2), S(1)-C(8) 1.780(2), C(1)-B(1) 1.569(3), C(1)-C(9) 1.440(3), C(8)-C(9) 1.423(3), C(11)-B(1) 1.587(3), C(20)-B(1) 1.594(3); C(29)-S(1)-C(8) 100.08(11), C(9)-C(1)-B(1) 126.1(2), C(9)-C(8)-S(1) 120.47(18), C(8)-C(9)-C(1) 123.1(2), C(1)-B(1)-C(11) 117.1(2), C(1)-B(1)-C(20) 122.0(2), C(11)-B(1)-C(20) 119.2(2).

**Table 14.** Crystal data, data collections, and structure refinements for **37** and **38**.

Crystal data	<b>37</b>	<b>38</b>
formula	C <sub>34</sub> H <sub>33</sub> BTe	C <sub>34</sub> H <sub>33</sub> BS
$M_r$	580.01	484.47
crystal size (mm <sup>3</sup> )	0.32 x 0.24 x 0.13	0.15 x 0.10 x 0.08
crystal system	Monoclinic	Monoclinic
space group	P2(1)/c	P2(1)/n
$a$ (Å)	15.3549(18)	15.337(2)
$b$ (Å)	12.2755(14)	12.0381(16)
$c$ (Å)	17.3029(14)	15.458(2)
$\alpha$ (°)	90	90
$\beta$ (°)	123.819(7)	111.1150(10)
$\gamma$ (°)	90	90
$V$ (Å <sup>3</sup> )	2709.6(5)	2662.5(6)
$Z$	4	4
$\rho_{\text{calc}}$ (g cm <sup>-3</sup> )	1.422	1.209
$\mu$ (mm <sup>-1</sup> )	1.119	0.143
$F(000)$	1176	1032
Data Collection		
$T$ (K)	110(2)	110(2)
scan mode	$\omega$	$\omega$
$hkl$ range	-20 → +20 -16 → +16 -22 → +23	-17 → +17 -13 → +13 -17 → +17
measd reflns	30557	26686
unique reflns [ $R_{\text{int}}$ ]	6497 [0.0509]	4174 [0.1727]
reflns used for refinement	6497	4174
Refinement		
refined parameters	325	325
Goof	1.001	1.000
$R_1$ , <sup>a</sup> $wR_2$ <sup>b</sup> all data	0.0325, 0.0835	0.0744, 0.1807
$\rho_{\text{fin}}$ (max/min) (e Å <sup>-3</sup> )	1.316, -0.433	0.513, -0.563

$$^a R_1 = \frac{\sum ||F_o| - |F_c||}{\sum |F_o|}. \quad ^b wR_2 = \left[ \frac{[\sum w(F_o^2 - F_c^2)^2]}{[\sum w(F_o^2)^2]} \right]^{1/2}.$$

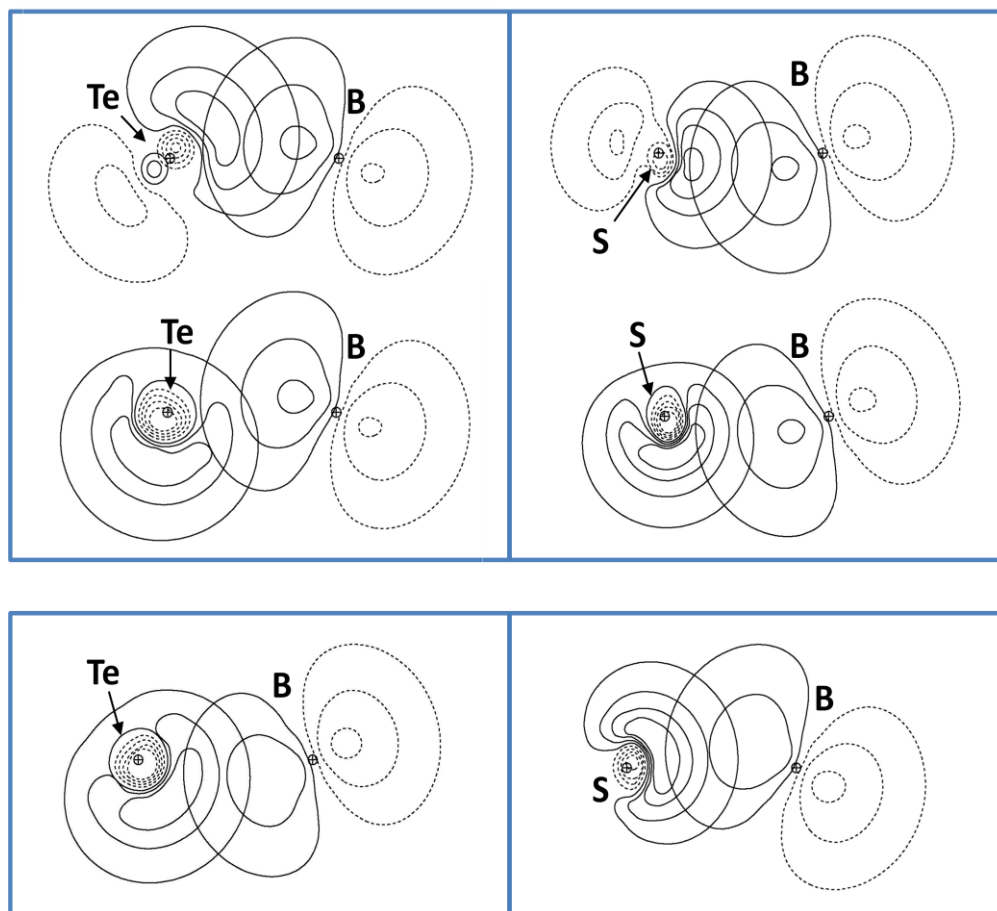


**Figure 46.** NBO contour plots showing the  $lp(\text{Ch}) \rightarrow p(\text{B})$  donor-acceptor interactions in **37** (top left), **38** (top right), **[37]OTf** (bottom left) and **[38]OTf** (bottom right). Two lone pairs of chalcogen atoms (one is  $p$ -orbital character and the other is  $s$ -orbital character) are involved in the donor-acceptor interactions in **37** and **38**. Only one lone pair of  $s$ -orbital character is involved in the donor-acceptor interactions in **[37]OTf** and **[38]OTf**.

To assess the effect of group 16 methylation on this lp(Ch)→p(B) donor-acceptor interaction, the crystal structures of [37]OTf and [38]OTf have also been determined (Figure 47 and Figure 48, Table 15).<sup>145</sup> While there are no unusual intermolecular contacts in the structure of [38]OTf, one of the oxygen atoms of the triflate anion in [37]OTf forms a short contact of 2.904(5) Å with the tellurium center in agreement with the anticipated higher Lewis acidity of the telluronium unit. Further examination of these structures show that: i) the boron atom in each cation becomes trigonal planar ( $\Sigma(\text{B-C-B}) = 359.8(5)^\circ$  for [37]OTf and  $359.7(2)^\circ$  for [38]OTf); ii) the B-Ch distance is significantly increased in the cationic species (B-Te = 3.244(6) Å for [37]OTf, B-S = 3.129(3) Å for [38]OTf). These structural features may be assigned to the lower donicity induced by oxidative methylation of the group 16 element. The increased bulk around the chalcogen atom in [37]OTf and [38]OTf may also play a role in the increased B-Ch separation, a conclusion supported by the large C(9)-C(1)-B angles of  $129.3(2)^\circ$  and  $129.4(5)^\circ$  observed in [37]OTf and [38]OTf, respectively. Further insights into the strength of the lp(Ch)→p(B) in [37]<sup>+</sup> and [38]<sup>+</sup> were obtained from computational studies carried out at the level of theory used for 37 and 38. The optimized structures of the two cations, which are close to those experimentally determined (B-Te<sub>calc</sub> = 3.222 Å and B-S<sub>calc</sub> = 3.091 Å), were subjected to NBO analyses. These analyses show that lp(Ch)→p(B) donor-acceptor interactions persist in [37]<sup>+</sup> and [38]<sup>+</sup>. These interactions, which account for  $E_{\text{del}} = 10.8$  kcal/mol and  $E_{\text{del}} = 8.2$  kcal/mol to the stability of [37]<sup>+</sup> and [38]<sup>+</sup>, are significantly lower than those in 37 and 38, in agreement with the lower donicity of the chalcogenium groups (Figure 46).

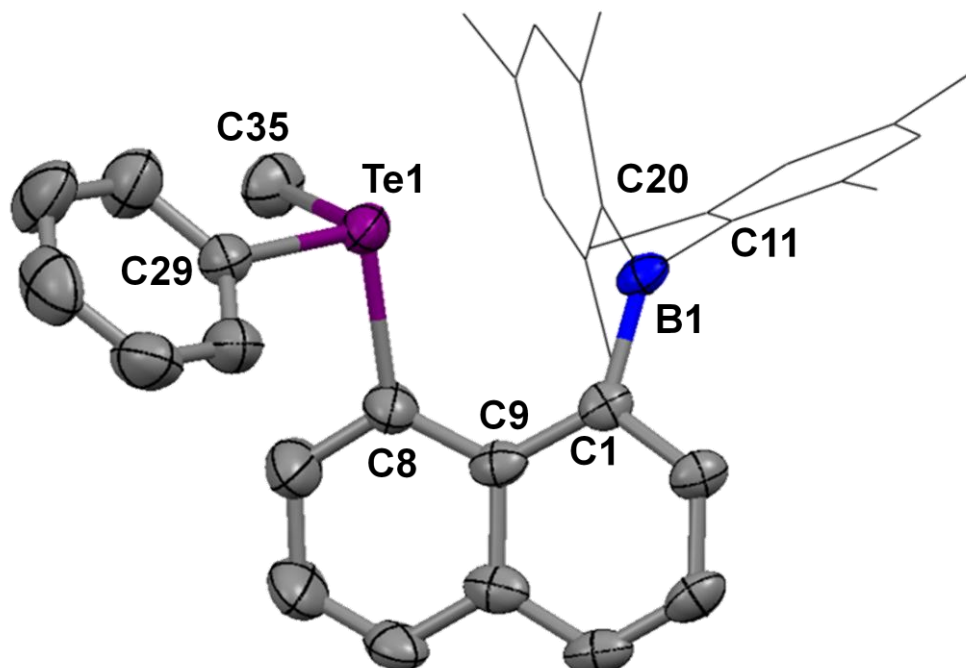


**Figure 47.** Crystal structure of the neutral borane [37]OTf (thermal ellipsoids are drawn at 50% probability levels; hydrogen atoms and triflate anion are omitted and the mesityl ligands are represented by thin lines for clarity). Selective bond distances [ $\text{\AA}$ ] and bond angles [ $^\circ$ ]: Te(1)-C(35) 2.102(6), Te(1)-C(29) 2.111(6), Te(1)-C(8) 2.134(5), C(1)-C(9) 1.437(7), C(1)-B(1) 1.586(7), C(8)-C(9) 1.414(8), C(11)-B(1) 1.573(8), C(20)-B(1) 1.572(7); C(35)-Te(1)-C(29) 99.9(2), C(35)-Te(1)-C(8) 96.3(2), C(29)-Te(1)-C(8) 94.7(2), C(9)-C(1)-B(1) 129.4(5), C(9)-C(8)-Te(1) 121.6(4), C(8)-C(9)-C(1) 125.0(5), C(20)-B(1)-C(11) 121.1(4), C(20)-B(1)-C(1) 122.7(5), C(11)-B(1)-C(1) 116.0(4).

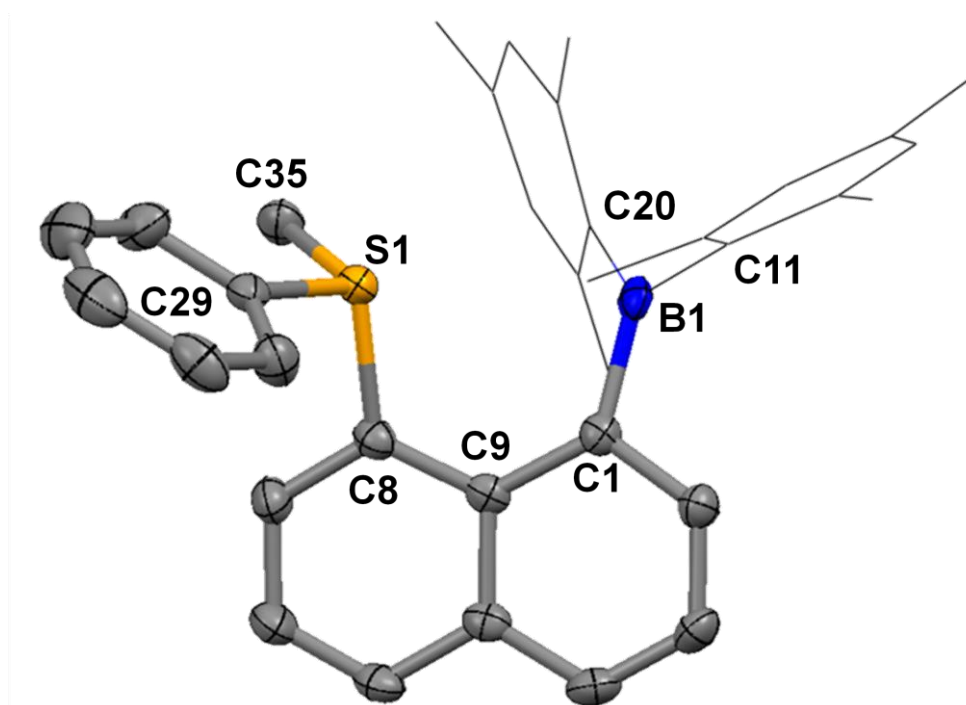


**Figure 48.** Crystal structure of the neutral borane [38]OTf (thermal ellipsoids are drawn at 50% probability levels; hydrogen atoms and triflate anion are omitted and the mesityl ligands are represented by thin lines for clarity). Selective bond distances [ $\text{\AA}$ ] and bond angles [ $^\circ$ ]: S(1)-C(8) 1.792(3), S(1)-C(29) 1.793(3), S(1)-C(35) 1.798(3), C(1)-C(9) 1.451(4), C(1)-B(1) 1.582(4), C(8)-C(9) 1.418(4), C(11)-B(1) 1.576(4), C(20)-B(1) 1.570(4); C(8)-S(1)-C(29) 101.92(13), C(8)-S(1)-C(35) 103.66(14), C(29)-S(1)-C(35) 105.11(14), C(9)-C(1)-B(1) 129.3(2), C(9)-C(8)-S(1) 119.9(2), C(8)-C(9)-C(1) 126.2(2), C(20)-B(1)-C(11) 120.8(2), C(20)-B(1)-C(1) 122.1(2), C(11)-B(1)-C(1) 116.8(2).

**Table 15.** Crystal data, data collections, and structure refinements for [37]OTf and [38]OTf.

Crystal data	[37]OTf	[38]OTf
formula	C <sub>36</sub> H <sub>36</sub> BF <sub>3</sub> O <sub>3</sub> STe	C <sub>36</sub> H <sub>36</sub> BF <sub>3</sub> O <sub>3</sub> S <sub>2</sub>
$M_r$	744.12	648.58
crystal size (mm <sup>3</sup> )	0.21 x 0.17 x 0.11	0.14 x 0.13 x 0.10
crystal system	Monoclinic	Triclinic
space group	P2(1)/c	P-1
$a$ (Å)	8.4011(16)	8.632(5)
$b$ (Å)	18.829(4)	10.482(6)
$c$ (Å)	21.449(4)	18.755(10)
$\alpha$ (°)	90	90.939(7)
$\beta$ (°)	97.903(2)	102.507(6)
$\gamma$ (°)	90	100.441(6)
$V$ (Å <sup>3</sup> )	3360.6(11)	1626.5(15)
$Z$	4	2
$\rho_{\text{calc}}$ (g cm <sup>-3</sup> )	1.471	1.324
$\mu$ (mm <sup>-1</sup> )	0.998	0.216
$F(000)$	1504	680
Data Collection		
$T$ (K)	110(2)	110(2)
scan mode	$\omega$	$\omega$
	-9 → +9	-11 → +11
$hkl$ range	-21 → +21	-13 → +13
	-24 → +24	-24 → +24
measd reflns	29312	19942
unique reflns [ $R_{\text{int}}$ ]	5284 [0.0547]	7878 [0.1168]
reflns used for refinement	5284	7878
Refinement		
refined parameters	406	406
Goof	1.002	0.999
R1, <sup>a</sup> wR2 <sup>b</sup> all data	0.0759 0.1730	0.1054 0.1405
$\rho_{\text{fin}}$ (max/min) (e Å <sup>-3</sup> )	1.874, -1.257	0.403, -0.423

$$^a R_1 = \frac{\sum ||F_o| - |F_c||}{\sum |F_o|}. \quad ^b wR_2 = \left[ \frac{[\sum w(F_o^2 - F_c^2)^2]}{[\sum w(F_o^2)^2]} \right]^{1/2}.$$

The UV-vis absorption spectra of these compounds in methanol (MeOH) display two distinct low energy bands centred at 353 nm and 312 nm in the case of  $[37]^+$  and 340 nm and 314 nm in case of  $[38]^+$  (Figure 49 and Figure 50). To elucidate the origin of these bands, the optimized structures of both cations were subjected to a Time Dependent-Density Functional Theory (TD-DFT) calculation (functional: MPW1PW91; mixed basis set: Te: aug-cc-pvTz-pp; B: 6-31+g(d'); S: 6-31+g(d); C, H: 6-31g)) using the PCM solvation with methanol as a solvent (PCM = Polarizable Continuum Model). Examination of the simulated spectra indicates that each of the low energy bands observed in the spectra of these cations mainly results from a few dominant excitations. The most red-shifted band at 353 nm for  $[37]^+$  and 340 nm for  $[38]^+$  arises from excitations ( $E_a$  and  $E_b$ , Figure 49 and Figure 50) which mostly involve the lowest unoccupied molecular orbital (LUMO) as the accepting orbital. The second band at 312 nm for  $[37]^+$  and 314 nm for  $[38]^+$  involves excitations ( $E_c$ , and  $E_d$  for  $[37]^+$ ,  $E_c$ ,  $E_d$  and  $E_e$  for  $[38]^+$ ) in which the LUMO+1, acts as the main accepting orbital.



Visualization of these orbitals indicate that the LUMO of  $[37]^+$  and  $[38]^+$ , bears an important contribution from the boron  $p_\pi$ -orbital (Figure 49 and Figure 50). This feature is reminiscent of simple triarylboranes which usually display a low energy band resulting from electronic excitations from filled orbitals into the boron-centred LUMO.<sup>5, 25, 146-149</sup> Interestingly, the LUMO+1 which is involved in the band detected at 312 nm for  $[37]^+$  and 314 nm for  $[38]^+$  bears an increased contribution from the Ch-C  $\sigma^*$ -orbital; this feature is especially noticeable in the case of the tellurium derivative  $[37]^+$  (Figure 49). The localization of the LUMO and LUMO+1 orbitals on the neighbouring heteroelements, as well as their involvement in the low energy electronic transitions, suggests that anion binding to these derivatives may be very efficiently monitored using spectrophotometric techniques.<sup>5</sup> It is also important to note that the localization of these two low lying vacant orbitals on the two heteroelements bodes well for the occurrence of anion chelation.

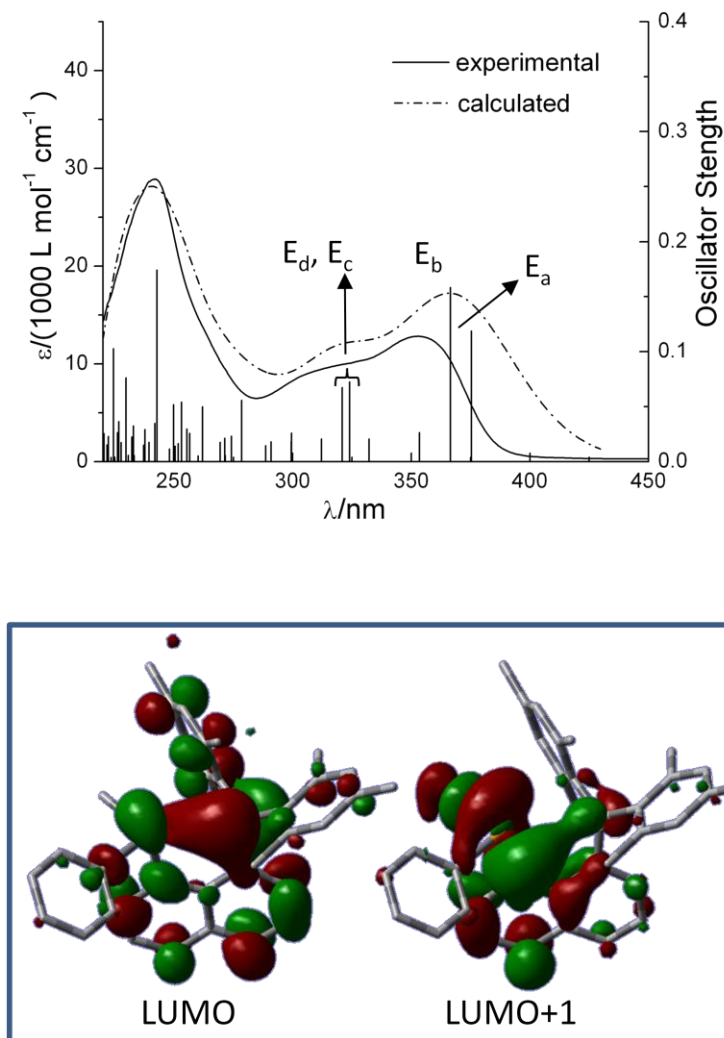


**Figure 49.** Photophysical properties of the chalcogenium borane  $[37]^+$ . Top: Experimental (methanol) and calculated UV-vis spectra. In addition to the simulated spectra, the computed excitations are shown as thin lines with heights proportional to the calculated oscillator strengths. Bottom: View of the LUMO and LUMO+1 (isovalue=0.03). These orbitals, which are implicated in  $E_{a-d}$ , bear a large component from the boron  $p_{\pi}$ - and Ch-C  $\sigma^*$ -orbitals.

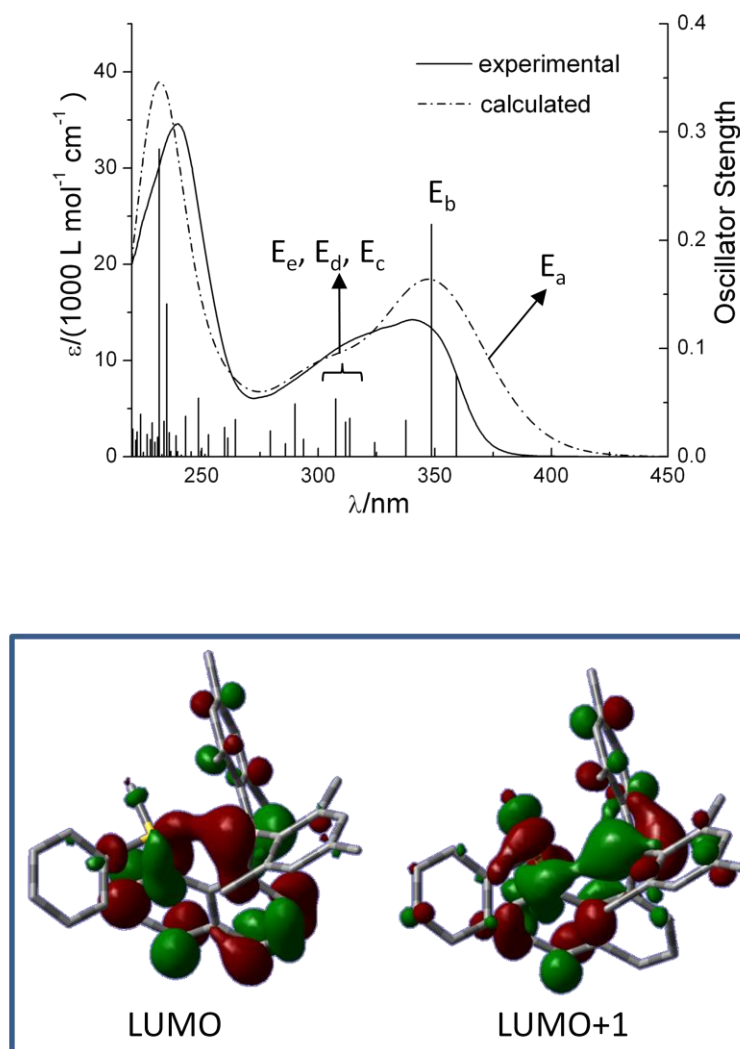


**Figure 50.** Photophysical properties of the chalcogenium borane  $[38]^+$ . Top: Experimental (methanol) and calculated UV-vis spectra. In addition to the simulated spectra, the computed excitations are shown as thin lines with heights proportional to the calculated oscillator strengths. Bottom: View of the LUMO and LUMO+1 (isovalue=0.03). These orbitals, which are implicated in  $E_{a-e}$ , bear a large component from the boron  $p_{\pi}$ - and Ch-C  $\sigma^*$ -orbitals.

### 4.3 Anion affinity of the sulfonium borane and telluronium borane

#### 4.3.1 Fluoride affinity

Having these two analogues in hand, we decided to investigate their fluoride ion affinity under dilute conditions in MeOH using UV-vis spectroscopy (Figure 51). Addition of fluoride ions to  $[37]^+$  (0.0673 mM) resulted in the progressive quenching of the two lowest energy bands, suggesting coordination of the fluoride anion to both the boron and tellurium atom. The resulting data was fitted to a 1:1 binding isotherm to afford  $K = 750 (\pm 100) \text{ M}^{-1}$  (Figure 51). By contrast, addition of 1000 eq. of fluoride ions to  $[38]^+$  did not result in any changes of the UV-vis spectrum, indicating that  $[38]^+$  has no or very little affinity for fluoride ions in this solvent. A similar behaviour was observed in the case of  $[1\text{-Mes}_2\text{B-8-Me}_2\text{S-C}_{10}\text{H}_6]^+$  which also shows no marked affinity for fluoride ions in MeOH.<sup>61</sup> Fluoride binding by  $[37]^+$  is also very selective as indicated by the absence of any response observed upon addition of  $\text{Cl}^-$ ,  $\text{Br}^-$ ,  $\text{I}^-$ ,  $\text{OAc}^-$ ,  $\text{NO}_3^-$ ,  $\text{H}_2\text{PO}_4^-$ , and  $\text{HSO}_4^-$  in MeOH.

In an effort to better understand the origin of the contrasting behaviour displayed by  $[37]^+$  and  $[38]^+$  toward fluoride anions, attempts to isolate **37-F** were undertaken (Figure 43). Addition of fluoride to a MeOH solution of  $[37]\text{OTf}$  led to the rapid precipitation of **37-F**. The  $^{11}\text{B}$  NMR resonance at 10.9 ppm is consistent with the presence of a four-coordinate boron centre. The  $^{19}\text{F}$  NMR signal of **37-F** appears at -130.4 ppm. This chemical shift is unusual and appears to shift significantly downfield when compared to other triarylfluoroborate species<sup>5, 47</sup> such as *o*- $\text{Mes}_2\text{FB}(\text{C}_6\text{H}_4)\text{NMe}_3$  (-158.0 ppm),  $[1,2-(\mu\text{-F})-\text{((C}_6\text{F}_5)_2\text{B)}_2\text{C}_6\text{H}_4]^-$  (-167.2 ppm) or  $[1-\{\text{Mes}_2\text{B}\}_v-(\mu\text{-F})\text{-8-}$

$\{(\text{C}_6\text{F}_5)\text{Hg}\}\text{C}_{10}\text{H}_6\text{]}^-$  (-164.3 ppm).<sup>27, 48, 57</sup> This downfield shift suggests that the fluoride anion in **37-F** is in an unusual chemical environment. In line with this argument, the  $^{19}\text{F}$  resonance of **37-F** features two satellites, indicating coupling to the  $^{125}\text{Te}$  nucleus ( $^1J_{\text{Te-F}} = 940$  Hz). This large  $^{125}\text{Te}$ - $^{19}\text{F}$  coupling is confirmed by the observation of a doublet ( $\delta = 713$  ppm) split by 940 Hz in the  $^{125}\text{Te}$  NMR spectrum. The magnitude of  $^1J_{\text{Te-F}}$  in **37-F** is comparable to that observed in *o*-( $\text{C}_6\text{H}_4\text{-CH}_2\text{NMe}_2$ ) $_2\text{TeF}_2$  (969 Hz).<sup>150</sup> Altogether, these spectroscopic features suggest that the fluorine atom is not only bound to the boron atom but also forms a strong bond with the tellurium atom. Although no evidence for the formation of **38-F** were obtained in MeOH under dilute conditions, formation of this fluoride adduct could be driven by precipitation through addition of an excess of KF to a MeOH solution of [**38**]OTf (Figure 43). Some of its salient spectroscopic features include a  $^{11}\text{B}$  NMR resonance at 8.7 ppm as well as a  $^{19}\text{F}$  NMR signal at -150.7 ppm in the range expected for typical triarylfluoroborate anions.<sup>5</sup>

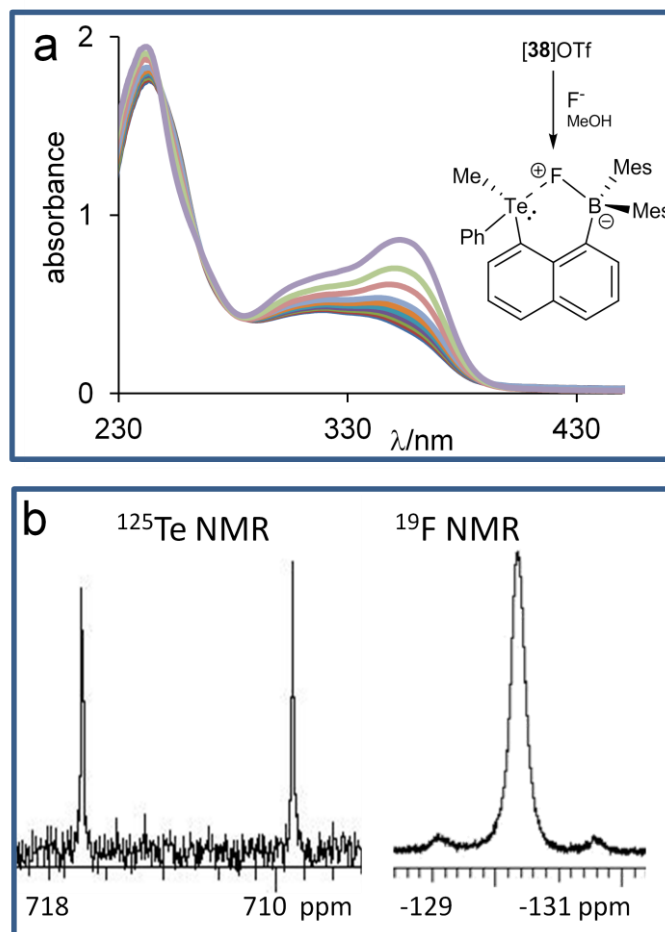


**Figure 51.** Spectroscopic evidence for the formation and structure of **37-F**. a, Changes observed in the UV-vis spectra of  $[37]^+$  ( $6.73 \times 10^{-5}$  M) in MeOH upon addition of a fluoride anions solution. The observed quenching of the low energy bands is consistent with the formation of **37-F**. b,  $^{125}\text{Te}$  NMR and  $^{19}\text{F}$  NMR spectra of **37-F**. The presence of a doublet ( $^1J_{\text{Te-F}} = 940$  Hz) in the  $^{125}\text{Te}$  NMR spectrum indicates the presence of a strong interaction between the fluorine and tellurium nuclei. Accordingly, the  $^{19}\text{F}$  NMR signal features two satellites resulting from coupling to the  $^{125}\text{Te}$  nucleus (7% natural abundance).

Compounds **37-F** and **38-F** were crystallized from dichloromethane.<sup>145</sup> The crystal structures of these compounds (Figure 52 and Figure 53, Table 16) clearly show that: i) the boron centre adopts a pyramidal geometry ( $\sum_{(C-B-C)} = 339.5(1)^\circ$  for **38-F** and  $343.0(3)^\circ$  for **37-F**); ii) that the B-F bond length in **38-F** (1.481(2) Å) is slightly shorter than that in **37-F** (1.514(4) Å); iii) that the F-Ch-C<sub>Ph</sub> angle is close to linearity ( $176.6(1)^\circ$  for **38-F** and  $174.0(1)^\circ$  for **37-F**); iv) that the S-F distance in **38-F** (2.548(1) Å) is slightly longer than the Te-F distance in **37-F** (2.506(2) Å) despite the larger size of the tellurium atom. In fact the Te-F bond distance in **37-F** is only moderately larger than the sum of the covalent radii of the two elements (1.95 Å).<sup>151</sup> This Te-F bond distance can also be compared to those observed in other Te(IV) monofluoride species such as  $[(\mu-F)Te(CF_3)_3-DMF]_\infty$  (DMF = dimethylformamide),<sup>152</sup> a fluoride-bridged polymeric species connected by Te-F linkages of 2.138(2) Å and 2.566(2) Å. The overall coordination geometry of the tellurium atom in **37-F** is best described as a seesaw with a stereoactive lone pair perpendicular to the F-Te-C<sub>Ph</sub> sequence.

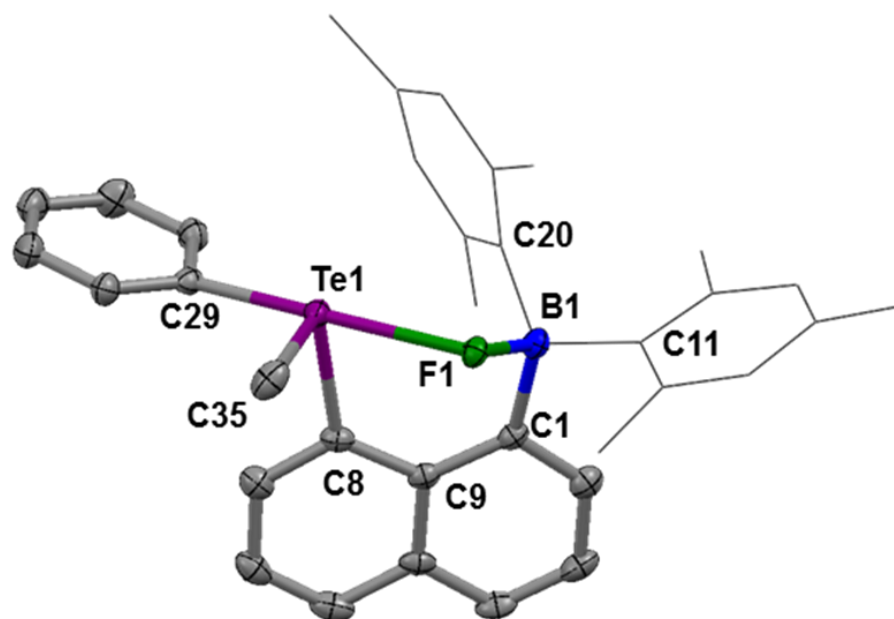


**Figure 52.** Crystal structure of the fluoride adduct **37-F** (thermal ellipsoids are drawn at 50% probability levels; hydrogen atoms are omitted and the mesityl ligands are represented by thin lines for clarity). Selective bond distances [ $\text{\AA}$ ] and bond angles [ $^\circ$ ]: Te(1)-C(35) 2.117(4), Te(1)-C(29) 2.124(3), Te(1)-C(8) 2.151(3), Te(1)-F(1) 2.5064(18), F(1)-B(1) 1.514(4), C(1)-C(9) 1.443(5), C(1)-B(1) 1.633(5), C(8)-C(9) 1.448(5), C(11)-B(1) 1.634(5), C(20)-B(1) 1.671(5); C(35)-Te(1)-C(29) 98.29(14), C(35)-Te(1)-C(8) 93.52(14), C(29)-Te(1)-C(8) 96.61(13), C(35)-Te(1)-F(1) 86.98(11), C(29)-Te(1)-F(1) 174.03(11), C(8)-Te(1)-F(1) 80.19(10), B(1)-F(1)-Te(1) 106.68(18), C(9)-C(1)-B(1) 126.2(3), C(9)-C(8)-Te(1) 125.9(2), C(1)-C(9)-C(8) 127.5(3), F(1)-B(1)-C(1) 103.0(3), F(1)-B(1)-C(11) 106.5(3), C(1)-B(1)-C(11) 112.5(3), F(1)-B(1)-C(20) 102.6(3), C(1)-B(1)-C(20) 115.8(3), C(11)-B(1)-C(20) 114.7(3).



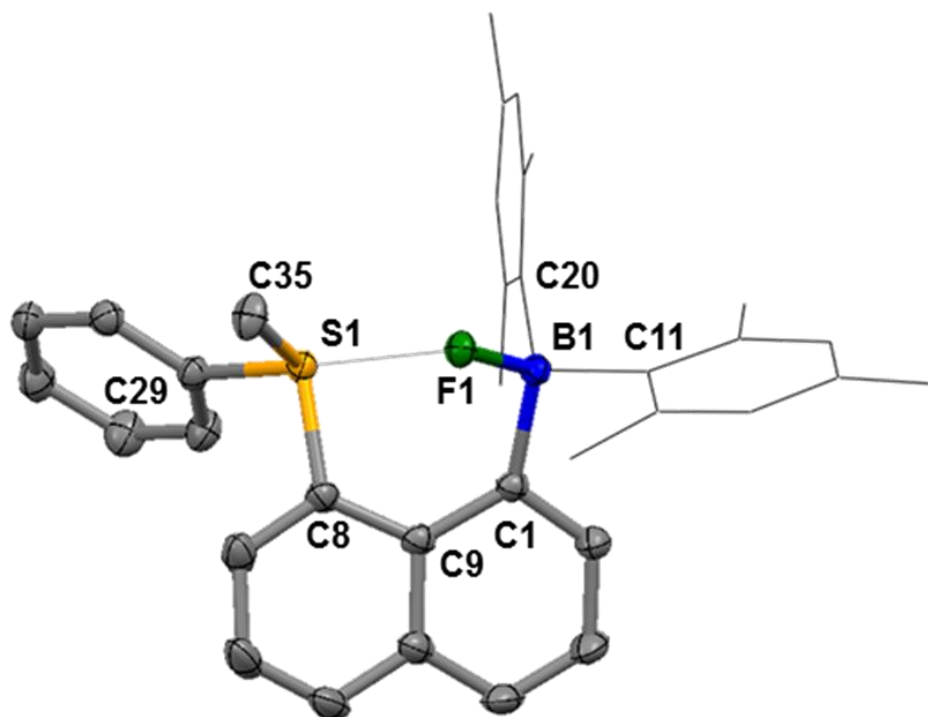


**Figure 53.** Crystal structure of the fluoride adduct **38-F** (thermal ellipsoids are drawn at 50% probability levels; hydrogen atoms are omitted and the mesityl ligands are represented by thin lines for clarity). Selective bond distances [ $\text{\AA}$ ] and bond angles [ $^\circ$ ]: S(1)-C(8) 1.7850(19), S(1)-C(34) 1.7896(18), S(1)-C(35) 1.7955(18), F(1)-B(1) 1.481(2), C(1)-C(9) 1.441(2), C(1)-B(1) 1.652(3), C(8)-C(9) 1.432(3), C(11)-B(1) 1.659(3), C(20)-B(1) 1.653(3); C(8)-S(1)-C(34) 100.50(8), C(8)-S(1)-C(35) 105.15(9), C(34)-S(1)-C(35) 102.84(9), C(9)-C(1)-B(1) 126.34(15), C(9)-C(8)-S(1) 119.07(13), F(1)-B(1)-C(1) 105.35(14), F(1)-B(1)-C(20) 104.34(13), C(1)-B(1)-C(20) 118.88(14), F(1)-B(1)-C(11) 106.63(13), C(1)-B(1)-C(11) 106.85(13), C(20)-B(1)-C(11) 113.80(14).

**Table 16.** Crystal data, data collections, and structure refinements for **37-F** and **38-F**.

Crystal data	<b>37-F</b>	<b>38-F</b>
formula	C <sub>35</sub> H <sub>36</sub> BFTe	C <sub>35</sub> H <sub>36</sub> BFS
$M_r$	614.05	518.51
crystal size (mm <sup>3</sup> )	0.34 x 0.27 x 0.16	0.21 x 0.17 x 0.15
crystal system	Monoclinic	Monoclinic
space group	P2(1)/n	P2(1)/n
$a$ (Å)	9.0099(9)	10.757(2)
$b$ (Å)	24.019(2)	8.8417(19)
$c$ (Å)	13.2080(12)	30.186(6)
$\alpha$ (°)	90	90
$\beta$ (°)	93.7740(10)	94.800(3)
$\gamma$ (°)	90	90
$V$ (Å <sup>3</sup> )	2852.1(5)	2861.0(10)
$Z$	4	4
$\rho_{\text{calc}}$ (g cm <sup>-3</sup> )	1.430	1.204
$\mu$ (mm <sup>-1</sup> )	1.072	0.142
$F(000)$	1248	1104
Data Collection		
$T$ (K)	110(2)	110(2)
scan mode	$\omega$	$\omega$
$hkl$ range	-12 $\rightarrow$ +11 -32 $\rightarrow$ +31 -17 $\rightarrow$ +17	-13 $\rightarrow$ +9 -11 $\rightarrow$ +11 -38 $\rightarrow$ +29
measd rflns	34846	15976
unique rflns [ $R_{\text{int}}$ ]	7069 [0.0680]	5849 [0.0302]
rflns used for refinement	7069	5849
Refinement		
refined parameters	343	343
GooF	1.001	0.999
$R_1$ , <sup>a</sup> $wR_2$ <sup>b</sup> all data	0.0610, 0.0757	0.0626, 0.1543
$\rho_{\text{fin}}$ (max/min) (e Å <sup>-3</sup> )	0.767 and -0.658	0.426 and -0.427

$$^a R_1 = \frac{\sum ||F_o| - |F_c||}{\sum |F_o|}, \quad ^b wR_2 = \left[ \frac{\sum w(F_o^2 - F_c^2)^2}{\sum w(F_o^2)^2} \right]^{1/2}$$

In order to investigate the nature of the interaction between the group 16 element and the fluorine atom in **37-F** and **38-F**, we carried out an NBO analysis at the DFT optimized structure (functional: BP86; mixed basis set: Te: aug-cc-pvTz-pp; B: 6-31+g(d'); S: 6-31+g(d); C, H: 6-31g). For both **37-F** and **38-F**, this analysis reveals the presence of two  $\text{lp}(\text{F}) \rightarrow \sigma^*(\text{Ch-C})$  donor-acceptor interactions. As depicted in Figure 54 in the case **37-F**, these two interactions involve two different fluorine lone-pair orbitals which differ by their *s* and *p* character. The concomitant deletion of these two interactions leads to an increase of the total energy of the molecule by  $E_{\text{del}} = 22.8$  kcal/mol for **37-F** and 9.2 kcal/mol for **38-F**, in line with the shorter Ch-F separation in **37-F**. The covalent component of the Ch-F interaction was further probed by performing an Atom-In-Molecule (AIM) analysis. This analysis shows that the value of the electron density at the bond critical point of the group 16-fluorine bond in **37-F** ( $\rho(r) = 0.047 \text{ e bohr}^{-3}$ ) is significantly larger than that in **38-F** ( $\rho(r) = 0.035 \text{ e bohr}^{-3}$ ), despite the increased diffuseness of the tellurium valence orbitals (Figure 54). Altogether, these structural and computational results point to the higher Lewis acidity anticipated for the telluronium of  $[\mathbf{37}]^+$  when compared to the sulfonium of  $[\mathbf{38}]^+$ . These observations, which are in line with previous studies on chalcogen-bonded species,<sup>136</sup> can be correlated to the lower energy of the Ch-C  $\sigma^*$ -orbital in **37-F**, as well as to the greater electropositivity and polarisability of tellurium when compared to sulfur.

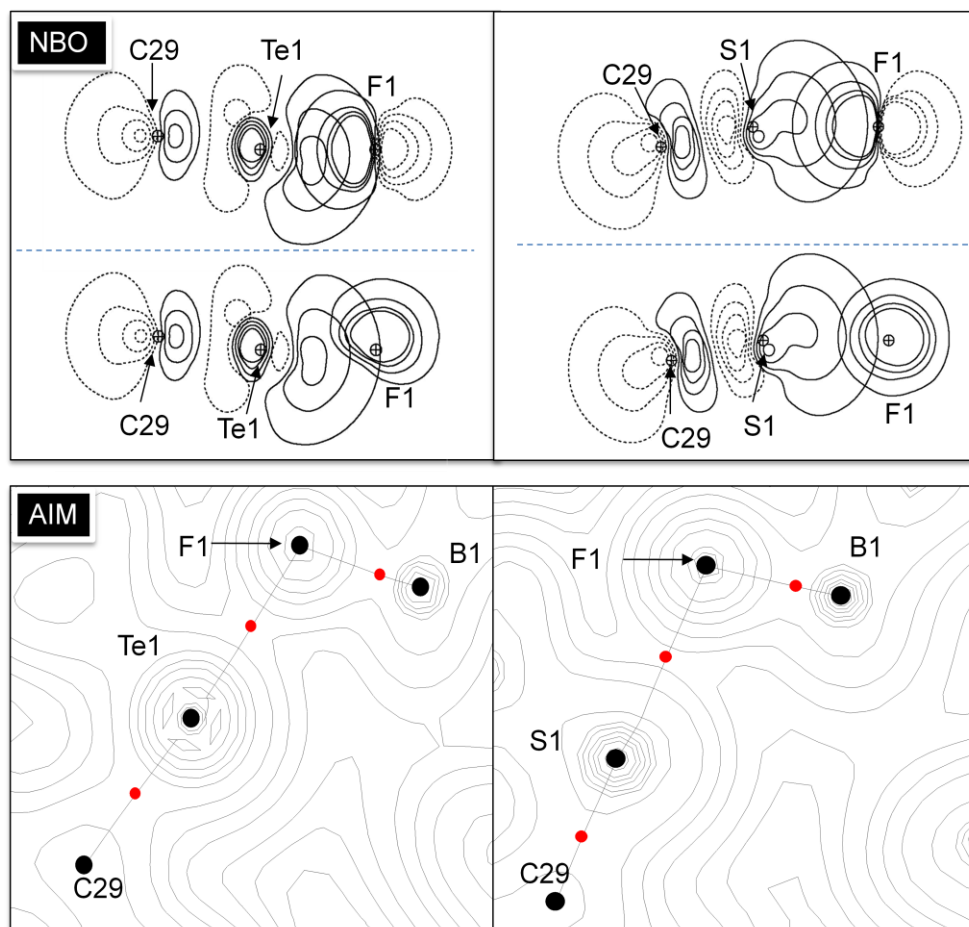


**Figure 54.** Top: NBO contour plots showing the two  $lp(F) \rightarrow \sigma^*(Ch-C)$  donor-acceptor interactions involved in **37-F** and **38-F**. Bottom: AIM electron density maps in the B-F-Ch plane of **37-F** and **38-F**. The thin lines connecting the atoms represent the bond paths. For each bond path, the red dot indicates the position of the bond critical point.

## 4.3.2 Cyanide affinity

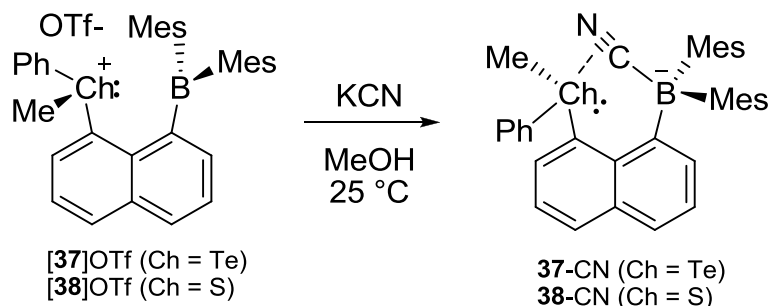


**Figure 55.** Synthesis of **37-CN** and **38-CN** in MeOH

We have studied the cyanide binding properties of **[37]OTf** and **[38]OTf** in methanol using UV/Vis spectroscopy. The addition of 5 equiv. of  $\text{CN}^-$  into a 0.054 mM methanolic solution of **[37]OTf** resulted in a total quenching of the absorption spectrum within 30 minutes. Similarly, addition of 10 equiv.  $\text{CN}^-$  into a 0.063 mM methanol solution of **[38]OTf** resulted in a total quenching of the absorption, again in 30 minutes. In both cases, the binding process is slow which precludes an accurate determination of the binding constant. Compound **37-CN** and **38-CN** were isolated from the reaction of KCN with **[37]OTf** and **[38]OTf**, respectively, in methanol at mM concentrations. These cyanide complexes have been characterized by multinuclear NMR spectroscopy, IR spectroscopy and single crystal X-ray diffraction (Figure 55). A  $^{11}\text{B}$ NMR resonance at -12.6 ppm for **37-CN** and -11.6 ppm for **38-CN** indicates the presence of the four-coordination of the boron center, and an intense IR band at  $2153\text{ cm}^{-1}$  for **37-CN** and  $2163\text{ cm}^{-1}$  for **38-CN** confirms the presence of a boron-bound cyano group.<sup>46, 61</sup> The

crystal structures of these two complexes show a substantial pyramidalization of the boron atom as indicated by the sum of the  $C_{\text{aryl}}\text{-B-}C_{\text{aryl}}$  angles ( $\Sigma_{(C-B-C)} = 340.8^\circ$  ppm for **37**-CN and  $340.4^\circ$  for **38**-CN). The B- $C_{\text{CN}}$ - bonds (1.638(5) Å for **37**-CN and 1.627(6) Å for **38**-CN) are comparable to those typically found in triarylcyanoborate anions such as  $[\text{Ph}_3\text{BCN}^-]$  (1.65 Å). The distance between the B and chalcogen atoms (Ch) in the cyanide adducts (3.446(4) Å for **37**-CN and 3.251(6) Å for **38**-CN) are longer than that in their cationic precursor ( $[\mathbf{37}]\text{OTf}$  (3.244(6) Å) and  $[\mathbf{38}]\text{OTf}$  3.129(3) Å), indicating an increase in steric crowding. The centroid of the  $\text{C}\equiv\text{N}$  ( $C_{\text{CN}}$ ) bond is separated from the chalcogen atom by only 2.958 Å for **37**-CN and 2.911 Å for **38**-CN. The  $C_{\text{CN}}\text{-Ch-}C_{\text{trans}}$  angle of  $167.98^\circ$  for **37**-CN and  $164.59^\circ$  for **38**-CN are close to linearity, which with the short  $C_{\text{CN}}\text{-Ch}$  separation are indicative of a possible interaction between the cyanide group and the chalcogen (Figure 56, Figure 57, Table 17).

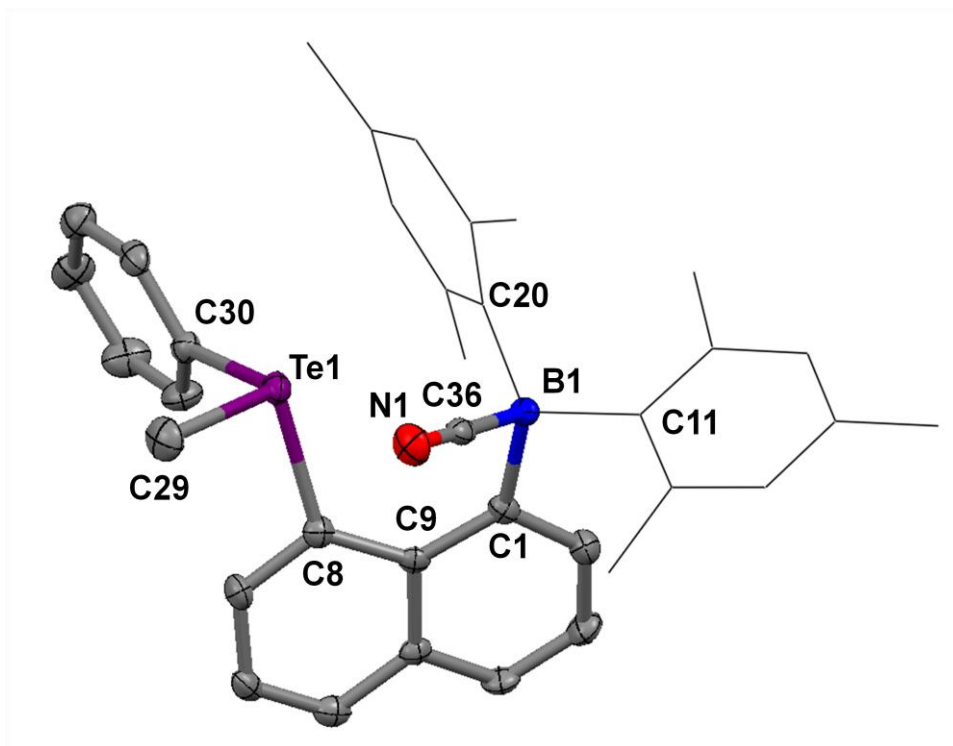


**Figure 56.** Crystal structure of the fluoride adduct **37-CN** (thermal ellipsoids are drawn at 50% probability levels; hydrogen atoms are omitted and the mesityl ligands are represented by thin lines for clarity). Selective bond distances [Å] and bond angles [°]: Te(1)-C(30) 2.120(3), Te(1)-C(29) 2.129(3), Te(1)-C(8) 2.143(3), N(1)-C(36) 1.152(4), C(1)-C(9) 1.436(4), C(1)-B(1) 1.659(5), C(9)-C(8) 1.441(4), C(11)-B(1) 1.677(5), C(20)-B(1) 1.652(5), C(36)-B(1) 1.638(5); C(30)-Te(1)-C(29) 96.82(13), C(30)-Te(1)-C(8) 97.15(13), C(29)-Te(1)-C(8) 97.21(14), C(9)-C(1)-B(1) 128.8(3), C(9)-C(8)-Te(1) 126.1(2), C(1)-C(9)-C(8) 127.9(3), N(1)-C(36)-B(1) 176.9(4), C(36)-B(1)-C(20) 104.1(3), C(36)-B(1)-C(1) 105.6(3), C(20)-B(1)-C(1) 114.1(3), C(36)-B(1)-C(11) 105.2(3), C(20)-B(1)-C(11) 117.4(3), C(1)-B(1)-C(11) 109.2(3).

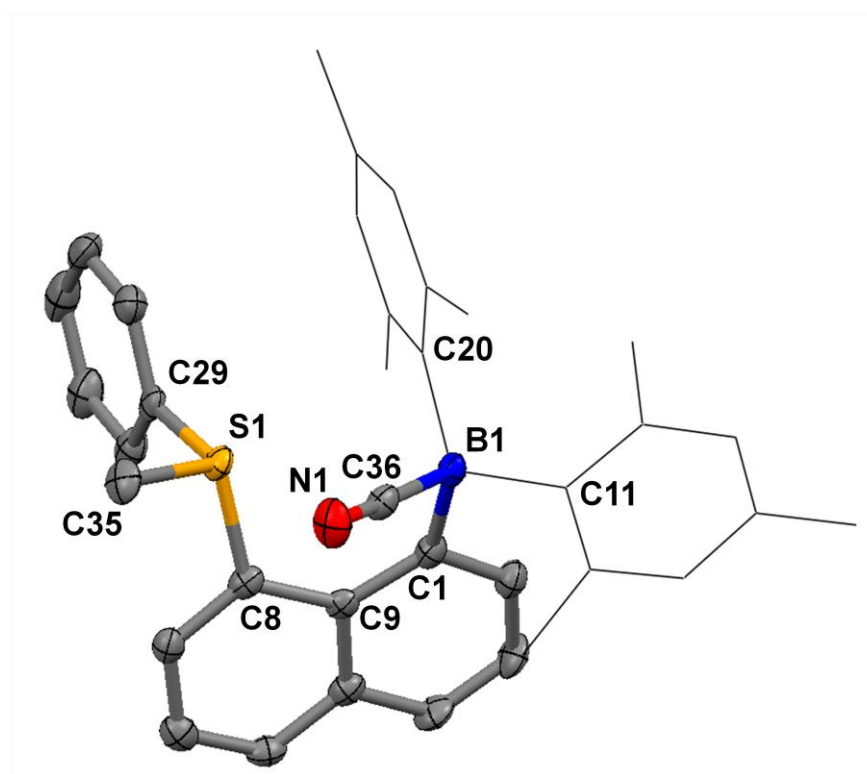


**Figure 57.** Crystal structure of the fluoride adduct **38-CN•CH<sub>2</sub>Cl<sub>2</sub>** (thermal ellipsoids are drawn at 50% probability levels; dichloromethane and hydrogen atoms are omitted and the mesityl ligands are represented by thin lines for clarity). Selective bond distances [Å] and bond angles [°]: S(1)-C(8) 1.780(4), S(1)-C(29) 1.803(5), S(1)-C(35) 1.804(4), B(1)-C(1) 1.673(7), C(1)-C(9) 1.446(6), C(9)-C(8) 1.442(6), C(11)-B(1) 1.667(6), C(20)-B(1) 1.658(6), C(36)-B(1) 1.627(6), C(36)-N(1) 1.145(6); C(8)-S(1)-C(29) 104.6(2), C(8)-S(1)-C(35) 105.9(2), C(29)-S(1)-C(35) 100.9(2), C(9)-C(1)-B(1) 128.8(4), C(9)-C(8)-S(1) 120.1(3), C(8)-C(9)-C(1) 127.5(4), N(1)-C(36)-B(1) 178.5(5), C(36)-B(1)-C(20) 103.1(3), C(36)-B(1)-C(11) 106.7(3), C(20)-B(1)-C(11) 114.5(4), C(36)-B(1)-C(1) 106.0(4), C(20)-B(1)-C(1) 118.7(4), C(11)-B(1)-C(1) 106.9(3).



**Table 17.** Crystal data, data collections, and structure refinements of **37-CN** and **38-CN**

Crystal data	<b>37-CN</b>	<b>38-CN</b> •CH <sub>2</sub> Cl <sub>2</sub>
formula	C <sub>36</sub> H <sub>36</sub> BNTe	C <sub>37</sub> H <sub>38</sub> BCl <sub>2</sub> NS
<i>M<sub>r</sub></i>	621.07	610.45
crystal size (mm <sup>3</sup> )	0.12 x 0.08 x 0.08	0.10 x 0.08 x 0.06
crystal system	Triclinic	Monoclinic
space group	P-1	P2(1)/c
<i>a</i> (Å)	9.5465(12)	9.6997(9)
<i>b</i> (Å)	10.0080(13)	16.7280(16)
<i>c</i> (Å)	15.470(2)	20.3173(19)
<i>α</i> (°)	93.260(2)	90
<i>β</i> (°)	97.636(2)	100.3250(10)
<i>γ</i> (°)	92.549(2)	90
<i>V</i> (Å <sup>3</sup> )	1460.5(3)	3242.2(5)
<i>Z</i>	2	4
$\rho_{\text{calc}}$ (g cm <sup>-3</sup> )	1.412	1.250
$\mu$ (mm <sup>-1</sup> )	1.044	0.291
<i>F</i> (000)	632	1288
Data Collection		
<i>T</i> (K)	110(2)	110(2)
scan mode	$\omega$	$\omega$
<i>hkl</i> range	-12 → +12	-11 → +11
	-13 → +13	-19 → +19
	-20 → +20	-23 → +23
measd reflns	18082	28371
unique reflns [ <i>R</i> <sub>int</sub> ]	7131 [0.0620]	5078 [0.0499]
reflns used for refinement	7131	5078
Refinement		
refined parameters	352	379
GooF	0.921	1.080
R1, <sup>a</sup> wR2 <sup>b</sup> all data	0.0681, 0.0691	0.1031, 0.2628
$\rho_{\text{fin}}$ (max/min) (e Å <sup>-3</sup> )	1.013 and -0.668	1.430 and -1.038

<sup>a</sup> R1 =  $\sum||F_o| - |F_c||/\sum|F_o|$ . <sup>b</sup> wR2 =  $[[\sum w(F_o^2 - F_c^2)^2]/[\sum w(F_o^2)^2]]^{1/2}$ .

In order to investigate the nature of the interaction between the group 16 element and the cyanide ligand in **37**-CN and **38**-CN, NBO analyses were carried out at the DFT optimized structures (functional: BP86; mixed basis set: Te: aug-cc-pvTz-pp; B: 6-31+g(d'); S: 6-31+g(d); C, H: 6-31g). For **37**-CN, this analysis reveals the presence of two  $\pi(\text{C}\equiv\text{N})\rightarrow\sigma^*(\text{Te}-\text{C})$  donor-acceptor interactions and one  $\text{lp}(\text{N})\rightarrow\sigma^*(\text{Te}-\text{C})$  donor-acceptor interaction (Figure 58). For **38**-CN, the NBO analysis shows a  $\pi(\text{C}\equiv\text{N})\rightarrow\sigma^*(\text{S}-\text{C})$  donor-acceptor interaction complemented by a back-bonding  $\text{lp}(\text{S})\rightarrow\pi^*(\text{C}\equiv\text{N})$  component. The concomitant deletion of these interactions leads to an increase of the total energy of the molecule by  $E_{\text{del}} = 9.57$  kcal/mol for **37**-CN and 4.50 kcal/mol for **38**-CN. These computational results show that the tellurium vacant orbitals are energetically and spatially more accessible than those of sulphur. These considerations serve to rationalize the higher Lewis acidity of the telluronium borane [**37**]<sup>+</sup> when compared to the sulfonium analogue [**38**]<sup>+</sup>.

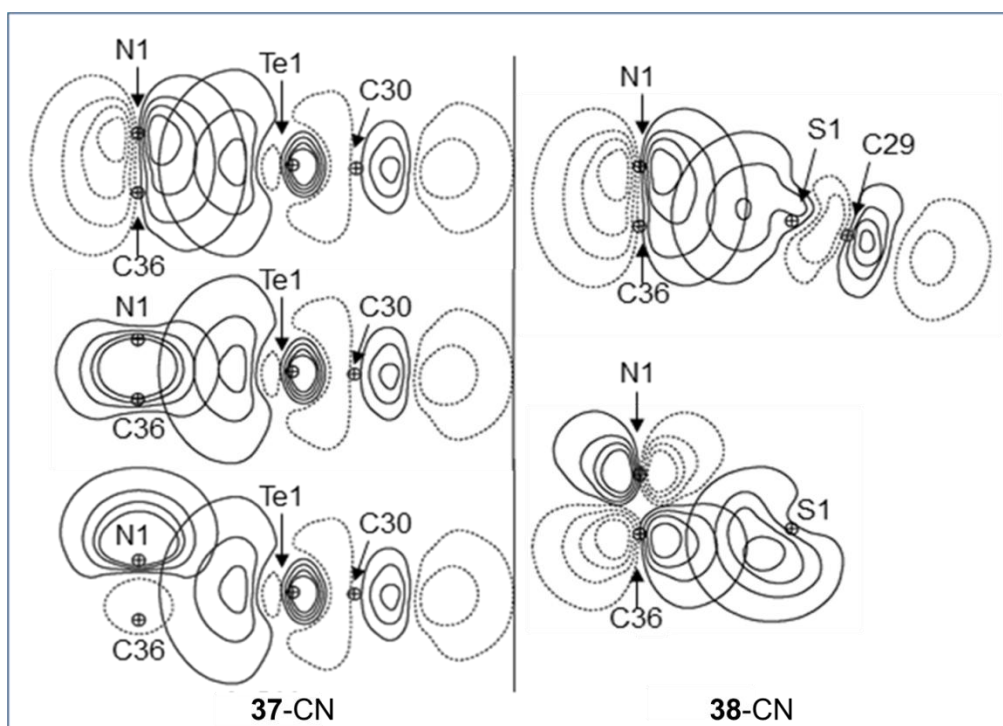


**Figure 58.** NBO NBO contour plots showing the donor-acceptor interactions involved in **37-CN** (left) and **38-CN** (right).

#### 4.4 Conclusion

The results presented in this chapter allow us to introduce a new strategy for the design of polyfunctional Lewis acids. This strategy, which is based on the use of heavier chalcogenium ions as Lewis acidic sites, takes advantage of the size, polarizability and electropositivity increases observed as the atom becomes larger. Although the increased polarizability and electropositivity of the tellurium atom in **37-F** lead to an enhancement of the ionic component of the group 16-anion interaction, its larger size allows for a reduction of intraligand repulsions, which makes interaction with the anionic guest more favorable. In turn, the anionic guest achieves a shorter approach to the tellurium atom,

which leads to an increase of the covalent component of the chalcogen–anion interaction. Cumulatively, these effects make the telluronium center of **[37]**<sup>+</sup> a stronger Lewis acid than the sulfonium center of **[38]**<sup>+</sup>, which thus provides a rationale for the enhanced fluoride affinity of **[37]**<sup>+</sup>. Although it was documented previously that heavier chalcogenium ions may act as acceptors, this property was not exploited in the context of molecular recognition. In turn, our work may lead to the development of novel Lewis acidic receptors or catalysts with telluronium ions as active sites.

#### 4.5 Experimental section

**General Considerations.** Tetrakis(THF)lithium dimesityl-1,8-naphthalenediylborate was synthesized by following the published procedure.<sup>56</sup> Dimesitylboron fluoride, methyl triflate, diphenyl ditelluride, potassium cyanide and potassium fluoride were purchased from Aldrich, diphenyl disulfide from TCI. Solvents were dried by passing through an alumina column (hexanes, dichloromethane, diethyl ether) or refluxing under N<sub>2</sub> over Na/K (Et<sub>2</sub>O). UV-vis spectra were recorded on an Ocean Optics USB4000 spectrometer with an Ocean Optics ISS light source. Elemental analyses were performed by Atlantic Microlab (Norcross, GA). NMR spectra were recorded on Varian Unity Inova 400 FT NMR (399.59 MHz for <sup>1</sup>H, 128.19 MHz for <sup>11</sup>B, 100.45 MHz for <sup>13</sup>C, 126.11 MHz for <sup>125</sup>Te) spectrometers at ambient temperature. Chemical shifts are given in ppm, and are referenced against external BF<sub>3</sub>·Et<sub>2</sub>O (<sup>11</sup>B, <sup>19</sup>F) and Ph<sub>2</sub>Te<sub>2</sub> (<sup>125</sup>Te). The crystallographic measurements were performed using a Bruker APEX-II CCD area detector diffractometer (Mo-K<sub>α</sub> radiation, λ = 0.71069 Å) for **37**,

[**37**]OTf, **37-F**, **37-CN**, **38**, [**38**]OTf, **38-F** and **38-CN**. In each case, a specimen of suitable size and quality was selected and mounted onto a nylon loop. The structures were solved by direct methods, which successfully located most of the non-hydrogen atoms. Subsequent refinement on  $F^2$  using the SHELXTL/PC package (version 5.1) allowed location of the remaining non-hydrogen atoms.

**Synthesis of 37.** Diphenyl ditelluride (0.70 g, 1.71 mmol) was added to a suspension of tetrakis(THF)lithium dimesityl-1,8-naphthalenediylborate (1.00 g, 1.49 mmol) in diethyl ether (60 mL) at  $-20\text{ }^\circ\text{C}$ . After stirring overnight at  $25\text{ }^\circ\text{C}$ , the reaction was quenched with water and extracted with dichloromethane (3 x 50 mL). The organic phases were combined, dried over  $\text{MgSO}_4$  and filtered. The solvent was removed under vacuum yielding a yellow solid. The solid was washed with hexanes to afford compound **37** (0.68 g, yield 79%). Characterization of **37**:  $^1\text{H}$  NMR (400 MHz,  $\text{CDCl}_3$ )  $\delta$  0.82 (s, 3H), 1.80 (s, 3H), 2.22 (s, 3H), 2.26 (s, 3H), 2.32 (s, 3H), 2.38 (s, 3H), 6.50 (s, 1H, Mes-CH), 6.80 (s, 1H, Mes-CH), 6.85 (s, 1H, Mes-CH), 6.87 (s, 1H, Mes-CH), 7.04-7.19 (m, 5H, ph-CH), 7.33 (t, 1H,  $^3J_{\text{H-H}} = 7.5\text{ Hz}$ , nap-CH), 7.40-7.47 (m, 2H, nap-CH), 7.89 (d, 1H,  $J_{\text{H-H}} = 7.5\text{ Hz}$ , nap-CH), 7.93 (d, 1H,  $J_{\text{H-H}} = 7.8\text{ Hz}$ , nap-CH), 8.03 (d, 1H,  $J_{\text{H-H}} = 7.2\text{ Hz}$ , nap-CH).  $^{13}\text{C}$  NMR (100 MHz,  $\text{CDCl}_3$ )  $\delta$  21.2, 22.9, 23.5, 25.5, 25.8, 120.5, 126.2, 126.6, 126.7, 127.2, 127.9, 128.9, 129.1, 129.7, 130.1, 130.2, 131.6, 133.8, 134.8, 135.1, 137.9, 139.8, 140.8, 141.3, 142.3, 143.4, 144.9.  $^{11}\text{B}$  NMR (128 MHz,  $\text{CDCl}_3$ )  $\delta$  + 60 (bs).  $^{125}\text{Te}$  NMR (126 MHz,  $\text{CDCl}_3$ )  $\delta$  646. Anal. Calcd for  $\text{C}_{33}\text{H}_{34}\text{BTe}$ : C, 70.40; H, 5.73. Found: C, 70.38; H, 5.72.

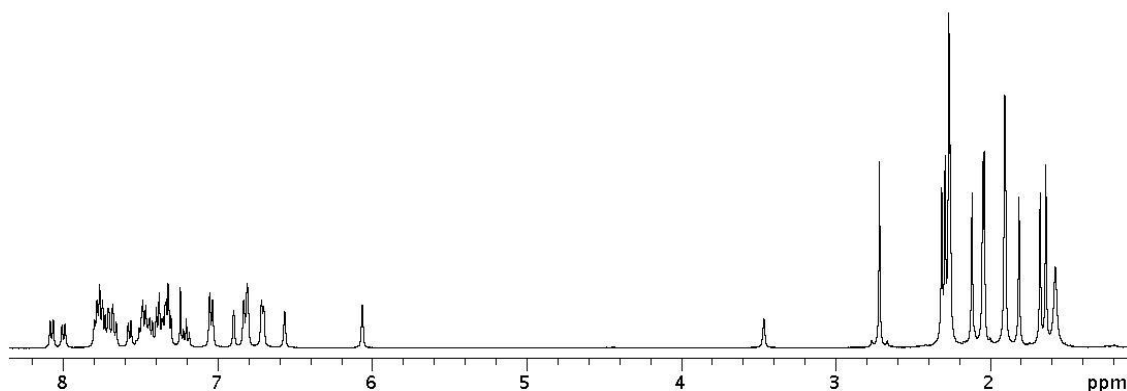
**Synthesis of [37]OTf.** Methyl triflate (0.40 g, 2.44 mmol) was added to a solution of compound **37** (0.67 g, 1.16 mmol) in dichloromethane (25 mL) at 25 °C. The mixture was refluxed overnight and cooled to 25 °C. The solvent was removed under vacuum to yield a sticky yellow solid which was washed by diethyl ether to afford [37]OTf as a pale yellow solid (0.40 g, yield 47 %). Single crystals of [37]OTf were obtained by slow evaporation of a dichloromethane solution. Characterization of [37]OTf: <sup>1</sup>H NMR (400 MHz, CDCl<sub>3</sub>) major diastereomer (71%): δ 0.75 (s, 3H), 1.79 (s, 3H), 2.19 (s, 3H), 2.27 (s, 3H), 2.31 (s, 3H), 2.36 (s, 3H), 2.53 (s, 3H, S-CH<sub>3</sub>), 6.60 (s, 1H, Mes-CH), 6.84 (s, 1H, Mes-CH), 6.97 (s, 1H, Mes-CH), 7.12 (s, 1H, Mes-CH), 7.14 (d, 1H, *J*<sub>H-H</sub> = 7.6 Hz, nap-CH), 7.26-7.42 (m, 5H, ph-CH), 7.50-7.61 (m, 2H, nap-CH), 7.82 (t, 1H, *J*<sub>H-H</sub> = 8.0 Hz, nap-CH), 8.07-8.13 (m, 2H, nap-CH). minor diastereomer (29%): δ 0.79 (s, 3H), 1.68 (s, 3H), 1.91 (s, 3H), 2.22 (s, 3H), 2.35 (s, 3H), 2.57 (s, 3H), 2.68 (s, 3H, S-CH<sub>3</sub>), 6.43 (s, 1H, Mes-CH), 6.46 (s, 1H, Mes-CH), 6.79 (s, 1H, Mes-CH), 7.00 (s, 1H, Mes-CH), 7.26-7.42 (m, 5H, ph-CH), 7.50-7.67 (m, 5H, nap-CH), 8.21 (d, 1H, *J*<sub>H-H</sub> = 7.6 Hz, nap-CH). <sup>13</sup>C NMR (100 MHz, CDCl<sub>3</sub>) major diastereomer: δ 11.9, 21.2, 21.3, 22.6, 22.7, 25.0, 25.1. minor diastereomer: δ 20.9, 21.0, 22.6, 22.7, 24.7, 24.7, 24.9. Remaining peaks for both diastereomers: δ 118.7, 120.6, 121.9, 124.4, 124.9, 125.2, 126.9, 127.5, 127.7, 127.9, 128.1, 128.3, 129.4, 129.5, 129.7, 129.9, 130.3, 130.5, 130.7, 131.0, 131.1, 131.6, 131.6, 131.9, 132.3, 132.6, 133.2, 133.3, 134.0, 134.2, 134.4, 134.5, 134.6, 136.8, 137.7, 138.9, 139.0, 139.7, 139.7, 139.8, 139.9, 140.1, 140.5, 140.8, 141.2, 141.7, 142.1, 142.8, 143.2, 145.9, 147.0. <sup>125</sup>Te NMR (126

MHz, CDCl<sub>3</sub>) δ 660, 677. Anal. Calcd for C<sub>36</sub>H<sub>36</sub>BO<sub>3</sub>F<sub>3</sub>STe: C, 58.11; H, 4.88. Found: C, 57.96; H, 4.88.

**Synthesis of 37-F.** [37]OTf (0.048 g, 0.074 mmol) was dissolved in a saturated KF methanol solution leading to the formation of a white precipitate. After 15 min., this precipitate was isolated by filtration, dried under vacuum to afford **37-F** (0.035 g, yield 88%). Single crystals of **37-F** were obtained by slow evaporation of a chloroform solution. Characterization of **37-F**: <sup>1</sup>H NMR (400 MHz, CDCl<sub>3</sub>) δ 1.69 (s, 3H), 1.93 (d, 3H, *J*<sub>H-F</sub> = 7.2 Hz), 2.02 (s, 3H), 2.14 (s, 3H), 2.21 (s, 3H), 2.27 (s, 3H), 2.72 (dd, 3H, *J*<sub>H-F</sub> = 2.4 Hz *J*<sub>H-Te</sub> = 16.3 Hz) 6.60 (s, 1H, Mes-CH), 6.72 (s, 2H, Mes-CH), 6.75 (s, 1H, Mes-CH), 7.15 (t, 1H, *J*<sub>H-H</sub> = 7.6 Hz, nap-CH), 7.27 (d, 1H, *J*<sub>H-H</sub> = 8.4 Hz, nap-CH), 7.36 (t, 1H, *J*<sub>H-H</sub> = 7.6 Hz, nap-CH), 7.46-7.53 (m, 5H, ph-CH), 7.64 (d, 1H, *J*<sub>H-H</sub> = 7.6 Hz, nap-CH), 7.70 (d, 1H, *J*<sub>H-H</sub> = 6.8 Hz, nap-CH), 7.94 (d, 1H, *J*<sub>H-H</sub> = 8.0 Hz, nap-CH). <sup>13</sup>C NMR (100 MHz, CDCl<sub>3</sub>) δ 13.06 (d, Te-CH<sub>3</sub>, *J*<sub>C-F</sub> = 11 Hz), 20.9, 21.0, 24.2 (d, Mes-CH<sub>3</sub>, *J*<sub>C-F</sub> = 7.3 Hz), 24.3, 24.8, 25.6, 123.7, 123.9, 126.7, 127.1, 127.8, 128.6, 129.1, 129.7, 129.9, 130.1, 130.5, 131.3, 132.9, 133.2, 134.8, 134.8, 135.3, 136.5, 136.5, 139.0, 141.0, 141.0, 142.1, 142.2, 142.3, 144.6. <sup>11</sup>B NMR (128 MHz, d<sub>6</sub>-acetone) δ + 10.9 (bs). <sup>19</sup>F-NMR (375.9 MHz, CDCl<sub>3</sub>) δ -130.4 (d, *J*<sub>Te-F</sub> = 940 Hz). <sup>125</sup>Te NMR (126 MHz, CDCl<sub>3</sub>) δ 713 (d, *J*<sub>Te-F</sub> = 940 Hz). Anal. Calcd for C<sub>35</sub>H<sub>36</sub>BF<sub>3</sub>Te: C, 68.46; H, 5.91. Found: C, 68.66; H, 5.94.

**Synthesis of 37-CN.** [37]OTf (0.048g, 0.074mmol) was added to saturated KCN methanol solution. After stirring 30 min, the white solid was formed. The solid was filtered, washed with methanol, and dried by vacuum to afford the product (0.040 mg,

yield 82%). Single crystals of **37-CN** were obtained by evaporation of chloroform solution. Anal. Calcd for  $C_{36}H_{36}BNTe$ : C, 69.62; H, 5.84. Found: C, 67.67; H, 5.66. (The EA result is not accurate, probably because the sample sent for analysis contains chloroform solvents, making lower C and H percentages.)  $^1H$  NMR (400 MHz,  $CDCl_3$ ) show there are two diastereomers in the solution. The NMR plot is shown:



**Synthesis of 38.** Diphenyl disulfide (0.703 g, 3.22 mmol) was added to a suspension of tetrakis(THF)lithium dimesityl-1,8-naphthalenediylborate (1.80 g, 2.68 mmol) in diethyl ether (60 mL) at  $-20$  °C. After stirring overnight at ambient temperature, the reaction was quenched with water and extracted with dichloromethane (3 x 50 mL). The organic phases were combined and dried over  $MgSO_4$  and filtered. The solvent was removed under reduced pressure yielding light yellow solid. The solid was washed with hexanes to afford compound **38** (0.893 g, yield 69%).  $^1H$  NMR (400 MHz,  $CDCl_3$ )  $\delta$  0.89 (s, 3H), 1.76 (s, 3H), 1.99 (s, 3H), 2.07 (s, 3H), 2.11 (s, 3H), 2.21 (s, 3H), 6.35 (bs, 1H, Mes-CH), 6.48 (bs, 1H, Mes-CH), 6.64-6.67 (m, 2H, ph-CH), 6.68 (bs, 1H, Mes-CH), 6.70 (bs, 1H, Mes-CH), 6.94-6.98 (m, 3H, ph-CH), 7.32-7.39 (m, 3H, nap-CH),



7.55 (d, 1H,  $J_{\text{H-H}} = 7.5$  Hz, nap-CH), 7.89 (d, 1H,  $J_{\text{H-H}} = 7.5$  Hz, nap-CH), 7.93 (d, 1H,  $J_{\text{H-H}} = 7.8$  Hz, nap-CH).  $^{13}\text{C}$  NMR (100 MHz,  $\text{CDCl}_3$ )  $\delta$  21.4, 23.3, 23.7, 24.4, 24.8, 125.9, 126.3, 126.8, 127.9, 128.6, 129.7, 130.7, 132.7, 132.9, 134.2, 134.4, 138.3, 138.7, 139.3, 140.4, 142.2, 143.5, 144.5, 149.8.  $^{11}\text{B}$  NMR (128 MHz,  $\text{CDCl}_3$ )  $\delta$  + 62 (bs).  
Anal. Calcd for  $\text{C}_{33}\text{H}_{34}\text{BS}$ : C, 84.29; H, 6.87. Found: C, 84.02; H, 6.91.

**Synthesis of [38]OTf.** Methyl triflate (0.328 g, 2.00 mmol) was added to a solution of compound **38** (0.8 g, 1.65 mmol) in dichloromethane (25 mL) at ambient temperature. The mixture was refluxed overnight and cooled to ambient temperature. The solvent was removed in *vacuo* to yield a yellow solid as crude. The solid was washed by diethyl ether to afford the pale product (0.944g, yield 88%). Single crystals of [38]OTf were obtained by evaporation of dichloromethane solution.  $^1\text{H}$  NMR (400 MHz,  $\text{CDCl}_3$ ) major diastereomer (79%):  $\delta$  0.77 (s, 3H), 1.79 (s, 3H), 2.15 (s, 3H), 2.23 (s, 3H), 2.32 (s, 3H), 2.38 (s, 3H), 2.74 (s, 3H, S- $\text{CH}_3$ ), 6.63 (s, 1H, Mes-CH), 6.84 (bs, 1H, Mes-CH), 6.90 (s, 1H, Mes-CH), 6.99 (s, 1H, Mes-CH), 7.48-7.53 (m, 5H, ph-CH), 7.60 (t, 1H,  $J_{\text{H-H}} = 8.0$  Hz, nap-CH), 7.81 (d, 1H,  $J_{\text{H-H}} = 8.0$  Hz, nap-CH), 7.84 (t, 1H,  $J_{\text{H-H}} = 8.0$  Hz, nap-CH), 8.12 (d, 1H,  $J_{\text{H-H}} = 8.4$  Hz, nap-CH), 8.27 (d, 1H,  $J_{\text{H-H}} = 7.6$  Hz, nap-CH), 8.41 (d, 1H,  $J_{\text{H-H}} = 7.2$  Hz, nap-CH). minor diastereomer (21%):  $\delta$  0.85 (s, 3H), 1.73 (s, 3H), 1.93 (s, 3H), 1.94 (s, 3H), 2.32 (s, 3H), 2.43 (s, 3H), 3.57 (s, 3H, S- $\text{CH}_3$ ), 6.11 (s, 1H, Mes-CH), 6.42 (bs, 1H, Mes-CH), 6.79 (s, 1H, Mes-CH), 6.99 (s, 1H, Mes-CH), 7.01 (d, 1H,  $J_{\text{H-H}} = 9.6$  Hz, nap-CH), 7.33 (t, 1H,  $J_{\text{H-H}} = 8.4$  Hz, nap-CH), 7.50 (t, 1H,  $J_{\text{H-H}} = 7.6$  Hz, nap-CH), 7.50-7.53 (m, 5H, ph-CH), 7.73 (d, 1H,  $J_{\text{H-H}} = 7.6$  Hz, nap-CH), 7.97 (d, 1H,  $J_{\text{H-H}} = 8.0$  Hz, nap-CH), 8.36 (d, 1H,  $J_{\text{H-H}} = 8.0$  Hz, nap-CH).  $^{13}\text{C}$

NMR (100 MHz, CDCl<sub>3</sub>) major diastereomer:  $\delta$  21.2, 21.3, 22.2, 22.7, 23.8, 25.0, 26.5.  
minor diastereomer:  $\delta$  21.0, 22.6, 22.7, 23.5, 24.5, 35.7. Remaining peaks for both diastereomers:  $\delta$  119.1, 122.3, 122.8, 123.5, 124.7, 127.5, 127.7, 128.0, 128.3, 128.6, 128.7, 129.3, 129.3, 129.6, 130.3, 130.4, 130.8, 131.3, 132.1, 133.3, 133.3, 133.8, 133.9, 134.5, 134.8, 134.8, 136.0, 136.4, 136.7, 137.0, 138.8, 139.5, 139.8, 140.0, 140.2, 141.2, 141.2, 141.3, 141.5, 141.8, 142.2, 142.2, 143.3, 143.5, 145.4. Anal. Calcd for C<sub>36</sub>H<sub>36</sub>BO<sub>3</sub>F<sub>3</sub>S<sub>2</sub>: C, 66.66; H, 5.59. Found: C, 66.46; H, 5.46.

**Synthesis of 38-F.** [38]OTf (0.050g, 0.077 mmol) was added to saturated KF methanol solution. After stirring 10 min, the white solid was formed. The solid was filtered, washed with methanol, and dried by vacuum to afford the product (0.031 g, yield 78%). Single crystals of 38-F were obtained by evaporation of dichloromethane solution. <sup>1</sup>H NMR (400 MHz, CDCl<sub>3</sub>)  $\delta$  1.75 (d, 3H,  $J_{\text{H-F}} = 5.6$  Hz), 1.91 (s, 3H), 1.94 (s, 3H), 2.10 (s, 3H), 2.18 (s, 3H), 2.23 (s, 3H), 3.51 (s, 3H) 6.45 (s, 1H, Mes-CH), 6.66 (s, 2H, Mes-CH), 6.68 (s, 1H, Mes-CH), 7.19 (d, 1H,  $J_{\text{H-H}} = 8.0$  Hz, nap-CH), 7.33-7.45 (m, 5H, ph-CH), 7.44-7.55 (m, 2H, nap-CH), 7.63 (d, 1H,  $J_{\text{H-H}} = 8.0$  Hz, nap-CH), 7.88 (d, 1H,  $J_{\text{H-H}} = 7.2$  Hz, nap-CH), 8.04 (d, 1H,  $J_{\text{H-H}} = 7.6$  Hz, nap-CH). <sup>13</sup>C NMR (100 MHz, CDCl<sub>3</sub>)  $\delta$  20.7, 20.9, 24.3, 24.4, 24.7, 27.7, 31.5 (d, S-CH<sub>3</sub>,  $J_{\text{C-F}} = 14.7$  Hz), 123.0, 125.5, 127.5, 127.7, 127.8, 128.1, 128.2, 128.3, 128.4, 129.0, 129.2, 130.2, 130.3, 131.4, 132.1, 132.7, 135.3, 136.2, 136.4, 138.6, 140.2, 141.2, 142.7, 143.1. <sup>11</sup>B NMR (128 MHz, d<sub>6</sub>-acetone)  $\delta$  + 8.7 (bs). <sup>19</sup>F NMR (375.9 MHz, CDCl<sub>3</sub>)  $\delta$  -150.7 (bs). Anal. Calcd for C<sub>35</sub>H<sub>36</sub>BFS: C, 81.07; H, 7.00. Found: C, 81.15; H, 7.00.

**Synthesis of 38-CN.** [38]OTf (0.050g, 0.077mmol) was added to saturated KCN methanol solution. After stirring 30 min, the white solid was formed. The solid was filtered, washed with methanol, and dried by vacuum to afford the product (0.034 mg, yield 84%). Single crystals of 38-CN were obtained by evaporation of dichloromethane solution.  $^1\text{H}$  NMR (400 MHz,  $\text{CDCl}_3$ )  $\delta$  1.36 (s, 3H), 1.74 (s, 3H), 1.77 (s, 3H), 2.07 (s, 3H), 2.23 (s, 3H), 2.34 (s, 3H), 2.57 (s, 3H), 5.78 (s, 1H, Mes-CH), 6.53 (d,  $J_{\text{H-H}} = 11.2$  Hz, 2H, Ph-CH), 6.66 (s, 1H, Mes-CH), 6.73 (s, 1H, Mes-CH), 6.82 (s, 1H, Mes-CH), 7.26-7.39 (m, 3H, Ph-CH), 7.46 (t, 1H,  $J_{\text{H-H}} = 10.0$  Hz, nap-CH), 7.65 (t, 1H,  $J_{\text{H-H}} = 9.6$  Hz, nap-CH), 7.72 (d, 1H,  $J_{\text{H-H}} = 10.8$  Hz, nap-CH), 7.85 (d, 1H,  $J_{\text{H-H}} = 10.0$  Hz, nap-CH), 7.91 (d, 1H,  $J_{\text{H-H}} = 9.2$  Hz, nap-CH), 8.30 (d, 1H,  $J_{\text{H-H}} = 10.4$  Hz, nap-CH).  $^{13}\text{C}$  NMR (100 MHz,  $\text{CDCl}_3$ )  $\delta$  20.65, 20.77, 24.96, 25.21, 28.07, 34.04, 122.95, 126.44, 127.39, 127.71, 128.74, 129.47, 129.53, 129.59, 129.95, 130.95, 131.46, 131.64, 132.62, 133.36, 136.05, 137.66, 138.22, 141.47, 141.78, 142.43, 142.54, 143.25.  $^{11}\text{B}$  NMR (128 MHz,  $\text{CDCl}_3$ )  $\delta$  -11.6. Anal. Calcd for  $\text{C}_{36}\text{H}_{36}\text{BNS} \cdot 1/6\text{CH}_2\text{Cl}_2$ : C, 80.49; H, 6.79. Found: C, 80.31; H, 6.85 (the single crystal contains  $\text{CH}_2\text{Cl}_2$  solvent, and partial solvent molecules were lost when sending out for elemental analysis)

**Computational details.** DFT calculations (full geometry optimization) were carried out with the Gaussian 03<sup>116</sup> program using the BP86 functional (Table 19, Table 20, Table 21, Table 22, Table 23, Table 24, Table 25, Table 26, Figure 59, Figure 60, Figure 61, Figure 62, Figure 63, Figure 64, Figure 65, Figure 66). Geometry optimization was carried out with the following mixed basis set: Te: aug-cc-pvTz-pp,, B, N, F: 6-31+g(d'); S: 6-31+g(d); C, H: 6-31g. Frequency calculations, which were carried out on the optimized structure of the compound, confirmed the absence of any imaginary frequencies. TD-DFT calculations were carried out with the Gaussian 03 program using the MPW1PW91 functional with and the aforementioned mixed basis set. The Natural Bond Orbital (NBO) analyses<sup>153</sup> were carried out using the stand along PC version of GENNBO 5.0 program. AIM analyses were carried out using the stand along PC version of AIM2000 program.<sup>154</sup>

**Electronic spectra simulation:** The UV-vis spectra were simulated based on the excitation energies and oscillator strengths generated by the TD-DFT calculations. The simulated spectra were generated by application of a Gaussian broadening with a  $\sigma$  value of 0.24 eV. Table 18 provides a listing of the main low energy excitations responsible for the two low energy bands observed in the spectra of [37]<sup>+</sup> and [38]<sup>+</sup>. The molecular orbital contribution of the different transitions to each excitation is also provided.

**Table 18.** Partial TD-DFT calculation output showing the nature of the low energy excitations for [37]<sup>+</sup> and [38]<sup>+</sup>.

[37] <sup>+</sup>				
Excitations	Energy	Oscillator strength.	MO-MO transitions	Contributions
Ea	375.31 nm 3.30 eV	0.1187	136 ->138	0.21924
			137 ->138	0.64571
Eb	366.45 nm 3.38 eV	0.1584	136 ->138	0.62784
			136 ->139	-0.13948
			137 ->138	-0.20235
Ec	323.97 nm 3.83 eV	0.0726	133 ->138	-0.34244
			136 ->139	-0.40535
			137 ->139	0.40643
Ed	320.84 nm 3.86 eV	0.0674	133 ->138	0.53907
			134 ->138	-0.12276
			136 ->138	-0.10795
			136 ->139	-0.32022
			137 ->139	0.12385
[38] <sup>+</sup>				
Excitations	Energy	Oscillator strength.	MO-MO transitions	Contributions
Ea	359.25 nm 3.45 eV	0.0752	133 ->134	0.66922
			133 ->135	-0.15660
Eb	348.62 nm 3.56 eV	0.2147	132 ->134	0.65582
			132 ->135	-0.13461
Ec	313.55 nm 3.95 eV	0.0355	129 ->134	0.64324
			132 ->135	0.20113
Ed	311.63 nm 3.9786 eV	0.0319	129 ->134	-0.15923
			131 ->135	0.15788
			132 ->134	0.12298
			132 ->135	0.60372
			133 ->135	-0.14495
Ed	307.46 nm 4.0325 eV	0.535	129 ->134	-0.10788
			132 ->135	0.11618
			133 ->134	0.16653
			133 ->135	0.63941

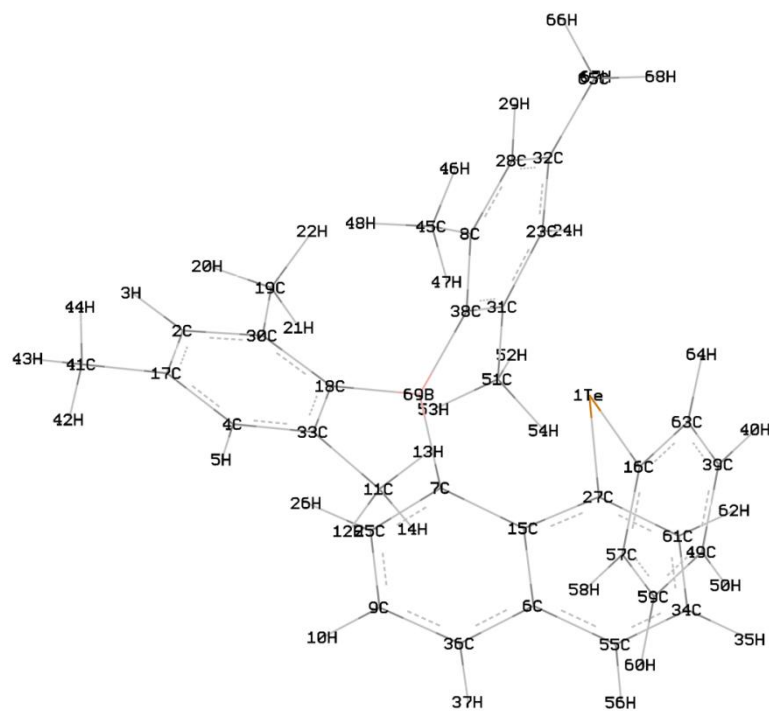


**Figure 59.** DFT optimized structure of **37**

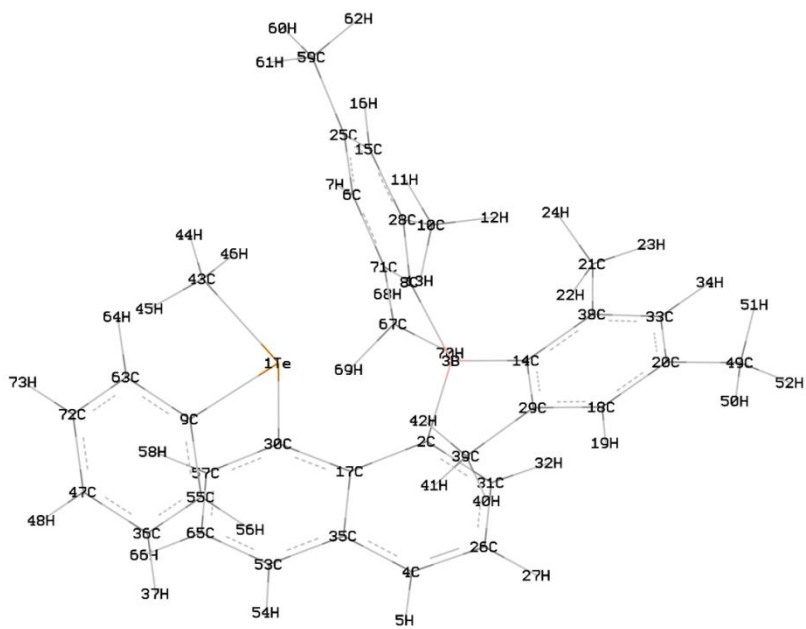


**Figure 60.** DFT optimized structure of **[37]<sup>+</sup>**

**Table 19:** Atom coordinates for the optimized structure of **37**

Center Number	Coordinates(Angstroms)		
	X	Y	Z
Te1	-0.917797	-1.108870	-0.944925
C2	4.251566	2.578519	0.199904
H3	4.724204	3.561945	0.081798
C4	4.424927	0.207493	0.588944
H5	5.033629	-0.687828	0.767907
C6	-1.828741	-0.136494	3.311640
C7	-0.041901	0.714111	1.763156
C8	0.144468	1.840175	-2.161674
C9	-0.011677	1.243177	4.192880
H10	0.487217	1.745549	5.027996
C11	2.443358	-1.304937	0.815859
H12	3.206719	-1.975895	1.247392
H13	2.087671	-1.764762	-0.126145
H14	1.577463	-1.278614	1.499027
C15	-1.230990	-0.085818	1.985713
C16	-0.774579	-3.255523	-0.823694
C17	5.066686	1.443563	0.388012
C18	2.185753	1.226043	0.340075
C19	2.076590	3.798575	-0.022119
H20	2.755590	4.661237	0.096807
H21	1.256956	3.914357	0.709348
H22	1.616342	3.867723	-1.024151
C23	-2.152827	3.326137	-1.521536
H24	-3.031038	3.929914	-1.261174
C25	0.555875	1.312933	2.890353
H26	1.482555	1.879593	2.752048
C27	-1.855177	-0.875349	0.956864
C28	-0.609895	2.483519	-3.163428
H29	-0.273263	2.407388	-4.204891
C30	2.843465	2.494929	0.166274
C31	-1.445664	2.682386	-0.480654
C32	-1.769697	3.229136	-2.870992
C33	3.017788	0.081357	0.584095
C34	-3.629522	-1.586621	2.491516
H35	-4.550469	-2.152431	2.662363
C36	-1.196501	0.550851	4.395389
H37	-1.656603	0.499841	5.388614
C38	-0.272705	1.890318	-0.773212
C39	-0.719462	-5.387929	-2.023482
H40	-0.802617	-5.947525	-2.961045
C41	6.579638	1.552811	0.370913
H42	7.050196	0.729126	0.935915
H43	6.922387	2.507918	0.807554
H44	6.973652	1.508178	-0.663526
C45	1.392709	1.105843	-2.625722
H46	1.386166	0.997666	-3.724523
H47	1.481155	0.098058	-2.180783
H48	2.312703	1.647234	-2.342052
C49	-0.470663	-6.066002	-0.814562
H50	-0.355334	-7.154408	-0.809145
C51	-1.962463	2.942163	0.927833
H52	-2.665704	3.793145	0.918854
H53	-1.152569	3.177830	1.637467
H54	-2.502720	2.072024	1.340842
C55	-3.026086	-0.885564	3.528477
H56	-3.457109	-0.900971	4.535772
C57	-0.515308	-3.937933	0.387754
H58	-0.429741	-3.380329	1.325368
C59	-0.372472	-5.338834	0.388545
H60	-0.177139	-5.861271	1.330959
C61	-3.033823	-1.589339	1.201160
H62	-3.492638	-2.175066	0.399075
C63	-0.876410	-3.987975	-2.030681
H64	-1.089730	-3.469583	-2.972588
C65	-2.576386	3.891191	-3.970386
H66	-1.924989	4.281275	-4.772825
H67	-3.179850	4.728907	-3.579809
H68	-3.275916	3.172255	-4.440191
B69	0.588420	1.152384	0.361088

**Table 20:** Atom coordinates for the optimized structure [37]<sup>+</sup>

Center Number	Coordinates(Angstroms)		
	X	Y	Z
Te1	1.453974	0.323877	-0.675331
C2	-0.810806	-1.003019	1.538351
B3	-1.539447	-0.116241	0.433760
C4	-0.122990	-2.302805	4.017578
H5	0.143638	-2.763731	4.974151
C6	-0.957324	3.698728	1.294746
H7	-0.836135	4.319366	2.190283
C8	-1.284594	1.452296	0.296852
C9	3.314298	-0.492220	-1.388897
C10	-1.659009	1.364738	-2.292831
H11	-1.374590	1.983915	-3.161323
H12	-2.735776	1.135310	-2.386224
H13	-1.136042	0.396386	-2.374309
C14	-2.679288	-0.825144	-0.398454
C15	-1.203421	3.505232	-1.098652
H16	-1.259747	3.970525	-2.089922
C17	0.557718	-0.950161	2.029324
C18	-3.477320	-2.623847	-1.890305
H19	-3.258337	-3.513162	-2.493007
C20	-4.798563	-2.138244	-1.843241
C21	-4.416962	0.891070	0.477911
H22	-4.009406	0.848963	1.504218
H23	-5.514212	0.966156	0.562619
H24	-4.054400	1.832715	0.026481
C25	-1.006458	4.326936	0.032251
C26	-1.398443	-2.436690	3.493094
H27	-2.160164	-3.016810	4.021424
C28	-1.370778	2.108292	-0.995054
C29	-2.427288	-2.003216	-1.180991
C30	1.666960	-0.347539	1.337245
C31	-1.725318	-1.798079	2.266716
H32	-2.746801	-1.891882	1.886813
C33	-5.050613	-0.991328	-1.057184
H34	-6.076124	-0.609417	-0.985946
C35	0.884464	-1.578531	3.304590
C36	4.706087	-2.453568	-1.764668
H37	4.896071	-3.521494	-1.624624
C38	-4.029403	-0.325998	-0.351982
C39	-1.029920	-2.581491	-1.347828
H40	-1.074299	-3.625293	-1.702741
H41	-0.463754	-2.570496	-0.400152
H42	-0.444123	-2.014558	-2.101431
C43	2.192598	2.328457	-0.395636
H44	2.276122	2.806965	-1.382481
H45	3.167585	2.266845	0.108959
H46	1.444423	2.848642	0.221353
C47	5.614803	-1.661747	-2.494839
H48	6.511915	-2.116685	-2.923642
C49	-5.919414	-2.825349	-2.595884
H50	-5.552423	-3.698648	-3.160013
H51	-6.402772	-2.136771	-3.313650
H52	-6.709482	-3.175905	-1.906025
C53	2.205464	-1.489354	3.840184
H54	2.406707	-1.962840	4.806531
C55	3.547604	-1.874936	-1.212129
H56	2.849864	-2.495204	-0.639947
C57	2.956207	-0.283539	1.877617
H58	3.780126	0.155425	1.306532
C59	-0.901422	5.831384	-0.099123
H60	-0.470340	6.127668	-1.070630
H61	-0.284803	6.269146	0.704320
H62	-1.902439	6.299789	-0.031849
C63	4.213688	0.305367	-2.129448
H64	4.033672	1.373452	-2.284102
C65	3.223474	-0.836099	3.156281
H66	4.231127	-0.772620	3.574794
C67	-1.092274	1.784928	2.885436
H68	-1.257549	2.619364	3.587306
H69	-0.134853	1.308686	3.162832
H70	-1.883234	1.037384	3.060414
C71	-1.088377	2.301538	1.453669
C72	5.369517	-0.287497	-2.676971
H73	6.073741	0.327045	-3.244979



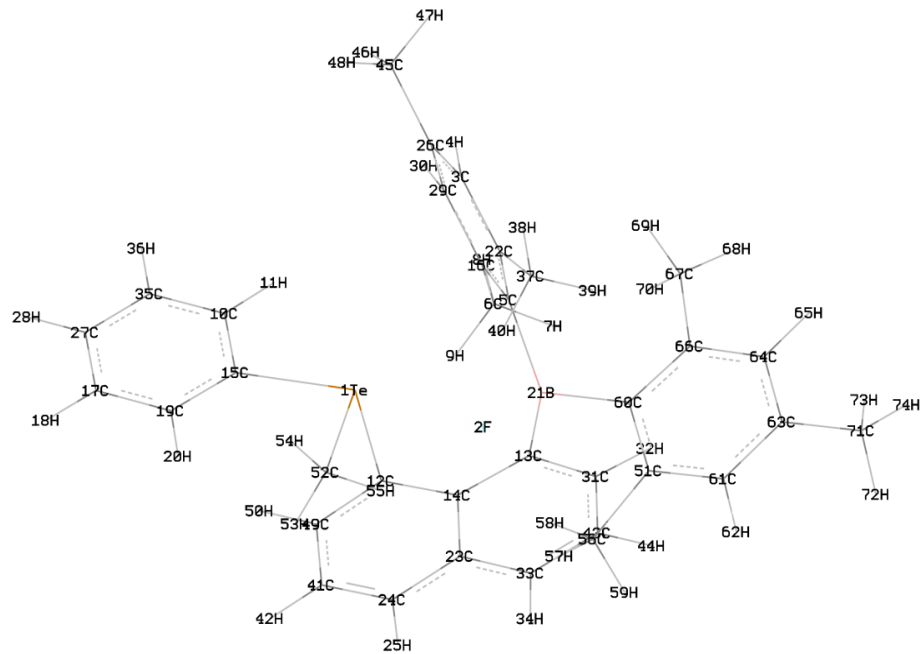


**Figure 61.** Computed structure of **37-F**

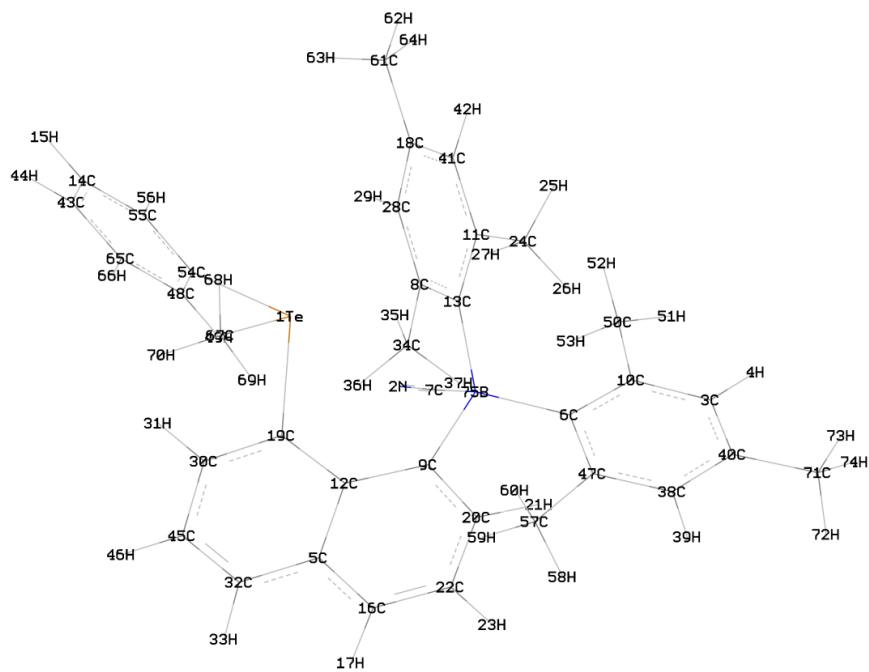


**Figure 62.** Computed structure of **37-CN**.

**Table 21:** Atom coordinates for the optimized structure of **37-F**

Center Number	Coordinates(Angstroms)		
	X	Y	Z
Te1	1.588376	0.129918	-0.904963
F2	-0.774471	-0.184813	-1.327475
C3	-0.041069	3.699109	0.078384
H4	-0.057664	4.552723	-0.612020
C5	-0.808681	1.397530	0.624050
C6	-0.098958	0.472884	2.964387
H7	-1.113383	0.093617	3.168529
H8	0.296807	0.905603	3.900661
H9	0.518413	-0.410053	2.719668
C10	4.191971	0.763187	0.568703
H11	3.463831	1.120882	1.306885
C12	1.285032	-1.783309	0.062375
C13	-1.167354	-1.401805	0.844515
C14	0.067008	-2.171791	0.751838
C15	3.749304	0.163772	-0.635248
C16	-0.090711	1.528057	1.862875
C17	6.075370	-0.104151	-1.339047
H18	6.805386	-0.435700	-2.084473
C19	4.697685	-0.262712	-1.592811
H20	4.377773	-0.718307	-2.535038
B21	-1.520951	0.007632	0.067148
C22	-0.802225	2.554680	-0.243483
C23	0.135816	-3.481585	1.412432
C24	1.295813	-4.308458	1.303246
H25	1.283134	-5.281594	1.806980
C26	0.722603	3.788735	1.261477
C27	6.511361	0.477084	-0.133247
H28	7.581624	0.596954	0.060867
C29	0.661327	2.698158	2.146012
H30	1.196834	2.758593	3.102908
C31	-2.202189	-1.950892	1.624069
H32	-3.144020	-1.396934	1.682524
C33	-0.965923	-3.954603	2.187689
H34	-0.878861	-4.932454	2.674268
C35	5.569001	0.911030	0.819947
H36	5.904380	1.369692	1.755419
C37	-1.609527	2.618798	-1.533932
H38	-1.540664	3.626981	-1.979536
H39	-2.673591	2.390011	-1.352492
H40	-1.264499	1.884259	-2.281736
C41	2.411662	-3.899111	0.593014
H42	3.297351	-4.535580	0.509428
C43	-2.114411	-3.190716	2.307444
H44	-2.963263	-3.547656	2.899990
C45	1.527758	5.033388	1.586439
H46	2.129825	4.894492	2.501268
H47	0.869562	5.908372	1.749997
H48	2.216953	5.299368	0.763216
C49	2.406280	-2.615508	-0.011976
H50	3.310944	-2.279413	-0.525875
C51	-3.700299	-0.720710	-1.323752
C52	1.694058	-0.650509	-2.916297
H53	2.226227	-1.613265	-2.899207
H54	2.209880	0.085676	-3.552248
H55	0.649723	-0.784919	-3.230157
C56	-2.888912	-1.714851	-2.146528
H57	-2.185546	-2.288602	-1.520117
H58	-2.286016	-1.212082	-2.924000
H59	-3.563816	-2.429314	-2.651733
C60	-3.129875	0.086035	-0.277779
C61	-5.079590	-0.646890	-1.624035
H62	-5.476322	-1.277700	-2.430676
C63	-5.961287	0.189176	-0.914660
C64	-5.422369	0.933546	0.150060
H65	-6.090265	1.561617	0.754371
C66	-4.047097	0.893920	0.479226
C67	-3.623675	1.730873	1.681270
H68	-4.514137	2.053317	2.250737
H69	-3.067881	2.638600	1.385238
H70	-2.968981	1.172768	2.372582
C71	-7.431622	0.280098	-1.279475
H72	-7.793110	-0.658081	-1.737563
H73	-7.618509	1.092583	-2.009526
H74	-8.056348	0.490244	-0.392633

**Table 22.** Atom coordinates for the optimized structure of **37-CN**

Center Number	Coordinates(Angstroms)		
	X	Y	Z
Te1	0.242009	-1.961422	0.381459
N2	-1.448128	-0.535751	2.320754
C3	-3.126840	4.554668	-0.449334
H4	-3.514090	5.075008	-1.335194
C5	3.119133	1.352524	1.564673
C6	-1.762887	2.701886	0.484299
C7	-1.230203	0.300123	1.510047
C8	-0.091539	0.194981	-2.086627
C9	0.784550	1.683328	0.671449
C10	-2.298346	3.422968	-0.640693
C11	-2.344095	-0.244954	-1.227417
C12	1.841597	0.775076	1.117211
C13	-1.080167	0.428653	-1.058225
C14	2.069090	-5.523124	-1.527873
H15	1.834767	-6.591769	-1.560260
C16	3.352873	2.758172	1.470260
H17	4.319061	3.148834	1.808128
C18	-1.533849	-1.473865	-3.215829
C19	1.806262	-0.680125	1.162614
C20	1.116841	3.049314	0.598098
H21	0.338279	3.741674	0.266106
C22	2.374772	3.593288	0.962514
H23	2.548211	4.670572	0.871972
C24	-3.537715	-0.005188	-0.312839
H25	-4.476791	-0.216897	-0.854939
H26	-3.572775	1.034762	0.048617
H27	-3.516738	-0.655745	0.581304
C28	-0.330463	-0.749158	-3.117060
H29	0.446320	-0.899509	-3.878222
C30	2.865260	-1.443442	1.670952
H31	2.810772	-2.535355	1.665313
C32	4.166000	0.538197	2.094063
H33	5.081703	1.036022	2.432072
C34	1.213593	0.976593	-2.205684
H35	1.632891	0.847557	-3.219452
H36	1.985321	0.659209	-1.482240
H37	1.063310	2.054624	-2.034800
C38	-2.886803	4.383713	1.929135
H39	-3.081610	4.766367	2.939668
C40	-3.460070	5.041121	0.826475
C41	-2.538447	-1.174547	-2.275361
H42	-3.514206	-1.669947	-2.364037
C43	3.156187	-5.013285	-2.262976
H44	3.770096	-5.685920	-2.869605
C45	4.045623	-0.838704	2.169370
H46	4.847714	-1.460812	2.576337
C47	-2.053637	3.250743	1.785808
C48	2.666611	-2.765827	-1.438853
H49	2.905343	-1.698880	-1.405605
C50	-2.005175	3.069164	-2.093378
H51	-2.301426	3.906665	-2.750562
H52	-2.552141	2.170770	-2.429802
H53	-0.934818	2.871876	-2.268341
C54	1.583771	-3.279836	-0.692126
C55	1.277495	-4.658643	-0.745752
H56	0.431364	-5.067178	-0.182481
C57	-1.474816	2.693988	3.081108
H58	-1.487835	3.474283	3.863413
H59	-0.432443	2.355185	2.962780
H60	-2.053354	1.833584	3.464023
C61	-1.758718	-2.481509	-4.328407
H62	-2.742308	-2.972565	-4.230911
H63	-0.983941	-3.270809	-4.324732
H64	-1.722929	-1.999084	-5.323865
C65	3.451892	-3.636659	-2.218901
H66	4.294836	-3.237344	-2.791534
C67	0.148289	-3.271687	2.113804
H68	-0.640642	-4.014140	1.912718
H69	-0.148902	-2.621095	2.948348
H70	1.119410	-3.758537	2.278828
C71	-4.390694	6.225937	1.005494
H72	-4.117471	6.826251	1.892096
H73	-5.439633	5.897549	1.146225
H74	-4.373177	6.891189	0.123694
B75	-0.818047	1.328634	0.331697

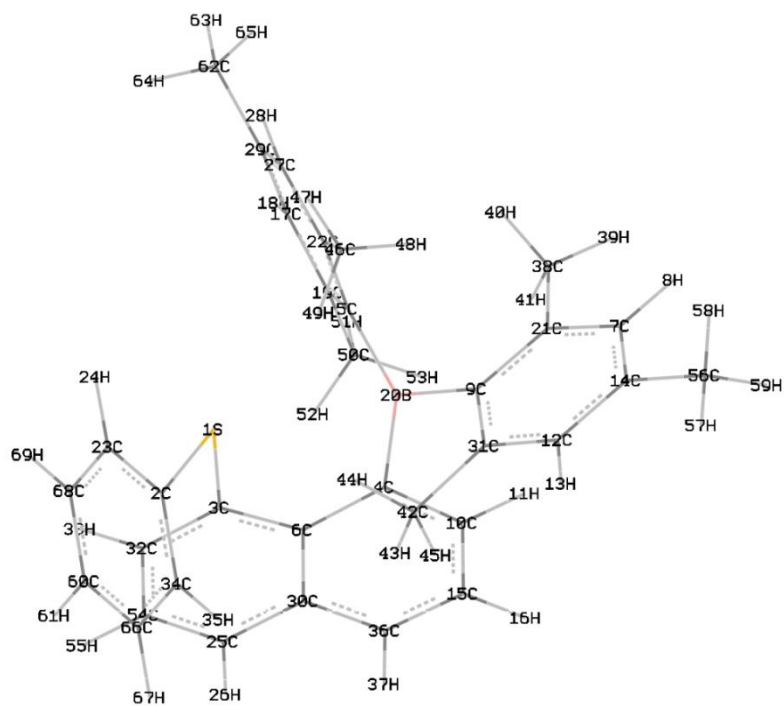


**Figure 63.** DFT optimized structure of **38**

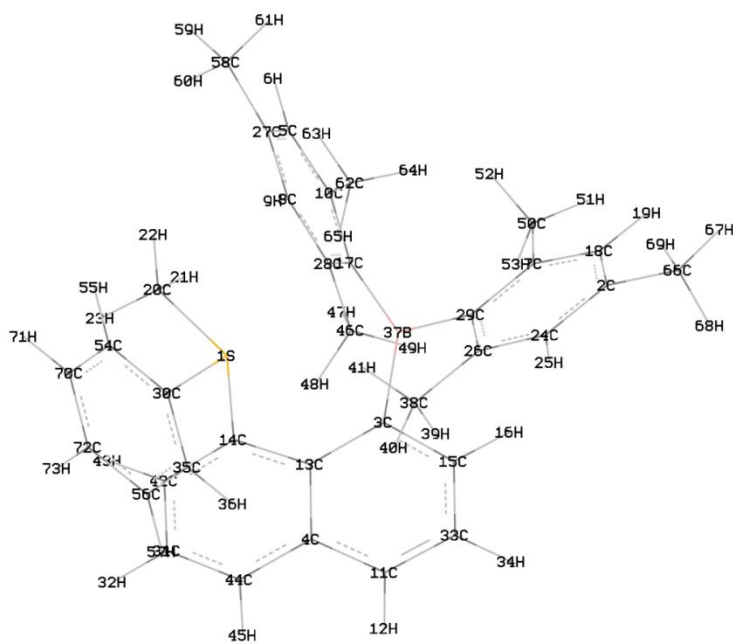


**Figure 64.** DFT optimized structure of **[38]<sup>+</sup>**

**Table 23:** Atom coordinates for the optimized structure of **38**

Center Number	Coordinates(Angstroms)		
	X	Y	Z
S1	1.614549	0.271494	-0.963642
C2	2.879431	-0.926936	-1.444761
C3	2.157023	0.736259	0.691000
C4	-0.095515	0.126957	1.711774
C5	-1.178065	1.450012	-0.485616
C6	1.283363	0.564776	1.823790
C7	-4.336185	-1.948539	0.184775
H8	-5.415282	-1.748711	0.201779
C9	-2.022549	-1.082894	0.260535
C10	-0.782910	-0.171999	2.904860
H11	-1.807062	-0.554065	2.836907
C12	-2.495659	-3.503052	0.106800
H13	-2.118096	-4.531606	0.049068
C14	-3.885279	-3.281805	0.094939
C15	-0.220286	0.046670	4.192861
H16	-0.809069	-0.180368	5.087463
C17	-1.328994	3.903860	-0.776563
H18	-1.315424	4.904315	-0.326000
C19	-1.147423	2.783746	0.062836
B20	-1.015089	0.143439	0.412323
C21	-3.444542	-0.857939	0.256293
C22	-1.416724	1.329678	-1.902963
C23	3.194470	-1.003820	-2.822862
H24	2.733708	-0.300475	-3.524166
C25	3.187847	1.302068	3.264881
H26	3.584898	1.489728	4.268552
C27	-1.569208	2.480904	-2.704045
H28	-1.727917	2.355714	-3.782445
C29	-1.529100	3.781137	-2.165269
C30	1.849610	0.819791	3.139562
C31	-1.567427	-2.442692	0.201125
C32	3.458400	1.228956	0.851774
H33	4.091591	1.365780	-0.029430
C34	3.488259	-1.824712	-0.537262
H35	3.246384	-1.772231	0.527622
C36	1.062181	0.561882	4.306721
H37	1.504082	0.760086	5.289600
C38	-4.055802	0.534716	0.351430
H39	-5.137525	0.463725	0.561816
H40	-3.930905	1.103089	-0.587767
H41	-3.597934	1.143268	1.151157
C42	-0.091106	-2.798395	0.191132
H43	0.453022	-2.305411	1.015388
H44	0.401419	-2.480264	-0.746206
H45	0.048549	-3.889003	0.288536
C46	-1.497605	-0.013968	-2.610745
H47	-1.499515	0.129257	-3.705575
H48	-2.414735	-0.565961	-2.339230
H49	-0.646843	-0.670950	-2.355641
C50	-0.981994	3.076098	1.548246
H51	-1.224743	4.133158	1.754699
H52	0.051692	2.899594	1.895203
H53	-1.638180	2.450851	2.177491
C54	3.974129	1.521886	2.139922
H55	4.994815	1.903477	2.238808
C56	-4.868021	-4.433605	-0.001533
H57	-4.348005	-5.406937	0.004254
H58	-5.465701	-4.377776	-0.931440
H59	-5.583872	-4.427015	0.841847
C60	4.719341	-2.858808	-2.379533
H61	5.434259	-3.605132	-2.739153
C62	-1.694945	5.005711	-3.044332
H63	-1.951822	4.725141	-4.080277
H64	-0.764655	5.604537	-3.080135
H65	-2.492260	5.671858	-2.665063
C66	4.409736	-2.777931	-1.007189
H67	4.879932	-3.466348	-0.297402
C68	4.105933	-1.971595	-3.284581
H69	4.345539	-2.020910	-4.351618

**Table 24:** Atom coordinates for the optimized structure of **[38]<sup>+</sup>**:

Center Number	Coordinates(Angstroms)		
	X	Y	Z
S1	0.086381	0.064947	1.819496
C2	3.224435	-0.391698	-4.153047
C3	-0.964501	-1.191268	-0.918628
C4	-2.641547	-2.622876	0.292056
C5	-0.069572	3.862406	-0.039988
H6	0.687810	4.606448	0.235562
C7	1.100226	0.689732	-3.504173
C8	-2.379328	3.255174	-0.386228
H9	-3.441806	3.525636	-0.399334
C10	0.354162	2.574293	-0.430286
C11	-2.933135	-3.298430	-0.935655
H12	-3.708114	-4.071413	-0.935226
C13	-1.618746	-1.582330	0.318532
C14	-1.324452	-1.051191	1.625288
C15	-1.257288	-1.957081	-2.068139
H16	-0.735326	-1.711079	-2.997725
C17	-0.615383	1.564845	-0.792033
C18	2.158282	0.491975	-4.416683
H19	2.146952	1.041666	-5.365222
C20	-0.657122	1.556442	2.592628
H21	-1.427120	1.909719	1.889399
H22	0.122770	2.325865	2.680958
H23	-1.089953	1.302017	3.570780
C24	3.201025	-1.104841	-2.935211
H25	4.020219	-1.796670	-2.704672
C26	2.153078	-0.957441	-2.006259
C27	-1.431067	4.232619	-0.017479
C28	-2.007844	1.947455	-0.771488
C29	1.073310	-0.042686	-2.267194
C30	1.018702	-0.682624	3.204365
C31	-3.060162	-2.382319	2.704394
H32	-3.606167	-2.663796	3.608016
C33	-2.229633	-2.993798	-2.089343
H34	-2.427452	-3.531991	-3.020514
C35	1.258012	-2.073183	3.170074
H36	0.808784	-2.702094	2.396870
B37	-0.133314	0.126287	-1.263478
C38	2.252661	-1.732932	-0.701171
H39	3.027510	-2.515476	-0.767607
H40	1.298373	-2.222756	-0.438960
H41	2.534016	-1.072387	0.144083
C42	-2.019380	-1.427004	2.781066
H43	-1.740539	-1.016796	3.756365
C44	-3.344246	-2.980989	1.481171
H45	-4.114111	-3.756453	1.415126
C46	-3.133687	1.024262	-1.218464
H47	-4.063022	1.600675	-1.361265
H48	-3.348982	0.231265	-0.479996
H49	-2.905738	0.518565	-2.172111
C50	0.001154	1.665924	-3.903699
H51	0.088347	1.926386	-4.972091
H52	0.056302	2.607384	-3.327217
H53	-1.011068	1.252634	-3.746572
C54	1.599083	0.137019	4.194414
H55	1.433562	1.216727	4.216593
C56	2.072432	-2.648384	4.162494
H57	2.254362	-3.726351	4.147823
C58	-1.856615	5.639877	0.346008
H59	-1.148484	6.112317	1.048200
H60	-2.861932	5.657715	0.800769
H61	-1.896742	6.281607	-0.555353
C62	1.855856	2.321077	-0.438880
H63	2.384582	3.122328	0.106046
H64	2.253862	2.301099	-1.468815
H65	2.137149	1.354592	0.015868
C66	4.354617	-0.580859	-5.144278
H67	4.224581	0.059319	-6.032398
H68	4.414250	-1.629873	-5.489727
H69	5.332769	-0.335967	-4.690300
C70	2.411174	-0.457815	5.180271
H71	2.856020	0.170164	5.956877
C72	2.647161	-1.844857	5.166633
H73	3.278781	-2.298736	5.934779

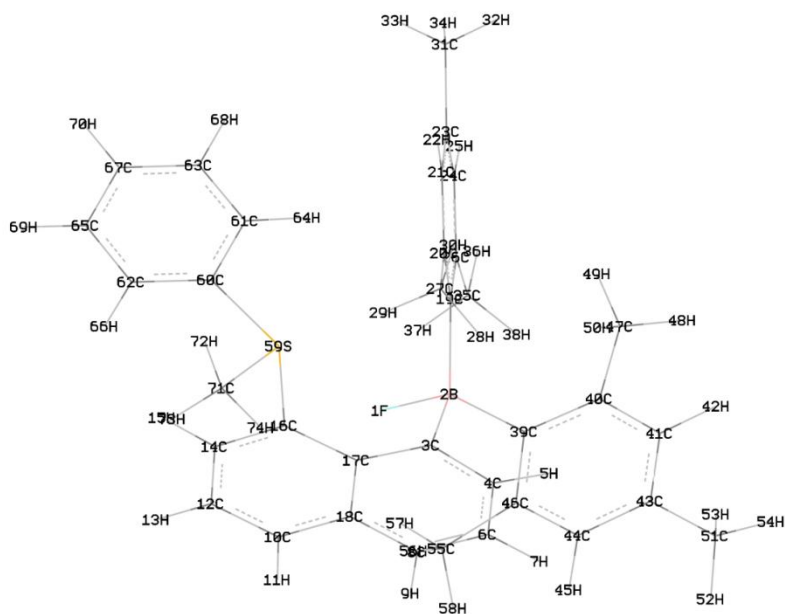


**Figure 65.** DFT optimized structure of **38-F**

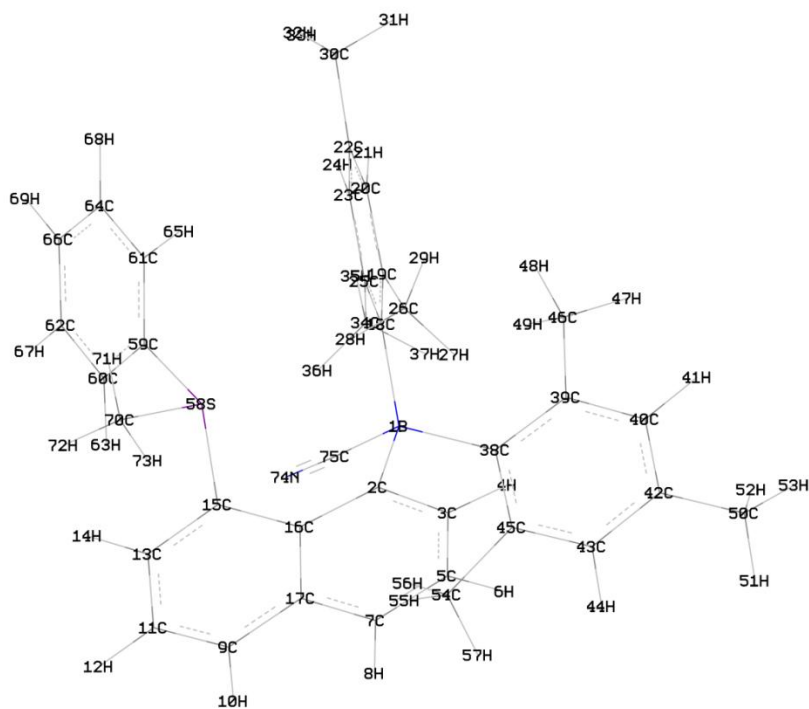


**Figure 66.** DFT optimized structure of **38-CN**

**Table 25:** Atom coordinates for the optimized structure of **38-F**

Center Number	Coordinates(Angstroms)		
	X	Y	Z
F1	-0.619404	-0.222778	0.124022
B2	-0.345380	-0.003002	1.621951
C3	1.031871	-0.893207	1.873956
C4	1.097373	-1.608946	3.084617
H5	0.271243	-1.481253	3.790580
C6	2.135743	-2.511310	3.429966
H7	2.110808	-3.026330	4.395932
C8	3.149675	-2.763820	2.521978
H9	3.943370	-3.486890	2.739048
C10	4.226383	-2.388495	0.352399
H11	4.965016	-3.140742	0.650780
C12	4.331943	-1.751217	-0.874376
H13	5.140683	-1.987896	-1.571094
C14	3.387336	-0.750329	-1.203368
H15	3.514747	-0.199132	-2.138917
C16	2.337741	-0.435011	-0.335172
C17	2.130433	-1.101119	0.938538
C18	3.173017	-2.085797	1.265906
C19	-0.221976	1.647309	1.783101
C20	-1.258837	2.463110	1.200666
C21	-1.199642	3.874073	1.258272
H22	-2.017374	4.453113	0.808304
C23	-0.142550	4.557098	1.891256
C24	0.862425	3.770868	2.482272
H25	1.682842	4.271312	3.014822
C26	0.841703	2.352598	2.444280
C27	-2.479667	1.865262	0.512139
H28	-2.873441	0.998760	1.068173
H29	-2.241839	1.497772	-0.502533
H30	-3.279921	2.621936	0.422882
C31	-0.113014	6.073112	1.964386
H32	-0.941179	6.464473	2.586312
H33	-0.218416	6.533613	0.963846
H34	0.832040	6.435545	2.406188
C35	1.987202	1.663703	3.180081
H36	2.605326	2.413808	3.705944
H37	2.653474	1.094368	2.507371
H38	1.626151	0.942195	3.933287
C39	-1.616914	-0.709342	2.427482
C40	-2.182166	-0.199742	3.647887
C41	-3.282401	-0.841405	4.265379
H42	-3.682553	-0.416742	5.195779
C43	-3.871299	-2.002512	3.735237
C44	-3.291990	-2.539231	2.571054
H45	-3.698270	-3.470102	2.152750
C46	-2.191851	-1.931630	1.924528
C47	-1.646101	1.029927	4.371735
H48	-2.069851	1.083133	5.391122
H49	-1.903945	1.967991	3.849620
H50	-0.547417	1.016192	4.466892
C51	-5.078135	-2.649664	4.389461
H52	-5.081302	-3.744488	4.239102
H53	-6.026053	-2.260732	3.966962
H54	-5.102426	-2.454134	5.476609
C55	-1.658174	-2.664879	0.698600
H56	-0.556051	-2.691925	0.681646
H57	-1.977039	-2.178192	-0.240358
H58	-2.030468	-3.705706	0.687418
S59	1.277180	0.964985	-0.878828
C60	2.475119	2.161966	-1.562309
C61	2.895262	3.150080	-0.643157
C62	2.915267	2.192636	-2.902935
C63	3.791430	4.148332	-1.066251
H64	2.500593	3.153705	0.379362
C65	3.803260	3.204836	-3.315138
H66	2.572837	1.452534	-3.631081
C67	4.249015	4.175377	-2.397868
H68	4.116695	4.913501	-0.355708
H69	4.143155	3.232349	-4.354782
H70	4.939786	4.958446	-2.724153
C71	0.502821	0.300440	-2.402045
H72	0.015293	1.137112	-2.926212
H73	1.241039	-0.202075	-3.043927
H74	-0.247887	-0.413267	-2.037485



**Table 26:** Atom coordinates for the optimized structure of **38-CN**

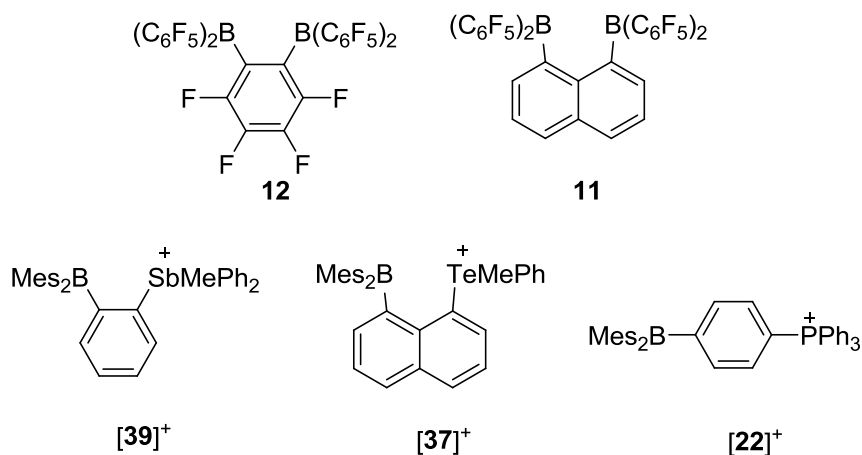
Center Number	Coordinates(Angstroms)		
	X	Y	Z
B1	-0.013526	-0.000183	-0.004992
C2	0.005769	-0.004488	1.687774
C3	1.290757	-0.008055	2.267544
H4	2.145219	-0.149045	1.600105
C5	1.558683	0.238464	3.639031
C6	2.591138	0.209322	4.002119
C7	0.522754	0.597220	4.485449
C8	0.707276	0.889614	5.524686
C9	-1.865421	1.029058	4.873388
H10	-1.591248	1.359770	5.881272
C11	-3.194371	1.031367	4.473749
H12	-3.986468	1.387836	5.137605
C13	-3.522828	0.505328	3.200159
H14	-4.577071	0.422107	2.924782
C15	-2.519100	0.074628	2.325214
C16	-1.101775	0.200929	2.616674
C17	-0.818750	0.605726	3.999879
C18	-0.360867	-1.432932	-0.800578
C19	-0.644027	-1.392981	-2.214723
C20	-0.976303	-2.570409	-2.925895
H21	-1.178263	-2.491281	-4.002392
C22	-1.026980	-3.835380	-2.311028
C23	-0.724945	-3.887981	-0.937990
H24	-0.723875	-4.861440	-0.429659
C25	-0.399306	-2.732805	-0.184750
C26	-0.570876	-0.116451	-3.043137
H27	0.273942	0.522467	-2.737513
H28	-1.484967	0.496972	-2.946782
H29	-0.444909	-0.365522	-4.112085
C30	-1.333841	-5.091402	-3.107072
H31	-0.438798	-5.455128	-3.649076
H32	-2.117605	-4.911812	-3.865752
H33	-1.672735	-5.913681	-2.451570
C34	-0.043785	-2.988134	1.275235
H35	-0.072905	-4.071814	1.487178
H36	-0.729163	-2.494599	1.987753
H37	0.967257	-2.622318	1.525497
C38	1.416953	0.729826	-0.509558
C39	2.526607	-0.000602	-1.068878
C40	3.686317	0.674578	-1.519459
H41	4.506770	0.078454	-1.940340
C42	3.832298	2.069696	-1.434591
C43	2.788042	2.781678	-0.820325
H44	2.889538	3.866519	-0.684107
C45	1.611072	2.150910	-0.354632
C46	2.582020	-1.520242	-1.182740
H47	3.622705	-1.841364	-1.371262
H48	1.956640	-1.909726	-2.004866
H49	2.239397	-2.023160	-0.263161
C50	5.065207	2.772318	-1.971691
H51	5.291725	3.689075	-1.397856
H52	4.929167	3.075457	-3.028875
H53	5.953851	2.116770	-1.933438
C54	0.612864	3.070179	0.338760
H55	0.138275	2.593116	1.212154
H56	-0.204350	3.387780	-0.333134
H57	1.128213	3.981785	0.692048
S58	-3.033214	-0.828231	0.843546
C59	-3.728432	-2.410311	1.451319
C60	-4.087092	-2.664181	2.788508
C61	-3.866592	-3.401156	0.453977
C62	-4.620935	-3.924031	3.123384
H63	-3.936345	-1.906934	3.561426
C64	-4.415773	-4.649013	0.802776
H65	-3.517039	-3.215247	-0.566158
C66	-4.794280	-4.910335	2.133615
H67	-4.895560	-4.131502	4.161810
H68	-4.526197	-5.420342	0.035424
H69	-5.210028	-5.886043	2.401969
C70	-4.573756	0.009054	0.287924
H71	-4.923908	-0.556593	-0.589664
H72	-5.345292	0.009729	1.070232
H73	-4.262978	1.020766	-0.017552
N74	-2.168825	1.658080	-0.661366
C75	-1.235624	0.981310	-0.396955

## CHAPTER V

ON THE SYNERGY OF COULOMBIC AND CHELATE EFFECTS IN BIDENTATE  
 DIBORANES: SYNTHESIS AND ANION BINDING PROPERTIES OF A CATIONIC  
 1,8-DIBORYLNAPHTHALENE

## 5.1 Introduction

The chemistry of boron-based bidentate Lewis acids<sup>19-24</sup> is an area of active investigation with application in the domains of anion complexation,<sup>25-26</sup> organometallic catalysis,<sup>27-30</sup> as well as small molecule activation.<sup>31-32</sup> Since the properties of these bidentate Lewis acids can be influenced by the respective positions and electronic features of the binding sites, a great deal of attention has been dedicated to the synthesis of compounds with juxtaposed electron-poor boron functionalities.<sup>27, 31</sup> Prototypical examples of such compounds include the fluorinated diboranes **12** and **11** which have both been shown to chelate small anions.<sup>27, 31</sup>



In a variant of this approach, several groups, including ours, have become interested in boron-based bidentate Lewis acids that bear a cationic group in proximity from the boron atom.<sup>30, 45, 49, 59-62, 155-158</sup> Examples of such compounds include **[39]**<sup>+</sup> and **[37]**<sup>+</sup> which have been investigated for the complexation of fluoride anions.<sup>59, 158</sup> For these compounds, the coordination of the anion is supported by the formation of a B-F→Sb (for **[39]**<sup>+</sup>) or B-F→Te (for **[37]**<sup>+</sup>) motif whose formation illustrates the Lewis acidic behavior of the heavy onium moiety. The stability of the resulting complexes also benefits from strong Coulombic effects which prevent dissociation of the anion from the cationic guest. The favorable influence of these Coulombic effects have also been demonstrated in the case of triarylboranes decorated by peripheral cationic moieties such as the phosphonium borane **[22]**<sup>+</sup> which, unlike neutral boranes, captures F<sup>-</sup> in aqueous solution.<sup>62</sup>

Building on these earlier achievements, we have now decided to target bidentate diboranes that incorporate a peripheral cationic functionality. From a simple conceptual viewpoint, we anticipate that the anion affinity of such system would benefit from: i) the chelate effect provided by the chelating diborane moiety; ii) the Coulombic effect imparted by the presence of a peripheral cationic group.

## 5.2 Synthesis and characterization of the cationic diborane

Inspired by Katz's seminal contribution on the anion affinity of 1,8-dimethylborylnaphthalene,<sup>20, 34-36</sup> our group has investigated the synthesis of numerous naphthalene-based diboranes<sup>56, 159-161</sup> including **10**,<sup>37, 162</sup> whose fluoride binding

constants exceed that of monofunctional analogues by at least 3 or 4 orders of magnitude. With the synthesis of a cationic bidentate borane as an objective, it occurred to us that the sulfur atom of the thiaborin<sup>163-166</sup> moiety could possibly be alkylated. With this in mind, **10** was allowed to react with MeOTf in refluxing dichloromethane to afford [40]OTf as a moisture sensitive compound (Figure 67). This salt has been characterized by NMR spectroscopy, UV-vis spectroscopy and single crystal X-ray diffraction. The <sup>1</sup>H NMR spectrum of this compound shows a singlet at 3.60 ppm corresponding to the methyl group of the sulfonium ion. In addition, six distinct methyl groups are observed for the mesityl substituents indicating that the structure of [40]<sup>+</sup> is sterically congested. Although the *S*-alkylation of thiaborins has, to our knowledge, never been reported, we note that related reactions are known for phosphaborins which can be easily converted into the corresponding phosphonium species.<sup>47, 167-168</sup>

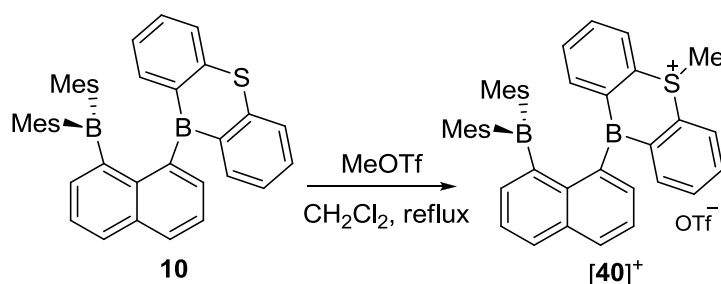


**Figure 67** Synthesis of the sulfonium diborane of [40]<sup>+</sup>

The crystal structure of [40]OTf shows that: 1) both boron centers B(1) and B(2) adopt a trigonal-planar coordination geometry as indicated by the sum of the C<sub>aryl</sub>-B-C<sub>aryl</sub> angles ( $\sum \angle \text{C-B(1)-C} = 356.02^\circ$ ,  $\sum \angle \text{C-B(2)-C} = 359.55^\circ$ ); 2) the distance separating the two boron atoms (3.276(3) Å) is almost identical to that of the neutral precursor **10**

(3.279(4) Å); 3) the sulfur-bound methyl group points outwards from the diboron pocket (Figure 68, Table 27). The UV-vis spectrum of [40]OTf in CHCl<sub>3</sub> exhibits a band centered at  $\lambda_{\text{max}} = 349$  nm.<sup>5</sup> This band, whose position is close to that observed for **10** ( $\lambda_{\text{max}} = 363$  nm in THF),<sup>37</sup> originates from the trigonal planar boron-centered chromophores thus implying that the triflate counteranion does not associate with [40]<sup>+</sup> in solution. To confirm this photophysical assignment, the structure of [40]<sup>+</sup> has been computationally optimized using DFT methods (functional: B3LYP; mixed basis set: B: 6-31+g(d'); S: 6-31+g(d); C, H: 6-31g). The optimized geometry, which is close to that determined experimentally, was subjected to a time-dependent DFT calculation using the PCM solvation model with chloroform as a solvent. The LUMO of [40]<sup>+</sup> is localized on the cationic and thus inherently electron-deficient sulfonium boryl moiety, with a dominating contribution from the *p<sub>z</sub>* orbital of the boron atom. The LUMO+1 is centered on the other boryl moiety, again with a large contribution from the *p<sub>z</sub>* orbital of the boron atom. These orbital characteristics contrast with those of the neutral precursor **10**, for which the LUMO shows an almost equal contribution from both boron *p<sub>z</sub>* orbitals (Figure 69).<sup>37, 162, 169</sup> These differences illustrate the asymmetry induced by the cationic sulfonium moiety, making one side of the molecule distinctly more electron-deficient than the other one. TD-DFT calculations indicate that both the LUMO and LUMO+1 of [40]<sup>+</sup> are the main accepting orbitals of the electronic transitions that contribute to the low energy band observed at  $\lambda_{\text{max}} 349$  nm. We have also compared the electrochemical properties of **10** and [40]<sup>+</sup>. Unlike the cyclic voltammogram of **10** which shows two reversible reduction waves at  $E_{1/2}$  -2.20 V and -2.57 V (vs. Fc/Fc<sup>+</sup>),<sup>162</sup> [40]<sup>+</sup> only

displays an irreversible wave at  $E_{\text{red}} -1.66 \text{ V}$  (vs.  $\text{Fc}/\text{Fc}^+$ ) in THF. The potential of this wave, which is much more positive than that of **10**, indicates that  $[\mathbf{40}]^+$  is substantially more electrophilic than **10**. Its irreversibility also suggests that the resulting neutral radical is unstable.

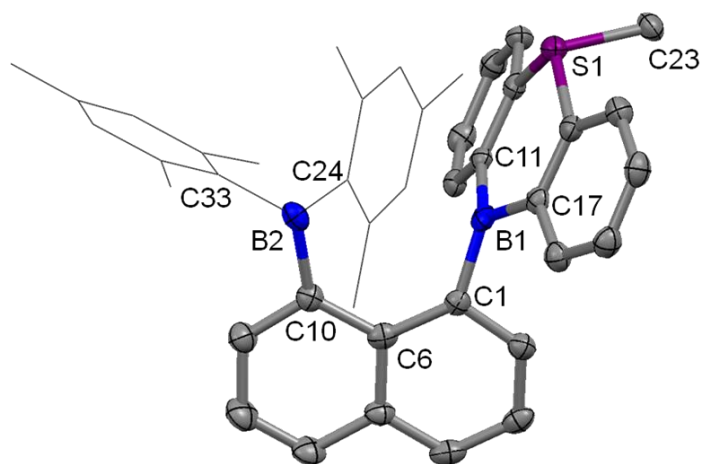


**Figure 68.** ORTEP drawing of  $[\mathbf{40}]^+$  with thermal ellipsoid plots (50% probability). For clarity, the hydrogen atoms and triflate anion are omitted and the mesityl substituents are represented by thin line. Selected bond lengths ( $\text{\AA}$ ) and angles ( $^\circ$ ): S(1)-C(23) 1.796(2), C(1)-B(1) 1.568(3), C(17)-B(1) 1.569(3), C(11)-B(1) 1.564(3), C(24)-B(2) 1.576(3), C(33)-B(2) 1.578(3), C(10)-B(2) 1.567(3); C(11)-B(1)-C(1) 117.23(18), C(11)-B(1)-C(17) 117.97(18), C(1)-B(1)-C(17) 120.82(18), C(10)-B(2)-C(24) 124.41(18), C(10)-B(2)-C(33) 116.85(17), C(24)-B(2)-C(33) 118.29(17), C(6)-C(10)-B(2) 128.27(17), C(6)-C(1)-B(1) 131.89(17).

**Table 27.** Crystal data, data collections, and structure refinement for [40]OTf•CH<sub>2</sub>Cl<sub>2</sub>.

Crystal data	[40]OTf•CH <sub>2</sub> Cl <sub>2</sub>
formula	C <sub>43</sub> H <sub>41</sub> B <sub>2</sub> Cl <sub>2</sub> F <sub>3</sub> O <sub>3</sub> S <sub>2</sub>
$M_r$	819.40
crystal size (mm <sup>3</sup> )	0.34 x 0.20 x 0.09
crystal system	Monoclinic
space group	P2(1)/c
$a$ (Å)	8.597(4)
$b$ (Å)	12.470(5)
$c$ (Å)	37.732(15)
$\alpha$ (°)	90
$\beta$ (°)	102.280(9)
$\gamma$ (°)	90
$V$ (Å <sup>3</sup> )	3952(3)
$Z$	4
$\rho_{\text{calc}}$ (g cm <sup>-3</sup> )	1.377
$\mu$ (mm <sup>-1</sup> )	0.324
$F(000)$	1704
Data Collection	
$T$ (K)	110(2)
scan mode	$\omega$
	-11 → +11
$hkl$ range	-16 → +16
	-49 → +50
measd reflns	45225
unique reflns [ $R_{\text{int}}$ ]	9592 [0.0805]
reflns used for refinement	9592
Refinement	
refined parameters	520
Goof	0.935
$R_1, {}^a wR_2^b$ all data	0.1035, 0.1550
$\rho_{\text{fin}}$ (max/min) (e Å <sup>-3</sup> )	0.971, -0.820

$${}^a R_1 = \frac{\sum ||F_o| - |F_c||}{\sum |F_o|}, {}^b wR_2 = \left[ \frac{[\sum w(F_o^2 - F_c^2)^2]}{[\sum w(F_o^2)^2]} \right]^{1/2}.$$

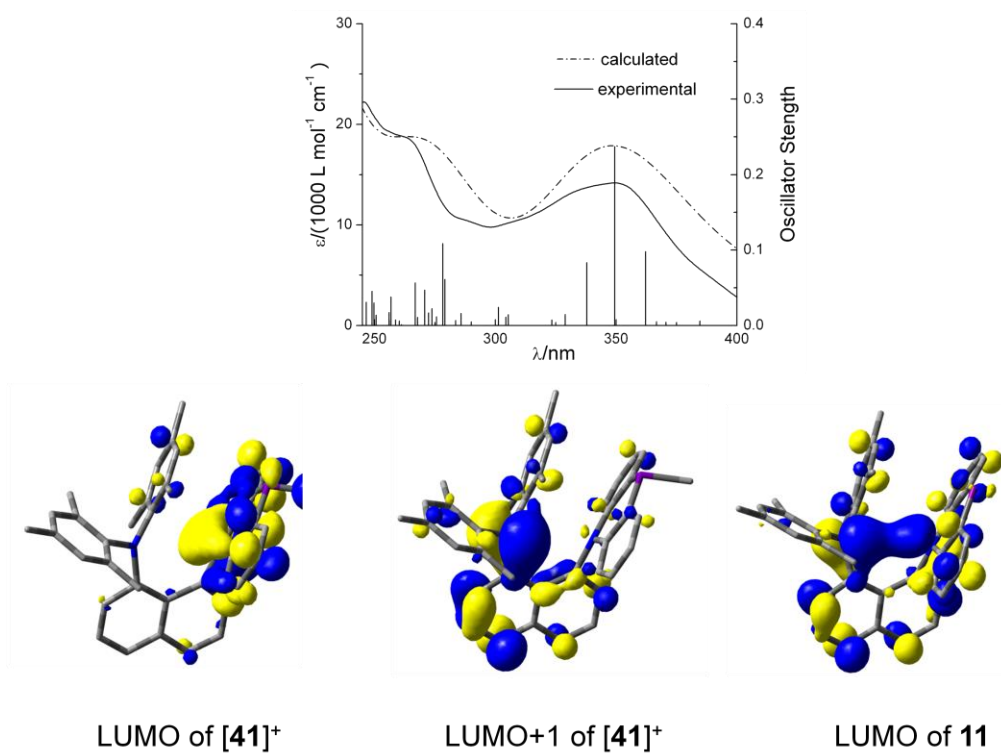


**Figure 69.** Top: Experimental (chloroform) and calculated UV-vis spectra for  $[40]^+$ . Bottom: Views of LUMO and LUMO+1 of  $[40]^+$  and LUMO of **10**. (isovalue = 0.035).

### 5.3 Fluoride anion complexation

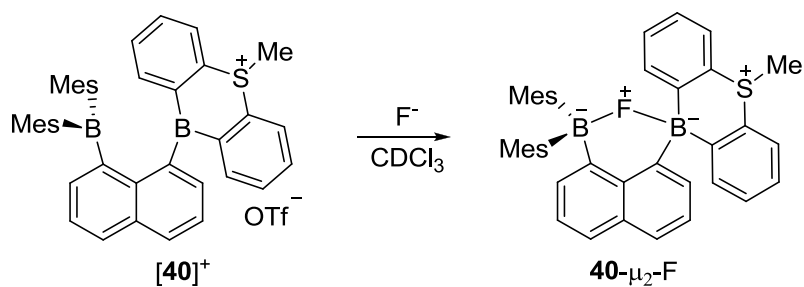


**Figure 70.** Reactions of  $[40]^+$  with fluoride in chloroform.



The cationic borane  $[40]^+$  quickly reacts with  $[n\text{Bu}_4\text{N}][\text{Ph}_3\text{SiF}_2]$  in  $\text{CDCl}_3$  to afford the corresponding fluoride complex  $40\text{-}\mu_2\text{-F}$  (Figure 70). This fluoride adduct, which is air and moisture stable, has been fully characterized. The  $^{11}\text{B}$  NMR resonances at -0.4 ppm and 4.4 ppm are consistent with the presence of two four-coordinate boron centers.<sup>37</sup> The  $^1\text{H}$  NMR resonance of the sulfur-bound methyl group appears at 3.28 ppm, upfield from that of  $[40]^+$  at 3.60 ppm. The  $^{19}\text{F}$  NMR signal at -174.4 ppm is comparable to the chemical shift observed in other fluoride chelate complexes<sup>27</sup> including  $[10\text{-}\mu_2\text{-F}]^-$  (-188.7 ppm).<sup>37</sup> The structure of  $40\text{-}\mu_2\text{-F}$  has also been determined by single crystal X-ray diffraction (Figure 71, Table 28). In contrast with the relatively symmetrical B-F-B bridge of  $[10\text{-}\mu_2\text{-F}]^-$  (B-F bond lengths = 1.585(5) Å and 1.633(5) Å),<sup>37</sup> the structure of  $40\text{-}\mu_2\text{-F}$  shows that the fluorine atom forms a short bond with B(1) (1.539(4) Å) and a long one with B(2) (1.822(4) Å). This unsymmetrical coordination is logically reflected by a notable difference in the extent of pyramidalization observed for each boron center ( $\Sigma(\angle\text{C-B(1)-C}) = 334.6^\circ$  and  $\Sigma(\angle\text{C-B(2)-C}) = 350.6^\circ$ ). The asymmetry of the B-F-B bridge in  $40\text{-}\mu_2\text{-F}$  can be correlated to the presence of a sulfonium moiety which enhances the Lewis acidity of the adjacent B(1) atom. This conclusion is in agreement with the computational studies of  $[40]^+$  which show that the  $p_z$  orbitals of the B(1) boron atom contributes to the LUMO while that of the B(2) atom contributes to the LUMO+1. It is also interesting to note that the sulfur-bound methyl group is oriented inwards. This surprising orientation places the C(41) atom at 3.452 Å from the fluorine atom, which is above the range that one would expect if a  $\text{C}_{\text{Me}}\text{-H}\cdots\text{F}$  interaction was present.

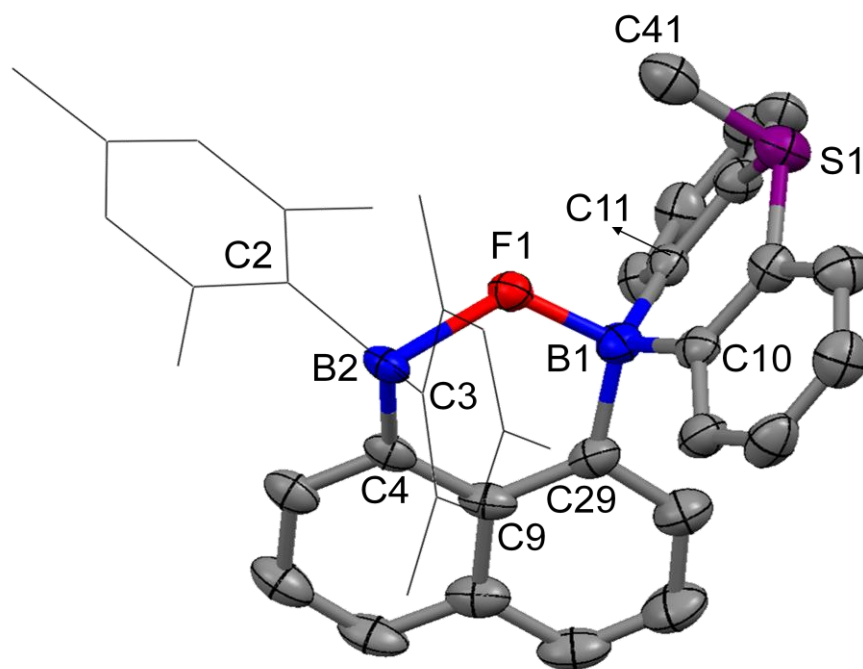


**Figure 71.** ORTEP drawings of **40- $\mu_2$ -F** with thermal ellipsoid plots (50% probability).

For clarity, the hydrogen atoms are omitted and the mesityl substituents are represented by thin line. Selected bond lengths (Å) and angles (°) for **40- $\mu_2$ -F**: F(1)-B(1) 1.540(5), F(1)-B(2) 1.822(4), C(2)-B(2) 1.608(6), C(3)-B(2) 1.626(5), C(4)-B(2) 1.599(6), C(10)-B(1) 1.622(6), C(11)-B(1) 1.631(6), C(29)-B(1) 1.604(6), S(1)-C(41) 1.760(4); B1-F1-B2 124.1(2), C(29)-B(1)-C(10) 112.8(3), C(29)-B(1)-C(11) 110.3(3), C(10)-B(1)-C(11) 111.5(3), C(9)-C(29)-B(1) 125.5(3), C(4)-B(2)-C(2) 112.3(3), C(4)-B(2)-C(3) 120.3(3), C(2)-B(2)-C(3) 118.0(3), C(9)-C(4)-B(2) 125.2(3).

**Table 28.** Crystal data, data collections, and structure refinement for **40- $\mu_2$ -F**.

Crystal data	<b>40-<math>\mu_2</math>-F</b>
formula	C <sub>41</sub> H <sub>39</sub> B <sub>2</sub> FS
$M_r$	604.40
crystal size (mm <sup>3</sup> )	0.10 x 0.08 x 0.06
crystal system	Monoclinic
space group	P2(1)/c
$a$ (Å)	12.492(2)
$b$ (Å)	12.127(2)
$c$ (Å)	21.474(4)
$\alpha$ (°)	90
$\beta$ (°)	94.187(2)
$\gamma$ (°)	90
$V$ (Å <sup>3</sup> )	3244.4(10)
$Z$	4
$\rho_{\text{calc}}$ (g cm <sup>-3</sup> )	1.237
$\mu$ (mm <sup>-1</sup> )	0.135
$F(000)$	1280
Data Collection	
$T$ (K)	110(2)
scan mode	$\omega$
	-14 $\rightarrow$ +14
$hkl$ range	-13 $\rightarrow$ +13
	-24 $\rightarrow$ +24
measd reflns	28175
unique reflns [ $R_{\text{int}}$ ]	5082 [0.0894]
reflns used for refinement	5082
Refinement	
refined parameters	402
Goof	0.926
$R_1, {}^a wR_2^b$ all data	0.1132, 0.1649
$\rho_{\text{fin}}$ (max/min) (e Å <sup>-3</sup> )	0.502, -0.404

$${}^a R_1 = \frac{\sum ||F_o| - |F_c||}{\sum |F_o|}. \quad {}^b wR_2 = \left[ \frac{[\sum w(F_o^2 - F_c^2)^2]}{[\sum w(F_o^2)^2]} \right]^{1/2}.$$

The structure of **40**- $\mu_2$ -F has been computationally optimized using DFT methods (functional: B3LYP; mixed basis set: B: 6-31+g(d'); S: 6-31+g(d); C, H: 6-31g). Interestingly, the optimized structure shows a large deviation from that observed experimentally (Figure 72). The largest deviation is observed in the B(2)-F(1) bond which converges to a value of 2.393 Å as opposed to 1.822(4) Å in the crystal structure. To elucidate the origin of this difference, we decided to study how variations in the B(2)-F(1) bond length affect the total energy of the structure. To this end, the structure of **40**- $\mu_2$ -F has been optimized with the B(2)-F(1) constrained at 1.600, 1.822, 2.000, 2.200, 2.400, 2.600, 2.800, 3.000 and 3.200 Å. As it can be seen from Figure 72, the total energy of the molecule varies by only 1.95 kcal/mol in the 1.822 < B(2)-F(1) < 2.800 Å range. This shallow energy well indicates that the B(2)-F(1) bond length has limited effect on the total energy of the molecule, the structure of which can therefore be influenced by subtle solvation or crystal packing effect.

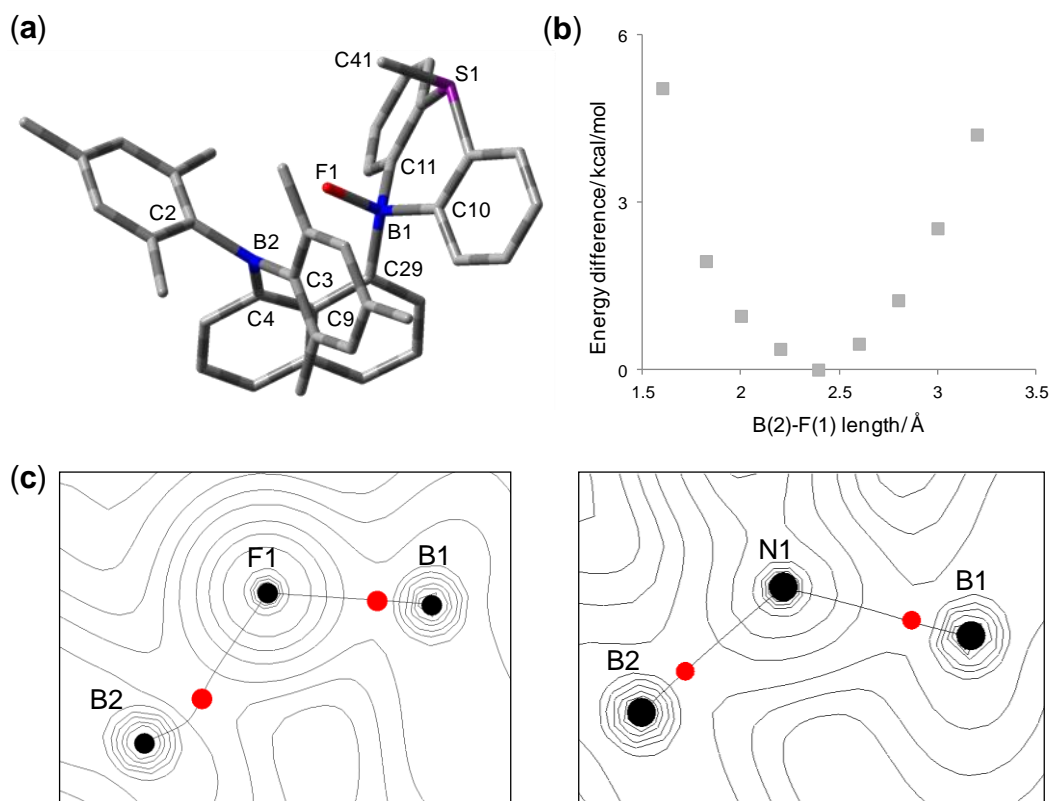


**Figure 72.** (a) Optimized structure of  $40-\mu_2-F$ . Calculated bond lengths (Å) and angles ( $^\circ$ ) for  $40-\mu_2-F$ : F(1)-B(1) 1.486, F(1)-B(2) 2.393, C(2)-B(2) 1.604, C(3)-B(2) 1.601, C(4)-B(2) 1.589, C(10)-B(1) 1.648, C(11)-B(1) 1.658, C(29)-B(1) 1.625, S(1)-C(41) 1.836; B1-F1-B2 116.9, C(29)-B(1)-C(10) 113.0, C(29)-B(1)-C(11) 109.6, C(10)-B(1)-C(11) 110.2, C(9)-C(29)-B(1) 127.2, C(4)-B(2)-C(2) 116.2, C(4)-B(2)-C(3) 122.0, C(2)-B(2)-C(3) 119.3, C(9)-C(4)-B(2) 129.0. (b) The energy changes based on different B(2)-F(1) lengths in the optimization calculations of  $40-\mu_2-F$ . (c) AIM electron density maps with relevant bond paths and bond critical points of B(1)-F(1)-B(2) bond in  $40-\mu_2-F$  (left) and B(1)-N(1)-B(2) bond in  $40-\mu_2-N_3$  (right).

A geometry optimization carried out by constraining the B(2)-F(1) bond length to its experimental value (B(2)-F(1) = 1.822 Å) afforded a structure that lies only 1.95 kcal/mol above the computed minimum with a B(1)-F(1) bond length of 1.555 Å (Figure 72). The latter is in good agreement with the B(1)-F(1) bond length of 1.540(5) Å determined by X-ray diffraction (Figure 71). An atom in molecules (AIM) calculation<sup>170</sup> carried out at this constrained geometry identifies a bond path for both the B(1)-F(1) and the B(2)-F(2) linkages (Figure 72). The electron density  $\rho(r)$  of 0.100 e bohr<sup>-3</sup> at the bond critical point (BCP) of the B(1)-F(1) bond is significantly larger than that of the B(2)-F(1) bond (0.053 e bohr<sup>-3</sup>), in agreement with the observed asymmetry of the B-F-B bridge. By contrast, AIM calculations carried out at the optimized geometry of the [10- $\mu_2$ -F] indicate a much more symmetrical B-F-B bridge, with similar electron density at the BCP of the B(1)-F(1) bond ( $\rho(r) = 0.074$  e bohr<sup>-3</sup>) and B(2)-F(1) bond ( $\rho(r) = 0.077$  e bohr<sup>-3</sup>).

To further understand the influence of the cationic sulfonium moiety in [40]<sup>+</sup>, we decided to measure the fluoride binding constant of [40]<sup>+</sup> and compare it to that of 10. Since we have previously shown that the binding constant of neutral 10 exceeds the range measurable by a direct titration with tetrabutylammonium fluoride (*n*Bu<sub>4</sub>NF),<sup>37</sup> we decided to employ the commercially available tetrabutylammonium difluorotriphenylsilicate (*n*Bu<sub>4</sub>NPh<sub>3</sub>SiF<sub>2</sub>) as fluoride source and determine the relative binding constant  $K_{\text{rel}}(\text{borane}) = K(\text{borane})/K(\text{Ph}_3\text{SiF})$  where  $K(\text{borane})$  is the absolute fluoride binding constant of the borane under study and  $K(\text{Ph}_3\text{SiF})$  is the absolute fluoride binding constant of Ph<sub>3</sub>SiF (see SI for details of the derivation).  $K_{\text{rel}}(\mathbf{10})$  could

be derived from the integrated  $^1\text{H}$  NMR and  $^{19}\text{F}$  NMR spectra of  $\text{CDCl}_3$  solutions containing **10** and  $[\text{nBu}_4\text{N}][\text{Ph}_3\text{SiF}_2]$  in different molar ratios, affording  $K_{\text{rel}}(\mathbf{10}) = 5.4 (\pm 1)$  (see Experimental section for details of the experiments). Analogous NMR experiments carried out with  $[\mathbf{40}]^+$  indicated the quantitative formation of  $\mathbf{40}\text{-}\mu_2\text{-F}$ . For this reason, we decided to resort to UV-vis spectroscopy, which is more appropriate to study large binding constants. However, addition of  $[\text{nBu}_4\text{N}][\text{Ph}_3\text{SiF}_2]$  to a dilute chloroform solution of  $[\mathbf{40}]^+$  ( $6.7 \times 10^{-5}$  M in  $\text{CHCl}_3$ ) resulted in the stoichiometric quenching of the absorbance of the boron-centered chromophore at 349 nm in agreement with the quantitative formation of the fluoride complex (Figure 73). These observations indicate the relative fluoride binding constant of  $[\mathbf{40}]^+$  ( $K_{\text{rel}}([\mathbf{40}]^+)$ ) exceeds the value of  $10^5 \text{ M}^{-1}$  and is thus at least four orders of magnitude greater than that of **10**. The drastic difference observed in the fluoride binding properties of **10** and  $[\mathbf{40}]^+$  underscores the higher fluoride affinity of  $[\mathbf{40}]^+$  which can be assigned to its cationic nature. Although  $\mathbf{40}\text{-}\mu_2\text{-F}$  is very stable, it slowly reacts with  $\text{B}(\text{C}_6\text{F}_5)_3$  to afford  $[\mathbf{40}][\text{FB}(\text{C}_6\text{F}_5)_3]$ , thus indicating that fluoride binding by  $[\mathbf{40}]^+$  is reversible. A similar reaction was observed for  $[\mathbf{10}\text{-}\mu_2\text{-F}]^-$  which also releases fluoride to  $\text{B}(\text{C}_6\text{F}_5)_3$ .<sup>37</sup>

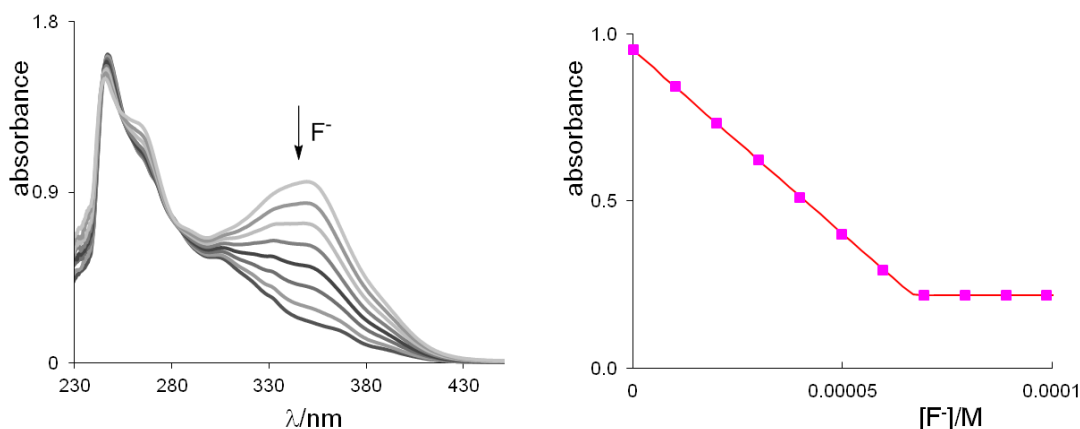


**Figure 73.** Left: Absorbance changes upon addition of  $n\text{Bu}_4\text{NPh}_3\text{SiF}_2$  to a  $\text{CHCl}_3$  solution of  $[\mathbf{40}]^+$  (0.067 mM). Right: Binding isotherm monitored at  $\lambda = 349$  nm ( $K_{\text{rel}}([\mathbf{40}]^+) \geq 10^5$ ,  $\epsilon = 10040$  for  $[\mathbf{40}]\text{OTf}$ ,  $\epsilon = 3270$  for  $\mathbf{40}\text{-}\mu_2\text{-F}$ ).

We also decided to compare the fluoride anion affinity of  $[\mathbf{40}]^+$  to that of another cationic borane. For the purpose of this study, we selected the phosphonium borane  $[\mathbf{28}]^+$  which was previously shown to react with fluoride to afford  $\mathbf{28}\text{-F}$ .<sup>49</sup> Interestingly, mixing equimolar amounts of  $[\mathbf{40}]^+$  and  $\mathbf{28}\text{-F}$  in  $\text{CDCl}_3$  at ambient temperature leads to the quantitative formation of  $[\mathbf{28}]^+$  and  $\mathbf{40}\text{-}\mu_2\text{-F}$ . Fluoride ion transfer from  $\mathbf{28}\text{-F}$  to  $[\mathbf{40}]^+$  is confirmed by  $^1\text{H}$ ,  $^{19}\text{F}$  and  $^{31}\text{P}$  NMR spectroscopy. Specifically, the  $^{31}\text{P}$  NMR spectrum shows full conversion of  $\mathbf{28}\text{-F}$  (28.3 ppm) into  $[\mathbf{28}]^+$  (23.9 ppm). Accordingly, the  $^{19}\text{F}$  NMR spectrum indicates formation of  $\mathbf{40}\text{-}\mu_2\text{-F}$ , the resonance of which appears at -174.4 ppm. Related changes are also observed in the  $^1\text{H}$  NMR spectrum where the *P*- or *S*-bound methyl signals of  $[\mathbf{40}]^+$  (3.60 ppm) and  $\mathbf{28}\text{-F}$  (3.12 ppm) disappear to give rise to those of  $\mathbf{40}\text{-}\mu_2\text{-F}$  (3.28 ppm) and  $[\mathbf{28}]^+$  (2.67 ppm) (Figure 74). This reaction indicates that  $[\mathbf{40}]^+$  is one of the most Lewis acidic cationic boranes ever investigated in our



group. Presumably the cumulative Coulombic and chelate effects occurring with this compound are responsible for this enhanced fluoride affinity.

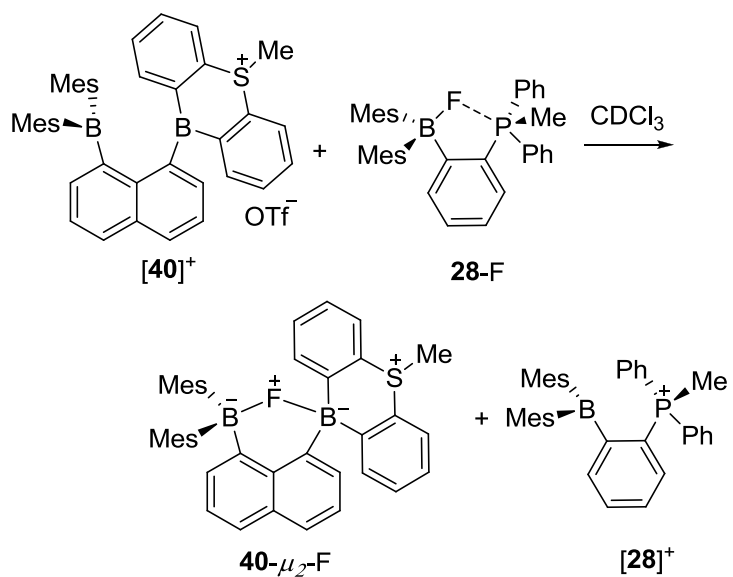


**Figure 74.** Competition reaction of  $[40]^+$  with  $28-F$  in  $CDCl_3$ .

## 5.4 Reaction with other anions

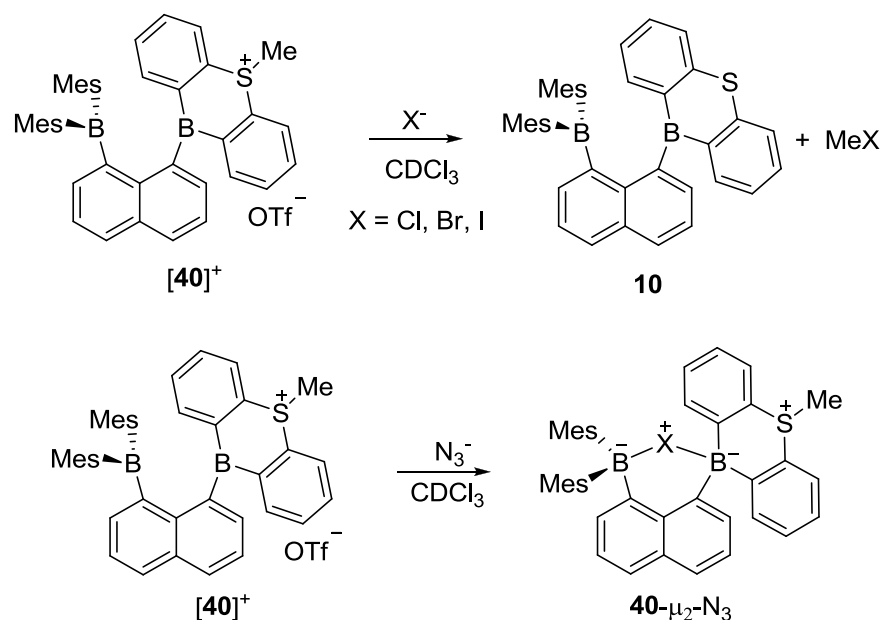


**Figure 75.** Reactions of **[40]<sup>+</sup>** with other anions in chloroform

To conclude this study, we decided to probe the reactivity of **[40]<sup>+</sup>** toward other anions. Interestingly, addition of TBACl, TBABr or TBAI to a CDCl<sub>3</sub> solution of **[40]<sup>+</sup>** resulted in the formation of the neutral diborane **10** indicating demethylation of the diarylmethylsulfonium (Figure 75). Such demethylation reactions are not unprecedented and have been observed in related sulfonium borane species.<sup>30, 171</sup> The reactivity of **[40]<sup>+</sup>** toward cyanide was also tested using TBACN as a cyanide source. In this case, however, the reaction afforded a mixture of compounds that could not be unambiguously identified. A cleaner anion complexation reaction was observed with TBAN<sub>3</sub> in CDCl<sub>3</sub>, leading to the corresponding azide complex **40-μ<sub>2</sub>-N<sub>3</sub>**. Formation of the latter, which

can be reverted by addition of  $B(C_6F_5)_3$ , could be monitored by UV-vis spectroscopy to afford a binding constant exceeding  $10^7 M^{-1}$  (Figure 76).

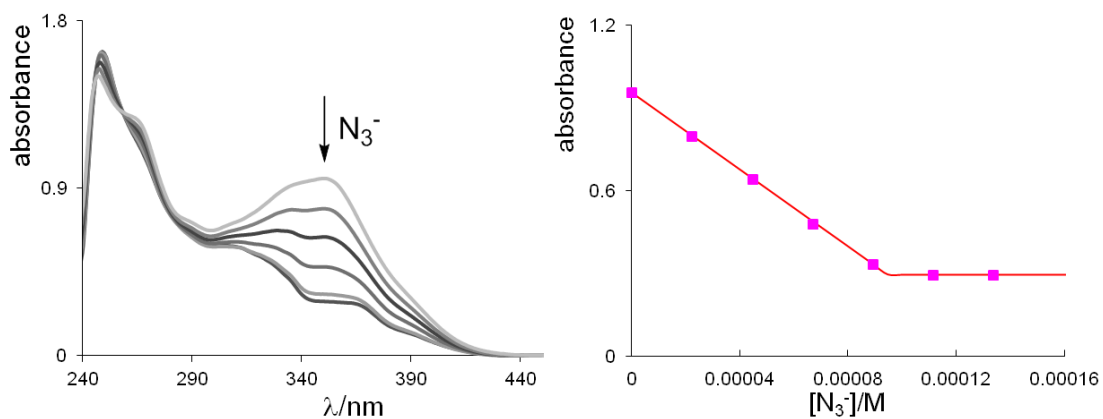


**Figure 76.** Left: Absorbance changes upon addition of  $nBu_4NN_3$  to a  $CHCl_3$  solution of  $[40]^+$  (0.095 mM). Right: Binding isotherm monitored at  $\lambda = 349$  nm ( $K \geq 10^7 M^{-1}$ ,  $\epsilon = 10040$  for  $[40]OTf$ ,  $\epsilon = 3100$  for  $40-\mu_2-N_3$ ).

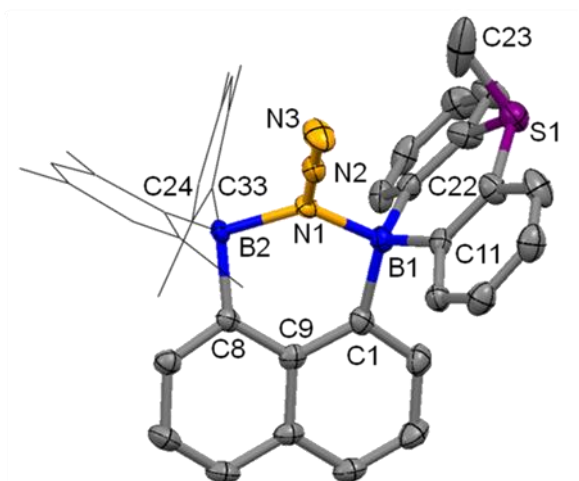


**Figure 77.** ORTEP drawings of **40**- $\mu_2$ -N<sub>3</sub> with thermal ellipsoid plots (50% probability).

For clarity, the hydrogen atoms are omitted and the mesityl substituents are represented by thin line. Selected bond lengths (Å) and angles (°): N(1)-N(2) 1.243(5), N(1)-B(1) 1.643(6), N(1)-B(2) 1.704(6), N(2)-N(3) 1.136(5), C(1)-B(1) 1.621(7), C(11)-B(1) 1.637(6), C(22)-B(1) 1.626(7), C(24)-B(2) 1.653(6), C(8)-B(2) 1.622(6), C(33)-B(2) 1.652(6), S(1)-C(23) 1.714(7); B(1)-N(1)-B(2) 124.3(3), C(9)-C(1)-B(1) 125.8(4), C(9)-C(8)-B(2) 124.4(4), C(1)-B(1)-C(11) 111.0(4), C(1)-B(1)-C(22) 111.8(4), C(11)-B(1)-C(22) 112.1(4), C(8)-B(2)-C(33) 115.9(4), C(8)-B(2)-C(24) 108.7(3), C(33)-B(2)-C(24) 119.5(4).

**Table 29.** Crystal data, data collections, and structure refinement for **40- $\mu_2$ - $N_3\cdot(CH_3)_2CO$** .

Crystal data	<b>40-<math>\mu_2</math>-<math>N_3\cdot(CH_3)_2CO</math></b>
formula	$C_{44}H_{45}B_2N_3OS$
$M_r$	685.51
crystal size (mm <sup>3</sup> )	0.12 x 0.08 x 0.06
crystal system	Monoclinic
space group	P2(1)/c
$a$ (Å)	14.5158(13)
$b$ (Å)	12.1583(11)
$c$ (Å)	21.037(2)
$\alpha$ (°)	90
$\beta$ (°)	98.0310(10)
$\gamma$ (°)	90
$V$ (Å <sup>3</sup> )	3676.3(6)
$Z$	4
$\rho_{\text{calc}}$ (g cm <sup>-3</sup> )	1.239
$\mu$ (mm <sup>-1</sup> )	0.127
$F(000)$	1456
Data Collection	
$T$ (K)	110(2)
scan mode	$\omega$
$hkl$ range	-15 $\rightarrow$ +15 -13 $\rightarrow$ +13 -23 $\rightarrow$ +23
measd reflns	29047
unique reflns [ $R_{\text{int}}$ ]	5138 [0.0561]
reflns used for refinement	5138
Refinement	
refined parameters	460
Goof	0.961
$R_1, {}^a wR_2^b$ all data	0.1048, 0.2359
$\rho_{\text{fin}}$ (max/min) (e Å <sup>-3</sup> )	1.898, -0.687

<sup>a</sup>  $R_1 = \frac{\sum ||F_o| - |F_c||}{\sum |F_o|}$ . <sup>b</sup>  $wR_2 = \left[ \frac{[\sum w(F_o^2 - F_c^2)^2]}{[\sum w(F_o^2)^2]} \right]^{1/2}$ .

The azide complex **40- $\mu_2$ -N<sub>3</sub>**, which could be isolated from the reaction of [40]OTf with TBAN<sub>3</sub> in dichloromethane, has been fully characterized. It features a broad <sup>11</sup>B NMR resonance at -4.6 ppm which, we speculate, corresponds to the overlapping signals of the two four-coordinate boron centers. In line with the coordination of an anion to the diborane, the resonance of the sulfur-bound methyl group at 3.26 ppm is close to that measured for **40- $\mu_2$ -F** (3.28 ppm). The crystal structure of **40- $\mu_2$ -N<sub>3</sub>** confirms formation of a chelate complex, with the azide anion bridging the two boron centers in a  $\mu$ - $\eta^1$  fashion (Figure 77, Table 29). While the structure of **40- $\mu_2$ -F** showed a rather unsymmetrical B-F-B bridge, the N(1)-B(1) (1.635 Å) and N(1)-B(2) (1.706 Å) bond lengths in **40- $\mu_2$ -N<sub>3</sub>** indicate a rather symmetrical B-N-B bridge, which is consistent with the propensity of the azide anion to adopt a  $\mu$ - $\eta^1$  coordination mode. The DFT optimized structure **40- $\mu_2$ -N<sub>3</sub>** (functional: B3LYP; mixed basis set: B, N: 6-31+g(d<sup>7</sup>); S: 6-31+g(d); C, H: 6-31g) features a B(1)-N(1) distance of 1.644 Å, which is very close to that experimentally observed. The calculated N(1)-B(2) distance of 1.832 Å is slightly elongated when compared to that experimentally observed, a phenomenon reminiscent of that observed in the computed structure of **40- $\mu_2$ -F**. Presumably, small variation of this bond length has only a limited effect on the total energy of the molecule, making subtle solvation or crystal packing effects the main culprit for this small discrepancy. An AIM analysis carried out at the optimized geometry affords consistent results with BCP electron densities  $\rho(r) = 0.108 \text{ e bohr}^{-3}$  for N(1)-B(1) and  $\rho(r) = 0.070 \text{ e bohr}^{-3}$  for N(1)-B(2), again illustrating the increased acidity of the sulfonium-decorated boryl moiety (Figure 72).

## 5.5 Conclusion

As demonstrated by our earlier work on naphthalene-based diboranes,<sup>25</sup> the fluoride binding constants of neutral bidentate derivatives exceed those of their monofunctional analogues by 3 or 4 orders of magnitude. The results presented in this paper show that the fluoride anion affinity of such diboranes can be further enhanced by the simple introduction of a cationic moiety in the proximity of one of the boron atoms. This conclusion is substantiated by the observation that the fluoride binding constant of **[40]<sup>+</sup>** exceeds that of its neutral precursor by at least four orders of magnitude. A more general lesson which can be derived from this work is that chelate effects and Coulombic effects are additive and can be combined to boost the anion affinity of bidentate Lewis acids.

## 5.6 Experimental Section

**General Considerations.** Commercially available chemicals were purchased and used as provided (Commercial sources: Aldrich for Mes<sub>2</sub>BF, TMEDA, Me<sub>3</sub>SiF<sub>2</sub>S(NMe<sub>2</sub>)<sub>3</sub>, *n*Bu<sub>4</sub>NPh<sub>3</sub>SiF<sub>2</sub>, TMSCl, *n*Bu<sub>4</sub>NF, *n*Bu<sub>4</sub>NCl, *n*Bu<sub>4</sub>NBr, *n*Bu<sub>4</sub>NI and *n*Bu<sub>4</sub>NN<sub>3</sub>; TCI America for Ph<sub>2</sub>S; Alpha Aesar for BBr<sub>3</sub> and *n*-butyllithium (2.8 M in hexanes). Diborane **10** was prepared by reaction of tetrakis(THF)lithium dimesityl-1,8-naphthalenediylborate<sup>56, 172</sup> with 10-Bromo-9-thia-10-boranthracene as previously described.<sup>37</sup> Solvents were dried by reflux under N<sub>2</sub> over drying agents, and freshly distilled prior to use. The drying agents employed were: CaH<sub>2</sub> for dichloromethane and Na/K for diethyl ether and THF. Air-sensitive compounds were handled under N<sub>2</sub>

atmosphere using standard Schlenk and glovebox techniques. UV-vis spectra were recorded on an Ocean Optics USB4000 spectrometer with an Ocean Optics ISS light source. Elemental analyses were performed at Atlantic Microlab (Norcross, GA). NMR spectra were recorded on Varian Unity Inova 400 FT NMR (399.59 MHz for  $^1\text{H}$ , 376.03 MHz for  $^{19}\text{F}$ , 128.19 MHz for  $^{11}\text{B}$ , 100.45 MHz for  $^{13}\text{C}$ ) spectrometers at ambient temperature. Chemical shifts  $\delta$  are given in ppm and are referenced against external  $\text{BF}_3 \cdot \text{Et}_2\text{O}$  ( $^{11}\text{B}$  and  $^{19}\text{F}$ ).

**Crystallography.** The crystallographic measurements were performed using a Bruker APEX-II CCD area detector diffractometer (Mo- $\text{K}_\alpha$  radiation,  $\lambda = 0.71069 \text{ \AA}$ ) for [40]OTf,  $40\text{-}\mu_2\text{-F}$ , and  $40\text{-}\mu_2\text{-N}_3$ . In each case, a specimen of suitable size and quality was selected and mounted onto a nylon loop. The structures were solved by direct methods, which successfully located most of the non-hydrogen atoms. Subsequent refinement on  $\text{F}^2$  using the SHELXTL/PC package (version 5.1) allowed location of the remaining non-hydrogen atoms.

**Synthesis of [40]OTf.** Methyl triflate (0.1 mL, 0.89 mmol) was added to a solution of diborane **10** (0.2 g, 0.35 mmol) in dichloromethane (10 mL) at room temperature. The mixture was refluxed overnight and then cooled to room temperature. The solvent was removed under vacuum to yield a solid which was washed with diethyl ether to afford [40]OTf as a pale yellow product (0.21g, yield 81%). Single crystals of [40]OTf- $\text{CH}_2\text{Cl}_2$  were obtained by slow diffusion of diethyl ether into a dichloromethane solution of [40]OTf at  $-25^\circ\text{C}$ .  $^1\text{H}$  NMR ( $\text{CDCl}_3$ ):  $\delta$  0.95 (s, 3H, Mes- $\text{CH}_3$ ), 1.39 (s, 3H, Mes- $\text{CH}_3$ ), 1.47 (s, 3H, Mes- $\text{CH}_3$ ), 1.82 (s, 3H, Mes- $\text{CH}_3$ ), 1.84 (s, 3H, Mes- $\text{CH}_3$ ), 2.23



(s, 3H, Mes-CH<sub>3</sub>), 3.60 (s, 3H, S-CH<sub>3</sub>), 5.71 (s, 1H, Mes-CH), 6.59 (s, 1H, Mes-CH), 6.60 (s, 1H, Mes-CH), 6.69 (s, 1H, Mes-CH), 7.39 (d, 1H, <sup>3</sup>J(HH) = 7.2 Hz, nap-CH), 7.46 (t, 1H, <sup>3</sup>J(HH) = 7.2 Hz, nap-CH), 7.52 (d, 1H, <sup>3</sup>J(HH) = 7.6 Hz, nap-CH), 7.53-7.63 (m, 3H, nap-CH), 7.77 (t, 1H, <sup>3</sup>J(HH) = 8.0 Hz, CH), 7.82 (t, 1H, <sup>3</sup>J(HH) = 7.6 Hz, CH), 7.88-7.94 (m, 2H, CH), 8.04 (d, 1H, <sup>3</sup>J(HH) = 8.4 Hz, CH), 8.13 (d, 1H, <sup>3</sup>J(HH) = 8.0 Hz, CH), 8.18 (d, 1H, <sup>3</sup>J(HH) = 8.0 Hz, CH), 8.23 (d, 1H, <sup>3</sup>J(HH) = 8.0 Hz, CH). <sup>13</sup>C NMR (CDCl<sub>3</sub>): δ 21.00 (Mes-CH<sub>3</sub>), 21.11 (Mes-CH<sub>3</sub>), 21.19 (Mes-CH<sub>3</sub>), 22.11 (Mes-CH<sub>3</sub>), 23.74 (Mes-CH<sub>3</sub>), 23.89 (Mes-CH<sub>3</sub>), 25.26 (S-CH<sub>3</sub>), 124.39, 126.51, 126.87, 127.40, 128.20, 128.29, 128.96, 130.12, 130.85, 130.88, 131.70, 132.28, 132.48, 132.51, 132.99, 133.13, 133.40, 133.98, 134.22, 135.93, 137.71, 138.64, 139.18, 139.76, 140.44, 141.47, 142.80, 143.49, 145.42, 147.93. <sup>11</sup>B NMR (CDCl<sub>3</sub>): not detected. Anal. Calcd for C<sub>42</sub>H<sub>39</sub>B<sub>2</sub>F<sub>3</sub>O<sub>3</sub>S<sub>2</sub>-1/2CH<sub>2</sub>Cl<sub>2</sub>: C 65.70; H 5.19. Found: C 65.74; H 5.28. (The sample used for EA was obtained by recrystallization from CH<sub>2</sub>Cl<sub>2</sub>; the EA results indicate partial loss of the interstitial CH<sub>2</sub>Cl<sub>2</sub> molecule found in the crystal structure).

**Synthesis of 40-μ<sub>2</sub>-F.** To a solution of [40]OTf (50 mg, 0.068 mmol) in CH<sub>2</sub>Cl<sub>2</sub> (5 mL) at 25°C, was added a CH<sub>2</sub>Cl<sub>2</sub> solution (5 mL) of Me<sub>3</sub>SiF<sub>2</sub>S(NMe<sub>2</sub>)<sub>3</sub> (21 mg, 0.076 mmol). After 15 minutes, the solvent was evaporated and the residue was dissolved in a mixture solvent of CH<sub>2</sub>Cl<sub>2</sub> (2 mL) and diethyl ether (18 mL). The resulting solution was filtered and evaporated to dryness to afford 40-μ<sub>2</sub>-F as a colorless solid (35 mg, 85% yield). Large colorless monocrystals of 40-μ<sub>2</sub>-F could be obtained by slow evaporation of an acetone solution of 40-μ<sub>2</sub>-F at room temperature. <sup>1</sup>H NMR (CDCl<sub>3</sub>): δ 0.86 (s, 3H, Mes-CH<sub>3</sub>), 1.63 (s, 3H, Mes-CH<sub>3</sub>), 1.79 (s, 3H, Mes-CH<sub>3</sub>), 1.92 (d, 3H, J(H-F) = 5.2 Hz,

Mes-CH<sub>3</sub>), 2.07 (s, 3H, Mes-CH<sub>3</sub>), 2.23 (s, 3H, Mes-CH<sub>3</sub>), 3.28 (s, 3H, S-CH<sub>3</sub>), 5.99 (s, 1H, Mes-CH), 6.37 (s, 1H, Mes-CH), 6.39 (s, 1H, Mes-CH), 6.62-6.66 (m, 2H, CH), 6.67 (s, 1H, Mes-CH), 6.78 (d, 1H, <sup>3</sup>J(HH) = 7.2 Hz, CH), 7.00 (t, 1H, <sup>3</sup>J(HH) = 7.6 Hz, CH), 7.12-7.25 (m, 5H, CH), 7.35 (t, 1H, <sup>3</sup>J(HH) = 7.6 Hz, CH), 7.49 (dd, 2H, <sup>3</sup>J(HH) = 6.8 Hz, CH), 7.75 (d, 1H, <sup>3</sup>J(HH) = 8.0 Hz, CH), 7.87 (d, 1H, <sup>3</sup>J(HH) = 8.0 Hz, CH). <sup>13</sup>C NMR (CDCl<sub>3</sub>): δ 20.74 (Mes-CH<sub>3</sub>), 21.01 (Mes-CH<sub>3</sub>), 22.89 (Mes-CH<sub>3</sub>), 24.58 (Mes-CH<sub>3</sub>), 25.16 (Mes-CH<sub>3</sub>), 25.24 (Mes-CH<sub>3</sub>), 39.23 (S-CH<sub>3</sub>), 124.20, 125.12, 125.92, 126.47, 126.68, 127.17, 127.47, 127.70, 127.92, 127.95, 128.01, 128.22, 129.16, 123.00 (d, J(CF) = 7.3 Hz), 130.50 (d, J(CF) = 7.1 Hz), 132.24 (d, J(CF) = 6.8 Hz), 132.61 (d, J(CF) = 2.7 Hz), 134.97 (d, J(CF) = 1.9 Hz), 135.10, 140.37, 140.76 (d, J(CF) = 6.2 Hz), 140.98, 141.57, 141.73 (d, J(CF) = 5.9 Hz), 141.84 (d, J(CF) = 6.1 Hz), 142.90. <sup>11</sup>B NMR (CDCl<sub>3</sub>): +0.4 (s), +4.4 (bs). <sup>19</sup>F NMR (CDCl<sub>3</sub>): -174.4 (s). Anal. Calcd for C<sub>41</sub>H<sub>39</sub>B<sub>2</sub>FS: C 80.47; H 6.50. Found: C 80.91; H 6.49.

**Synthesis of 40- $\mu_2$ -N<sub>3</sub>.** To a solution of [40]OTf (84 mg, 0.11 mmol) in CH<sub>2</sub>Cl<sub>2</sub> (5 mL) at 25°C, was added a CH<sub>2</sub>Cl<sub>2</sub> solution (5 mL) of *n*Bu<sub>4</sub>NN<sub>3</sub> (35 mg, 0.12 mmol). After 15 minutes, the solvent was evaporated and the residue was dissolved in a mixture solvent of CH<sub>2</sub>Cl<sub>2</sub> (2 mL) and diethyl ether (18 mL). The resulting solution was filtered and evaporated to dryness to afford 40- $\mu_2$ -N<sub>3</sub> as a colorless solid (41 mg, 59% yield). Large colorless monocrystals of 40- $\mu_2$ -N<sub>3</sub> could be obtained by slow evaporation of an acetone/hexane mixture of 40- $\mu_2$ -N<sub>3</sub> at room temperature. <sup>1</sup>H NMR (CDCl<sub>3</sub>): δ 1.25 (s, 3H, Mes-CH<sub>3</sub>), 1.73 (s, 3H, Mes-CH<sub>3</sub>), 1.81 (s, 3H, Mes-CH<sub>3</sub>), 2.10 (s, 6H, Mes-CH<sub>3</sub>), 2.23 (s, 3H, Mes-CH<sub>3</sub>), 3.26 (s, 3H, S-CH<sub>3</sub>), 6.15 (bs, 1H, Mes-CH), 6.34 (bs, 1H, Mes-

CH), 6.38 (d, 2H,  $^3J(\text{HH}) = 8.0$  Hz, CH), 6.73 (bs, 1H, Mes-CH), 6.86 (bs, 1H, Mes-CH), 6.78 (m, 2H, CH), 7.06 (t, 1H,  $^3J(\text{HH}) = 6.0$  Hz, CH), 7.18-7.33 (m, 4H, CH), 7.40-7.48 (m, 3H, CH), 7.66 (d, 1H,  $^3J(\text{HH}) = 8.0$  Hz, CH), 7.77 (d, 1H,  $^3J(\text{HH}) = 8.0$  Hz, CH).  $^{13}\text{C}$  NMR ( $\text{CDCl}_3$ ): 20.73 (Mes- $\text{CH}_3$ ), 23.87 (Mes- $\text{CH}_3$ ), 25.41 (Mes- $\text{CH}_3$ ), 26.08 (Mes- $\text{CH}_3$ ), 30.95 (Mes- $\text{CH}_3$ ), 41.16 (S- $\text{CH}_3$ ), 123.73, 123.83, 125.03, 125.18, 126.08, 126.15, 126.31, 126.37, 126.86, 127.83, 128.15, 129.07, 129.57, 130.06, 130.68, 131.50, 132.52, 132.87, 133.07, 133.57, 133.95, 139.74, 140.53, 142.75.  $^{11}\text{B}$  NMR ( $\text{CDCl}_3$ ): -4.6. Anal. Calcd for  $\text{C}_{41}\text{H}_{39}\text{B}_2\text{N}_3\text{S}$ : C 78.48; H 6.26. Found: C 78.36; H 6.37.

**Anion ( $\text{X}^-$ ) complexation in  $\text{CHCl}_3$ .** A  $\text{CHCl}_3$  solution of [40]OTf (3 ml,  $c = 6.73 \times 10^{-5}$  M for  $\text{X}^- = \text{F}^-$  and  $c = 9.5 \times 10^{-5}$  M for  $\text{X}^- = \text{N}_3^-$ ) was placed in a cuvette and titrated with incremental amounts of the anion by addition of a  $\text{CHCl}_3$  solution of  $n\text{Bu}_4\text{NPh}_3\text{SiF}_2$  for  $\text{X}^- = \text{F}^-$  (7.2 mM) or  $n\text{Bu}_4\text{NN}_3$  for  $\text{X}^- = \text{N}_3^-$  (33.5 mM). For both experiments, the absorbance of the diborane was monitored at  $\lambda = 349$  nm, showing stoichiometric complexation of the anion ( $\epsilon = 10040$  for [40]OTf,  $\epsilon = 3270$  for **40- $\mu_2$ -F**,  $\epsilon = 3100$  for **40- $\mu_2$ -N $_3$** ).

**NMR study of the reaction of diborane **10** with  $n\text{Bu}_4\text{NPh}_3\text{SiF}_2$  in  $\text{CDCl}_3$ .** In a typical assay, a mixture of diborane **10** and  $n\text{Bu}_4\text{NPh}_3\text{SiF}_2$  in  $\text{CDCl}_3$  was placed in an NMR tube and analyzed by  $^1\text{H}$  NMR and  $^{19}\text{F}$  NMR spectroscopy. Integration of the spectra was used to determine the respective concentration of the relevant species. Two data sets (labeled as experiments 1 and 2) are provided below, along with the derivation of the equation used to calculate  $K_{\text{rel}}(\mathbf{10})$  ( $F_0$  is the initial concentration of  $\text{Ph}_3\text{SiF}_2^-$ , and  $B_0$  is the initial concentration of the diborane **10**).

	<b>10</b>	+	$\text{Ph}_3\text{SiF}$	+	$2 \times \text{F}^-$	$\Leftrightarrow$	<b>10F</b>	+	$\text{Ph}_3\text{SiF}_2^-$
	$B_0 - x$		$F_0 - y$		$F_0 - x - y$		$x$		$Y$
<b>Experiment 1</b>	5.1		51				51		100
<b>Experiment 2</b>	70		100				100		25

$$K_1 = [\mathbf{10F}] / ([\mathbf{10}] * [\text{F}^-]) = x / [(B_0 - x) * (F_0 - x - y)]$$

$$K_{\text{Ph}_3\text{SiF}_2^-} = [\text{Ph}_3\text{SiF}_2^-] / ([\text{Ph}_3\text{SiF}] * [\text{F}^-]) = y / [(F_0 - y) * (F_0 - x - y)]$$

$$\Rightarrow K_{\text{rel}}(\mathbf{10}) = K_1 / K_{\text{Ph}_3\text{SiF}_2^-} = [x * (F_0 - y)] / [y * (B_0 - x)] = 5.4 (\pm 1)$$

**Electrochemistry.** Electrochemical experiments were performed with an electrochemical analyzer from CH Instruments (Model 610A) with a glassy carbon working electrode, a platinum auxiliary electrode and a reference silver electrode. The reference electrode solution was built by immersing a silver wire in Vycor-capped glass tube containing a THF solution of TBAPF<sub>6</sub> (0.1 M) and AgNO<sub>3</sub> (0.005 M). All the three electrodes were placed in a THF solution (3 mL) containing TBAPF<sub>6</sub> (0.1 M) as a support electrolyte and [40]OTf (0.010 M). Ferrocene was used as an internal standard and the potentials are reported relative to the  $E_{1/2}$  of the Fc<sup>+</sup>/Fc redox couple.

**Computational details.** DFT calculations (full geometry optimization) were carried out with the Gaussian 03 program using the gradient-corrected Becke exchange functional (B3LYP) and the Lee-Yang-Parr correlation functional (Table 30, Table 31, Figure 78, Figure 79). Geometry optimization was carried out with the following mixed basis set: 6-31+g(d') for the boron, nitrogen and fluorine atoms, 6-31+g(d) for the sulfur atom, 6-31g basis set was used for other remained carbon and hydrogen atoms. Frequency calculations, which were carried out on the optimized structure of the compound, confirmed the absence of any imaginary frequencies. DT-DFT calculation was carried out with the Gaussian 03 program using B3LYP functional with the same basis sets as DFT calculation

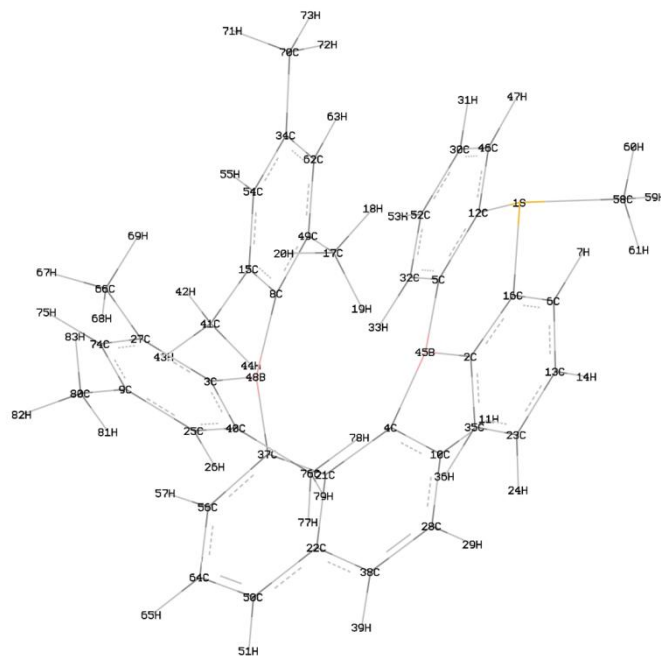


**Figure 78.** DFT optimized structure of  $[40]^+$

**Table 30.** Atom coordinates for the optimized structure of  $[40]^+$

Center Number	Coordinates(Angstroms)		
	X	Y	Z
S1	-3.158224	-1.636815	1.547687
C2	-1.242174	0.403136	1.887870
C3	2.975786	-0.582492	-0.180676
C4	-0.862226	2.322599	0.002165
C5	-2.753231	0.399897	-0.362082
C6	-1.668142	-1.171180	3.753131
H7	-2.165005	-2.056745	4.137791
C8	0.407163	-0.726466	-1.060410
C9	5.458859	-1.918645	0.379721
C10	-1.826820	3.339274	0.107328
H11	-2.855990	3.073228	0.334191
C12	-3.519983	-0.712726	0.042717
C13	-0.763277	-0.481355	4.564288
H14	-0.572917	-0.828727	5.573482
C15	-0.178747	-0.470449	-2.345295
C16	-1.912308	-0.702284	2.455026
C17	0.701935	-2.402464	0.891502
H18	0.084328	-3.163923	1.380839
H19	0.848501	-1.580928	1.595947
H20	1.687262	-2.846868	0.713049
C21	0.503565	2.685584	-0.320846
C22	0.782031	4.097688	-0.495156
C23	-0.114487	0.654130	4.066042
H24	0.577976	1.202520	4.694813
C25	4.858273	-1.080175	1.322218
H26	5.342299	-0.934682	2.284721
C27	3.594795	-1.442703	-1.146114
C28	-1.527733	4.709498	-0.036711
H29	-2.309462	5.452175	0.080430
C30	-4.988509	-0.573358	-1.865814
H31	-5.833253	-0.946476	-2.434073
C32	-3.174906	1.005634	-1.572935
H33	-2.618162	1.859638	-1.936031
C34	-1.392412	-2.603989	-2.279180

**Table 30.** Continued

Center Number	Coordinates(Angstroms)		
	X	Y	Z
C35	-0.346288	1.075336	2.754686
H36	0.168562	1.949895	2.377188
C37	1.607440	1.745797	-0.499960
C38	-0.237013	5.076622	-0.335067
H39	0.026977	6.122132	-0.462320
C40	3.650200	-0.411959	1.065558
C41	0.145486	0.765160	-3.164354
H42	-0.278701	0.677669	-4.168899
H43	1.223138	0.922777	-3.274382
H44	-0.255576	1.676219	-2.708615
B45	-1.507148	0.955785	0.436191
C46	-4.602707	-1.220626	-0.690602
H47	-5.137816	-2.107877	-0.365664
B48	1.611175	0.164514	-0.526303
C49	0.068379	-1.960156	-0.415268
C50	2.088766	4.548183	-0.836791
H51	2.249198	5.614361	-0.966661
C52	-4.271411	0.546815	-2.302754
H53	-4.559480	1.050964	-3.218690
C54	-1.043723	-1.409006	-2.924283
H55	-1.445100	-1.208348	-3.914230
C56	2.869749	2.279810	-0.813694
H57	3.701377	1.596343	-0.932813
C58	-4.660046	-1.271562	2.554679
H59	-4.526127	-1.730095	3.535555
H60	-5.516958	-1.722391	2.051697
H61	-4.784340	-0.191768	2.642820
C62	-0.835604	-2.850195	-1.015952
H63	-1.066409	-3.785999	-0.511456
C64	3.120076	3.655505	-0.997390
H65	4.117134	3.994354	-1.257067
C66	3.016803	-1.683884	-2.530738
H67	3.753270	-2.187771	-3.163842
H68	2.741027	-0.752768	-3.037109
H69	2.122415	-2.315624	-2.501283
C70	-2.322133	-3.596955	-2.936760
H71	-1.968036	-3.868679	-3.938087
H72	-3.330600	-3.179993	-3.057948
H73	-2.406363	-4.517433	-2.351169
C74	4.809320	-2.076043	-0.853057
H75	5.266782	-2.704070	-1.613560
C76	3.082895	0.419921	2.199231
H77	3.883721	0.768902	2.859570
H78	2.394027	-0.172857	2.816504
H79	2.536945	1.294677	1.841673
C80	6.766110	-2.621413	0.664892
H81	7.141923	-2.377925	1.663104
H82	7.537471	-2.338007	-0.061829
H83	6.654910	-3.711357	0.604935

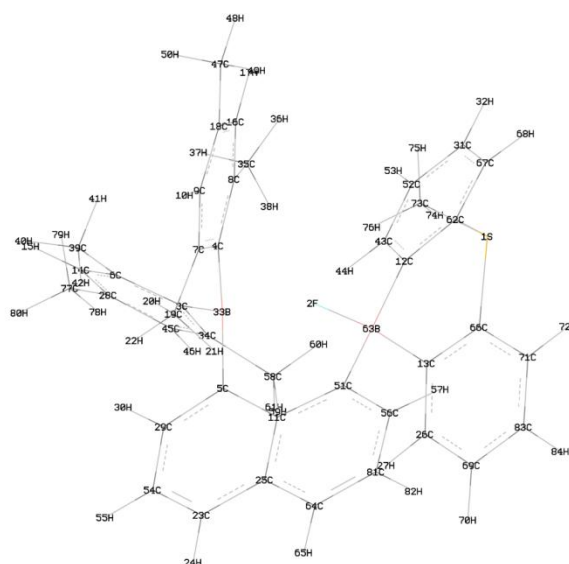


**Figure 79.** DFT optimized structure of **40-μ<sub>2</sub>-F**

**Table 31.** Atom coordinates for the optimized structure of **40-μ<sub>2</sub>-F**

Center Number	Coordinates(Angstroms)		
	X	Y	Z
S1	3.234204	-0.484771	-2.503270
F2	0.155097	-0.425737	-0.446635
C3	-2.587073	-0.684602	-0.564363
C4	-1.253982	1.647135	0.171470
C5	-1.221773	-0.674879	1.762166
C6	-3.860339	-0.053463	-0.742628
C7	-1.224637	2.574763	1.263283
C8	-1.115784	2.210017	-1.137045
C9	-0.999371	3.943596	1.035611
H10	-0.988342	4.615966	1.891137
C11	0.034457	-0.744247	2.479642
C12	2.318671	0.919339	-0.270622
C13	2.266657	-1.792737	-0.241016
C14	-4.862817	-0.664994	-1.512417
H15	-5.817758	-0.154750	-1.623144
C16	-0.872481	3.582418	-1.317079
H17	-0.756286	3.965293	-2.329248
C18	-0.798370	4.471837	-0.243517
C19	-1.475698	2.196337	2.714460
H20	-1.616393	3.102167	3.314039
H21	-0.644873	1.636196	3.153206
H22	-2.367481	1.576155	2.835764
C23	-1.196890	-1.515264	4.493651
H24	-1.183239	-1.796198	5.543687
C25	0.023374	-1.115709	3.877186
C26	2.180697	-2.989238	0.508842
H27	1.597404	-2.980818	1.421995
C28	-4.680466	-1.908216	-2.127705
C29	-2.369070	-1.124301	2.415718
H30	-3.313524	-1.120018	1.880733
C31	3.746165	3.254845	-1.136701
H32	4.290191	4.136769	-1.457397
B33	-1.430378	0.030463	0.331265
C34	-2.440436	-1.988121	-1.126256
C35	-1.299305	1.416019	-2.421502
H36	-0.728402	1.875568	-3.238018
H37	-2.354395	1.413332	-2.725250
H38	-1.007600	0.372851	-2.330258



**Table 31** Continued

Center Number	Coordinates(Angstroms)		
	X	Y	Z
C39	-4.238945	1.271106	-0.095051
H40	-5.326479	1.401116	-0.125970
H41	-3.786704	2.130338	-0.600794
H42	-3.930482	1.325087	0.952974
C43	2.290108	2.131691	0.454311
H44	1.703894	2.169244	1.363342
C45	-3.465415	-2.558087	-1.902210
H46	-3.311522	-3.550468	-2.321412
C47	-0.540785	5.948359	-0.452400
H48	-0.434228	6.186763	-1.515933
H49	0.376396	6.274332	0.055918
H50	-1.360638	6.559893	-0.053968
C51	1.298977	-0.448336	1.854780
C52	2.973198	3.275446	0.031306
H53	2.904511	4.186230	0.617218
C54	-2.365190	-1.551439	3.766440
H55	-3.291854	-1.879929	4.228444
C56	2.439728	-0.400971	2.657150
H57	3.400228	-0.174423	2.198757
C58	-1.212027	-2.852652	-0.907324
H59	-0.871148	-2.809974	0.129799
H60	-0.365088	-2.546321	-1.530605
H61	-1.438931	-3.897257	-1.147590
C62	3.098974	0.955350	-1.442948
B63	1.521521	-0.408464	0.261254
C64	1.227625	-1.071605	4.633100
H65	1.192341	-1.341600	5.685469
C66	3.057500	-1.889018	-1.402230
H67	3.818481	2.079645	-1.884093
H68	4.425600	2.033835	-2.783751
C69	2.822838	-4.168456	0.120309
H70	2.716513	-5.061634	0.727979
C71	3.740134	-3.049301	-1.807490
H72	4.360660	-3.046156	-2.699122
C73	1.651746	-0.499768	-3.428836
H74	1.643900	-1.398096	-4.050216
H75	1.623366	0.394838	-4.054188
H76	0.824387	-0.502680	-2.721339
C77	-5.772247	-2.535808	-2.966652
H78	-5.466355	-3.515663	-3.348348
H79	-6.028787	-1.907085	-3.829494
H80	-6.694566	-2.676492	-2.388033
C81	2.412492	-0.687413	4.041838
H82	3.328625	-0.636607	4.623321
C83	3.612803	-4.204158	-1.036597
H84	4.129063	-5.112543	-1.327764

## CHAPTER VI

## LEWIS ACIDITY BEHAVIOR OF TRIS(PENTACHLOROPHENYL)BORANE

## 6.1 Introduction

Tris(pentafluorophenyl)borane, in which the small electronegative fluorine substituents induce strong Lewis acidity, has attracted a great deal of attention in catalysis, synthesis and small molecule activation.<sup>6-15</sup> Tuning the Lewis acidity of such triarylboranes has been achieved by simple modifications in the electronic and steric properties of the aryl substituents. As previously shown by Norton and Jaekle, substitution of a pentafluorophenyl group with a mesityl group in the  $\text{Mes}_n\text{B}(\text{C}_6\text{F}_5)_{(3-n)}$  ( $n = 1, 2, 3$ ) series results in a gradual decrease of the electron affinity and thus Lewis acidity of the borane.<sup>173</sup> Recently, O'Hare and coworkers have reported the synthesis of a new family of triarylboranes,  $(\text{C}_6\text{Cl}_5)_n\text{B}(\text{C}_6\text{F}_5)_{(3-n)}$  ( $n = 1, 2, 3$ ), and investigated how substitution of a pentafluorophenyl by a pentachlorophenyl groups affects the properties of the molecule.<sup>174</sup> Cyclic voltammetry and NMR data show that the electron affinity of the borane increases as  $n$ , the number of pentachlorophenyl group, increases. This effect is rationalized by the greater  $\sigma$ -Hammett parameter of the chlorine substituents, making the pentachlorophenyl group a more electron withdrawing substituent. Somewhat paradoxically, this group decreases the Lewis acidity of the boron center because the increased bulk of the chlorine atom hinders pyramidalization of the boron atom. In line with this argument, the O'Hare group observed that  $\text{B}(\text{C}_6\text{Cl}_5)_3$  fails to interact with triethylphosphine oxide in chloroform as indicated by  $^{31}\text{P}$  NMR spectroscopy. Intrigued

by this presumed lack of Lewis acidity, we decided to carry out a more careful investigation of its Lewis acidity. In this study, we report a series of results which shows that  $B(C_6Cl_5)_3$  is a potent Lewis acid which binds anions and neutral molecules in organic solvents.

## 6.2 Fluoride ion complexation of $B(C_6Cl_5)_3$

First of all, we examined the spectroscopic property of  $B(C_6Cl_5)_3$  by UV-vis spectroscopy. Like other triarylboranes,  $B(C_6Cl_5)_3$  shows a broad low-energy absorption band at  $\lambda_{max} = 331$  nm in dichloromethane corresponding to the boron-centered chromophore. Since binding of a Lewis base to the boron center will interrupt  $\pi$ -conjugation in this chromophore and thus quench the absorption band, the binding process can be easily monitored by UV-vis spectroscopy.

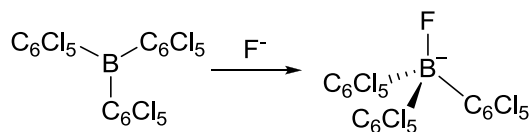


**Figure 80.** The reaction of  $B(C_6Cl_5)_3$  with fluoride anion.

Next, the reactivity of  $B(C_6Cl_5)_3$  toward fluoride was investigated by mixing an equimolar quantities of  $B(C_6Cl_5)_3$  and TASF (tris(dimethylamino)sulfonium difluorotrimethylsilicate) in  $CDCl_3$  (Figure 80). Both the  $^{19}F$  NMR resonance at -168

ppm (broad) and the  $^{11}\text{B}$  NMR resonance at 6.5 ppm (broad) indicate the formation of a triarylfluoroborate species.<sup>26</sup> This new species,  $[\text{FB}(\text{C}_6\text{Cl}_5)_3][\text{S}(\text{NMe}_2)_3]^+$ , has been isolated from the reaction of  $\text{B}(\text{C}_6\text{Cl}_5)_3$  with TASF in THF. Large single crystals of  $[\text{FB}(\text{C}_6\text{Cl}_5)_3][\text{S}(\text{NMe}_2)_3]^+$  were obtained by slow diffusion of pentane into a THF solution of  $[\text{FB}(\text{C}_6\text{Cl}_5)_3][\text{S}(\text{NMe}_2)_3]^+$ . This salt crystallized in a hexagonal P-3C1 space group (Figure 81, Table 32). The crystal structure is affected by a complicated disorder thus precluding an accurate determination of the bond distances and angles. Nevertheless, the crystal structure has shown that: 1) the B(1)-F(1) bond length of 1.43 Å is comparable to those measured for other reported triarylfluoroborate species; 2) the boron center becomes clearly pyramidalized as indicated by the sum of the  $\text{C}_{\text{aryl}}\text{-B-C}_{\text{aryl}}$  angles ( $\Sigma_{(\text{C-B-C})} = 335.1^\circ$ ); 3) the distance between the sulfur atom of the counter cation and the boron-bound fluoride is 3.09 Å which is within the sum of Van der Waals radii (3.27 Å), indicating a potential weak interaction between the sulfonium center of the counter cation and the fluorine atom.

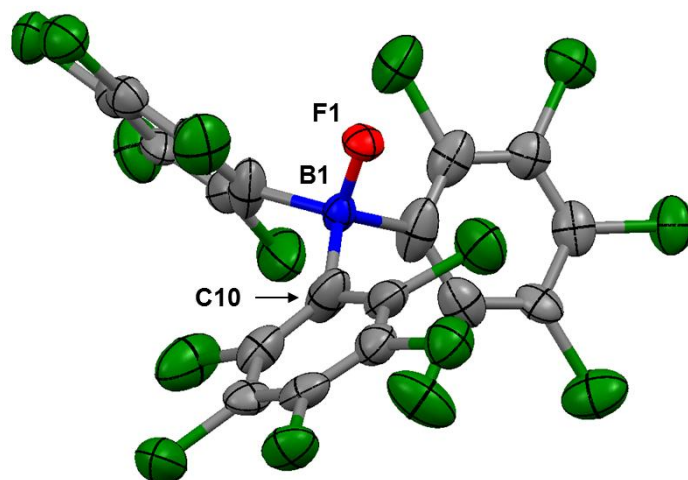


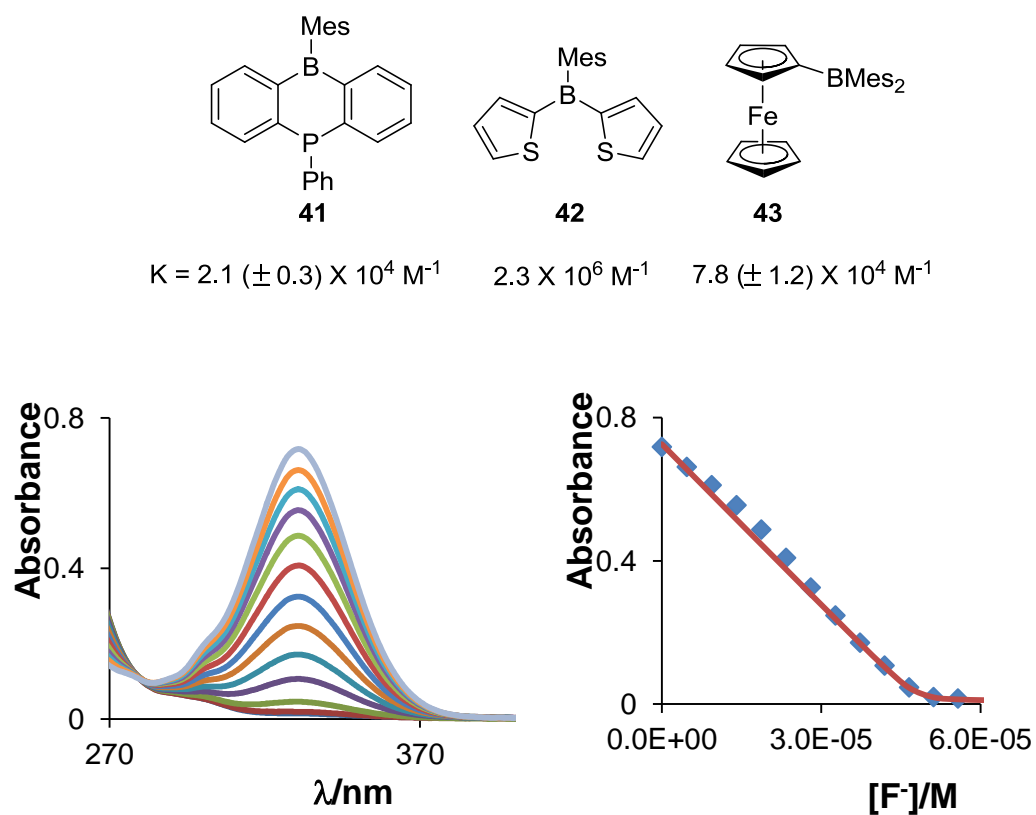
**Figure 81.** ORTEP drawing of  $[\text{FB}(\text{C}_6\text{Cl}_5)_3][\text{S}(\text{NMe}_2)_3]^+$  with thermal ellipsoid plots (50% probability). For clarity, the counter cation  $[\text{S}(\text{NMe}_2)_3]^+$  and hydrogen atoms are omitted. Selected bond lengths ( $\text{\AA}$ ) and angles ( $^\circ$ ): B(1)-F(1) 1.43(3), B(1)-C(10) 1.710(16); F(1)-B(1)-C(10) 107.1(12), C(10)-B(1)-C(10)<sub>#2</sub> 111.7(10).

**Table 32.** Crystal data, data collections, and structure refinement for  $[\text{FB}(\text{C}_6\text{Cl}_5)_3]^- [\text{S}(\text{NMe}_2)_3]^+ \cdot 1.5\text{THF}$ .

Crystal data	$[\text{FB}(\text{C}_6\text{Cl}_5)_3]^- [\text{S}(\text{NMe}_2)_3]^+ \cdot 1.5\text{THF}$
formula	$\text{C}_{30}\text{H}_{60}\text{BCl}_{15}\text{FN}_3\text{O}_{1.5}\text{S}$
$M_r$	1050.19
crystal size ( $\text{mm}^3$ )	0.15 x 0.14 x 0.10
crystal system	Hexagonal
space group	P-3C1
$a$ ( $\text{\AA}$ )	13.7551(10)
$b$ ( $\text{\AA}$ )	13.7551(10)
$c$ ( $\text{\AA}$ )	25.562(4)
$\alpha$ ( $^\circ$ )	90
$\beta$ ( $^\circ$ )	90
$\gamma$ ( $^\circ$ )	120
$V$ ( $\text{\AA}^3$ )	4188.5(7)
$Z$	2
$\rho_{\text{calc}}$ ( $\text{g cm}^{-3}$ )	1.665
$\mu$ ( $\text{mm}^{-1}$ )	1.073
$F(000)$	2112
Data Collection	
$T$ (K)	110(2)
scan mode	$\omega$
	-14 $\rightarrow$ +14
$hkl$ range	-14 $\rightarrow$ +14
	-27 $\rightarrow$ +27
measd reflns	29279
unique reflns [ $R_{\text{int}}$ ]	1825 [0.0495]
reflns used for refinement	1825
Refinement	
refined parameters	
GooF	1.027
$R_1$ , <sup>a</sup> $wR_2$ , <sup>b</sup> all data	0.1588, 0.2580
$\rho_{\text{fin}}$ (max/min) ( $\text{e \AA}^{-3}$ )	1.541, -2.007

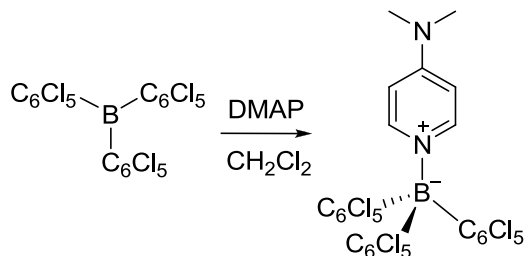
<sup>a</sup>  $R_1 = \Sigma ||F_o| - |F_c|| / \Sigma |F_o|$ . <sup>b</sup>  $wR_2 = [(\Sigma w(F_o^2 - F_c^2)^2) / (\Sigma w(F_o^2)^2)]^{1/2}$ .

A fluoride titration was carried out by monitoring the absorption of  $\text{B}(\text{C}_6\text{Cl}_5)_3$  at  $\lambda_{\text{max}} = 331 \text{ nm}$  with UV-vis spectroscopy. The fluoride binding constant of  $\text{B}(\text{C}_6\text{Cl}_5)_3$  in dichloromethane is  $1.5 (\pm 0.2) \times 10^7 \text{ M}^{-1}$  (Figure 82). Under these conditions, the fluoride binding constants of other neutral triarylboranes, such as **41**, **42** and **43** which are also air stable, are in the range of  $10^4$  and  $10^6 \text{ M}^{-1}$ .<sup>157, 167, 175</sup> These results show that  $\text{B}(\text{C}_6\text{Cl}_5)_3$  is more fluorophilic than most other neutral triarylboranes. Encouraged by these results, we tested the ability of  $\text{B}(\text{C}_6\text{Cl}_5)_3$  to extract fluoride from water into a less polar solvent. Shaking a biphasic mixture consisting of tetrabutylammonium fluoride (TBAF) in  $\text{D}_2\text{O}$  (0.13 M, 0.5 ml) and  $\text{B}(\text{C}_6\text{Cl}_5)_3$  in  $\text{CDCl}_3$  (0.013 M, 0.5 ml) results in the formation of the corresponding fluoride adduct  $[\text{FB}(\text{C}_6\text{Cl}_5)_3][n\text{Bu}_4\text{N}]^+$  after a few minutes, as indicated by the presence of  $^{19}\text{F}$  NMR resonance at -148 ppm and a  $^{11}\text{B}$  NMR signal at 5.1 ppm. Both the  $^{19}\text{F}$  NMR and  $^{11}\text{B}$  NMR spectra show that the boron and fluorine nuclei are coupled by  $J_{\text{B-F}} = 52 \text{ Hz}$ . The difference of the chemical shifts (both  $^{19}\text{F}$  NMR and  $^{11}\text{B}$  NMR) between biphasic conditions and pure chloroform probably results from cation effect and solvation effect. Besides the formation of the fluoride adduct, another compound was also formed under biphasic conditions. This other compound is assigned to  $[(\text{C}_6\text{Cl}_5)_3\text{BOH}]^-$ , as indicated by the presence of  $^{11}\text{B}$  NMR resonance at 1.5 ppm. To our knowledge, such a biphasic fluoride capture is unprecedented for any neutral triarylboranes and diboranes.



**Figure 82.** Left: Absorbance changes upon addition of TBAF ( $4.7 \times 10^{-3} \text{ M}$  in  $\text{CH}_2\text{Cl}_2$ ) to a  $\text{CH}_2\text{Cl}_2$  solution of  $\text{B}(\text{C}_6\text{Cl}_5)_3$  ( $4.84 \times 10^{-5} \text{ M}$ ). Right: Binding isotherm monitored at  $\lambda = 331 \text{ nm}$  ( $\epsilon = 15000$  for  $\text{B}(\text{C}_6\text{Cl}_5)_3$ ,  $\epsilon = 150$  for  $[\text{FB}(\text{C}_6\text{Cl}_5)_3]$ ).



6.3 DMAP complexation of  $B(C_6Cl_5)_3$ 

**Figure 83.** The reaction of  $B(C_6Cl_5)_3$  with DMAP.

In order to gain more insights into the Lewis acidity of  $B(C_6Cl_5)_3$ , we decided to investigate its reactivity toward *p*-dimethylaminopyridine (DMAP) in organic solvents. First of all, we studied the reaction of  $B(C_6Cl_5)_3$  with DMAP in  $CDCl_3$  by  $^1H$  NMR and  $^{11}B$  NMR spectroscopy (DMAP: 0.027 M;  $CDCl_3$ : 0.7 ml) (Figure 83). The proton signal of the DMAP *CH* group ortho to the nitrogen atom showed a progressing upfield shift when gradual amounts of  $B(C_6Cl_5)_3$  were added to the solution. These changes indicate the formation of a new species, identified as  $B(C_6Cl_5)_3$ -DMAP. The  $^{11}B$  NMR resonance at 1.8 ppm also confirmed the presence of the adduct  $B(C_6Cl_5)_3$ -DMAP. The precipitation of  $B(C_6Cl_5)_3$ -DMAP did not allow for an NMR determination of the DMAP binding constant. Nevertheless, the equilibrium could be studied by UV-vis spectroscopy under more dilute conditions, in dichloromethane. Addition of 34 equivalents of DMAP in a dichloromethane solution of  $B(C_6Cl_5)_3$  resulted in a 84% quenching of the absorption spectrum indicating the formation of the adduct  $B(C_6Cl_5)_3$ -DMAP. More careful titration carried out in dichloromethane afforded a binding

constant of  $3.0 (\pm 0.3) \times 10^4 \text{ M}^{-1}$  (Figure 84). This binding constant is smaller than that of fluoride, which can be correlated to the bulk of DMAP as well as its neutrality.

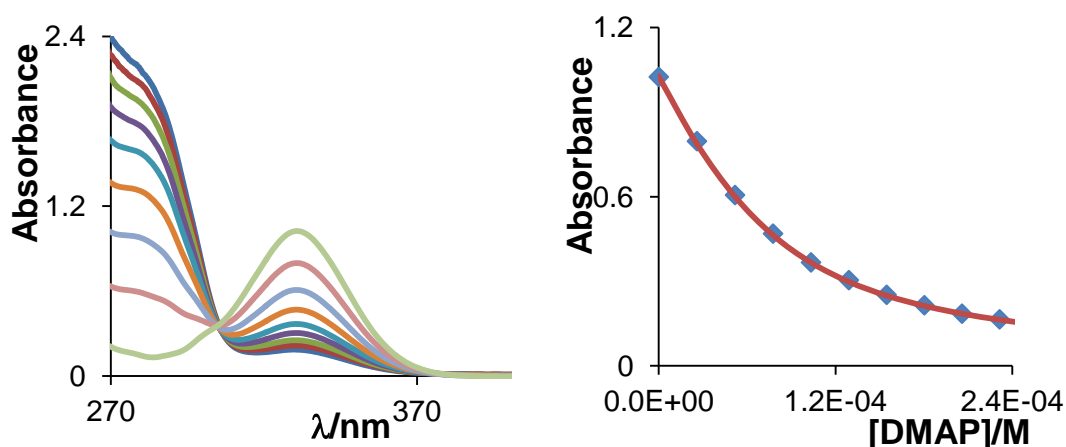


**Figure 84.** Left: Absorbance changes upon addition of DMAP (0.026 M in  $\text{CH}_2\text{Cl}_2$ ) to a  $\text{CH}_2\text{Cl}_2$  solution of  $\text{B}(\text{C}_6\text{Cl}_5)_3$  ( $6.8 \times 10^{-5} \text{ M}$ ). Right: Binding isotherm monitored at  $\lambda = 331 \text{ nm}$  ( $\epsilon = 15000$  for  $\text{B}(\text{C}_6\text{Cl}_5)_3$ ,  $\epsilon = 0$  for  $\text{B}(\text{C}_6\text{Cl}_5)_3\text{-DMAP}$ ).

Large single crystals of  $\text{B}(\text{C}_6\text{Cl}_5)_3\text{-DMAP}$  were obtained by slow diffusion of pentane into a THF solution of equimolar amounts of  $\text{B}(\text{C}_6\text{Cl}_5)_3$  and DMAP. This adduct crystallizes in a triclinic  $P-1$  space group (Figure 85, Table 33). The  $\text{B}(1)\text{-N}(1)$  bond ( $1.615(4) \text{ \AA}$ ) is slightly shorter than those measured in the adducts of triarylboranes, such as  $\text{Ph}_3\text{B-DMAP}$ ,  $\text{B-N}_{\text{DMAP}} = 1.636(2) \text{ \AA}$ .<sup>164, 176</sup> Coordination of the DMAP molecule to the boron center leads to a distinct pyramidalization of the latter, as indicated by the sum of the  $\text{C}_{\text{aryl}}\text{-B-C}_{\text{aryl}}$  angles ( $\Sigma_{(\text{C-B-C})} = 335.9^\circ$ ).

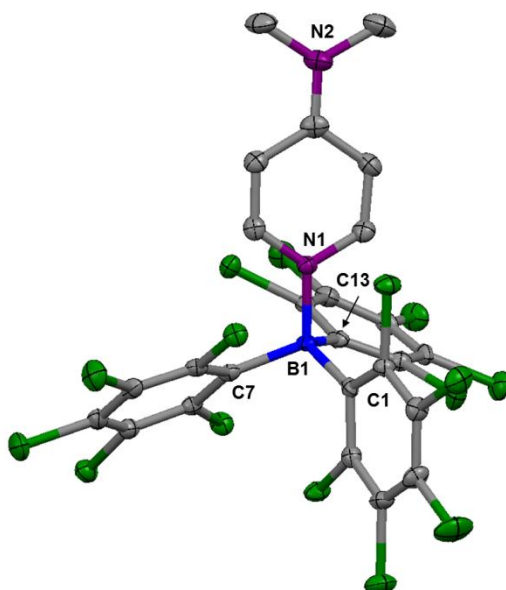


**Figure 85.** ORTEP drawing of  $B(C_6Cl_5)_3$ -DMAP with thermal ellipsoid plots (50% probability). For clarity, hydrogen atoms are omitted. Selected bond lengths ( $\text{\AA}$ ) and angles ( $^\circ$ ): N(1)-B(1) 1.615(4), C(1)-B(1) 1.688(5), C(7)-B(1) 1.688(5), C(13)-B(1) 1.687(5); N(1)-B(1)-C(13) 98.3(2), N(1)-B(1)-C(7) 110.0(3), C(13)-B(1)-C(7) 116.4(3), N(1)-B(1)-C(1) 112.8(3), C(13)-B(1)-C(1) 115.4(3), C(7)-B(1)-C(1) 104.1(3).

**Table 33.** Crystal data, data collections, and structure refinement for B(C<sub>6</sub>Cl<sub>5</sub>)<sub>3</sub>-DMAP.

Crystal data	B(C <sub>6</sub> Cl <sub>5</sub> ) <sub>3</sub> -DMAP•3.5THF
formula	C <sub>37</sub> H <sub>26</sub> BCl <sub>15</sub> N <sub>2</sub> O <sub>3.5</sub>
<i>M</i> <sub>r</sub>	1097.16
crystal size (mm <sup>3</sup> )	0.12 x 0.11 x 0.07
crystal system	Triclinic
space group	P-1
<i>a</i> (Å)	13.427(3)
<i>b</i> (Å)	13.490(3)
<i>c</i> (Å)	14.172(4)
<i>α</i> (°)	68.329(3)
<i>β</i> (°)	67.007(3)
<i>γ</i> (°)	79.508(3)
<i>V</i> (Å <sup>3</sup> )	2193.7(10)
<i>Z</i>	2
<i>ρ</i> <sub>calc</sub> (g cm <sup>-3</sup> )	1.661
<i>μ</i> (mm <sup>-1</sup> )	0.982
<i>F</i> (000)	1100
Data Collection	
<i>T</i> (K)	110(2)
scan mode	<i>ω</i>
	-15 → +15
<i>hkl</i> range	-16 → +16
	-16 → +16
measd reflns	21110
unique reflns [ <i>R</i> <sub>int</sub> ]	7695 [0.0381]
reflns used for refinement	7695
Refinement	
refined parameters	
Goof	1.006
<i>R</i> <sub>1</sub> , <sup>a</sup> <i>wR</i> <sub>2</sub> <sup>b</sup> all data	0.0577, 0.1229
<i>ρ</i> <sub>fin</sub> (max/min) (e Å <sup>-3</sup> )	0.905, -0.559

$$^a R_1 = \frac{\sum ||F_o| - |F_c||}{\sum |F_o|}, \quad ^b wR_2 = \left[ \frac{\sum w(F_o^2 - F_c^2)^2}{\sum w(F_o^2)^2} \right]^{1/2}.$$

#### 6.4 Complexation of other anions and molecules by $B(C_6Cl_5)_3$

Encouraged by these results, we moved on to test the affinity of  $B(C_6Cl_5)_3$  for other common anions. Table 34 has shown the binding constants of  $B(C_6Cl_5)_3$  with cyanide and azide, compared to those of fluoride and DMAP in dichloromethane. The binding constants decrease in the order: fluoride > azide > cyanide. Presumably the larger bulk of the azide and cyanide anions are responsible for their lower tendency to associate with the borane. We also decided to test if neutral molecules other than DMAP would also bind to the borane. Only weak binding was observed for pyridine in dichloromethane; the less competitive solvent THF (acceptor number = AN = 8.9 for THF vs. 20.4 for  $CH_2Cl_2$ ) was therefore employed (Table 34). As shown in Table 34, the binding constant of pyridine is much smaller than that of DMAP due to the lower basicity of pyridine ( $pK_a(\text{pyridine}) = 5.2$  vs.  $pK_a(\text{DMAP}) = 9.2$ ).

**Table 34.** The binding constants of  $B(C_6Cl_5)_3$  with different Lewis bases in dichloromethane and/or THF.

	Fluoride ( $CH_2Cl_2$ )	Azide ( $CH_2Cl_2$ )	Cyanide ( $CH_2Cl_2$ )	DMAP ( $CH_2Cl_2$ )	DMAP (THF)	Pyridine (THF)
K/ $M^{-1}$	$1.5 (\pm 0.2) \times 10^7$	$6.0 (\pm 0.6) \times 10^6$	$1.8 (\pm 0.2) \times 10^6$	$3.0 (\pm 0.3) \times 10^4$	$1.0 (\pm 0.1) \times 10^7$	36 ( $\pm 4$ )

#### 6.5 Conclusion

In conclusion, we report the Lewis acidic behavior of  $B(C_6Cl_5)_3$  which can capture fluoride, azide and cyanide in dichloromethane with large binding constants.

$B(C_6Cl_5)_3$  can also extract fluoride ions from aqueous environments into less polar phases. In addition,  $B(C_6Cl_5)_3$  is found to also bind neutral molecule, such as pyridine and DMAP, in organic solvents. The results in this work may lead to the development of the chlorinated triarylboranes with potential applications in sensing, catalysis, synthesis and small molecule activation.

## 6.6 Experimental section

**General Considerations.** Commercially available chemicals were purchased and used as provided (Commercial sources: Aldrich for  $Me_3SiF_2S(NMe_2)_3$  (TASF),  $nBu_4NF$ ,  $nBu_4NCN$ ,  $nBu_4NN_3$ ,  $BCl_3$  in *n*-heptane, DMAP; Alpha Aesar for *n*-butyllithium (2.6 M in hexanes)).  $B(C_6Cl_5)_3$  was prepared by reaction of pentachlorophenyl lithium with  $BCl_3$  as reported by O'Hare group. Diethyl ether and THF were dried by refluxing under  $N_2$  over Na/K and freshly distilled prior to use. Dichloromethane and pentane were dried over  $AlCl_3$  column. Air-sensitive compounds were handled under  $N_2$  atmosphere using standard Schlenk and glovebox techniques. UV-vis spectra were recorded on an Ocean Optics USB4000 spectrometer with an Ocean Optics ISS light source. Elemental analyses were performed at Atlantic Microlab (Norcross, GA). NMR spectra were recorded on Varian Unity Inova 400 FT NMR (399.59 MHz for  $^1H$ , 376.03 MHz for  $^{19}F$ , 128.19 MHz for  $^{11}B$ , 100.45 MHz for  $^{13}C$ ) spectrometers at ambient temperature. Chemical shifts  $\delta$  are given in ppm and are referenced against external  $BF_3 \cdot Et_2O$  ( $^{11}B$  and  $^{19}F$ ).

**Crystallography.** The crystallographic measurements were performed using a Bruker APEX-II CCD area detector diffractometer (Mo-K $\alpha$  radiation,  $\lambda = 0.71069 \text{ \AA}$ ) for [FB(C<sub>6</sub>Cl<sub>5</sub>)<sub>3</sub>][S(NMe<sub>2</sub>)<sub>3</sub>]<sup>+</sup> and B(C<sub>6</sub>Cl<sub>5</sub>)<sub>3</sub>-DMAP. In each case, a specimen of suitable size and quality was selected and mounted onto a nylon loop. The structures were solved by direct methods, which successfully located most of the non-hydrogen atoms. Subsequent refinement on F<sup>2</sup> using the SHELXTL/PC package (version 5.1) allowed location of the remaining non-hydrogen atoms.

**Synthesis of [FB(C<sub>6</sub>Cl<sub>5</sub>)<sub>3</sub>][S(NMe<sub>2</sub>)<sub>3</sub>]<sup>+</sup>.** TASF (11 mg, 0.040 mmol) was added to a solution of B(C<sub>6</sub>Cl<sub>5</sub>)<sub>3</sub> (30 mg, 0.040 mmol) in THF (5 mL) at room temperature. The mixture was stirred for ten minutes. The solvent was removed under vacuum to yield a solid which was washed with diethyl ether to afford [FB(C<sub>6</sub>Cl<sub>5</sub>)<sub>3</sub>][S(NMe<sub>2</sub>)<sub>3</sub>]<sup>+</sup> as a pale product (35 g, yield 84%). Single crystals were obtained by slow diffusion of pentane into a THF solution of [FB(C<sub>6</sub>Cl<sub>5</sub>)<sub>3</sub>][S(NMe<sub>2</sub>)<sub>3</sub>]<sup>+</sup> at -25°C. <sup>1</sup>H NMR (399.59MHz, CDCl<sub>3</sub>):  $\delta$  2.96 (N-CH<sub>3</sub>) <sup>13</sup>C NMR (100.45 MHz, CDCl<sub>3</sub>):  $\delta$  38.65 (N-CH<sub>3</sub>), 129.03, (s, ortho- C<sub>6</sub>Cl<sub>5</sub>), 130.23, 130.66, 136.89, 137.49. <sup>11</sup>B NMR (128.19 MHz, CDCl<sub>3</sub>): 6.8 (broad signal). <sup>19</sup>F NMR (376.03 MHz, CDCl<sub>3</sub>) -168 (broad). Anal. Calcd for C<sub>24</sub>H<sub>18</sub>BFCl<sub>15</sub>S-1/2THF: C 31.93; H 2.27. Found: C 31.99; H 2.38. (The sample used for EA was obtained by recrystallization from THF, and the initial crystal contains THF molecules).

**Lewis bases (X) complexation in CH<sub>2</sub>Cl<sub>2</sub>.** A CH<sub>2</sub>Cl<sub>2</sub> solution of B(C<sub>6</sub>Cl<sub>5</sub>)<sub>3</sub> (3 ml,  $c = 4.84 \times 10^{-5} \text{ M}$  for X = F<sup>-</sup>,  $c = 5.80 \times 10^{-5} \text{ M}$  for X = N<sub>3</sub><sup>-</sup>,  $c = 7.20 \times 10^{-5} \text{ M}$  for X = CN<sup>-</sup>,  $c = 6.84 \times 10^{-5} \text{ M}$  for X = DMAP) was placed in a cuvette and titrated with

incremental amounts of the Lewis base by addition of a  $\text{CH}_2\text{Cl}_2$  solution of  $n\text{Bu}_4\text{NF}$  for  $\text{X} = \text{F}^-$  (4.7 mM),  $n\text{Bu}_4\text{NN}_3$  for  $\text{X} = \text{N}_3^-$  (30 mM),  $n\text{Bu}_4\text{NCN}$  for  $\text{X} = \text{CN}^-$  (3.6 mM), or DMAP (26 mM). For these experiments, the absorbance of  $\text{B}(\text{C}_6\text{Cl}_5)_3$  was monitored at  $\lambda = 331$  nm, showing the complexation of the Lewis bases.

**NMR study of the reaction of  $\text{B}(\text{C}_6\text{Cl}_5)_3$  with DMAP in  $\text{CDCl}_3$ .** A  $\text{CDCl}_3$  solution of DMAP (0.027 M, 0.7 ml) was placed in an NMR tube and was added  $\text{B}(\text{C}_6\text{Cl}_5)_3$  4 mg each time.  $^1\text{H}$  NMR spectra were recorded correspondingly each time.



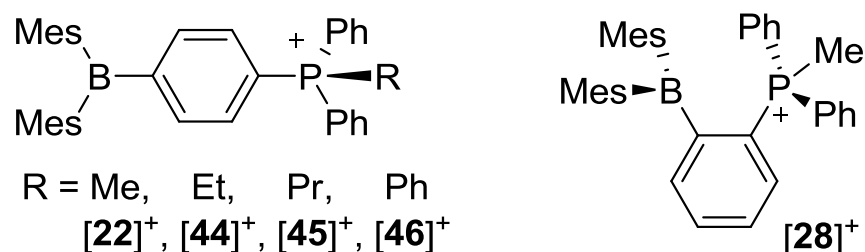
CHAPTER VII  
THE HYDROPHOBIC EFFECTS IN THE FLUORIDE COMPLEXATION BY  
A SERIES OF SULFONIUM BORANES

### 7.1 Introduction

The recognition of the fluoride anion has been attracting a great deal of attention because of toxicity concerns.<sup>1-3</sup> Since fluoride has found widespread applications in industry and medicine, the potential toxicity of this anion has been the subject of numerous discussions and polemics leading to some rather strict regulations for human intake. For example, the Environment Protection Agency (EPA) recommends of fluoride concentration of just 0.7 ppm for drinking water. The same agency has also set the drinking water maximum contaminant level of fluoride to 4 ppm in drinking water. For these reasons, fluoride anion sensors that can operate in water in the low concentration range are worthwhile targets.

Previous results from the Gabbai group have shown that the introduction of cationic moieties into organoboranes increases their Lewis acidity as well as the water solubility.<sup>25-26, 45-46, 48, 177</sup> For example, onium boranes such as the phosphonium boranes **[22]<sup>+</sup>**, **[44]<sup>+</sup>**, **[45]<sup>+</sup>** and **[46]<sup>+</sup>** capture fluoride ions in aqueous solution,<sup>62</sup> Investigation of these four boranes indicates that an increase in the hydrophobicity of the cationic boranes leads to an increase of their anion affinity. On the other hand, the anion affinity could be further elevated by placing the cationic moieties next to the boron atom as in **[22]<sup>+</sup>** and **[28]<sup>+</sup>**.<sup>25</sup> These precedents lead us to speculate that the incorporation of

hydrophobic groups in close proximity to the boron center may actually result in a more significant Lewis acidity increase. Considering the fact that  $[28]^+$  is not stable in water, we have now synthesized a series of sulfonium boranes of varying hydrophobicity and investigated their Lewis acidity and fluoride affinity in aqueous environment.



## 7.2 Synthesis and characterization of sulfonium boranes

Using a similar synthetic strategy to that employed in the case of  $[47]^+$ ,<sup>61</sup> we found that the related sulfonium boranes  $[48]^+$ ,  $[49]^+$  and  $[50]^+$  could be readily synthesized by reaction of 1-Li-2-SPh-C<sub>6</sub>H<sub>4</sub>, 1-Li-4-SMe-C<sub>6</sub>H<sub>4</sub> or 1-Li-4-SPh-C<sub>6</sub>H<sub>4</sub> with Mes<sub>2</sub>BF and subsequent methylation of the corresponding neutral thiophenyl boranes with MeOTf (Figure 86). These triflate salts have been characterized by multinuclear NMR spectroscopy. In all four cases, the boron center remains trigonal planar in agreement with the detection of a broad <sup>11</sup>B-NMR resonance in the 70 - 80 ppm range in CDCl<sub>3</sub>. Like  $[47]^+$ , these new sulfonium boranes feature a low energy UV absorption band detected at 334 nm for  $[48]^+$ , 325 nm for  $[49]^+$ , and 319 nm for  $[50]^+$  in H<sub>2</sub>O/MeOH (95:5 vol.), which also confirms the presence of a coordinatively unsaturated boron center.<sup>146-147, 178</sup> The resulting boron-centered chromophores are fluorescent and give rise to a broad emission band at 470 nm for  $[47]^+$  and  $[48]^+$ , 494 nm

for  $[49]^+$  and 499 nm for  $[50]^+$  in H<sub>2</sub>O/MeOH (95:5 vol.), respectively when excited at 340 nm. The crystal structure of the sulfonium borane salt  $[48]OTf$  has been obtained (Table 35, Figure 87). These structure shows that: 1) the boron center remains trigonal planar geometry indicated by the sum of the C<sub>aryl</sub>-B-C<sub>aryl</sub> angles ( $\sum C_{aryl}-B-C_{aryl} = 360.0^\circ$ ); 2) that the boron-sulfur separation (3.158 Å) is slightly longer than that in  $[47]^+$  (3.070 Å). The NBO analysis carried out at DFT optimized geometry of  $[48]^+$  indicates the presence of a lp(S)→p(B) interaction, whose deletion energy (2.54 kcal/mol) is similar to that of  $[47]^+$ , but much weaker than that of  $[37]^+$ . These analyses indicate that the lp(S) and p(B) orbitals of  $[48]^+$  are in a divergent orientation like those of  $[47]^+$ .

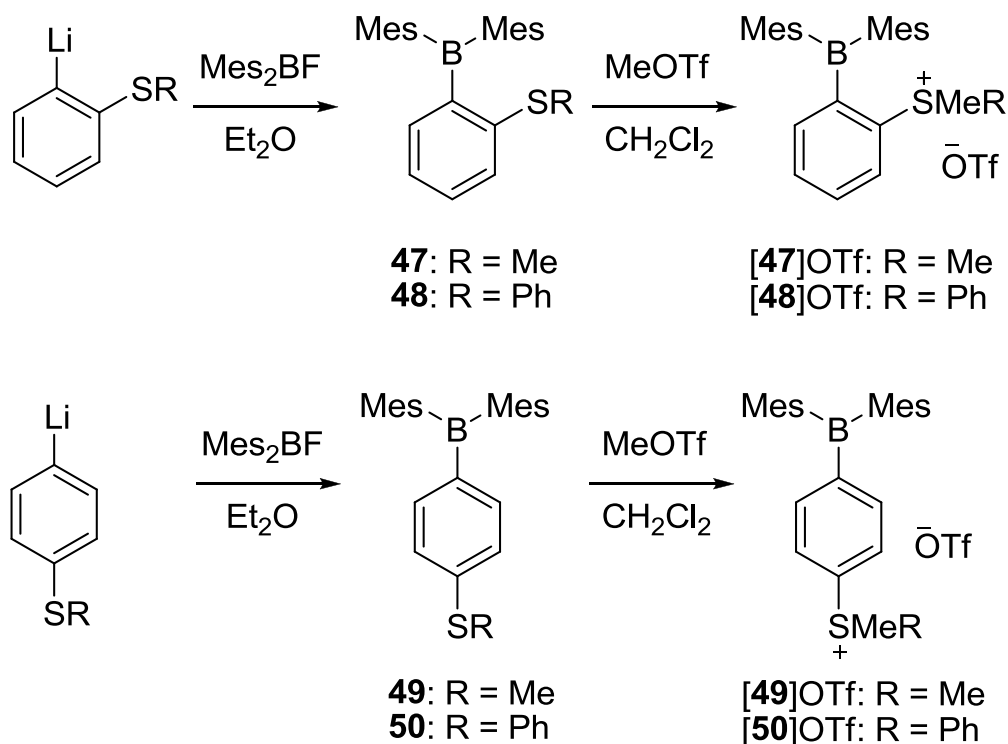


**Figure 86.** Synthesis of the sulfonium boranes  $[47]^+$ ,  $[48]^+$ ,  $[49]^+$  and  $[50]^+$ .

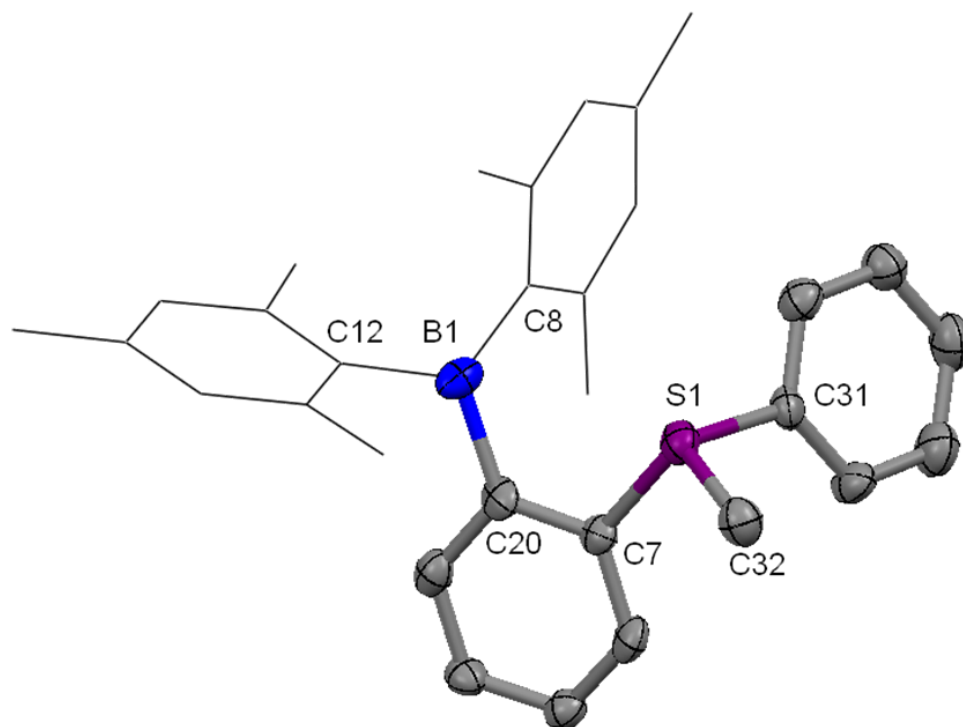


**Figure 87.** ORTEP drawing of of  $[48]^+$  (thermal ellipsoids drawn at 50%; for clarity purposes, the hydrogen atoms and triflate anion are omitted, and the mesityl ligands are represented by thin lines). Selected bond lengths (Å) and angles (°): S(1)-C(32) 1.783(5), S(1)-C(31) 1.784(5), S(1)-C(7) 1.787(5), C(8)-B(1) 1.555(8), C(12)-B(1) 1.576(8), C(20)-B(1) 1.595(7); C(32)-S(1)-C(31) 104.0(2), C(32)-S(1)-C(7) 103.8(2), C(31)-S(1)-C(7) 106.8(2), C(8)-B(1)-C(12) 122.8(5), C(8)-B(1)-C(20) 121.6(5), C(12)-B(1)-C(20) 115.3(5), C(23)-C(38)-C(39) 120.0(5).

**Table 35.** Crystal data, data collections, and structure refinement for [48]OTf.

Crystal data	[48]OTf
formula	C <sub>32</sub> H <sub>34</sub> BF <sub>3</sub> O <sub>3</sub> S <sub>2</sub>
$M_r$	598.52
crystal size (mm <sup>3</sup> )	0.15 x 0.11 x 0.08
crystal system	Triclinic
space group	P-1
$a$ (Å)	8.363(6)
$b$ (Å)	11.161(8)
$c$ (Å)	16.749(12)
$\alpha$ (°)	82.596(10)
$\beta$ (°)	78.412(10)
$\gamma$ (°)	79.602(10)
$V$ (Å <sup>3</sup> )	1499.2(19)
$Z$	2
$\rho_{\text{calc}}$ (g cm <sup>-3</sup> )	1.326
$\mu$ (mm <sup>-1</sup> )	0.228
$F(000)$	628
Data Collection	
$T$ (K)	110(2)
scan mode	$\omega$
	-9 → +9
$hkl$ range	-12 → +12
	-19 → +19
measd reflns	13194
unique reflns [ $R_{\text{int}}$ ]	4698 [0.1093]
reflns used for refinement	4698
Refinement	
refined parameters	370
GooF	0.991
$R_1, {}^a wR_2^b$ all data	0.1418, 0.1921
$\rho_{\text{fin}}$ (max/min) (e Å <sup>-3</sup> )	0.455, -0.448

$${}^a R_1 = \frac{\sum ||F_o| - |F_c||}{\sum |F_o|}, {}^b wR_2 = \left[ \frac{[\sum w(F_o^2 - F_c^2)^2]}{[\sum w(F_o^2)^2]} \right]^{1/2}.$$

### 7.3 Lewis acidity and pH stability range studies

In order to compare the Lewis acidity of these four sulfonium boranes and study their compatibility with aqueous environments, we investigated their behavior in aqueous solutions. Since hydroxide binding is expected to quench the absorption of low energy band in the UV-vis spectra of these boranes, we monitored the absorbance as a function of pH.<sup>5</sup> In all cases, the absorption of the low energy band is quenched as the pH of the solution increases. Acidification of the solution results in a revival of the absorbance, indicating that the hydroxide binding process is reversible. This simple equilibrium can be parameterized using eq. 1. In the case of  $[48]^+$  (H<sub>2</sub>O/MeOH, 95:5 vol.), a 9% decrease of the absorbance is observed at pH = 6.1. Further elevation of the pH induces the formation of a precipitate, thus preventing completion of the titration. A similar behavior is observed with  $[47]^+$ , which undergoes a 9% quenching at pH 6.9, followed by precipitation at more basic pH. These results indicate that  $[48]^+$  is more Lewis acidic than  $[47]^+$ . Extrapolation of the limited data obtained suggest the following equilibrium constants:  $pK_{R^+} = 7.89(\pm 0.05)$  for  $[47]^+$ , and  $pK_{R^+} = 7.02(\pm 0.05)$  for  $[48]^+$  (Figure 88). We note in passing that these  $pK_{R^+}$  values are mathematically equal to the pH value at which 50% of the borane is neutralized by hydroxide. The same experiments were performed for  $[49]^+$  and  $[50]^+$  under similar conditions (H<sub>2</sub>O/MeOH, 95:5 vol.). Fitting of the titration data to the equilibrium described in eq 1 afforded  $pK_{R^+} = 8.84(\pm 0.05)$  for  $[49]^+$ , and  $pK_{R^+} = 8.54(\pm 0.05)$  for  $[50]^+$ , suggesting that  $[50]^+$  is slightly more Lewis acidic than  $[49]^+$ . In turn, comparison of the  $pK_{R^+}$  values obtained for the *ortho*-phenylene derivatives  $[47]^+$ ,  $[48]^+$  and *para*-phenylene derivatives  $[49]^+$ ,

[50]<sup>+</sup> further support the conclusion that the Lewis acidity of the compounds is increased when the cationic moiety and the boron atom are placed in close proximity. Another conclusion from these studies is the fact that the anion affinity appears to increase with the hydrophobic character of the molecule. This is reflected by the lowering p*K*<sub>R+</sub> values on moving from the dimethylsulfonium derivatives to the methylphenylsulfonium derivatives.<sup>62</sup> More interestingly, the decrease of p*K*<sub>R+</sub> value from [47]<sup>+</sup> to [48]<sup>+</sup> (ca. 0.8) is more significant than that from [49]<sup>+</sup> to [50]<sup>+</sup> (ca. 0.3). In turn, these results suggest that hydrophobic effect is more acute when the hydrophobic substituent is placed closed to the boron center. To further assess the validity of this conclusion, we decided to investigate the fluoride anion binding properties of these compounds.

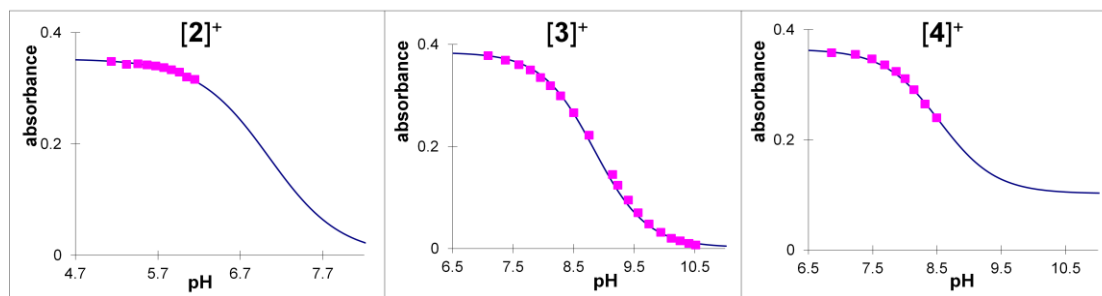
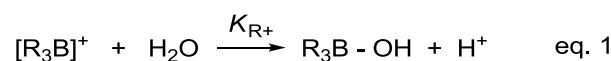


**Figure 88.** Spectrophotometric acid-base titration curve of [48]<sup>+</sup>, or [49]<sup>+</sup> and [50]<sup>+</sup> in H<sub>2</sub>O/MeOH (95:5 vol.). The titrations of [48]<sup>+</sup> and [50]<sup>+</sup> could not be finished due to the precipitation of 48-OH and 50-OH. (The acid-base titration data of [47]<sup>+</sup> was published previously by the Gabbai group.<sup>61</sup>)

#### 7.4 Fluoride ion complexation in methanol

Since anion binding to the boron center of these sulfonium boranes should result in a quenching of the low energy absorption band observed in their UV-vis spectra, we monitored the fluoride binding process by UV-vis spectroscopy. Addition of fluoride ions to MeOH solution of these boranes leads to the progressive quenching of the low energy absorption band, indicating fluoride coordination to the boron center. Fitting of the resulting titration data afforded the following fluoride binding constants:  $K = 4.0(\pm 0.5) \times 10^4 \text{ M}^{-1}$  for  $[\mathbf{47}]^+$ ,  $K = 8.5(\pm 0.5) \times 10^4 \text{ M}^{-1}$  for  $[\mathbf{48}]^+$ ,  $K = 260(\pm 20) \text{ M}^{-1}$  for  $[\mathbf{49}]^+$ , and  $K = 420(\pm 40) \text{ M}^{-1}$  for  $[\mathbf{50}]^+$ . These results clearly show that: i) the fluoride affinity increases slightly with the hydrophobicity increase of the boranes in MeOH when comparing the binding constants of  $[\mathbf{47}]^+$  and  $[\mathbf{48}]^+$ , or  $[\mathbf{49}]^+$  and  $[\mathbf{50}]^+$ ; ii) such fluoride affinity enhancement when phenyl group replaces methyl group in the *ortho*-sulfonium boranes is similar to that of *para*-sulfonium boranes; iii) for the cationic moiety of similar hydrophobicity, the proximity of the sulfonium unit to the boron center leads to a notable increase. Last but not least, these four cationic boranes do not bind other common anions such as  $\text{Cl}^-$ ,  $\text{Br}^-$ ,  $\text{I}^-$ ,  $\text{NO}_3^-$ ,  $\text{H}_2\text{PO}_4^-$ , and  $\text{HSO}_4^-$ , suggesting that they are highly selective.



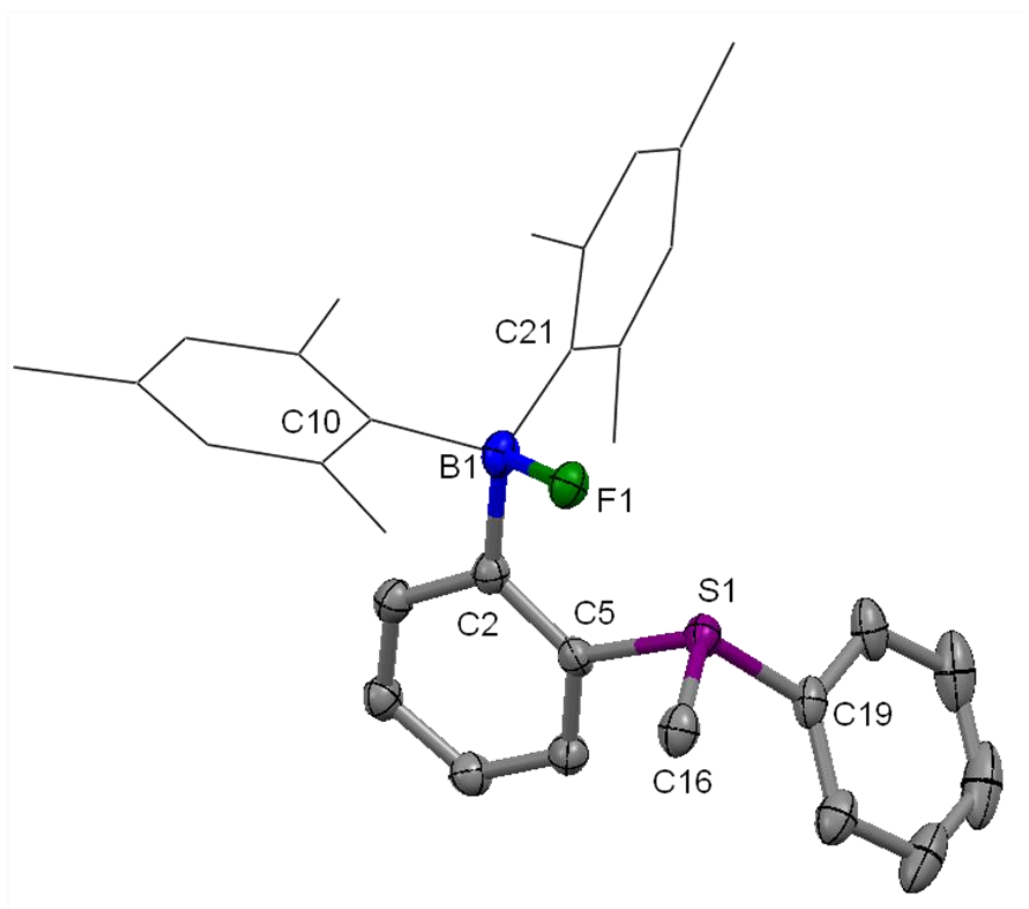


**Figure 89.** ORTEP drawing of **48-F**. (thermal ellipsoids drawn at 50%; for clarity purposes, the hydrogen atoms are omitted, and the mesityl ligands are represented by thin lines). Selected bond lengths (Å) and bond angles (°): S(1)-C(19) 1.762(3), S(1)-C(16) 1.791(3), S(1)-C(5) 1.793(2), F(1)-B(1) 1.477(3), C(2)-B(1) 1.642(4), C(10)-B(1) 1.641(4), C(21)-B(1) 1.649(4); C(19)-S(1)-C(16) 104.51(12), C(19)-S(1)-C(5) 104.48(11), C(16)-S(1)-C(5) 101.54(12), C(10)-B(1)-C(2) 106.9(2), C(10)-B(1)-C(21) 113.8(2), C(2)-B(1)-C(21) 116.9(2).

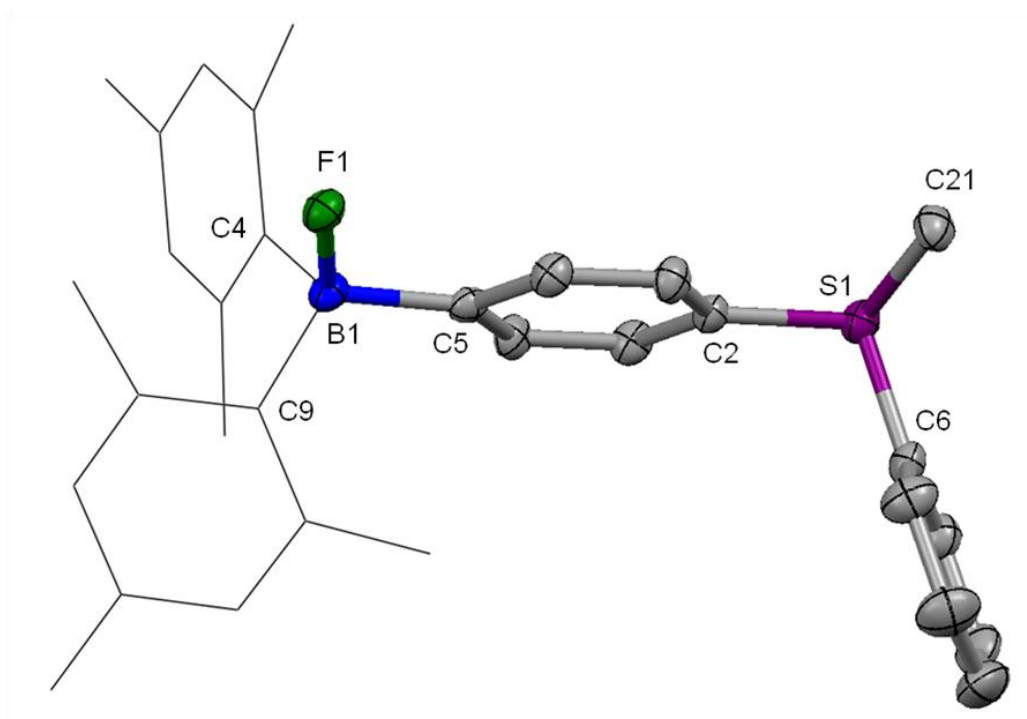


**Figure 90.** ORTEP drawing of **50-F**. (thermal ellipsoids drawn at 50%; for clarity purposes, the hydrogen atoms are omitted, and the mesityl ligands are represented by thin lines). Selected bond lengths (Å) and bond angles (°): S(1)-C(6) 1.777(3), S(1)-C(2) 1.777(2), S(1)-C(21) 1.791(2), F(1)-B(1) 1.466(3), C(4)-B(1) 1.661(4), C(5)-B(1) 1.640(4), C(9)-B(1) 1.667(4); C(6)-S(1)-C(2) 105.53(11), C(6)-S(1)-C(21) 103.09(12), C(2)-S(1)-C(21) 104.82(12), C(5)-B(1)-C(4) 107.2(2), C(5)-B(1)-C(9) 118.3(2), C(4)-B(1)-C(9) 113.2(2).

**Table 36.** Crystal data, data collections, and structure refinements of **48-F** and **50-F**

Crystal data	<b>48-F</b>	<b>50-F</b>
formula	C <sub>31</sub> H <sub>34</sub> BFS	C <sub>31</sub> H <sub>34</sub> BFS
$M_r$	468.45	468.45
crystal size (mm <sup>3</sup> )	0.15 x 0.11 x 0.08	0.12 x 0.11 x 0.06
crystal system	Orthorhombic	triclinic
space group	P2(1)/c	P-1
$a$ (Å)	8.464(5)	10.0180(10)
$b$ (Å)	12.829(8)	10.1978(10)
$c$ (Å)	22.897(14)	14.357(2)
$\alpha$ (°)	90	92.035(2)
$\beta$ (°)	90	90.491(2)
$\gamma$ (°)	90	118.5870(10)
$V$ (Å <sup>3</sup> )	2486(3)	1286.6(3)
$Z$	4	2
$\rho_{\text{calc}}$ (g cm <sup>-3</sup> )	1.252	1.209
$\mu$ (mm <sup>-1</sup> )	0.156	0.150
$F(000)$	1000	500
Data Collection		
$T$ (K)	110(2)	110(2)
scan mode	$\omega$	$\omega$
$hkl$ range	-10 $\rightarrow$ +11 -16 $\rightarrow$ +16 -30 $\rightarrow$ +30	-11 $\rightarrow$ +11 -12 $\rightarrow$ +12 -17 $\rightarrow$ +17
measd reflns	28371	12579
unique reflns [ $R_{\text{int}}$ ]	6035 [0.0934]	4515 [0.0478]
reflns used for refinement	6035	4515
Refinement		
refined parameters	307	307
GooF	1.000	1.008
R1, <sup>a</sup> wR2 <sup>b</sup> all data	0.1055, 0.1300	0.0762, 0.1104
$\rho_{\text{fin}}$ (max/min) (e Å <sup>-3</sup> )	0.366 and -0.492	0.496 and -0.507

<sup>a</sup> R1 =  $\sum ||F_o| - |F_c|| / \sum |F_o|$ . <sup>b</sup> wR2 =  $[[\sum w(F_o^2 - F_c^2)^2] / [\sum w(F_o^2)^2]]^{1/2}$ .

Attempts to isolate the fluoride adducts were also undertaken. Addition of excess KF to a concentrated MeOH solution of  $[47]^+$ ,  $[48]^+$ ,  $[49]^+$  and  $[50]^+$  led to the precipitation of the corresponding fluoride complexes **47-F**, **48-F**, **49-F**, and **50-F**, respectively. These compounds have been characterized by multinuclear NMR spectroscopy. The  $^{11}\text{B}$  NMR resonances at  $\delta = 6.0$  ppm for **47-F**,  $\delta = 6.8$  ppm for **48-F**,  $\delta = 6.6$  ppm for **49-F** and  $\delta = 7.0$  ppm for **50-F** confirm the presence of a four-coordinate boron center. The  $^{19}\text{F}$  NMR resonances ( $\delta = -153.3$  ppm for **47-F**,  $\delta = -156.5$  ppm for **48-F**,  $\delta = -178.7$  ppm for **49-F** and  $\delta = -178.8$  ppm for **50-F**) are also close to those observed in compounds featuring triarylfluoroborate moieties. The crystal structures of **47-F**, **48-F** and **50-F** have been determined by single crystal X-ray diffraction (Figure 89 and Figure 90, Table 36; **47-F** was synthesized and characterized by Youngmin Kim, a former student in the Gabbai group). In all cases, the B-F bond length (B-F = 1.494 Å for **47-F**, B-F = 1.477 Å for **48-F** and B-F = 1.465 Å for **50-F**) is comparable to those found in triarylfluoroborate moiety and the boron center adopts a pyramidal geometry as indicated by the sum of the  $\text{C}_{\text{aryl}}\text{-B-C}_{\text{aryl}}$  angles ( $\Sigma_{(\text{C-B-C})} = 340.3^\circ$  for **47-F**,  $\Sigma_{(\text{C-B-C})} = 337.6^\circ$  for **48-F** and  $\Sigma_{(\text{C-B-C})} = 338.7^\circ$  for **50-F**). In the case of **47-F** and **48-F**, the separation between sulfur and fluoride (2.665 Å in **47-F** and 2.639 Å in **48-F**) is well within the sum of van der Waals radii of the two elements and the F-S- $\text{C}_{\text{ph}}$  angle ( $170.82^\circ$  for **47-F** and  $163.93^\circ$  for **48-F**) is close to linearity. These characteristics indicate the presence of a B-F $\rightarrow$ S donor-acceptor interaction involving a fluorine lone pair (lp) and the  $\sigma^*$  orbital of S-C bond. To investigate the strength of the lp(F) $\rightarrow\sigma^*(\text{S-C})$  interaction, the geometries of **47-F** and **48-F** were optimized using DFT methods (functional: B3LYP;

mixed basis set: B: 6-31+g(d<sup>3</sup>); S: 6-31+g(d); C, H: 6-31g). NBO analysis, carried out on the optimized structure, confirms the presence of the  $\text{lp}(\text{F}) \rightarrow \sigma^*(\text{S}-\text{C})$  interaction. Deletion calculations show that this interaction contributes to the stability of the molecule by 5.35 kcal/mol for **47-F** and 4.51 kcal/mol for **48-F**, which are close to the interaction identified by *o*-Mes<sub>2</sub>BF-ph-PMePh<sub>2</sub>.<sup>49</sup> This donor-acceptor interaction accounts for the higher anion affinity of the *ortho*-phenylene linked isomers [**47**]<sup>+</sup> and [**48**]<sup>+</sup> when compared to the *para*-phenylene linked isomers [**49**]<sup>+</sup> and [**50**]<sup>+</sup>.

### 7.5 Fluoride ion complexation in water

Having established the pH stability range of these cationic boranes as well as their ability to bind fluoride in organic solvents, their anion binding behavior was investigated in aqueous media (H<sub>2</sub>O/MeOH, 95:5 vol.). Careful titrations of [**49**]<sup>+</sup> and [**50**]<sup>+</sup> with fluoride ions monitored by UV-vis spectroscopy under dilute conditions (0.052 mM for [**49**]<sup>+</sup> and 0.042 mM for [**50**]<sup>+</sup>) afforded  $K = 8.5(\pm 0.5) \text{ M}^{-1}$  for [**49**]<sup>+</sup> and  $K = 33(\pm 1) \text{ M}^{-1}$  for [**50**]<sup>+</sup> (Figure 91). The highest fluoride anion affinity of [**50**]<sup>+</sup> maybe correlated to its increased hydrophobicity, as speculated in the case of the phosphonium analogs of these compounds.<sup>62</sup> Considering the poor solubility of the fluoride adducts **47-F** and **48-F** in aqueous environments, we carried out fluorescence quenching titrations of [**47**]<sup>+</sup> and [**48**]<sup>+</sup> monitored by fluorescence spectroscopy under more dilute conditions (see Experimental section for details). Fitting the data to a 1:1 binding isotherm using eq. 2 afforded  $K = 60(\pm 5) \text{ M}^{-1}$  for [**47**]<sup>+</sup> and  $K = 1670(\pm 50) \text{ M}^{-1}$  for [**48**]<sup>+</sup> (Figure 91).

The fluoride affinity of the latter cation **[48]**<sup>+</sup> is almost 30 times higher than that of **[47]**<sup>+</sup>, again reinforcing the major role played by hydrophobic effects especially when the hydrophobic group is positioned near the anion binding site. The advantages of the *ortho*-positioned sulfonium moiety in **[48]**<sup>+</sup> include: i) The cationic charge provides a Coulombic and inductive drive for the formation of the fluoride adduct and increases the solubility of the receptor in water as well; ii) The hydrophobic group in close proximity to the boron center results in a significant Lewis acidity increase probably by facilitating the covalent ion pairing process between the borane and fluoride ion; iii) The *ortho*-positioned S-C moiety engages the fluoride anion in a stabilizing  $\text{lp}(\text{F}) \rightarrow \sigma^*(\text{S}-\text{C})$  interaction in **48-F**. In turn, **[48]**<sup>+</sup> is the best receptor for fluoride ions among these four cationic boranes.

$$(\text{I}_0 - \text{I})/\text{I}_0 = [\text{F}^-]/(1/K + [\text{F}^-]) \quad \text{eq 2}$$

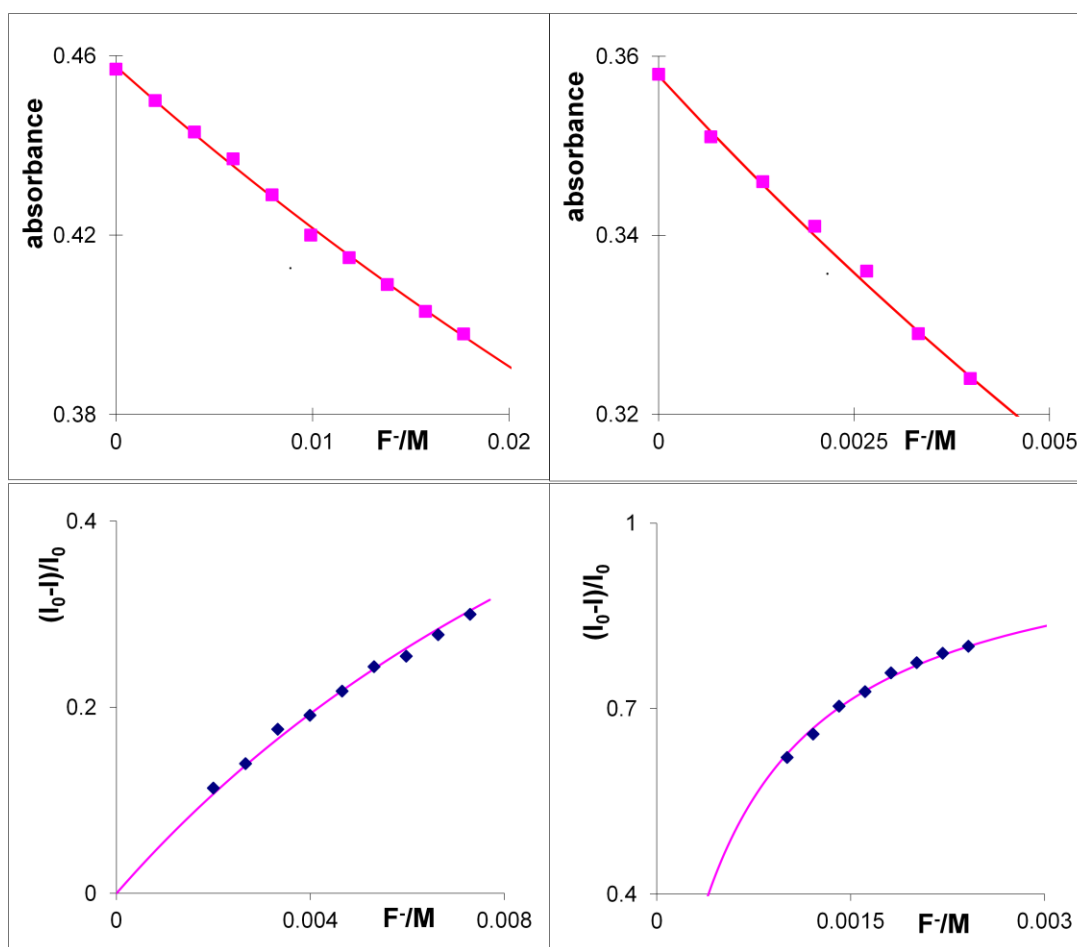


**Figure 91.** Top: Experimental data and calculated 1:1 binding isotherm with  $K = 8.5(\pm 0.5) \text{ M}^{-1}$  for  $[\mathbf{49}]^+$  (left) and  $K = 33(\pm 1) \text{ M}^{-1}$  for  $[\mathbf{50}]^+$  (right) monitored by UV-vis spectroscopy. Bottom: Fluorescence quenching titration data and calculated 1:1 binding isotherm with  $K = 60(\pm 5) \text{ M}^{-1}$  for  $[\mathbf{47}]^+$  (left) and  $K = 1670(\pm 50) \text{ M}^{-1}$  for  $[\mathbf{48}]^+$  (right).

### 7.6 Lewis acidity and fluoride affinity in the presence of CTABr

Since the cation  $[\mathbf{48}]^+$  is the strongest Lewis acid among the four boranes, we decided to investigate its fluoride affinity in water in the presence of CTABr which is expected to increase the solubility and fluoride affinity of the receptors in water.<sup>179</sup> We

first set out to determine the  $pK_{R+}$  of  $[48]^+$  by monitoring the absorbance as a function of pH. The hydroxide binding process is still reversible in  $H_2O/MeOH$  (95:5 vol.) with different concentrations of CTABr. The acid-base titrations of the compound  $[48]^+$  afforded  $pK_{R+} = 6.07(\pm 0.05)$  with 0.95 mM CTABr,  $pK_{R+} = 5.57(\pm 0.05)$  with 9.5 mM CTABr and  $pK_{R+} = 5.90$  with 47.5mM CTABr. In turn, the acidity of  $[48]^+$  is the highest in the presence of 9.5 mM CTABr. Next, we decided to study the anion binding properties of  $[48]^+$  in a  $H_2O/MeOH$  (95:5 vol.) solution containing CTABr (9.5 mM). The changes observed in the UV-vis spectrum of  $[48]^+$  upon addition of fluoride ions (Figure 92) could be fitted to a 1:1 binding isotherm affording a binding constant of  $2.65(\pm 0.2) \times 10^4 M^{-1}$ . As shown in Figure 92, 0.76 and 1.52 ppm of fluoride ions cause 32% and 56% quenching of the absorbance in the UV-vis spectra, respectively. In addition, this detection process is rapid and only takes one minute. These results demonstrate that  $[48]^+$  is capable of detecting fluoride ions in the ppm range, which is relevant to drinking water analysis.



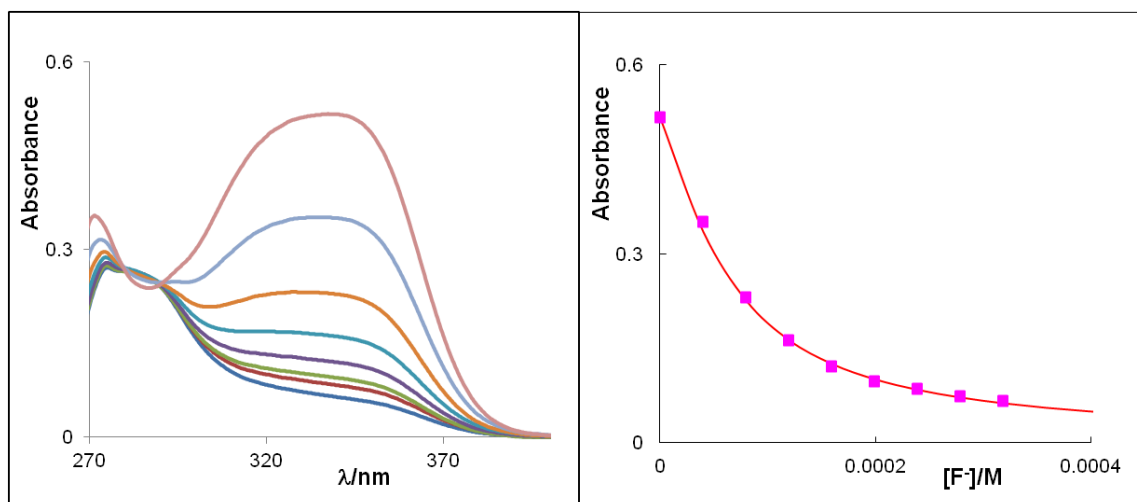


**Figure 92.** Left: Absorbance change of a solution of  $[48]^+$  after successive additions of fluoride anions in  $H_2O/MeOH$  (95:5, vol.; 9.5 mM pyridine buffer, pH = 4.6). Right: Experimental data and calculated 1:1 binding isotherm with  $K = 2.65(\pm 0.2) \times 10^4 M^{-1}$  for  $[48]^+$  using  $\epsilon([48]^+) = 9200 M^{-1} cm^{-1}$ ,  $\epsilon(48-F) = 0 M^{-1} cm^{-1}$ .

To test the anion binding selectivity of  $[48]^+$ , its absorption spectrum has been monitored upon the addition of various anions including  $Cl^-$ ,  $Br^-$ ,  $I^-$ ,  $NO_3^-$ ,  $H_2PO_4^-$ , and  $HSO_4^-$ . The absorbance of  $[48]^+$  shows no or negligible quenching after the addition of 5 equivalents of these anions, suggesting that  $[48]^+$  has no or little affinity for these anions. Next, we tested the reversibility of the fluoride binding process of  $[48]^+$ . Addition of an aqueous solution of  $Al^{3+}$  to a solution containing **48-F** led to a revival of the absorbance of  $[48]^+$  showing that fluoride binding is reversible.

## 7.7 Conclusion

In summary, the results presented in this chapter show that sulfonium boranes are

water stable and react reversibly with hydroxide and fluoride ions in aqueous environments. More interestingly, we also demonstrate that the incorporation of hydrophobic groups in close proximity to the boron center actually results in a more significant Lewis acidity increase. The presence of CTABr further enhances the Lewis acidity of the cationic boranes. In turn, the integration of Coulombic, chelate and hydrophobic effects makes **[48]**<sup>+</sup> sufficiently fluorophilic to sense fluoride at ppm level in water.

## 7.8 Experimental section

**General Considerations.** Methyl triflate and potassium fluoride were purchased from Aldrich, diphenyl disulfide from TCI, *n*-butyllithium from Alfa Aesar. dimesitylboron fluoride and 1-dimesitylboryl-4-methylthio-benzene were prepared by following the published steps.<sup>180-181</sup> Solvents were dried by passing through an alumina column (hexanes, dichloromethane) or refluxing under N<sub>2</sub> over Na/K (diethyl ether, THF). UV-vis spectra were recorded on an Ocean Optics USB4000 spectrometer with an Ocean Optics ISS light source. Elemental analyses were performed by Atlantic Microlab (Norcross, GA). The pH measurements were carried out with a Radiometer PHM290 pH meter equipped with a VWR SympHony electrode. Fluorescence measurements were carried out using a PTI, QuantaMaster spectrofluorometer. NMR spectra were recorded on Varian Unity Inova 400 FT NMR (399.59 MHz for <sup>1</sup>H, 375.99 MHz for <sup>19</sup>F, 128.19 MHz for <sup>11</sup>B, 100.45 MHz for <sup>13</sup>C) spectrometers at ambient temperature. Chemical shifts are given in ppm, and are referenced against external

$\text{BF}_3 \cdot \text{Et}_2\text{O}$  ( $^{11}\text{B}$ ,  $^{19}\text{F}$ ). The crystallographic measurements were performed using a Bruker APEX-II CCD area detector diffractometer (Mo- $\text{K}_\alpha$  radiation,  $\lambda = 0.71069 \text{ \AA}$ ) for **47-F**, **[48]OTf**, **48-F** and **50-F**. In each case, a specimen of suitable size and quality was selected and mounted onto a nylon loop. The structures were solved by direct methods, which successfully located most of the non-hydrogen atoms. Subsequent refinement on  $\text{F}^2$  using the SHELXTL/PC package (version 5.1) allowed location of the remaining non-hydrogen atoms.

**Synthesis of 47-F.** **[47]OTf** (0.08 g, 0.15 mmol) was dissolved in MeOH (5 mL) and treated with excess amount of KF which resulted in the formation of a white solid. After 30 min, the solid was isolated by filtration, washed with MeOH, and dried in *vacuo* to afford **47-F** as a white solid (65% yield).  $^1\text{H}$  NMR (400 MHz,  $\text{CDCl}_3$ )  $\delta$  1.90 (s, 12H), 2.23 (s, 6H), 2.75 (s, 6H), 6.66 (s, 4H), 7.30-7.36 (m, 3H), 7.39-7.41 (m, 1H).  $^{13}\text{C}$  NMR (100 MHz,  $\text{CDCl}_3$ )  $\delta$  21.03, 24.90, 29.24, 123.31, 127.14, 128.85, 128.94, 131.97, 133.41, 137.39 (d,  $J_{\text{C-F}} = 6.1 \text{ Hz}$ ), 141.87, 151.24 (bs), 168.85 (bs).  $^{11}\text{B}$  NMR (128 MHz,  $\text{CDCl}_3$ )  $\delta$  +6.02 (bs).  $^{19}\text{F}$  NMR (376 MHz,  $\text{CDCl}_3$ )  $\delta$  -153.32 (s). Anal. Calcd for  $\text{C}_{26}\text{H}_{32}\text{BFS}$  (**2-F**): C, 76.84; H, 7.94. Found: C, 75.47; H, 7.75.

**Synthesis of [48]OTf.** 1,2-dibromobenzene (3.9 g, 16.6 mmol) was allowed to react with *n*BuLi (6.8 ml, 2.8 M in hexane) in THF/ $\text{Et}_2\text{O}$  solution at  $-110 \text{ }^\circ\text{C}$  for 1 h. Freshly made PhSI in THF (from mixing equimolar PhSSPh and  $\text{I}_2$ ) was added and the reaction was kept at ambient temperature overnight. The reaction was quenched with water (40 mL) and extracted with dichloromethane. The organic layer was separated, dried over  $\text{MgSO}_4$ , filtered, and concentrated in *vacuo* to afford a colorless oil (**2-**

Bromophenyl)(phenyl) sulfane.  $^1\text{H}$  NMR. (400 MHz,  $\text{CDCl}_3$ )  $\delta$  7.02 (d, 1H, ph-CH), 7.12 (t, 1H, ph-CH), 7.24 (t, 1H, ph-CH), 7.48-7.52 (m, 3H, SPh-CH), 7.54-7.58 (m, 2H, SPh-CH), 7.66 (d, 1H, ph-CH).

(2-Bromophenyl)(phenyl) sulfane (2 g, 7.54 mmol) was allowed to react with *n*BuLi (3.0 mL, 8.4 mmol, 2.8M in hexanes) in diethyl ether (60 mL) at  $-0^\circ\text{C}$ . After stirring the reaction mixture for 3 h, dimesitylboryl fluoride (2.0 g, 7.46 mmol) was added to the resulting solution. The reaction mixture was warmed to ambient temperature and stirred overnight. The reaction was quenched with water (40 mL) and extracted with dichloromethane. The organic layer was separated, dried over  $\text{MgSO}_4$ , filtered, and concentrated in vacuo to afford a yellow solid. This solid was washed with hexanes (10 mL) to afford 1-dimesitylboryl-2-phenylthio-benzene as a pale solid (1.8 g, 55% yield).  $^1\text{H}$  NMR (400 MHz,  $\text{CDCl}_3$ )  $\delta$  2.04 (s, 12H, Mes-CH<sub>3</sub>), 2.28 (s, 6H, Mes-CH<sub>3</sub>), 6.76 (s, 4H, Mes-CH), 7.07-7.13 (m, 2H, Ph-CH), 7.19-7.24 (m, 7H, Ph-CH).  $^{11}\text{B}$  NMR (128 MHz,  $\text{CDCl}_3$ )  $\delta$  81 (bs)

Without additional purification, 1-dimesitylboryl-2-phenylthio-benzene (1.0 g, 2.30 mmol) was allowed to react with methyl triflate (0.5 g, 3.05 mmol) in dichloromethane (20 ml). The resulting mixture was heated to reflux, stirred overnight and then cooled to ambient temperature. The solvent was removed in vacuo to afford a foamy solid. The solid was washed by diethyl ether to yield a white solid (1.2 g, 87% yield).  $^1\text{H}$  NMR (400 MHz,  $\text{CDCl}_3$ )  $\delta$  2.11 (bs, 9H, Mes-CH<sub>3</sub>), 2.28 (s, 3H, Mes-CH<sub>3</sub>), 2.32 (s, 6H, Mes-CH<sub>3</sub>), 3.36 (bs, 3H, S-CH<sub>3</sub>), 6.87 (s, 4H, Mes-CH), 7.49 (d, 2H,  $J_{\text{H-H}} = 7.6$  Hz, Ph-CH), 7.60-7.73 (m, 5H, SPh-CH), 7.82-7.96 (m, 2H, Ph-CH).  $^{13}\text{C}$  NMR (100

MHz, CDCl<sub>3</sub>) 21.32, 22.04, 27.88, 30.77, 120.15, 131.42, 134.14, 134.45, 135.65, 141.03, 141.64. <sup>11</sup>B NMR (128 MHz, CD<sub>3</sub>OD) 81.3 (bs). Anal. Calcd for C<sub>32</sub>H<sub>34</sub>BF<sub>3</sub>O<sub>3</sub>S<sub>2</sub>: C, 64.21, H, 5.73. Found: C, 63.90, H, 5.68.

**Synthesis of 48-F.** [48]OTf (0.050 g, 0.084 mmol) was dissolved in an excess KF methanol solution leading to the formation of a white precipitate. After 15 min., this precipitate was isolated by filtration, dried under vacuum to afford **48-F** (0.035 g, 89% yield). Single crystals of **48-F** were obtained by slow evaporation of a dichloromethane solution. <sup>1</sup>H NMR (400 MHz, CDCl<sub>3</sub>) δ 1.95 (s, 6H, Mes-CH<sub>3</sub>), 2.00 (s, 6H, Mes-CH<sub>3</sub>), 2.24 (s, 3H, Mes-CH<sub>3</sub>), 2.26 (s, 3H, Mes-CH<sub>3</sub>), 3.19 (s, 3H, S-CH<sub>3</sub>), 6.71 (s, 2H, Mes-CH), 6.72 (s, 2H, Mes-CH), 6.96 (d, 1H, *J*<sub>H-H</sub> = 8.0 Hz, Ph-CH), 7.13 (t, 1H, *J*<sub>H-H</sub> = 8.0 Hz, Ph-CH), 7.22 (t, 1H, *J*<sub>H-H</sub> = 7.6 Hz, Ph-CH), 7.38 (d, 1H, *J*<sub>H-H</sub> = 7.6 Hz, Ph-CH), 7.50 (d, 2H, *J*<sub>H-H</sub> = 8.0 Hz, SPh-CH), 7.56-7.66 (m, 3H, SPh-CH). <sup>13</sup>C NMR (100 MHz, CDCl<sub>3</sub>) δ 20.91, 20.93, 24.73, 24.78, 24.91, 24.95, 28.74 (d, 1C, *J*<sub>H-C</sub> = 6.1 Hz, S-CH<sub>3</sub>), 126.23, 127.00, 128.66, 129.12, 130.55, 130.97, 132.64, 133.24, 133.39, 137.31, 137.37, 142.04, 142.37. <sup>11</sup>B NMR (128 MHz, CDCl<sub>3</sub>) δ +7.0 (s). <sup>19</sup>F NMR (375.9 MHz, CDCl<sub>3</sub>) δ -156.5 (s). Anal. Calcd for C<sub>31</sub>H<sub>34</sub>BFS: C, 79.48, H, 7.32. Found: C, 79.27, H, 7.40.

**Synthesis of [49]OTf.** 1-dimesitylboryl-4-methylthio-benzene (0.20 g, 0.54 mmol) was allowed to react with methyl triflate (0.10 g, 0.61 mmol) in dichloromethane (5 ml). The resulting mixture was heated to reflux, stirred overnight and then cooled to ambient temperature. The solvent was removed in vacuo to afford a foamy solid. The solid was washed by diethyl ether to yield a white solid (0.18 g, 62% yield). <sup>1</sup>H NMR (400 MHz, CDCl<sub>3</sub>) δ 1.95 (s, 12H, Mes-CH<sub>3</sub>), 2.31 (s, 6H, Mes-CH<sub>3</sub>), 3.41 (s, 6H, S-

CH<sub>3</sub>), 6.83 (s, 4H, Mes-CH), 7.73 (d, 2H,  $J_{\text{H-H}} = 8.4$  Hz, Ph-CH), 7.89(d, 2H,  $J_{\text{H-H}} = 8.0$  Hz, Ph-CH). <sup>13</sup>C NMR (100 MHz, CDCl<sub>3</sub>) δ 21.26, 23.50, 29.30 (s, 2C, S-CH<sub>3</sub>), 121.17, 128.59, 128.74, 137.68, 140.04, 140.76. <sup>11</sup>B NMR (128 MHz, CD<sub>3</sub>OD) δ 82 (bs). The purity of this compound was established by NMR spectroscopy (Figure 93).

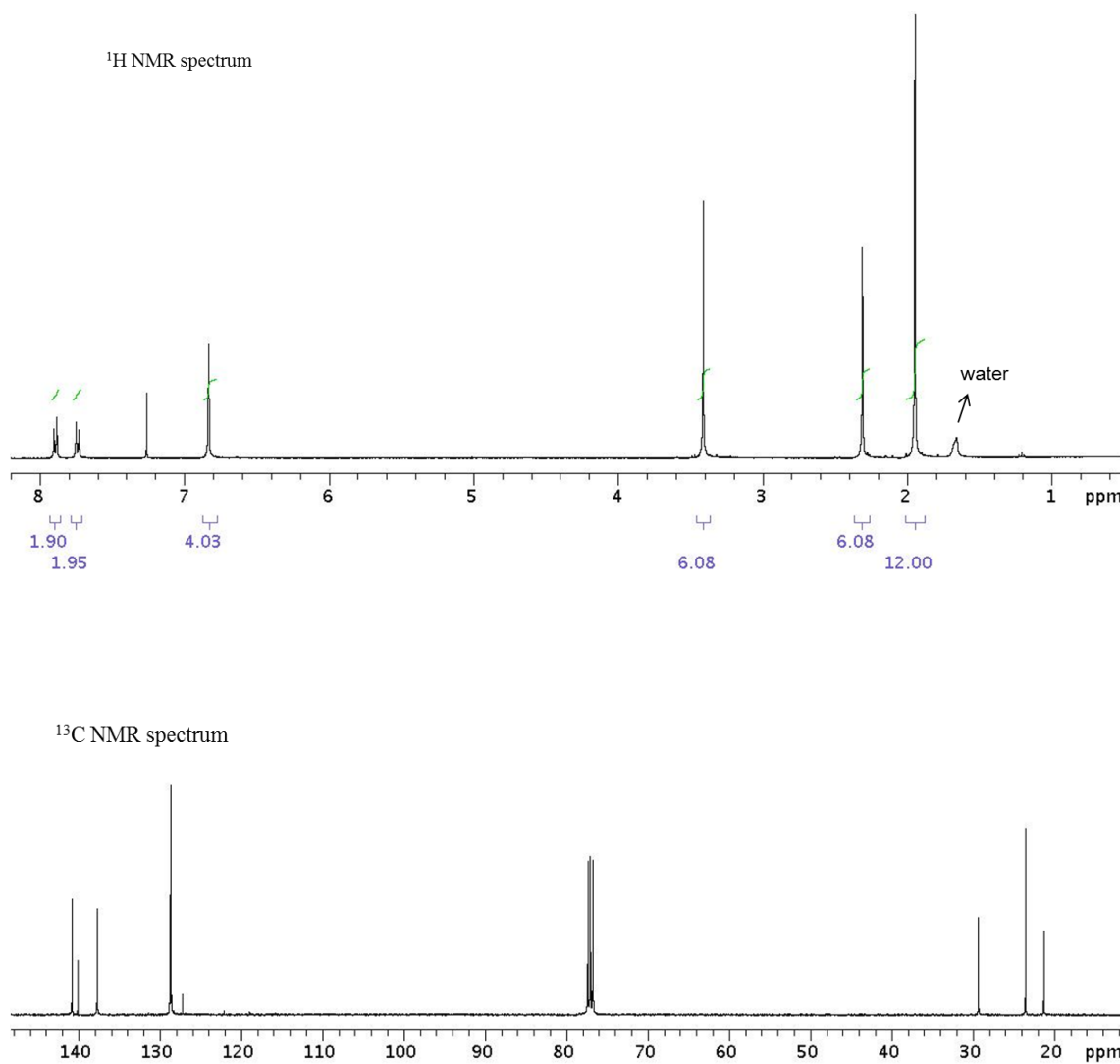


**Figure 93.** <sup>1</sup>H NMR and <sup>13</sup>C NMR spectra of [49]OTf.

**Synthesis of 49-F.** [49]OTf (0.050 g, 0.093 mmol) was dissolved in an excess KF methanol solution leading to the formation of a white precipitate. After 15 min., this precipitate was isolated by filtration, dried under vacuum to afford **49-F** (0.030 g, 79% yield).  $^1\text{H}$  NMR (400 MHz, DMSO- $d_6$ )  $\delta$  1.78 (s, 12H, Mes-CH<sub>3</sub>), 2.06 (s, 6H, Mes-CH<sub>3</sub>), 3.14 (s, 6H, S-CH<sub>3</sub>), 6.38 (s, 4H, Mes-CH), 7.14 (bs, 1H, Ph-CH), 7.51 (bs, 1H, Ph-CH), 7.62 (bs, 1H, Ph-CH), 7.90 (bs, 1H, Ph-CH).  $^{13}\text{C}$  NMR (100 MHz, DMSO- $d_6$ )  $\delta$  20.96, 25.37, 25.41, 29.00, 119.16, 126.78, 128.51, 131.30, 140.90.  $^{11}\text{B}$  NMR (128 MHz, DMSO- $d_6$ )  $\delta$  +6.6 (bs).  $^{19}\text{F}$  NMR (375.9 MHz, DMSO- $d_6$ )  $\delta$  -178.7 (s). The purity of this compound was established by NMR spectroscopy ( Figure 94).

**Synthesis of [50]OTf.** 1-dimesitylboryl-4-phenylthio-benzene (0.50 g, 1.15 mmol) was allowed to react with methyl triflate (0.23 g, 1.38 mmol) in dichloromethane (20 ml). The resulting mixture was heated to reflux, stirred overnight and then cooled to ambient temperature. The solvent was removed in *vacuo* to afford a foamy solid. The solid was washed by diethyl ether to yield a white solid (0.54 g, 78% yield).  $^1\text{H}$  NMR (400 MHz, CDCl<sub>3</sub>)  $\delta$  1.93 (s, 12H, Mes-CH<sub>3</sub>), 2.29 (s, 6H, Mes-CH<sub>3</sub>), 3.73 (s, 3H, S-CH<sub>3</sub>), 6.81 (s, 4H, Mes-CH), 7.63-7.74 (m, 5H, SPh-CH), 7.77 (d, 2H,  $J_{\text{H-H}} = 8.8$  Hz, Ph-CH), 7.90 (d, 2H,  $J_{\text{H-H}} = 8.0$  Hz, Ph-CH).  $^{13}\text{C}$  NMR (100 MHz, CDCl<sub>3</sub>)  $\delta$  21.24, 23.48, 28.89, 125.44, 128.19, 128.56, 128.74, 130.13, 130.17, 131.48, 134.56, 137.65, 139.97, 140.74.  $^{11}\text{B}$  NMR (128 MHz, CD<sub>3</sub>OD)  $\delta$  78 (bs). The purity of this compound was established by NMR spectroscopy (Figure 95).

**Synthesis of 50-F.** [50]OTf (0.050 g, 0.115 mmol) was dissolved in an excess KF methanol solution leading to the formation of a white precipitate. After 15 min., this

precipitate was isolated by filtration, dried under vacuum to afford **3-F** (0.046 g, 85% yield).  $^1\text{H}$  NMR (400 MHz,  $\text{DMSO-}d_6$ )  $\delta$  1.74 (s, 12H, Mes-CH<sub>3</sub>), 2.04 (s, 6H, Mes-CH<sub>3</sub>), 3.67 (s, 3H, S-CH<sub>3</sub>), 6.37 (s, 4H, Mes-CH), 7.15 (bs, 1H, Ph-CH), 7.53 (bs, 1H, Ph-CH), 7.63-7.71 (m, 5H, SPh-CH), 7.88 (d, 2H,  $J_{\text{H-H}} = 7.2$  Hz, Ph-CH).  $^{13}\text{C}$  NMR (100 MHz,  $\text{DMSO-}d_6$ )  $\delta$  20.95, 25.30, 25.33, 27.20, 119.51, 127.31, 128.54, 129.59, 129.66, 131.09, 131.36, 133.71, 135.80, 140.89.  $^{11}\text{B}$  NMR (128 MHz,  $\text{DMSO-}d_6$ )  $\delta$  +7.0 (bs).  $^{19}\text{F}$  NMR (375.9 MHz,  $\text{DMSO-}d_6$ )  $\delta$  -178.8 (s). The purity of this compound was established by NMR spectroscopy (Figure 96).

**Computational details.** DFT calculations (full geometry optimization) were carried out with the Gaussian 03 program using the gradient-corrected Becke exchange functional (B3LYP) and the Lee-Yang-Parr correlation functional (Figure 97, Figure 98, Table 37, Table 38). Geometry optimization was carried out with the following mixed basis set: 6-31+g(d') for the boron, and fluorine atoms, 6-31+g(d) for the sulfur atom, 6-31g basis set was used for other remained carbon and hydrogen atoms. Frequency calculations, which were carried out on the optimized structure of the compound, confirmed the absence of any imaginary frequencies. DT-DFT calculation was carried out with the Gaussian 03 program using B3LYP functional with the same basis sets as DFT calculation



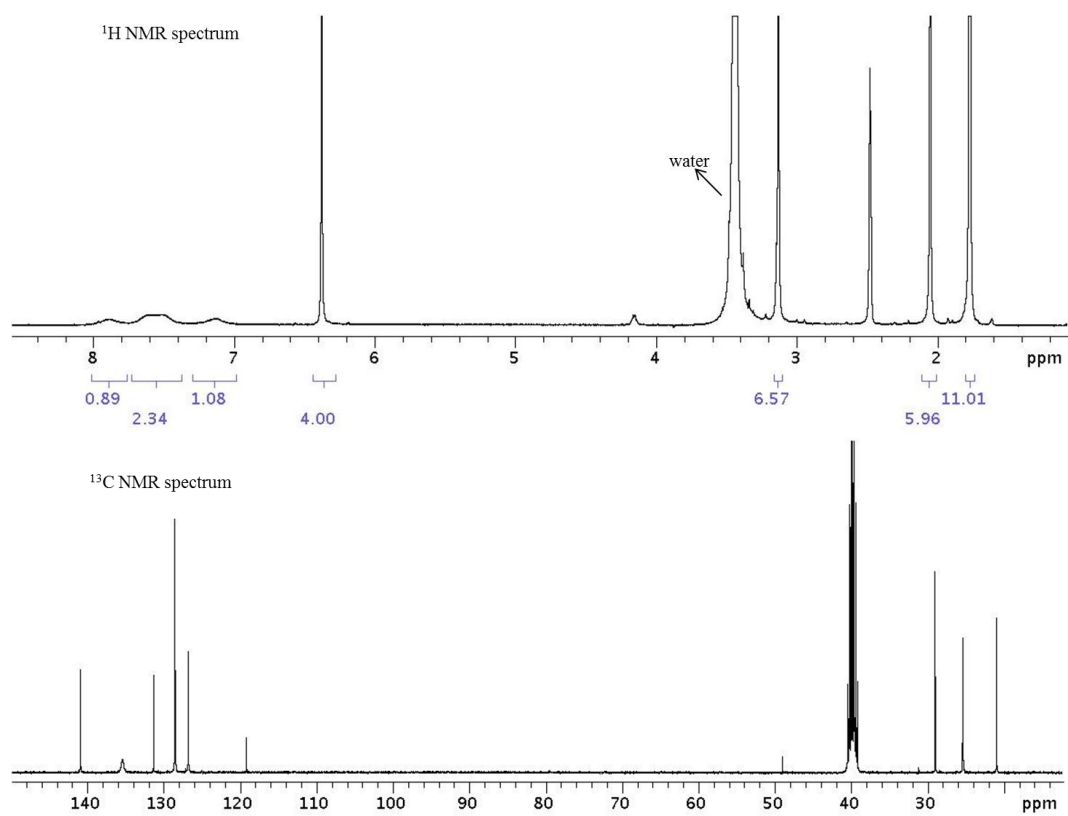


**Figure 94.** <sup>1</sup>H NMR and <sup>13</sup>C NMR spectra of **49-F**.

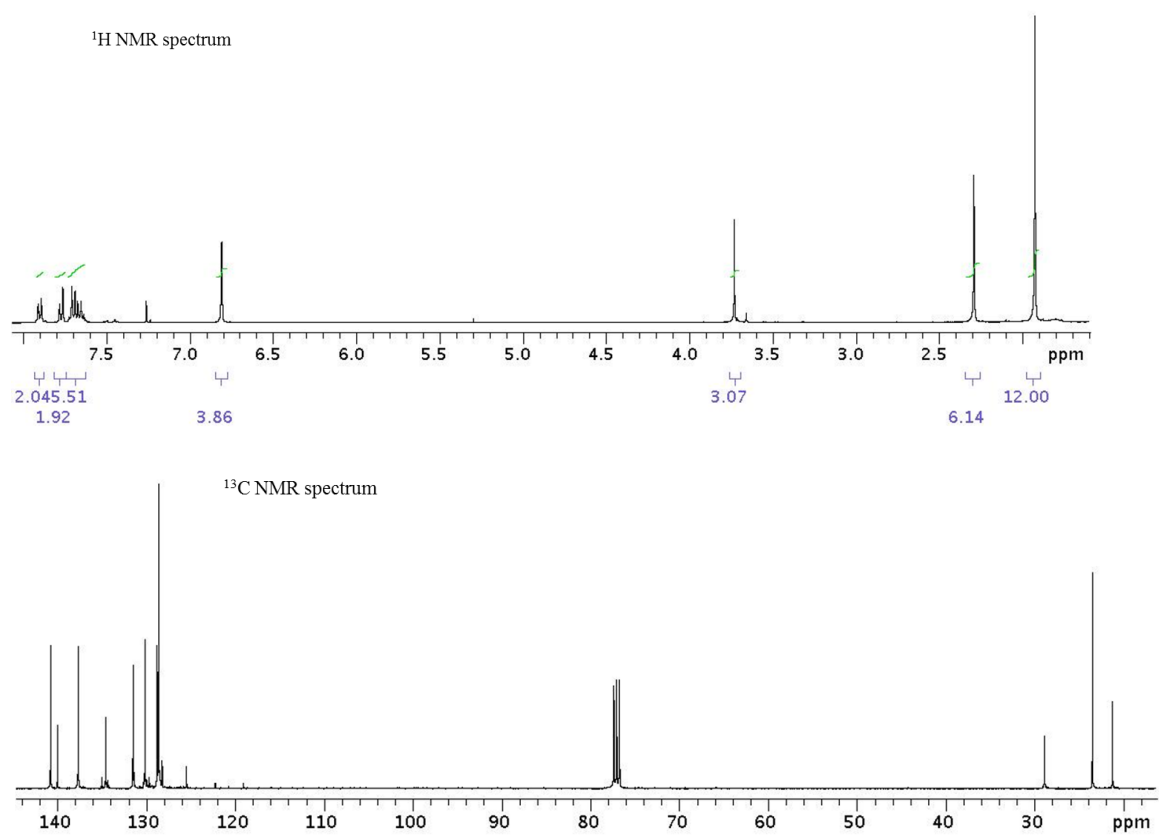


**Figure 95.** <sup>1</sup>H NMR and <sup>13</sup>C NMR spectra of [50]OTf.

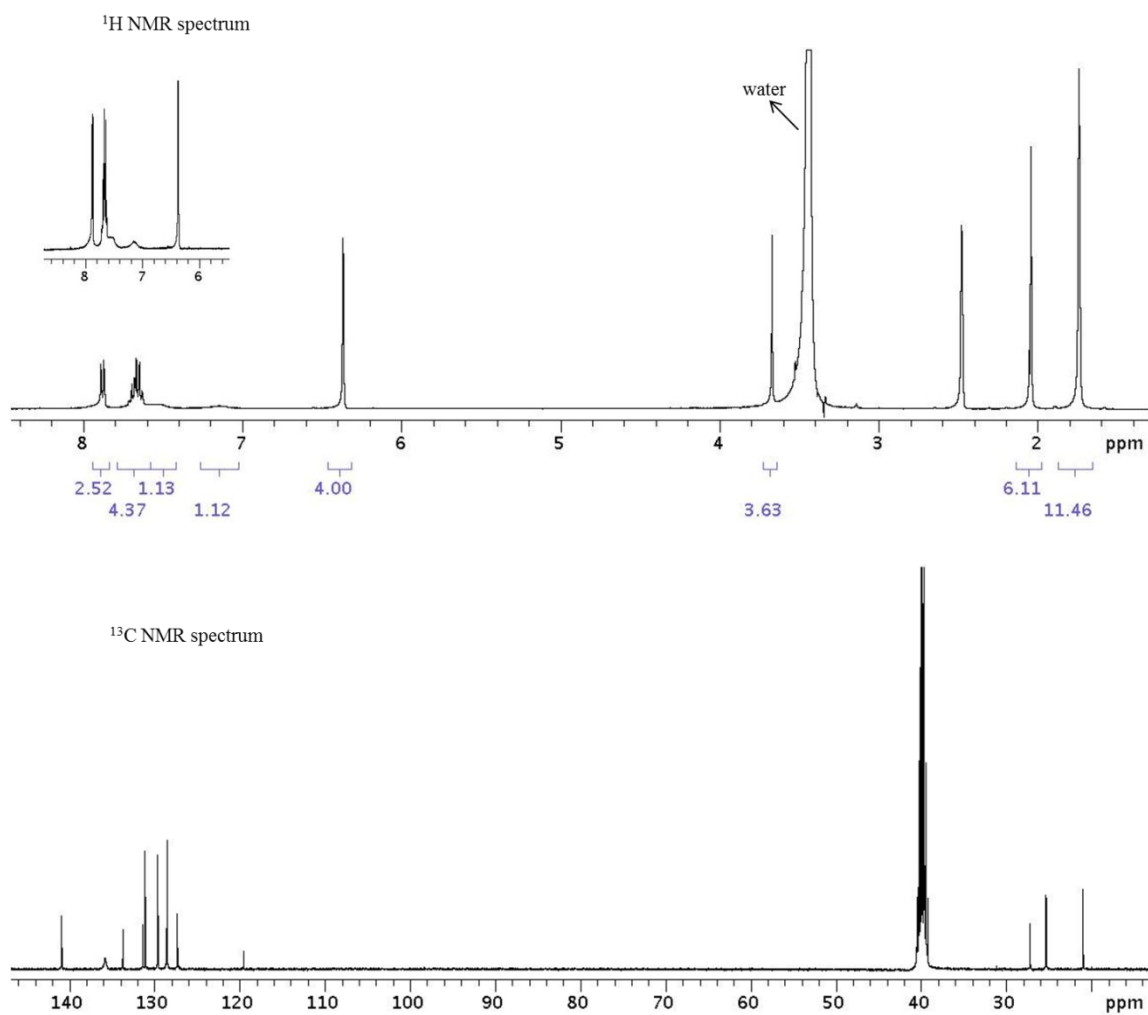


**Figure 96.** <sup>1</sup>H NMR and <sup>13</sup>C NMR spectra of **50-F**.

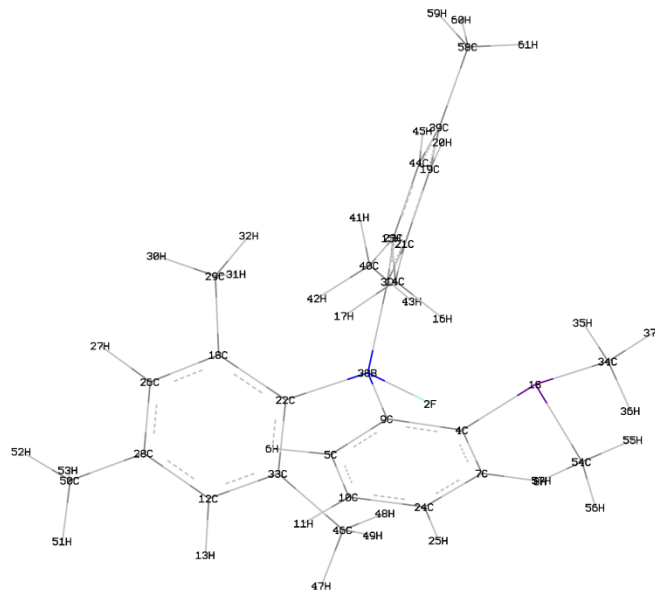


**Figure 97.** DFT optimized structure of **47-F**.

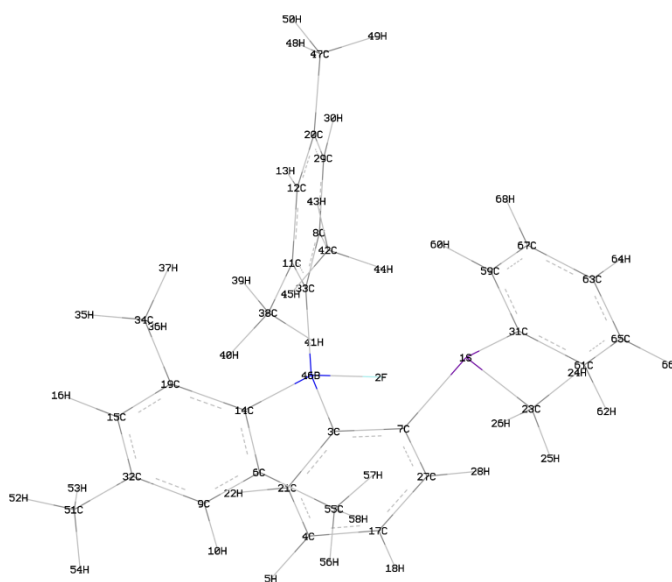


**Figure 98.** DFT optimized structure of **48-F**.

**Table 37.** Atom coordinates for the optimized structure of **47-F.**

Center Number	Coordinates(Angstroms)		
	X	Y	Z
S1	0.171623	-0.233476	0.249971
F2	-0.150780	0.266484	2.745903
C3	2.335051	0.128888	2.685448
C4	0.341943	1.573167	0.290507
C5	0.949598	3.530063	1.503047
H6	1.288812	4.004087	2.417975
C7	0.018264	2.336104	-0.844148
H8	-0.352372	1.880454	-1.756309
C9	0.810855	2.122722	1.502686
C10	0.649753	4.314333	0.387973
H11	0.772596	5.392172	0.436454
C12	-0.488659	3.342098	5.792578
H13	-1.481274	3.693159	6.068917
C14	1.262855	-1.320346	4.544908
H15	1.615898	-2.091262	5.239431
H16	0.307984	-1.652161	4.123648
H17	1.050528	-0.412825	5.116718
C18	2.044955	2.456843	5.035032
C19	3.261613	-2.081209	3.277538
H20	3.204559	-2.976493	3.894330
C21	2.302270	-1.074349	3.462819
C22	0.935754	2.079104	4.217694
C23	3.430832	0.267685	1.782532
C24	0.178687	3.721094	-0.792173
H25	-0.065336	4.327254	-1.658298
C26	1.859420	3.236727	6.191629
H27	2.731187	3.502259	6.786229
C28	0.600929	3.682737	6.599646
C29	3.482526	2.064180	4.734495
H30	4.162055	2.570596	5.428979
H31	3.788273	2.335327	3.720170
H32	3.645142	0.986622	4.832542
C33	-0.347453	2.566079	4.630522
C34	0.546551	-0.658153	-1.489286
H35	1.574674	-0.349528	-1.687997
H36	-0.132595	-0.188324	-2.202062
H37	0.477445	-1.745861	-1.572266
B38	1.067260	1.181888	2.841158
C39	4.296713	-1.963774	2.341295
C40	3.715575	1.532628	0.980042
H41	4.763650	1.540369	0.660158
H42	3.543371	2.442110	1.561219
H43	3.101946	1.621553	0.074850
C44	4.370854	-0.770027	1.620813
H45	5.195949	-0.624567	0.925551
C46	-1.631775	2.294757	3.860819
H47	-2.438892	2.932603	4.238947
H48	-1.946154	1.250961	3.959296
H49	-1.522007	2.491347	2.789878
C50	0.421556	4.491330	7.866048
H51	-0.379591	5.232216	7.759618
H52	1.341093	5.023755	8.133997
H53	0.156953	3.849904	8.718595
C54	-1.633716	-0.510275	0.267311
H55	-1.817833	-1.568312	0.063399
H56	-2.129594	0.122269	-0.471627
H57	-1.959592	-0.261129	1.277013
C58	5.305702	-3.074327	2.143186
H59	5.714496	-3.421481	3.100315
H60	6.144607	-2.743920	1.521144
H61	4.854959	-3.948450	1.652847

**Table 38.** Atom coordinates for the optimized structure of **48-F**.

Center Number	Coordinates(Angstroms)		
	X	Y	Z
S1	0.686010	-1.576134	1.382780
F2	0.260745	0.985769	1.489116
C3	-1.415755	-0.236688	0.209517
C4	-3.643036	-1.252464	-0.079413
H5	-4.668268	-1.158755	-0.425065
C6	-1.911389	2.976665	1.099632
C7	-1.038435	-1.460785	0.799480
C8	2.139212	1.447343	-0.649244
C9	-2.615787	4.189220	1.024549
H10	-3.155135	4.535493	1.904401
C11	0.933149	-0.186308	-1.981205
C12	2.127738	-0.464008	-2.677300
H13	2.099557	-1.175835	-3.501031
C14	-1.184488	2.471373	-0.028045
C15	-1.970521	4.464202	-1.253697
H16	-1.994961	5.030588	-2.182514
C17	-3.212628	-2.453033	0.503745
H18	-3.891434	-3.292959	0.608884
C19	-1.251300	3.254812	-1.220919
C20	3.334024	0.173586	-2.375153
C21	-2.762971	-0.177365	-0.217409
H22	-3.111386	0.749902	-0.660031
C23	0.520631	-1.447160	3.195257
H24	1.481115	-1.701050	3.649060
H25	-0.278135	-2.087906	3.570936
H26	0.281776	-0.397795	3.369630
C27	-1.895254	-2.562324	0.950973
H28	-1.549397	-3.492598	1.388830
C29	3.306378	1.146903	-1.369115
H30	4.215136	1.703091	-1.145787
C31	1.144627	-3.303032	1.121053
C32	-2.651664	4.960605	-0.140867
C33	0.912664	0.754455	-0.907844
C34	-0.570045	2.865494	-2.522865
H35	-0.871152	3.551485	-3.322481
H36	-0.826336	1.853012	-2.845746
H37	0.520868	2.902722	-2.444497
C38	-0.305320	-0.905277	-2.503065
H39	-0.128980	-1.251451	-3.527900
H40	-1.184223	-0.256835	-2.522275
H41	-0.579368	-1.785093	-1.907582
C42	2.246831	2.562299	0.378591
H43	3.109986	3.199798	0.155020
H44	2.367461	2.169302	1.393732
H45	1.350239	3.187443	0.392862
B46	-0.369543	1.043394	0.103479
C47	4.610856	-0.151112	-3.120227
H48	4.404335	-0.699092	-4.046245
H49	5.287632	-0.770818	-2.515025
H50	5.162862	0.758783	-3.384809
C51	-3.387917	6.281747	-0.188742
H52	-3.650378	6.555999	-1.216606
H53	-2.775801	7.098095	0.220119
H54	-4.313093	6.248320	0.398991
C55	-1.982521	2.258326	2.439222
H56	-2.767455	2.702207	3.062262
H57	-1.034730	2.328116	2.982625
H58	-2.204613	1.192985	2.326802
C59	1.782427	-3.558258	-0.105285
H60	1.955922	-2.748606	-0.809046
C61	0.939418	-4.333204	2.049830
H62	0.459629	-4.142757	3.002746
C63	1.988110	-5.894926	0.515287
H64	2.316115	-6.902208	0.281557
C65	1.366985	-5.629982	1.741140
H66	1.212497	-6.429041	2.458424
C67	2.194607	-4.860139	-0.405096
H68	2.684781	-5.060539	-1.351539

## CHAPTER VIII

## SUMMARY

## 8.1 Lewis acidity of a sulfonium borane and its application in fluorination chemistry

Since the sulfonium ions are inherently Lewis acidic due to its low lying  $\sigma^*$  orbitals, the incorporation of the sulfonium moiety into the borane system has been performed. The sulfonium borane  $[30]^+$  has been synthesized, and its anion binding properties have been investigated.  $[30]^+$  reacts with fluoride in MeOH to afford **30-F**. Furthermore, **30-F** also precipitates from MeOH/H<sub>2</sub>O solutions. The structural and computational analyses have indicated the presence of a B-F→S chelate motif. The boron-bound fluorine atom is separated from the sulfur atom by an average distance of 2.53 Å, which is well within the sum of van der Waals radii of the two elements (ca. 3.3 Å).<sup>58</sup> The average F-S-C<sub>Me</sub> angle of 171.7° indicates that the fluorine atom occupies an axial coordination site directly opposite to one of the sulfur-bound methyl groups. NBO analysis indicates that the short F-S separation present in **30-F** corresponds to two lp(F)→ $\sigma^*(S-C)$  donor-acceptor interactions which contribute 7.0 kcal/mol to the stability of the molecule. Altogether, these results suggest that the ability of  $[30]^+$  to complex F<sup>-</sup> in wet methanol arises from favorable Coulombic effects which are complemented by the formation of a B-F→S chelate motif.

Realizing that the absence of such interactions would greatly increase the liability of the boron-bound fluoride anion, we have discovered that the demethylation of the sulfonium moiety could be used to trigger the release of the fluoride anion. When

nucleophiles, such as TBAI, TBAN<sub>3</sub>, TBACN and TBASPh, are employed in dry CD<sub>3</sub>CN or THF, the demethylation of the sulfonium ion occurs and the new anionic fluoride adduct, namely **30-F**<sup>-</sup>, is formed. However, when TBACN is used as a nucleophile, the demethylation of the sulfonium moiety requires an elevated temperature while for other three nucleophiles, the demethylation can proceed at ambient temperature. When TBAI and TBAN<sub>3</sub> work as nucleophiles, MeF can be afforded, which could consume some **30-F**<sup>-</sup>. For these reasons, the phenylthiolate anion (p*K*<sub>a</sub> = 10.3, TBASPh) is employed as a good nucleophile, which can result in the process of demethylation at ambient temperature within 30 minutes and the formation of **30-F**<sup>-</sup>. Further studies clearly show that the fluoroborate **30-F**<sup>-</sup> can transfer its fluoride ions to a variety of substrates, including *p*-tolylsulfonyl chloride, benzoyl chloride, 1-chloro-2-cyano-3-nitrobenzene, benzyl chloride, and 1-bromooctane, through nucleophilic fluorination reactions in organic solvents. This process may be applicable for the preparation of <sup>18</sup>F-labeled compound in PET technology.

[**30**]<sup>+</sup> reacts with KCN in MeOH affording the zwitterionic cyanoborate, **30-CN**. The crystal structure of **30-CN** shows that the centroid of the C<sub>CN</sub>-N (C<sub>tCN</sub>) bond is separated from the sulfur atom by only 2.95 Å and forms a C<sub>tCN</sub>-S-C<sub>Me</sub> angle of 157.9°. NBO analysis reveals the presence of a π(C≡N)→σ\*(S—C) donor-acceptor interaction unexpectedly complemented by a back-bonding lp(S)→π\*(C≡N) component. The concomitant deletion of these two interactions leads to an increase of the total energy of the molecule by 4.1 kcal/mol, an energy comparable to that of a strong hydrogen bond.



## 8.2 Fluoride affinity of a telluronium borane

Realizing that the  $\sigma^*$  orbital energy decreases as the size of the group 15 or 16 elements increases, we are now investigating the Lewis acidic properties of heavier onium derivatives. In a first incarnation of this idea, we have synthesized the telluronium derivative  $[37]^+$  and compared its fluoride affinity with its sulfur analog  $[38]^+$ .<sup>59</sup>  $[37]^+$  and  $[38]^+$  can be synthesized by the methylation of the corresponding neutral boranes **37** and **38**, respectively. The structural and computational studies indicate a  $lp(\text{Ch}) \rightarrow p(\text{B})$  donor-acceptor interaction in both neutral boranes with a stabilizing energy of 32.4 kcal/mol in the case of **37** and 16.5 kcal/mol in the case of **38** by NBO deletion calculations. The oxidative methylation of the chalcogen element has lowered the donicity and thus has increased the Lewis acidity of the chalcogenium moiety indicated by the longer Ch-B distance and smaller NBO deletion energy ( $E_{\text{del}} = 10.8$  kcal/mol for  $[37]^+$  and  $E_{\text{del}} = 8.2$  kcal/mol for  $[38]^+$ ). The UV-vis spectra of both  $[37]^+$  and  $[38]^+$  in MeOH bear two distinct low-energy bands, involving electron excitations in which LUMO and LUMO+1 are main accepting orbitals. The LUMO carries an important contribution from the boron  $p$ -orbital and LUMO+1 bears an increased contribution from Ch-C  $\sigma^*$ -orbital which is especially noticeable in  $[37]^+$ . The localization of the LUMO and LUMO+1 orbitals on the boron and chalcogen moieties bodes well for the occurrence of anion chelation.

The fluoride titration in MeOH affords a binding constant of  $750 (\pm 100) \text{ M}^{-1}$  for  $[37]^+$ , while  $[38]^+$  shows no or very little fluoride affinity under dilute conditions in MeOH. The origin of the contrasting behavior displayed by  $[37]^+$  and  $[38]^+$  results from

the spectroscopic, structural and computational analyses of the fluoride adducts **37-F** and **38-F**. The  $^{11}\text{B}$  NMR signals of both fluoride adducts (10.9 ppm for **37-F** and 8.7 ppm for **38-F**) and the  $^{19}\text{F}$  NMR signal of **38-F** (-150.7 ppm) appear in the expected range for typical triarylfluoroborate anions. However, the  $^{19}\text{F}$  NMR signal of **37-F** at -130.4 ppm appears to move significantly downfield. Both  $^{19}\text{F}$  NMR and  $^{125}\text{Te}$  NMR spectra feature a Te-F coupling at 940 Hz, which is comparable to that observed in  $o\text{-(C}_6\text{H}_4\text{-CH}_2\text{NMe}_2)_2\text{TeF}_2$ . These spectroscopic features suggest that the boron bound fluorine atom in **37-F** also forms a strong bond with the tellurium atom. The crystal structure shows that Te-F distance in **37-F** is slightly shorter than S-F distance in **38-F**, despite the larger size of the tellurium atom, and the F-Te-C<sub>ph</sub> angle is close to linearity. The NBO analysis confirms a much stronger  $\text{lp}(\text{F})\rightarrow\sigma^*(\text{Ch-C})$  interaction in **37-F** ( $E_{\text{del}} = 22.8$  kcal/mol) than that in **38-F** ( $E_{\text{del}} = 9.2$  kcal/mol), and the AIM analysis shows that the electron density at the bond critical point of Ch-F bond in **37-F** ( $\rho(r) = 0.047$  e bohr<sup>-3</sup>) is obviously larger than that in **38-F** ( $\rho(r) = 0.035$  e bohr<sup>-3</sup>). Altogether, these analyses confirm the stronger Lewis acidity and thus higher fluoride affinity of [**37**]<sup>+</sup> than [**38**]<sup>+</sup>.

### 8.3 Anion affinity of a cationic diborane

The neutral diboranes have been used to chelate small anions by forming B-X-B bridging bonds. The fluoride binding constants of **51** exceed that of monofunctional analogues by at least 3 or 4 orders of magnitude. The favorable influence of the Coulombic effect in anion complexation has been demonstrated in the case of

triarylboranes decorated by peripheral cationic moieties such as the phosphonium borane  $[22]^+$  which, unlike neutral boranes, captures  $F^-$  in aqueous solution.<sup>62</sup>

Encouraged by these results, we have synthesized  $[40]OTf$  to investigate if the chelate effects and the Coulombic effects can be combined to boost anion affinity.  $[40]^+$  reacts with fluoride and azide ions to afford  $40-\mu_2-F$  and  $40-\mu_2-N_3$ , respectively, in organic solvents. The fluoride binding constant of  $[40]^+$  exceeds that of its neutral precursor by at least four orders of magnitude. The azide binding constant of  $[40]^+$  exceeds  $10^7 M^{-1}$ . The structural and computational analyses have shown that the B-F-B bridging bond in  $40-\mu_2-F$  is asymmetrical when compared to that of  $[52-\mu_2-F]^-$ . The B-N-B bridging bond in  $40-\mu_2-N_3$  is relatively symmetrical indicated by the N(1)-B(1) (1.635 Å) and N(1)-B(2) (1.706 Å) bond lengths.

The structure of  $40-\mu_2-F$  shows that the fluorine atom forms a short bond with B(1) (1.539(4) Å) and a long one with B(2) (1.822(4) Å), in contrast with the relatively symmetrical B-F-B bridge of  $[53-\mu_2-F]^-$  (B-F bond lengths = 1.585(5) Å and 1.633(5) Å).<sup>37</sup> AIM calculation identifies a bond path for both B(1)-F(1) and B(2)-F(2) linkages (Figure 72). The electron density  $\rho(r)$  of 0.100 e bohr<sup>-3</sup> at BCP of the B(1)-F(1) bond is significantly larger than that of the B(2)-F(1) bond (0.053 e bohr<sup>-3</sup>), in agreement with the observed asymmetry of the B-F-B bridge. By contrast, AIM calculations of  $[54-\mu_2-F]^-$  indicate a much more symmetrical B-F-B bridge, with similar electron density at the BCP of the B(1)-F(1) bond ( $\rho(r) = 0.074$  e bohr<sup>-3</sup>) and B(2)-F(1) bond ( $\rho(r) = 0.077$  e bohr<sup>-3</sup>).

These results clearly show that chelate effects and Coulombic effects are additive and can be combined to boost the anion affinity of bidentate Lewis acids.

#### 8.4 Lewis acidity behavior of $B(C_6Cl_5)_3$

Tris(pentafluorophenyl)borane,  $B(C_6F_5)_3$ , has been investigated extensively with successful applications in catalysis, synthesis and small molecule activation. However, the investigation of  $B(C_6Cl_5)_3$  is rare and new in this area.  $B(C_6Cl_5)_3$  can react with fluoride, azide and cyanide in dichloromethane with large binding constants,  $1.5 (\pm 0.2) \times 10^7 M^{-1}$  for fluoride,  $6.0 (\pm 0.6) \times 10^6 M^{-1}$  for azide, and  $1.8 (\pm 0.2) \times 10^6 M^{-1}$  for cyanide. Furthermore,  $B(C_6Cl_5)_3$  can react with neutral Lewis bases, such as DMAP and pyridine, with the binding constants of  $3.0 (\pm 0.3) \times 10^4 M^{-1}$  ( $CH_2Cl_2$ ),  $1.0 (\pm 0.1) \times 10^7 M^{-1}$  (THF) for DMAP and  $36 (\pm 4) M^{-1}$  (THF) for pyridine. The binding constants decrease in the order of fluoride, azide, cyanide and DMAP, in which the bulk steric is probably the main effect to control the affinity of  $B(C_6Cl_5)_3$  with different Lewis bases. The binding constant of pyridine is much smaller than that of DMAP due to the lower basicity of pyridine ( $pK_a(\text{pyridine}) = 5.2$  vs.  $pK_a(\text{DMAP}) = 9.2$ ).

The single crystals of  $[FB(C_6Cl_5)_3]^- [S(NMe_2)_3]^+$  and  $B(C_6Cl_5)_3$ -DMAP have been obtained from the diffusion of pentane into a THF solution of equimolar of  $B(C_6Cl_5)_3$  and TSAF, or  $B(C_6Cl_5)_3$  and DMAP. The crystal structure of  $[FB(C_6Cl_5)_3]^- [S(NMe_2)_3]^+$  shows that the B-F bond length is 1.43 Å, which is comparable with other reported triarylfluoroborate species, and the boron center becomes clearly pyramidalized as indicated by the sum of the  $C_{\text{aryl}}\text{-B-}C_{\text{aryl}}$  angles ( $\Sigma_{(C-B-C)} = 335.1^\circ$ ). As for  $B(C_6Cl_5)_3$ -

DMAP, the B-N bond (1.615 Å), is slightly shorter than those measured in other DMAP adducts of triarylboranes. Coordination of the DMAP molecule to the boron center leads to a distinct pyramidalization of the latter, as indicated by the sum of the  $C_{\text{aryl}}\text{-B-C}_{\text{aryl}}$  angles ( $\Sigma_{(C-B-C)} = 335.9^\circ$ ).

### 8.5 Hydrophobic effects in the fluoride complexation by cationic boranes

In order to speculate how the incorporation of hydrophobic functionality in close proximity to the boron center can affect the fluoride affinity of cationic boranes, a series of sulfonium borane have been synthesized. Direct methylation of the neutral thiophenyl boranes **47**, **48**, **49** and **50** can afford the corresponding sulfonium boranes  $[\mathbf{47}]^+$ ,  $[\mathbf{48}]^+$ ,  $[\mathbf{49}]^+$  and  $[\mathbf{50}]^+$ . These four sulfonium boranes feature a coordinatively unsaturated boron center confirmed by NMR spectroscopy, UV-vis spectroscopy and single crystal X-ray diffraction. The Lewis acidity of these boranes has been investigated in aqueous solutions (H<sub>2</sub>O/MeOH, 95:5 vol.) by monitoring the absorbance of the boranes as a function of pH, which affords  $pK_{R^+} = 7.89(\pm 0.05)$  for  $[\mathbf{47}]^+$ ,  $7.02(\pm 0.05)$  for  $[\mathbf{48}]^+$ ,  $8.84(\pm 0.05)$  for  $[\mathbf{49}]^+$ , and  $8.54(\pm 0.05)$  for  $[\mathbf{50}]^+$ . Comparison of these  $pK_{R^+}$  values reveals that the replacement of methyl with phenyl group in the *ortho* position of boron center (0.87) can increase the Lewis acidity more significantly than that in the *para* position of boron center (0.30).

The fluoride affinity of these four boranes has also been studied under same conditions. Fluoride titrations of  $[\mathbf{49}]^+$  and  $[\mathbf{50}]^+$  monitored by UV-vis spectroscopy under dilute conditions (0.052 mM for  $[\mathbf{49}]^+$  and 0.042 mM for  $[\mathbf{50}]^+$ ) afford  $K =$

8.5(±0.5) M<sup>-1</sup> for [49]<sup>+</sup> and 33(±1) M<sup>-1</sup> for [50]<sup>+</sup>. Due to the poor solubility of the fluoride adducts 47-F and 48-F in aqueous environment, the fluoride titrations of [47]<sup>+</sup> and [48]<sup>+</sup> are monitored by fluorescence spectroscopy under more diluted conditions, affording  $K = 60(\pm 5) \text{ M}^{-1}$  for [47]<sup>+</sup> and 1670(±50) M<sup>-1</sup> for [48]<sup>+</sup>. The fluoride affinity of [48]<sup>+</sup> is around 28 times higher than that of [47]<sup>+</sup>, while the fluoride affinity of [50]<sup>+</sup> is only about four times than that of [49]<sup>+</sup>. These results indicate that the replacement of the *ortho*-methyl moiety in [47]<sup>+</sup> with an *ortho*-phenyl moiety in [48]<sup>+</sup> results in a more significant increase of the fluoride affinity when compared to the replacement of a *para*-methyl with a *para*-phenyl moiety from [49]<sup>+</sup> to [50]<sup>+</sup>. However, these boranes in non-aqueous environments show different changes in the fluoride affinity. The titrations in MeOH afford the following binding constants:  $K = 4.0(\pm 0.5) \times 10^4 \text{ M}^{-1}$  for [47]<sup>+</sup>,  $8.5(\pm 0.5) \times 10^4 \text{ M}^{-1}$  for [48]<sup>+</sup>, 260(±20) M<sup>-1</sup> for [49]<sup>+</sup>, and 420(±40) M<sup>-1</sup> for [50]<sup>+</sup>. These data show that the fluoride affinity increases slightly from methyl to phenyl group in both *para* and *ortho* positions to boron center in MeOH. These different results in MeOH and H<sub>2</sub>O/MeOH (95:5 vol.) indicate that the increase in the hydrophobicity in close proximity to the boron center can result in a significant increase in Lewis acidity as well as fluoride affinity.

The presence of CTABr further enhances the Lewis acidity of the cationic boranes. The anion binding properties of the cation [48]<sup>+</sup> in a H<sub>2</sub>O/MeOH (95:5 vol.) solution of 9.5 mM CTABr are monitored by UV-vis spectroscopy, affording a binding constant of  $2.65(\pm 0.2) \times 10^4 \text{ M}^{-1}$ . 0.76 and 1.52 ppm of fluoride ions cause 32% and 56% quenching of the absorbance of [48]<sup>+</sup> in the UV-vis spectra, respectively. In addition,

this detection process is rapid and takes only one minute. These results demonstrate that [48]<sup>+</sup> is capable of detecting fluoride ions at the level of drinking water standard with a rapid response. In turn, the integration of Coulombic, chelating, and hydrophobic effects leads to [48]<sup>+</sup> fluorophilic sufficiently to sense fluoride at ppm level with a rapid response.

## REFERENCES

1. Holland, M. A.; Kozlowski, L. M., *Clin. Pharmacy* **1986**, *5*, 737.
2. Baud, F. J., *Hum. Exp. Toxicol.* **2007**, *26*, 191.
3. Aaseth, J.; Shimshi, M.; Gabrilove, J. L.; Birketvedt, G. S., *J. Trace Elem. Exp. Med.* **2004**, *17*, 83.
4. Carton, R. J., *Fluoride* **2006**, *39*, 163.
5. Yamaguchi, S.; Akiyama, S.; Tamao, K., *J. Am. Chem. Soc.* **2001**, *123*, 11372.
6. Piers, W. E.; Chivers, T., *Chem. Soc. Rev.* **1997**, *26*, 345.
7. Ishihara, K.; Yamamoto, H., *Eur. J. Org. Chem.* **1999**, 527.
8. Chen, E. Y.-X.; Marks, T. J., *Chem. Rev.* **2000**, *100*, 1391.
9. Erker, G., *Dalton Trans.* **2005**, 1883.
10. Piers, W. E., *Adv. Organomet. Chem.* **2005**, *52*, 1.
11. Stephan, D. W., *Dalton Trans.* **2009**, 3129.
12. Stephan, D. W., *Org. Biomol. Chem.* **2008**, *6*, 1535.
13. Cardoso, A. P.; Mirione, E.; Ernesto, M.; Massaza, F.; Cliff, J.; Haque, M. R.; Bradbury, J. H., *J. Food Compos. Anal.* **2005**, *18*, 451.
14. Nahrstedt, L. P.; Vennesland, B.; Conn, E. E.; Knowles, C. J.; Westley, J.; Wissing, F., *Cyanide in Biology*. 1981; p 145.
15. Yeoh, H. H., *Biotechnol. Tech.* **1993**, *7*, 761.
16. Huh, J. O.; Kim, H.; Lee, K. M.; Lee, Y. S.; Do, Y.; Lee, M. H., *Chem. Commun.* **2010**, *46*, 1138.
17. Kaim, W.; Schulz, A., *Angew. Chem. Int. Ed.* **1984**, *23*, 615.
18. Zhao, S.-B.; Wucher, P.; Hudson, Z. M.; McCormick, T. M.; Liu, X.-Y.; Wang, S.; Feng, X.-D.; Lu, Z.-H., *Organometallics* **2008**, *27*, 6446.



19. Biallas, M. J.; Shriver, D. F., *J. Am. Chem. Soc.* **1966**, *88*, 375.
20. Katz, H. E., *Inclusion Compd.* **1991**, *4*, 391.
21. Schmidtchen, F. P.; Berger, M., *Chem. Rev.* **1997**, *97*, 1609.
22. Gabbaï, F. P., *Angew. Chem., Int. Ed.* **2003**, *42*, 2218.
23. Melaïmi, M.; Gabbaï, F. P., *Adv. Organomet. Chem.* **2005**, *53*, 61.
24. Wang, H.; Sole, S.; Gabbaï, F. P., *ACS Symp. Ser.* **2006**, *917*, 208.
25. Hudnall, T. W.; Chiu, C.-W.; Gabbaï, F. P., *Acc. Chem. Res.* **2009**, *42*, 388.
26. Wade, C. R.; Broomsgrove, A. E. J.; Aldridge, S.; Gabbaï, F. P., *Chem. Rev.* **2010**, *110*, 3958.
27. Williams, V. C.; Piers, W. E.; Clegg, W.; Elsegood, M. R. J.; Collins, S.; Marder, T. B., *J. Am. Chem. Soc.* **1999**, *121*, 3244.
28. Piers, W. E.; Irvine, G. J.; Williams, V. C., *Eur. J. Inorg. Chem.* **2000**, 2131.
29. Lewis, S. P.; Taylor, N. J.; Piers, W. E.; Collins, S., *J. Am. Chem. Soc.* **2003**, *125*, 14686.
30. Zhao, H.; Gabbaï, F. P., *Org. Lett.* **2011**, 1444.
31. Jiang, C.; Blacque, O.; Berke, H., *Chem. Commun.* **2009**.
32. Zhao, X.; Stephan, D. W., *Chem. Commun.* **2011**, 47.
33. Shriver, D. F.; Biallas, M. J., *J. Am. Chem. Soc.* **1967**, *89*, 1078.
34. Katz, H. E., *Organometallics* **1987**, *6*, 1134.
35. Katz, H. E., *J. Org. Chem.* **1985**, *50*, 5027.
36. Katz, H. E., *J. Am. Chem. Soc.* **1985**, *107*, 1420.
37. Solé, S.; Gabbaï, F. P., *Chem. Commun.* **2004**, 1284.
38. Sun, Y.; Wang, S., *Inorg. Chem.* **2010**, *49*, 4394.
39. Dash, R. R.; Gaur, A.; Balomajumder, C., *J. Hazard. Mater.* **2009**, *163*, 1.

40. Dusemund, C.; Sandanayake, K. R. A. S.; Shinkai, S., *Chem. Commun.* **1995**, 333.
41. Wade, C. R.; Gabbai, F. P., *Inorg. Chem.* **2009**, *49*, 714.
42. Wade, C. R.; Gabbai, F. P., *Dalton Trans.* **2009**, 9169.
43. Zhao, Q.; Li, F.; Liu, S.; Yu, M.; Liu, Z.; Yi, T.; Huang, C., *Inorg. Chem.* **2008**, *47*, 9256.
44. Sun, Y.; Ross, N.; Zhao, S. B.; Huszarik, K.; Jia, W. L.; Wang, R. Y.; Macartney, D.; Wang, S., *J. Am. Chem. Soc.* **2007**, *129*, 7510.
45. Chiu, C.-W.; Gabbai, F. P., *J. Am. Chem. Soc.* **2006**, *128*, 14248.
46. Chiu, C.-W.; Gabbai, F. P., *Dalton Trans.* **2008**, 814.
47. Lee, M. H.; Agou, T.; Kobayashi, J.; Kawashima, T.; Gabbai, F. P., *Chem. Commun.* **2007**, 1133.
48. Hudnall, T. W.; Gabbai, F. P., *J. Am. Chem. Soc.* **2007**, *129*, 11978.
49. Hudnall, T. W.; Kim, Y.-M.; Bebbington, M. W. P.; Bourissou, D.; Gabbai, F. P., *J. Am. Chem. Soc.* **2008**, *130*, 10890.
50. Picard, C.; Cazaux, L.; Jaud, J., *J. Chem. Soc. Perk. Trans. 2* **1981**, 1554.
51. Akiba, K.-Y.; Takee, K.; Ohkata, K.; Iwasaki, F., *J. Am. Chem. Soc.* **1983**, *105*, 6965.
52. Iwasaki, F.; Akiba, K.-Y., *Acta Crystallographica Section B-Structural Science* **1985**, *41*, 445.
53. Akiba, K.-Y.; Takee, K.; Shimizu, Y.; Ohkata, K., *J. Am. Chem. Soc.* **1986**, *108*, 6320.
54. Kuti, M.; Rabai, J.; Kapovits, I.; Kucsman, A.; Parkanyi, L.; Argay, G.; Kalman, A., *J. Mol. Struct.* **1994**, *318*, 161.
55. Erhart, M.; Mews, R., *Z. Anorg. Allg. Chem.* **1992**, *615*, 117.
56. Hoefelmeyer, J. D.; Gabbai, F. P., *Organometallics* **2002**, *21*, 982.
57. Melaïmi, M.; Gabbai, F. P., *J. Am. Chem. Soc.* **2005**, *127*, 9680.

58. Batsanov, S. S., *Inorg. Mater.* **2001**, *37*, 871.
59. Zhao, H.; Gabbai, F. P., *Nat. Chem.* **2010**, *2*, 984.
60. Wade, C. R.; Zhao, H.; Gabbai, F. P., *Chem. Commun.* **2010**, *46*, 6380.
61. Kim, Y.; Zhao, H.; Gabbai, F. P., *Angew. Chem., Int. Ed.* **2009**, *48*, 4957.
62. Kim, Y.; Gabbai, F. P., *J. Am. Chem. Soc.* **2009**, *131*, 3363.
63. Filler, R.; Saha, R., *Future Med. Chem.* **2009**, *1*, 777.
64. Reid, D. G.; Murphy, P. S., *Drug Discovery Today* **2008**, *13*, 473.
65. Purser, S.; Moore, P. R.; Swallow, S.; Gouverneur, V., *Chem. Soc. Rev.* **2008**, *37*, 320.
66. Hagmann, W. K., *J. Med. Chem.* **2008**, *51*, 4359.
67. Mueller, K.; Faeh, C.; Diederich, F., *Science* **2007**, *317*, 1881.
68. Ting, R.; Harwig, C.; auf dem Keller, U.; McCormick, S.; Austin, P.; Overall, C. M.; Adam, M. J.; Ruth, T. J.; Perrin, D. M., *J. Am. Chem. Soc.* **2008**, *130*, 12045.
69. Dolle, F.; Roeda, D.; Kuhnast, B.; Lasne, M.-C., *Fluorine and Health* **2008**, *3*.
70. Cai, L.; Lu, S.; Pike, V. W., *Eur. J. Org. Chem.* **2008**, 2853.
71. Le Bars, D., *J. Fluorine Chem.* **2006**, *127*, 1488.
72. Cahard, D.; Xu, X.; Couve-Bonnaire, S.; Pannecoucke, X., *Chem. Soc. Rev.* **2010**, *39*, 558.
73. Brown, J. M.; Gouverneur, V., *Angew. Chem., Int. Ed.* **2009**, *48*, 8610.
74. Pacheco, M. C.; Purser, S.; Gouverneur, V., *Chem. Rev.* **2008**, *108*, 1943.
75. Lommerse, J. P. M.; Stone, A. J.; Taylor, R.; Allen, F. H., *J. Am. Chem. Soc.* **1996**, *118*, 3108.
76. Brunet, V. A.; O'Hagan, D., *Angew. Chem., Int. Ed.* **2008**, *47*, 1179.
77. Prakash, G. K. S.; Beier, P., *Angew. Chem., Int. Ed.* **2006**, *45*, 2172.

78. Pihko, P. M., *Angew. Chem., Int. Ed.* **2006**, *45*, 544.
79. Nyffeler, P. T.; Duron, S. G.; Burkart, M. D.; Vincent, S. P.; Wong, C.-H., *Angew. Chem., Int. Ed.* **2005**, *44*, 192.
80. Kiselyov, A. S., *Chem. Soc. Rev.* **2005**, *34*, 1031.
81. Jadhav, V. H.; Jang, S. H.; Jeong, H.-J.; Lim, S. T.; Sohn, M.-H.; Chi, D. Y.; Kim, D. W., *Org. Lett.* **2010**, *12*, 3740.
82. Kim, D. W.; Jeong, H.-J.; Lim, S. T.; Sohn, M.-H., *Angew. Chem., Int. Ed.* **2008**, *47*, 8404.
83. Kim, D. W.; Ahn, D. S.; Oh, Y. H.; Lee, S.; Kil, H. S.; Oh, S. J.; Lee, S. J.; Kim, J. S.; Ryu, J. S.; Moon, D. H.; Chi, D. Y., *J. Am. Chem. Soc.* **2006**, *128*, 16394.
84. Katcher, M. H.; Doyle, A. G., *J. Am. Chem. Soc.* **2010**, *132*, 17402.
85. Kalow, J. A.; Doyle, A. G., *J. Am. Chem. Soc.* **2010**, *132*, 3268.
86. Bejot, R.; Fowler, T.; Carroll, L.; Boldon, S.; Moore, J. E.; Declerck, J.; Gouverneur, V., *Angew. Chem., Int. Ed.* **2009**, *48*, 586.
87. Sun, H.; DiMagno, S. G., *Chem. Commun.* **2007**, 528.
88. Sun, H.; DiMagno, S. G., *Angew. Chem. Int. Ed.* **2006**, *45*, 2720.
89. Sun, H.; DiMagno, S. G., *J. Am. Chem. Soc.* **2005**, *127*, 2050.
90. Gingras, M.; Chabre, Y. M.; Raimundo, J. M., *Synthesis* **2006**, 182.
91. Schwesinger, R.; Link, R.; Wenzl, P.; Kossek, S., *Chem. Eur. J.* **2006**, *12*, 438.
92. Pilcher, A. S.; Ammon, H. L.; Deshong, P., *J. Am. Chem. Soc.* **1995**, *117*, 5166.
93. Wang, H.; Gabbai, F. P., *unpublished results*.
94. Cox, D. P.; Terpinski, J.; Lawrynowicz, W., *J. Org. Chem.* **1984**, *49*, 3216.
95. Clark, J. H.; Macquarrie, D. J., *Tetrahedron Lett.* **1987**, *28*, 111.
96. Smith, R. G., *J. Am. Chem. Soc.* **1929**, *51*, 1171.
97. Liotta, C. L.; Harris, H. P., *J. Am. Chem. Soc.* **1974**, *96*, 2250.

98. Lou, B.; Chen, Z. Q.; Bian, Z. Q.; Huang, C. H., *New J. Chem.* **2010**, *34*, 132.
99. Liu, Z. M.; Yasserli, A. A.; Lindsey, J. S.; Bocian, D. F., *Science* **2003**, *302*, 1543.
100. Leroy, J.; Hebert, E.; Wakselman, C., *J. Org. Chem.* **1979**, *44*, 3406.
101. Schmidbaur, H.; Mitschke, K.-H.; Buchner, W.; Stuhler, H.; Weidlein, J., *Chem. Ber.* **1973**, *106*, 1226.
102. Gao, L.; Peay, M. A.; Partyka, D. V.; Updegraff, J. B., III; Teets, T. S.; Esswein, A. J.; Zeller, M.; Hunter, A. D.; Gray, T. G., *Organometallics* **2009**, *28*, 5669.
103. Partyka, D. V.; Esswein, A. J.; Zeller, M.; Hunter, A. D.; Gray, T. G., *Organometallics* **2007**, *26*, 3279.
104. Arnendola, V.; Bonizzoni, M.; Esteban-Gomez, D.; Fabbrizzi, L.; Licchelli, M.; Sancenon, F.; Taglietti, A., *Coord. Chem. Rev.* **2006**, *250*, 1451.
105. Christe, K. O.; Wilson, W. W.; Wilson, R. D.; Bau, R.; Feng, J. A., *J. Am. Chem. Soc.* **1990**, *112*, 7619.
106. Daunert, S.; Bachas, L. G., *Anal. Chem.* **1989**, *61*, 499.
107. Zelder, F. H., *Inorg. Chem.* **2008**, *47*, 1264.
108. Christe, K. O.; Dixon, D. A.; Sanders, J. C. P.; Schrobilgen, G. J.; Wilson, W. W., *Inorg. Chem.* **1993**, *32*, 4089.
109. Shang, L.; Dong, S., *J. Anal. Chem.* **2009**, *81*, 1465.
110. Cho, D. G.; Kim, J. H.; Sessler, J. L., *J. Am. Chem. Soc.* **2008**, *130*, 12163.
111. Hassan, S. S. M.; Hamza, M. S. A.; Kelany, A. E., *Talanta* **2007**, *71*, 1088.
112. Touceda-Varela, A.; Stevenson, E. I.; Galve-Gasion, J. A.; Dryden, D. T. F.; Mareque-Rivas, J. C., *Chem. Commun.* **2008**, 1998.
113. Lou, X.; Zhang, L.; Qin, J.; Li, Z., *Chem. Commun.* **2008**, 5848.
114. Liu, S. J.; Zhao, Q.; Xu, W. J.; Huang, W., *Prog. Chem.* **2008**, *20*, 1708.
115. Carroll, R. L.; Gorman, C. B., *Angew. Chem.-Int. Edit.* **2002**, *41*, 4379.

116. M. J. Frisch; G. W. Trucks; H. B. Schlegel; G. E. Scuseria; M. A. Robb; J. R. Cheeseman; V. G. Zakrzewski; J. A. Montgomery; R. E. Stratman; J. C. Burant; S. Dapprich; J. M. Millam; A. D. Daniels; K. N. Kudin; M. C. Strain; O. Farkas; J. Tomasi; V. Barone; M. Cossi; R. Cammi; B. Mennucci; C. Pomelli; C. Adamo; S. Clifford; J. Ochterski; G. A. Petersson; P. Y. Ayala; Q. Cui; K. Morokuma; D. K. Malick; A. D. Rabuck; K. Raghavachari; J. B. Foresman; J. Cioslowski; J. V. Ortiz; A. G. Baboul; B. B. Stefanov; G. Liu; A. Liashenko; P. Piskorz; I. Komaromi; R. Gomperts; R. Martin; D. J. Fox; T. Keith; M. A. Al-Laham; C. Y. Peng; A. Nanayakkara; C. Gonzalez; M. Challacombe; P. M. W. Gill; B. Johnson; W. Chen; M. W. Wong; J. L. Andres; M. Head-Gordon; E. S. Replogle; J. A. Pople, Gaussian 03; C.02 ed. Pittsburgh PA: 2006.
117. Reed, A. E.; Curtiss, L. A.; Weinhold, F., *Chem. Rev.* **1988**, *88*, 899.
118. Wuest, J. D., *Acc. Chem. Res.* **1999**, *32*, 81.
119. Wedge, T. J.; Hawthorne, M. F., *Coord. Chem. Rev.* **2003**, *240*, 111.
120. Shur, V. B.; Tikhonova, I. A., *Russ. Chem. Bull.* **2003**, *52*, 2539.
121. Taylor, T. J.; Burrell, C. N.; Gabbaï, F. P., *Organometallics* **2007**, *26*, 5252.
122. Kilyanek, S. M.; Fang, X.; Jordan, R. F., *Organometallics* **2009**, *28*, 300.
123. Emslie, D. J. H.; Piers, W. E.; Parvez, M., *Angew. Chem. Int. Ed.* **2003**, *42*, 1252.
124. Uhl, W.; Hannemann, F., *J. Organomet. Chem.* **1999**, *579*, 18.
125. Tagne Kuate, A. C.; Reeske, G.; Schurmann, M.; Costisella, B.; Jurkschat, K., *Organometallics* **2008**, *27*, 5577.
126. Zobel, B.; Duthie, A.; Dakternieks, D.; Tiekink, E. R. T., *Organometallics* **2001**, *20*, 3347.
127. Tamao, K.; Hayashi, T.; Ito, Y.; Shiro, M., *Organometallics* **1992**, *11*, 2099.
128. Newcomb, M.; Horner, J. H.; Blanda, M. T.; Squattrito, P. J., *J. Am. Chem. Soc.* **1989**, *111*, 6294.
129. Kawachi, A.; Tani, A.; Shimada, J.; Yamamoto, Y., *J. Am. Chem. Soc.* **2008**, *130*, 4222.
130. Boshra, R.; Venkatasubbaiah, K.; Doshi, A.; Lalancette, R. A.; Kakalis, L.; Jäkle, F., *Inorg. Chem.* **2007**, *46*, 10174.

131. Lee, M. H.; Gabbaï, F. P., *Inorg. Chem.* **2007**, *46*, 8132.
132. Metrangolo, P.; Resnati, G., *Chem. Eur. J.* **2001**, *7*, 2511.
133. Sudha, N.; Singh, H. B., *Coord. Chem. Rev.* **1994**, *135*, 469.
134. Burling, F. T.; Goldstein, B. M., *J. Am. Chem. Soc.* **1992**, *114*, 2313.
135. Gleiter, R.; Werz, D. B.; Rausch, B. J., *Chem. Eur. J.* **2003**, *9*, 2676.
136. Bleiholder, C.; Werz, D. B.; Köppel, H.; Gleiter, R., *J. Am. Chem. Soc.* **2006**, *128*, 2666.
137. Tripathi Santosh, K.; Patel, U.; Roy, D.; Sunoj Raghavan, B.; Singh Harkesh, B.; Wolmershauser, G.; Butcher Ray, J., *J. Org. Chem.* **2005**, *70*, 9237.
138. Hayashi, S.; Nakanishi, W., *Bull. Chem. Soc. Jpn.* **2008**, *81*, 1605.
139. Chandrasekhar, V.; Thirumoorthi, R., *Inorg. Chem.* **2009**, *48*, 10330.
140. Klapötke, T. M.; Krumm, B.; Scherr, M., *Eur. J. Inorg. Chem.* **2008**, *2008*, 4413.
141. Naumann, D.; Tyrre, W.; Hermann, R.; Pantenburg, I.; Wickleder, M. S., *Z. Anorg. Allg. Chem.* **2002**, *628*, 833.
142. Sato, S.; Kondo, N.; Horn, E.; Furukawa, N., *Organometallics* **1998**, *17*, 1897.
143. Laali, K.; Chen, H. Y.; Gerzina, R. J., *J. Org. Chem.* **1987**, *52*, 4126.
144. Saito, S.; Zhang, J.; Tanida, K.; Takahashi, S.; Koizumi, T., *Tetrahedron* **1999**, *55*, 2545.
145. Burger, B. J.; Cotter, W. D.; Coughlin, E. B.; Chacon, S. T.; Hajela, S.; Herzog, T. A.; Kohn, R.; Mitchell, J.; Piers, W. E.; et al., *Ziegler Catal.* **1995**, 317.
146. Entwistle, C. D.; Marder, T. B., *Angew. Chem., Int. Ed.* **2002**, *41*, 2927.
147. Yamaguchi, S.; Wakamiya, A., *Pure Appl. Chem.* **2006**, *78*, 1413.
148. Parab, K.; Venkatasubbaiah, K.; Jäkle, F., *J. Am. Chem. Soc.* **2006**, *128*, 12879.
149. Hudson, Z. M.; Wang, S., *Acc. Chem. Res.* **2009**, *42*, 1584.

150. Hammerl, A.; Klapötke, T. M.; Krumm, B.; Scherr, M., *Z. Anorg. Allg. Chem.* **2007**, *633*, 1618.
151. Cordero, B.; Gomez, V.; Platero-Prats, A. E.; Reves, M.; Echeverria, J.; Cremades, E.; Barragan, F.; Alvarez, S., *Dalton Trans.* **2008**, 2832.
152. Kirij, N. V.; Yagupolskii, Y. L.; Tyrra, W.; Pantenburg, I.; Naumann, D., *Z. Anorg. Allg. Chem.* **2007**, *633*, 943.
153. Reed, A. E. C., Larry A.; Weinhold, F., *Chem. Rev.* **1988**, *88*, 899.
154. Konig, F. B.; Schonbohm, J.; Bayles, D., *J. Comput. Chem.* **2001**, *22*, 545.
155. Kim, Y.; Hudnall, T. W.; Bouhadir, G.; Bourissou, D.; Gabbai, F. P., *Chem. Commun.* **2009**, 3729.
156. Agou, T.; Sekine, M.; Kobayashi, J.; Kawashima, T., *Chem. Eur. J.* **2009**, *15*, 5056.
157. Broomsgrove, A. E. J.; A. Addy, D.; Di Paolo, A.; Morgan, I. R.; Bresner, C.; Chislett, V.; Fallis, I. A.; Thompson, A. L.; Vidovic, D.; Aldridge, S., *Inorg. Chem.* **2010**, *49*, 157.
158. Wade, C. R.; Gabbai, F. P., *Organometallics* **2011**, *30*, 4479.
159. Hoefelmeyer, J. D.; Gabbai, F. P., *J. Am. Chem. Soc.* **2000**, *122*, 9054.
160. Hoefelmeyer, J. D.; Schulte, M.; Tschinkl, M.; Gabbai, F. P., *Coord. Chem. Rev.* **2002**, *235*, 93.
161. Hoefelmeyer, J. D.; Solé, S.; Gabbai, F. P., *Dalton Trans.* **2004**, 1254.
162. Melaiimi, M.; Sole, S.; Chiu, C.-W.; Wang, H.; Gabbai, F. P., *Inorg. Chem.* **2006**, *45*, 8136.
163. Agou, T.; Kobayashi, J.; Kawashima, T., *Chem. Eur. J.* **2007**, *13*, 8051.
164. Matsumoto, T.; Wade, C. R.; Gabbai, F. P., *Organometallics* **2010**, *29*, 5490.
165. Agou, T.; Kobayashi, J.; Kawashima, T., *Phosphorus Sulfur Silicon and the Related Elements* **2010**, *185*, 947.
166. Rohr, A. D.; Banaszak, H. M. M.; Kampf, J. W.; Ashe, A. J., *Organometallics* **2011**, *30*, 3698.



167. Agou, T.; Kobayashi, J.; Kawashima, T., *Inorg. Chem.* **2006**, *45*, 9137.
168. Agou, T.; Kobayashi, J.; Kim, Y.; Gabbai, F. P.; Kawashima, T., *Chem. Lett.* **2007**, *36*, 976.
169. Dorsey, C. L.; Jewula, P.; Hudnall, T. W.; Hoefelmeyer, J. D.; Taylor, T. J.; Honesty, N. R.; Chiu, C.-W.; Schulte, M.; Gabbai, F. P., *Dalton Trans.* **2008**, 4442.
170. Bader, R. F. W., *Atoms in Molecules: A Quantum Theory*. 1994; p 454 pp.
171. Kim, Y.; Kim, M.; Gabbai, F. P., *Org. Lett.* **2010**, *12*, 600.
172. Schulte, M.; Gabbai, F. P., *Chem. Eur. J.* **2002**, *8*, 3802.
173. Cummings, S. A.; Iimura, M.; Harlan, C. J.; Kwaan, R. J.; Trieu, I. V.; Norton, J. R.; Bridgewater, B. M.; Jäkle, F.; Sundararaman, A.; Tilset, M., *Organometallics* **2006**, *25*, 1565.
174. Ashley, A. E.; Herrington, T. J.; Wildgoose, G. G.; Zaher, H.; Thompson, A. L.; Rees, N. H.; Krämer, T.; O'Hare, D., *J. Am. Chem. Soc.* **2011**, *133*, 14727.
175. Miyasaka, S.; Kobayashi, J.; Kawashima, T., *Tetrahedron Lett.* **2009**, *50*, 3467.
176. Chisholm, M. H.; Gallucci, J. C.; Yin, H., *Dalton Trans.* **2007**, 4811.
177. Baud, F. J., *Hum. Exp. Toxicol.* **2007**, *26*, 191.
178. Aaseth, J.; Shimshi, M.; Gabrilove, J. L.; Birketvedt, G. S., *J. Trace Elem. Exp. Med.* **2004**, *17*, 83.
179. Chiu, C.-W.; Kim, Y.; Gabbai, F. P., *J. Am. Chem. Soc.* **2009**, *131*, 60.
180. Elbing, M.; Bazan, G. C., *Angew. Chem., Int. Ed.* **2008**, *47*, 834.
181. Cametti, M.; Dalla Cort, A.; Bartik, K., *ChemPhysChem* **2008**, *9*, 2168.
182. Brown, H. C.; Dodson, V. H., *J. Am. Chem. Soc.* **1957**, *79*, 2302.
183. Yuan, Z.; Entwistle, C. D.; Collings, J. C.; Albesa-Jove, D.; Batsanov, A. S.; Howard, J. A. K.; Taylor, N. J.; Kaiser, H. M.; Kaufmann, D. E.; Poon, S.-Y.; Wong, W.-Y.; Jardin, C.; Fathallah, S.; Boucekkine, A.; Halet, J.-F.; Marder, T. B., *Chem. Eur. J.* **2006**, *12*, 2758.

## VITA

Name: Haiyan Zhao

Address: Department of Chemistry, Texas A&M University, TAMU 3255,  
College Station, TX 77843

Email Address: zhao@chem.tamu.edu

Education: Ph. D., Chemistry, Texas A&M University, May 2012  
B.S., Chemistry, Nankai University, China, June 2007

## Publications:

Zhao, H.; Gabbai, F. P. *Organometallics*. Accepted.

Zhao, H.; Gabbai, F. P. *Nature Chem.* **2010**, *2*, 984.

Zhao, H.; Gabbai, F. P. *Org. Lett.* **2011**, *13*, 1444. (highlighted in *Chemical and Engineering News* March 7, **2011** - Volume 89, Number 10 - p 42)

Cao, D.; Zhao, H. (equal contribution); Gabbai, F. P. *New J. Chem.* **2011**, *35*, 2299.

Kim, Y.; Huh, H-S.; Lee, M-H.; Lenov, I. L.; Zhao, H.; Gabbai, F. P. *Chem. Eur. J.* 2011, *17*, 2057.

Wade, C. R.; Zhao, H.; Gabbai, F. P. *Chem. Commun.* **2010**, *46*, 6380.

Kim, Y.; Zhao, H.; Gabbai, F. P. *Angew. Chem. Int. Ed.* **2009**, *48*, 4957. (highlighted in *Chemical and Engineering News* June 15, **2009** - Volume 87, Number 24 - p 27)